FUNDAMENTAL STUDIES ON TUBE HYDROFORMING AND LASER ASSISTANCE IN THE MANUFACTURE OF MICRO-PARTS

DOCTORAL THESIS

Presented in Partial Fulfilment of the Requirements for the
Doctoral Degree of Philosophy in the
Faculty of Engineering of
The University of Strathclyde, Glasgow

By
JÖRN LUNGERSHAUSEN

* * * * *

Department of
Design, Manufacture and Engineering Management
University of Strathclyde
2012

This thesis is the result of the author's original research. It has been composed by the author and has not been previously submitted for examination which has led to the award of a degree.

Signed:

Date:

ABSTRACT

This PhD-Thesis focuses on initial investigations of tube hydroforming (THF) as a new technology in the field of micro-part manufacture.

THF has been widely adopted in the automotive industry for approximately fifteen years and is now commonly used in many other industries. In the forming process the semi-finished part is formed with the aid of a forming liquid which acts inside the hole of the tube. Under the influence of hydrostatic pressure and additional mechanical loads the tubular blank is forced to conform to a given die cavity giving the part its final shape.

In comparison to "conventional" procedures for the manufacturing of hollow-shaped constructional work pieces, as for instance the welding of deep-drawn metal sheets, THF offers many advantages by enabling the production of parts having:

- Complex and variable cross sections in their longitudinal axis
- High strength due to cold-work hardening and homogenous grain structure
- High rigidity achieved by closed cross-sections
- Narrow tolerances in their outer dimensions
- Optimized transitions for fluid transport

Further on, THF especially offers a considerable time saving potential for manufacturing hollow shaped components compared to currently used techniques based on the removal of material. However, current state-of-the-art manufacturing of hydroformed parts is still restricted to conventional parts which well exceed micro-part dimensions.

Micro-THF as a new technology would add all these advantages to the micro technology sector and can establish access to other new fields and application. Examples of micro-hydroformed components are all hollow straight as well as bent components with complex shapes which currently cannot be (mass-)produced with any other micro manufacturing technology; components such as elements for micro-fluidic chips, micro heat exchangers and fluidic sensors or tubular parts for endoscopes etc.

The research performed aimed at carrying out the fundamentals of process design necessary for hydroforming micro-parts. Investigations were carried out on tubular parts having an outer diameter smaller than 1 mm and a length of ca. 10 mm. Extensive studies regarding material properties of micro-tubes especially its forming abilities were conducted and procedure limitations identified and analysed. In order to examine extended forming limits and to approach the so-called size effects which arise from scaling down a traditional forming process to micro-level, the process has further been investigated under the influence of laser energy. A diode Laser was used to increase the temperature of the tube material during forming, reducing the flow stress and increasing the ductility in the required area of the part. Additionally, numerous theoretical design studies had been performed which led to the development of the entire forming machine components.

As a result of the intensive research and development work carried out, process specific fundamentals suitable for an industrial application were established as well as the world's first micro tube hydroforming prototype machine was constructed that successfully manufactured hollow shaped micro components.

ACKNOWLEDGEMENTS

I express my sincere thanks to my advisors, Prof. Dr. Yi Qin, Strathclyde University and Prof. Dr. Ch. Hartl, Cologne University of Applied Sciences for taking the time to mentor and tutor me throughout the years of my graduate study program. Their insight, wisdom, support, and trust were indispensable. I also would like to give special thank all of my colleagues at the Institute of Production and Production Engineering of University of Applied Sciences Northwestern Switzerland, especially to Prof. Dr. Arne Wahlen and to the members of the Laser Applications Technology Research Group as well as to my colleagues at the Institute of Production of Cologne University of Applied Sciences who have all helped make this research effort possible.

Their invaluable assistance in technical areas and their uplifting emotional support will always be remembered.

I also wish to thank Chris Blomfield-Brown, my Australian friend for his precious time for carefully checking my manuscript as well as Angela Furrer from ETH Zurich (Swiss Federal Institute of Technology) for her support in material testing.

Further, I would like to thank the following facilities for their generous financial and technical support:

- Cologne University of Applied Sciences, in particular the electric's and mechanic's workshop
- All MASMICRO project partners
- University of Applied Sciences Northwestern Switzerland
- ETH Zurich

In closing, I would like to express my gratitude to my entire family, especially to my wife Sonja and my boys Lasse and Mads for their unyielding love and patience.

VITA

November 30, 1967 ……Born – Köln, Germany

2005 ……Dipl.-Ing. Automotive Engineering,
Cologne University of Applied Sciences,
Institute of Automotive Systems

2005 - 2008 .....….....Project Engineer,
Cologne University of Applied Sciences,
Institute of Production

2005 - 2012 …….……Doctoral Candidate,
University of Strathclyde, Glasgow,
Faculty of Engineering,
Department of Design, Manufacture and Engineering Management

2009 - …….……Senior Scientist and Lecturer,
University of Applied Sciences Northwestern Switzerland,
Institute of Product and Production Engineering

PUBLICATIONS

Studies on the hydroforming of micro-components (orig. Untersuchungen zum Innenhochdruckumformen von Mikro-Bauteilen). Proceedings from 9th Int. Symposium of Students and Young Mechanical Engineers „Advances in Mechanical Engineering“, Gdansk University of Technology 6-7 April 2006, pp. 129-134

Study of Hydroforming Processes for the Production of Micro-Components. Proceedings from 1st Jubilee Scientific Conference Manufacturing Engineering in Time of information Society, Gdansk, PL, June 1-2, 2006

Micro hydro-forming process and machine system for miniature/micro products. Proceedings from Euspen, 7th International Conference, Bremen; Germany; May 20-24, 2007

Micro-forming with high pressure (orig. Mikroumformen mit Hochdruck). Maschinenmarkt - Das Industriemagazin, October 15, 2007, pp. 26-28

Laser System for microforming applications, Internationale Leitmesse der angewandten Mikrosystemtechniken und Nanotechnologien, FORUM "Innovations for Industry", Hannover Messe, IVAM, Fachverband für Mikrotechnik, May 2008

Development of tools and machines for micro-hydroforming with improved accuracy. 20th Polish-German Conf. Development Trends in Design of Machines and Vehicles, Warsaw, PL, 17.-21- June 2008

A fiber laser system for 3D-processing of hydroformed micro components (orig. Faserlasersystem für die 3D-Bearbeitung von Miniatur-Umformteilen), LASER-Ausgabe 6 – Europäischer LASER Markt. Jan. 05, 2009

Investigation into reduction of die cavity deflection in micro-hydroforming processes using FEA, Int. J. of Advanced Manufacturing Technology. Springer, June 2009

Formability of stainless steel micro-tubes for micro-hydroforming processes, International Symposium on Plasticity: PLASTICITY 2011. Conference Proceedings, January 3-8, 2011

Formability of Micro-Tubes in Hydroforming, The 14th International ESAFORM Conference on Material Forming: ESAFORM 2011. AIP Conference Proceedings, Volume 1353, pp. 529-534 (2011).

TABLE OF CONTENTS

LIST OF FIGURES

LIST OF TABLES

NOMENCLATURE

Forces

F_a	*Axial load*	*[N]*
F_c	*Closing force of the press*	*[N]*
F_f	*Friction force*	*[N]*
F_u	*Forming force*	*[N]*
F_p	*Sealing (reaction) force applied on the punches due to internal pressure*	*[N]*

Stresses, strains and pressures

σ_{UTS}	*Ultimate tensile strength*	*[N/mm^2]*
σ_{yp}	*Yield strength*	*[N/mm^2]*
σ_t	*Tangential (hoop) stress*	*[N/mm^2]*
σ_z	*Longitudinal (meridional) stress*	*[N/mm^2]*
σ_v	*Effective stress*	*[N/mm^2]*
σ_N	*Normal stress*	*[N/mm^2]*
ε_t	*True (logarithmic) strain*	*[-][%]*
ε_u	*Uniform strain*	*[-][%]*
ε_z	*Elongation at fracture*	*[-][%]*
E	*Young's modulus*	*[N/mm^2]; [GPa]*
p_i	*Internal pressure*	*[N/mm^2]; [MPa]*
$p_{i,\,max}$	*Maximum internal pressure*	*[N/mm^2]; [MPa]*
$p_{i,\,min}$	*Minimum internal pressure*	*[N/mm^2]; [MPa]*
p_{ib}	*Bursting pressure*	*[N/mm^2]; [MPa]*
p_n	*Contact pressure between tube wall and sealing punch*	*[N/mm^2]; [MPa]*

Tube dimensions

d_0	*Initial inner diameter of tube*	*[µm]; [mm]*
D_0	*Initial outer diameter of tube*	*[µm]; [mm]*
D_1	*Instantaneous or final outer diameter of tube or die cavity diameter*	*[µm]; [mm]*
D_{1b}	*Final outer diameter of tube at bursting*	*[mm]*
t	*Wall thickness of the tube, in general or local*	*[µm]*
t_0	*Initial wall thickness of the tube*	*[µm]*
L_0	*Initial length of tube*	*[mm]*
L_f	*Length of tube in contact with die where friction occurs*	*[mm]*
r_c	*Corner radius of formed tube*	*[µm]*

Specific flaring and bulge test parameters

d_f	*Maximum achievable flaring diameter (after a crack occurred in flaring test)*	*[mm]*
ε_f	*Relative expansion ratio in the flaring test*	*[-]; [%]*
ε_b	*Relative expansion ratio in the hydraulic bulge forming experiments*	*[-]; [%]*
Δd	*Increase in inner tube diameter,* $d_f - d_o$	*[mm]*
v_a	*Spindle displacement rate during flaring tests (velocity of the conical forming tool)*	*[mm/min]*
α	*Semi-angle of the conical forming tool*	*[°]*
h_h	*Height of the tube holder (flaring test)*	*[mm]*
s	*Spindle stroke of the conical tool during flaring test*	*[mm]*

Laser parameters

$P_{out,l}$	*Laser source output power*	*[W]*
w_f	*Focal radius laser beam*	*[mm]*
A_N	*Numerical aperture*	*[mm]*
γ	*Opening angle laser beam at fibre*	*[°]*
n	*refractive index of the immersion medium*	*[-]*
Δx_{def}	*Amount of defocusing*	*[mm]*
w_{def}	*Radius of laser beam at defocused position*	*[mm]*
λ	*Wave length of the laser source*	*[nm]*

Other parameters

A_p	*Projected component surface (orthogonal to the press closing direction)*	*[mm²]*
t_f	*Forming time*	*[s]*
V_{fl}	*Volume flow*	*[ml/min.]*
ϑ_f	*Forming temperature*	*[°C]*
T_i	*Initial tube specimen*	*[-]*
T_1	*Tube specimen N° 1*	*[-]*
s	*Standard deviation*	
x	*Stroke of the axial punch*	*[mm]*
μ	*Friction coefficient*	*[-]*
d_k	*grain size*	*[µm]*

CHAPTER 1

INTRODUCTION

1.1 Background of the research - problems and development needs

The on-going trend towards miniaturization of products in many fields of daily life requires a large number of small metallic parts combined with a wide spectrum of part geometries/shapes. The growing demand for miniaturization encompasses a wide range of needs in the electronic and medical field for instance. Increasingly more functional devices are sought after as well as high precision medical equipment such as sensor technology and optoelectronics require mechanical parts such as levers, connector pins, resistor caps, tiny screws, contact springs and lead-frames [1].

Due to high production rates, achievable accuracy, minimized or zero material loss and excellent mechanical final part properties etc., metal-forming processes became more and more established for the manufacture of the above-mentioned micro-parts, in particular for bulk production. As a consequence, a lot of research has been done in the recent past which predominantly dealt with sheet and bulk forming [2]. So far, no investigations have been conducted to enable the forming of hollow-shaped micro parts, although there is an increasing demand for tubular micro-components in particular in the field of medical engineering. Elements for micro-fluidic chips, micro-needles, hose couplings for medical technology and implanted micro-tubes for drug delivery or tubular parts for endoscopes are only a few examples. Non-medical applications of micro-tubular components concern, for example, elements for micro heat exchangers, fluidic sensors and shafts for micro motors and cameras [3,4].

Against this background, tube hydroforming (THF) as a “new” technology for the manufacture of hollow-shaped micro-parts would not only offer a considerable time-

saving potential compared to techniques based on the removal of material. Furthermore it would lead to an enhanced spectrum of part geometries due to the possibility of forming hollow micro-components with complex shapes [3], which cannot be realized using conventional machining technologies.

At present, mass production of tubular hydroformed components is limited to the manufacture of parts with cross sections above about 20 mm in width [5]. The typical work areas and the limits of tube hydroforming are presented in *Table 1* [6]. For tubes covering the shown dimension ranges the process parameters as well as workpiece parameters such as attainable strains are largely known. But so far, no systematic studies - which would be of particular interest for micro-technology - on the hydroforming of tubular micro parts with outer diameters smaller than 1 mm can be found in the literature. Also, no solutions have been suggested yet.

Against this background, it shall be hypothesised in the here presented research study that hydroforming is a viable process for the manufacture of tubular micro-components with lengths of approx. 10-20 mm and diameters between approx. 0.75 and 1 mm at production rates of approx. 6 parts per minute.

Main parameter	Most common area in mm	Maximum values in mm
Length of tube	up to 500 (2,000)	12,000
Tube diameter	20 - 120	600
Wall thickness	0.5 - 4	50

Table 1: Work areas and limitations of tube hydroforming [6]

Problems in the micro range

The development and design of a tube hydroforming process for the manufacture of micro-parts require that specific issues/problems when scaling down a process on a one-to-one basis have taken into account [7,8].

Basic research in the field of microforming, e.g. [7-11], has shown that scaling down a process from macro to microscale is subjected to so-called size effects (cf. *Chap. 2.1 The state of the art of micro-manufacturing)*. As a consequence general process knowledge of conventional forming processes (bending extrusion, upsetting and others) cannot simply be transferred to microscale [12].

Since an ordinary 'macro' component has in general much larger workpiece dimensions in comparison to the grain size of the material from which it is made, conventional macro-mechanics (continuum) FE modelling is effective for simulating typical 'macro' forming processes [13]. However, if at microscale only a few grains are located in the forming zone, microstructural effects like strain non-uniformity and localization, grain size, grain structure (e.g. the direction between the crystal slip system and the local stress direction and the effect of adjacent grains with significant plastic mismatch) have shown an important influence on forming results [7,8,11,12]. The effects can be generally understood and often anticipated by means of numerical analysis applying special single crystal models, but this cannot be done for polycrystals [13]. This in turn still leads to the situation that the design of micro metal forming processes is often based on the empirically and experimentally gained know-how.

According to [7], the following 3 issues/groups also have to be considered when miniaturizing a production process:

1. Process
2. Tools
3. Machines/Equipment

The process itself is strongly coupled with the material, which has to be kept in mind when designing a micro forming process. Effects concerning the tribology, springback, the scatter of the results and further the accuracy of the produced parts have to be taken into consideration. Also these effects determine the applicability of FEA-based simulations for micro-process design and layout which are further reasons for the above mentioned mostly empirically obtained know-how [8].

Regarding the tooling, main problem is the manufacturing of the high-precision forming tools [7]. In particular the realization of an adequate surface quality of the dies and/or the inner shapes of its forming radii may be difficult. Other problems which have to be addressed are found in the forming loads which may have an important influence on the stiffness of the tooling and in turn on the accuracy of the part to be produced. A tool deflection of a few microns may lead to a much higher relative tolerance of finished micro parts compared to the same deflection which has a less important influence on the production accuracy of a component having macro dimensions.

An essential problem for micro forming machines is the handling of the initial/formed part with the required precision and safety in an appropriate time [8]. Regarding a bulk production the machine has to transfer the micro part within a few seconds and position it in the die with an accuracy of a few microns. Another problem is the weight of the micro-formed components which might be too low to overcome adhesion forces and in particular the finished part which is often moistened with forming fluid probably might stick to the grappler of a handling system.

1.2 Aims and objectives of the study

Based on the observations made, the aims and objectives of the study shall be summarized by the following:

Overall aim:
To develop fundamentals of a hydroforming process for the production of tubular micro-parts by theoretical and experimental work and to derive concepts for tools and for a micro hydroforming machine capable of economical mass production.

From this three specific aims can be derived:

- Establishment of material properties assessment methods
- Demonstration of a micro-THF prototype process
- Manufacture of 6 tubular micro-parts per minute

The objectives of the proposed work are:

- Investigation of the tubes' relative expansion ratios and the change in formability of micro-tubes compared to macro-sized tubes which feature a geometrical similarity
- Investigation of "conventional" testing methods to find out, if and/or how far they can also be used for the examination of micro-tubes
- Verification of technological laws and formulas used to design a macro hydroforming process if they can also be applied (and if, how far) for the development of a down-scaled process.
- Verification of an increase in formability and a decreased influence of size-effects during warm forming.
- Examination and quantification of size-effects, since as mentioned above, the development and design of a micro-forming process in general require that these 'negative' size-dependent effects have to be taken into account.

1.3 Approach

To achieve the aims and objectives of the study, the following research phases were planned and realized:

(1) State-of-the-art review of the tube hydroforming technology, understanding of the physical and technological background, design models and rules, etc.

(2) State-of-the-art review in micro-forming, study of scaling effects, material behaviour in the micro range, micro-forming and miniaturized production processes, etc.

(3) Investigation and quantification of the forming ability of micro-tubes and the change of formability compared to macro-sized tubes by applying the 'flaring test' and the 'bulge test' to get information about workpiece, machine and process parameters, such as maximum achievable expansion ratios, maximum internal pressures, forming loads, etc.

(4) Introduction of thermal laser energy to get information about enhanced material formability and/or reduction of scaling effects

(5) Development of tool and machine concepts based on the fundamentals gained from the experimental investigations

(6) Carry out first hydroforming experiments on a prototype machine to be able to draw a conclusion to the achieved research results

1.4 The research performed

To create a fundamental basis, first of all, the mechanisms that characterize the conventional tube hydroforming process had to be understood and analysed. Analysed, in terms of e.g. which laws and principles, design rules, relationships etc. can probably be applied on a one-to-one basis in the micro-range.

In order to be able to describe and analyse the forming behaviour of the investigated micro-tubes, extensive material analyses such as tensile and hardness tests of the tube specimens as well as grain structure investigations had been performed prior to the experiments.

The material analyses were followed by experimental investigations. To examine the forming behaviour of the selected micro-tubes, two kinds of testing methods had been conducted:

(1) Standardized, mechanical cone test (flaring test)
(2) Free expansion test of micro-tubes (hydraulic free-bulging test)

First test was mainly used to get initial information about a general forming ability of chosen micro-tubes and amounts of forming loads to be expected. Although its applicability as an easy-to-use "method" for the examination of tubular raw material provided for miniaturized hydroforming processes in the future should be verified.

Whereas the intention of the latter test was to investigate the forming behaviour, and the mechanical properties of tubes respectively, more in depth and closer to reality. Compared to the flaring test, hydraulic free-bulging tests enable the examination of

tubular material under bi-axial stresses without frictional influence. Furthermore, hydraulic free-bulging is even part of a hydroforming process.

Additionally, to investigate extended process limits due to the increase in formability and due to a decrease of size-effects, both flaring as well as bulge tests were accompanied by laser-assistance to conduct warm-forming experiments.

Based on the results obtained from the theoretical and experimental work, studies were performed in order to design a micro-THF tool and a prototype machine system.

Concluding, first micro-hydroforming experiments were carried out using the prototype machine to verify the applicability of the conducted testing methods and to draw a conclusion on the process, tools and the machine.

1.5 Thesis organization

Finally, the outline of this thesis proposal by chapters is:

Chapter 1: Introduction, background of the research and problem statement

Chapter 2: Literature review, state-of-the-art of micro-manufacturing and the tube hydroforming technology, hydroforming fundamentals

Chapter 3: Selection of micro-tube dimensions and materials, analyses of the material

Chapter 4: Experimental investigations of the tubes' formability with flaring tests (tests at room temperature as well as laser-assisted warm forming tests)

Chapter 5: Experimental investigation of tubes' mechanical properties with hydraulic free-bulging (tests at room temperature as well as laser-assisted warm forming tests)

Chapter 6: Forming machine development: Concept studies for forming tools and micro-hydroforming machine components

Chapter 7: Forming experiment using the prototype machine system and analysis

Chapter 8: Conclusions and future work

CHAPTER 2

LITERATURE REVIEW

2.1 The state of the art in micro-manufacturing

The persistent trend towards higher miniaturization, particularly in the field of electronics production, but also in the areas of micro electro-mechanical systems (MEMS) and micro systems technology (MST), is not only induced by consumers, who wish for more convenient electronic devices including more integrated functions, i.e. mobile phones, digital cameras. The increasing demand on miniature/micro-metal-products is also driven by technical applications such as actuator and sensor technology mainly within the automotive sector, medical equipment and optoelectronics. Typical examples of mechanical parts which contain all these products, besides electronic components, are pins for IC-carriers, fasteners, micro-screws, lead frames, micro-cups and connectors, as well as medical implants.

There are various techniques which can be used for manufacturing micro-products. MEMS-based manufacturing involves, largely, techniques such as photolithography, chemical-etching, plating, LIGA, laser fabrication, etc. while non–MEMS-based manufacturing often involves techniques such as mechanical machining, EDM, laser-cutting/patterning/drilling, embossing, injection-moulding, extrusion, stamping, etc. [15]. In most cases mass production can be realized by applying these technologies, but with regard to high final part accuracy, costs are comparable high and cycle times often very long.

Due to its advantages like good surface quality, minimized or zero material loss, excellent material properties and high accuracy at concurrent high quantity, in the first

instance metal forming technologies are predestined to substitute machining processes for the manufacturing of micro parts in serial production.

Influence of "size-effects"

The forming of small/miniature metallic parts is not new. Industry has experienced this for many years. But if it comes to a reduction of sizes down to tens or hundreds of a micrometre, challenges arise. When scaling down process and process dimensions, according to the similarity theory, so called size-effects appear [16]. Compared to conventional forming processes, some parameters remain constant. For instance, the microstructure of the material is independent of the dimensions of the process. Further on, the topography of the material stays also constant [17]. As a result, the ratio of the component dimensions or surface and the microstructure changes with miniaturization. Further, the forming behaviour, tribological conditions and operation accuracy are influenced by the size-effects. This leads to the fact that the existing know-how of conventional forming processes cannot be transferred unrestrictedly to micro-scale. Thus, fundamental studies have been studied intensively over the last ten years [1,7-9,11-14, 16,18]. Major issues concerned the understanding of material deformation mechanisms and material/tool interfacial conditions. Other examinations were related to materials property characterization, process modelling and analysis, qualification of forming limits, process design optimization, etc., with emphasis on the related size-effects. The following summarizes major key aspects mentioned by [19]:

- Conventional metal-forming process-configurations such as forging, extrusion, stamping, coining, deep-drawing, etc., may be equally used for the forming of miniature/micro-parts, process capabilities are likely to be constrained more, due to additional material, interfacial and tooling considerations in micro-forming.
- The types of material which could be formable at micro-levels are prescribed more significantly than for forming at macro-levels by the micro-structures and grain-boundary properties of the materials. The forming limits for these materials

are, therefore, somewhat different, compared to those for the forming of macro-parts.

- Size-effects may exist in material property and tool-material interfacial property characterization, depending largely on the micro-structures of the materials, which leads to the requirement of the definition of these parameters with reference to the actual materials and interfaces to be used.

Machines and forming tools

Traditionally, micro-manufacturing (non-MEMS manufacturing) was effected with large scale equipment, such as that for micro-mechanical-machining, micro-EDM and micro-metal-forming [15]. To perform micro-manufacturing tasks with the equipment, significant efforts have been made to improve the precision of mechanical structures, compensate for any mechanical and thermal errors, as well as increase functionality, resolution and reliability for online geometrical inspection.

During last 15 years bench-type machines or so called miniature manufacturing systems have been gradually developed and introduced to industry. The development of such machines/systems has attracted a lot of interest from research organisations and industries. Various new concepts are being experimented upon to design and fabricate prototypes of the machines and systems. A main consideration is that conventional facilities for manufacturing miniature/micro-products are not compatible, in sizes, to the products to be made in miniature/micro-manufacturing [15].

2.2 Tube hydroforming

Hydroforming is a general term for a forming technology where a pressurized fluid is used as the forming media. The method can be applied to either sheets or tubular geometries, where the latter is the topic of this work.

2.2.1 History of the technology

In the past, Tube Hydroforming (THF) has been called with many other names depending on the time and place it was applied and investigated [20]. Two early terms for THF, for instance, were Bulge Forming of Tubes (BFT) and liquid bulge forming (LBF). Hydraulic Pressure Forming or Hydrostatic Pressure Forming (HPF) was used for a short time by several investigators. One of the first general used terms was Internal High Pressure Forming (IHPF, german *Innenhochdruckumformen IHU*) which has mostly been used in Germany. Throughout this paper, the well-established acronym THF will be used.

Even though THF processes have been in industrial use since only approximately one and a half decades, the development of the techniques and the establishment of the theoretical background go back to the 1940s. Grey et al. investigated the manufacture of copper T-fittings by using hydraulic pressure and axial load. He applied for and achieved an US patent [21] which should give an indication of the coming period of THF.

First experimental and theoretical investigations on instability of thin walled-cylinders have been accomplished in the 1960s by many researchers in different countries. Mellor [22] presented fundamental investigations on thin- and thick-walled cylinders leading to theoretical improvements in LBF operations. Use of hydrostatic pressure, in particular for bulging of tubular parts, was initially reported by Fuchs [23] and Ogura et al., [24] in the late 60s.

In the 1970s, studies on new shapes, materials, different tooling configurations and new machine concepts, both experimentally and theoretically, continued by various researchers. For instance, to provide internal pressure, materials like polyurethane, rubber and elastomer were applied by Al-Qureshi, [25]. Woo [26] and Sauer, [27] investigated the free expansion of rotationally symmetrical workpiece shapes in order to determine material parameters and their influence on the forming behaviour. Applying the Membrane Theory and the Levi and von Mises correlations, initial computer-based programs to model THF processes could be designed.

In 1987 Klaas [28] applied the Membrane Theory, the Theory of Shells and the Continuum Theory of Plasticity for the study of relations between loads, stresses and strains for spherically formed tubes under the simultaneous influence of internal pressure and axial forces at the tube ends. In the late 1980s, the forming technology started to spread industrially, especially in Germany, after theoretical studies [29, 30] with 'real and new' industrial applications had been conducted.

After Schmoeckel et al. [31] had developed an algorithm for a pressure-dependent determination of axial stroke and force parameters based on the Membrane Theory, one began more and more using computer controls in experimental works, e.g. [32]. Also in the early 1990s, researchers started utilizing the capabilities of continuously developing the Finite Element Method in their analytical works. Dohmann [33], for instance, experimentally investigated the wall thickness distribution of rotationally symmetrical expanded components and compared the results to FE simulations. In the late 1990s, use of FEA was now a standard tool for THF process simulations: most of the research work is aimed towards the investigation of component materials and dimensions and the selection and control of the process parameters, examples can be found in [34].

Present applications

In today's industrial production, THF technology is widely used for forming lightweight or complicated shaped components. Series parts can predominantly be found in the automotive industry with a constantly increasing number of applications [6]. Typical THF components are chassis parts, including the engine cradle, front and rear axles, exhaust systems, space frame structure body parts and assembly components such as camshafts. *Fig. 1a* represents a rear axle frame made of four hydroformed aluminium tubes combined with other hydroformed light materials, in order to realize a low axle weight and improved driving kinematics. The axle is been manufactured on one of the first fully automated production lines.

Besides the products in the automotive industry, further THF applications are to be found in the areas of sanitary products *Fig. 1b&d* such as T-fittings which have been

one of first hydroformed products as mentioned above. Also hydroforming has gained increasing interest in the aerospace industry in the production of some complicated structural parts [35] and in the bicycle industry *Fig. 1c*, due to the demand for weight reduction in these fields. However, the automotive industry is currently the driving factor in the research and development work carried out on the area of hydroforming technology by research facilities, supplier industry and users. Their research and investigations during the past few years have supported the increasing application of this technology which offers decisive advantages regarding the manufacturing of complex shaped lightweight components [36].

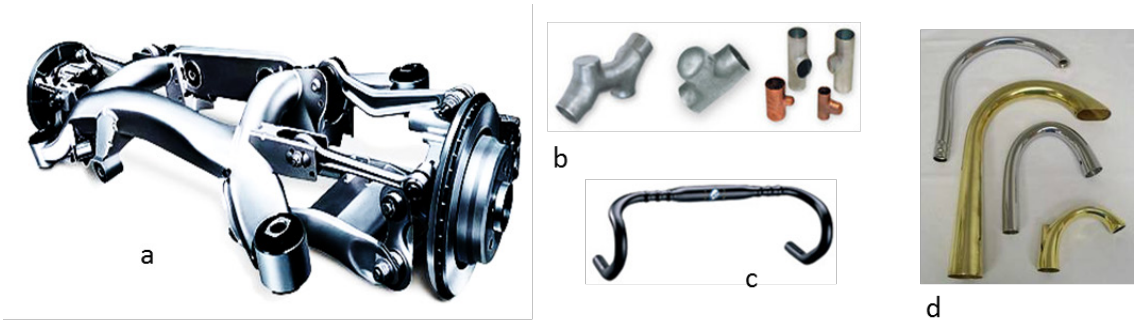

Fig. 1: Hydroformed components for automotive and non-automotive applications: a) BMW 5er series rear axle, b) T-fittings and Y-shaped tubes (American Hydroformers Inc.), c) Road handlebar (Yeu Chueh), d) Water Tap (H & H Tube's)

Pre-forming of complex shaped tubes for THF process

In order to achieve the desired shapes, many THF operations - such as for the manufacture of the products represented in *Fig. 1c&d* - require a pre-forming of the tube. Bending processes (in general rotary draw bending for complex bent components and press bending for less complex shapes with large bend radii) are necessary to ensure that the initial tube can be inserted into the hydroforming die [37]. However preforming not only comprises the bending of the semi-finished tubular material by itself, it usually includes crushing operations as well as annealing operations to remove residual stresses [34].

2.2.2 Hydroforming fundamentals

2.2.2.1 Process principle

In the process of tube hydroforming a straight or a bended tube is been formed under the influence of a hydrostatic pressure accompanied by mechanical loads. Initially the tube is placed into the die cavity of a split forming tool. The shape of the cavity corresponds to the final shape of the component. Following process steps include the closing of the dies as well as the sealing of the tube ends performed by axial sealing punches. A forming fluid which passes the boreholes of the punches is inserted and pressurized by a hydraulic power unit affecting the expansion of the component (internal pressure p_i). Axially compressed by the sealing punches tube material can additionally be forced into the main forming zone of the die cavity (axial force F_a). During the course of the process the internal pressure is continuously increased under the simultaneously controlled action of F_a until the formed tube entirely touches the inner surface of the die. *Fig. 2* shows the sequence of a typical tube hydroforming process including the filling of the tube, the forming under internal pressure and additional axial feeding and the relief of the loads.

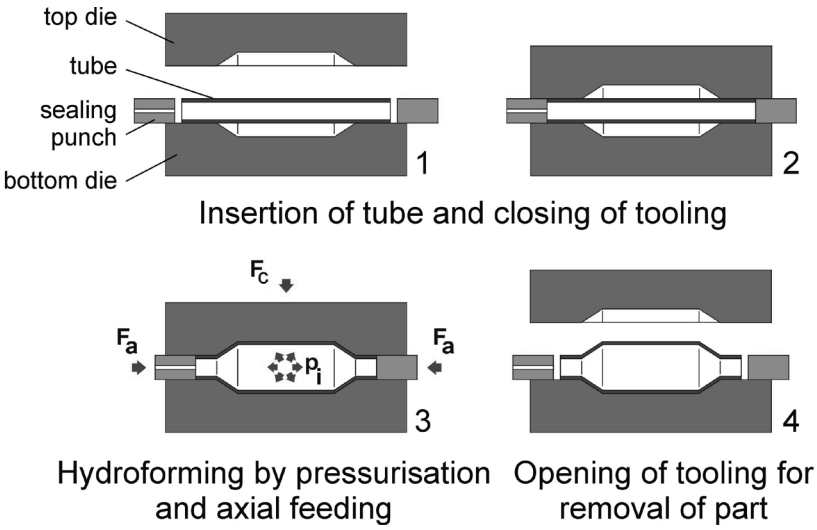

Fig. 2: Tube hydroforming principle [38]

2.2.2.2 Tube materials and testing methods

Process designers have to select materials, which optimally meet the component requirements. User-specified combinations of strength and good formability are required. Thus, for today's industrial hydroforming processes suitable and reliable testing methods to obtain material parameters which characterize the forming behaviour of the initial workpiece are essential [39]. However, the testing methods are also used as a tool for quality control of the incoming tubular raw material to reduce the number of scrap parts during manufacture [40]. As the formability of tubular material depends on the material composition, rolling process, state of heat treatment etc. even smallest differences - especially between materials of two or more delivery batches - can lead to different achievable expansion ratios for instance, which cause a run of defective parts, due to early bursting during the hydroforming process.

Currently, predominantly traditional material testing methods are used [6] which are standardized and thus easy to perform.

One of the most commonly used methods to describe the forming behaviour of the tubular material is the standardized uniaxial tensile test. Though, the suitability of the test is often limited due to the fact that the typical biaxial stress state of the THF process is not reproducible. For roll-formed products, a distinction has to be drawn between the application of this test to the initial sheet material before roll-forming and its application to the welded and roll-formed workpieces. If testing the initial sheet material, changes in material properties caused by the manufacturing process remain unconsidered [39]. The same applies to drawn tubular components formed from bulk material. Consequently, samples for tensile tests are predominantly taken from the finished tubular part in a longitudinal as well as in a tangential direction. However, this requires the specimens to be flattened before testing which influences the material properties [39]. Major characteristics obtained by tensile tests are: yield strength σ_{yp}, ultimate tensile strength σ_{UTS}, uniform strain ε_u, elongation at fracture ε_z, strain hardening coefficient n and elastic modulus E.

Further standardized methods [6] for testing the semi-finished products are:

(a) the expansion (or flaring) test, cf. *Chap.4*: expansion performed by a conical tool
(b) the ring expanding test: a cut tube section is expanded by a conical tool until fracture occurs
(c) ring tensile test: a cut tube section (ring) is expanded until it breaks
(d) the flattening test (flattening of the tube or tube cross section by compressive forces)

All tests are predominantly used to determine the formability and for the detection of defects on the surface and cross section of tubes.

To improve the characterization of tubes suitable for hydroforming applications, a process-specific burst test (also 'bulge test', cf. *Chap.5*) has been developed and numerous investigations have been carried out e.g. by [28,34,40]. According to *Fig. 3*, a tube specimen is clamped at both tube ends and is pressurized by a forming liquid until the tube bursts. During the test tube expansion and internal pressure are measured. With this method, the maximum attainable circumferential expansion of the tube can be determined.

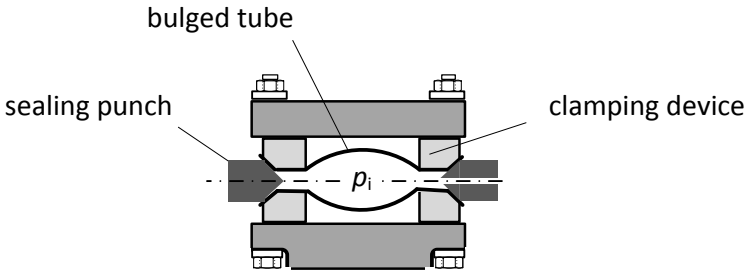

Fig. 3: Tube bulge test, schematically

Further common testing methods are hardness tests and non-destructive methods which work with ultrasonic or Foucault current. Detailed information regarding those tests can be found in the literature, i.e [6,39].

2.2.2.3 Process Design

When developing a THF part, an in-depth analysis of the boundary conditions is essential. An optimal component design considering the process limits (described later in this chapter) increases the reliability and the economy during the working process. The boundary conditions must be specifically applied so that the forming of the workpiece with its given wall thickness, cross section ratios etc. is guaranteed. The result depends on numerous parameters, like e.g. the initial tube dimensions, tube material, expand geometry and the controlling of the loads [41]. Their interaction during the process to the point of the final result is very complex.

In order to successfully accomplish the THF process and to achieve the aspired forming result, it must be known, in which way axial force and internal pressure e.g. as a function of the feeding path or the time have to be applied and/or increased. Generally the forming process consists of four steps:

1. Sealing and Filling

   After placing the initial workpiece into the die cavity the dies are closed. In order to obtain the sealing, the axial punches move towards the tube ends and simultaneously insert the forming liquid which is then pressurized. However the internal pressure p_i is still beneath the yield start.

2. Free Forming

   Due to the increase in pressure now, the material starts to flow. The pressure is raised until scarcely below burst limit. Axial loads F_a are further increased, in order to keep the system close. The punches are continued to move forward to feed material into the forming zone. At the end of this step the workpiece largely conforms to the shape of the die cavity.

3. Calibration

   During calibration, the tube totally conforms to the shape of the die cavity. The pressure level is high. Due to material friction, minor feeding is possible. The axial strokes and the axial loads respectively are used to prevent leakage. The calibration pressure $p_{i,\,max}$ is significantly influenced by the ratio of the

smallest component radius r_c to the wall thickness t_0, the stress condition inside the component as well as the current yield stress of the tube material.

4. Pressure Relief
   When forming is completed the pressure is released. After decreasing the axial loads and the press force, the dies are opened and the hydroformed part can be removed.

2.2.2.4 Prediction of forming loads

For the design of a suitable process control for a hydroforming operation the determination of the forming loads is essential. Nevertheless, the prediction of the forming parameters requires appropriate fundamentals first of all. As already mentioned above, technological principles had been developed by plasto-mechanical approaches as well as by means of FE simulations, which can all be found in the literature, e.g. by [28,42-50].

However, important fundamentals which are meanwhile established in practical experiences for a first determination of necessary loads and which are of a high interest for a 'new' micro hydroforming process shall be presented in the following. In conventional THF technology all introduced theoretical fundamentals serve in many cases as a basis for a more detailed determination of process control.

Yield pressure at process start

During the hydroforming process the forming loads internal pressure p_i and the axial force F_a cause stresses in the tube wall, which can be referred to as plane strain for the sake of simplicity in case of thin-walled components. For the cylindrical shape of the component the stress state can be described by a stress acting in circumferential direction, tangential stress σ_t and a transverse so-called longitudinal or meridional stress σ_z. Regarding the process start with a cylindrical tube under axial force F_a and internal pressure p_i (*Fig. 4*), the circumferential and axial stresses can be derived

from the force equilibrium at a tube section for a thin walled tube according to [28] as follows:

$$\sigma_t = p_i \frac{D_0 - t_0}{2t_0} \tag{1}$$

$$\sigma_z = \frac{F_a}{\pi (D_0 - t_0) t_0} \tag{2}$$

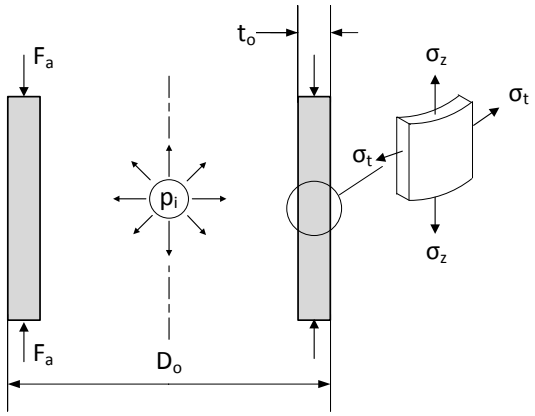

Fig. 4: Tube section under internal pressure and axial compression according to [28]

Expansion of the tube is ensured under the assumption according to [28] that the effective stress σ_v, which results from the combination of these stresses, corresponds to the local yield strength σ_{yp} of the tube material:

$$\sigma_v = \sqrt{\sigma_t^2 + \sigma_z^2 - \sigma_t \sigma_z} \tag{3}$$

Determination of the closing force

The parameters of the forming machine and units mounted on the tool are derived from the maximum loads necessary for the forming process. Moreover, they determine the design of the hydroforming tool with regard to rigidity and strength.

Decisive for the closing force F_c of the hydroforming machine is the projected component surface A_p located orthogonal to the press closing direction and the maximum internal pressure $p_{i,\ max}$. The following applies for the minimum required closing force $F_{c,\ min}$:

$$F_{c,\,\min} = A_p\, p_{i,\,\max} \tag{4}$$

The maximum value $p_{i,\ max}$ determines also the pressure intensifiers to be used. The characteristic data of the drives for the axial punch stroke is given from the necessary axial force F_a. For the determination of the amount of stroke, the amount of tube material to be supplied during the forming process is to be determined.

Internal pressure

In tube hydroforming process, the internal pressure p_i versus the time needs to be determined. Its variation depends mainly on the material properties and strain hardening behaviour, on the tube wall thickness, and on intricate sections sizes of the component such as small corner radii. Hence, the amount of internal pressure p_i as a function of time should satisfy the following criteria [34]:

- Sufficiently high to start the plastic deformation of the tube. A minimum required internal pressure $p_{i,\ min}$ must be present to avoid buckling and/or wrinkling of the tube due to axial forces F_a at the beginning of forming.
- Sufficiently high to prevent the tube from wrinkling during intermediate forming stages due to excessive compressive axial force F_a.
- Sufficiently high to form the tube wall into intricate sections of the die cavity during calibration. The so called calibration pressure $p_{i\ max}$ is dependent on the wall thickness t_0, corner radius r_c and flow stress of the material (however, usually ultimate tensile strength σ_{UTS} is used instead).
- Low enough not to cause instabilities by necking or bursting of the tube wall. The amount of the burst pressure p_{ib} may not be exceeded.

Maximum internal pressure

At the end of the forming process the tube wall has to be formed into corner radii of the die cavity which have not been formed during the main expansion of the tube. This requires the raise of the internal pressure up to its maximum value $p_{i,\,max}$. One possibility to determine $p_{i,\,max}$ has been developed by [34]:

$$p_{i,\max} = \frac{2}{\sqrt{3}} \sigma_{yp} \ln\left(\frac{r_c}{r_c - t}\right)\left(2 - \frac{\sigma_{yp}}{\sigma_{UTS}}\right) \tag{5}$$

with the yield strength σ_{yp}, the ultimate tensile strength σ_{UTS} of the tube material, the wall thickness t (*Fig. 5*) at the formed radius and the outside corner radius r_c of the die cavity which is to be formed.

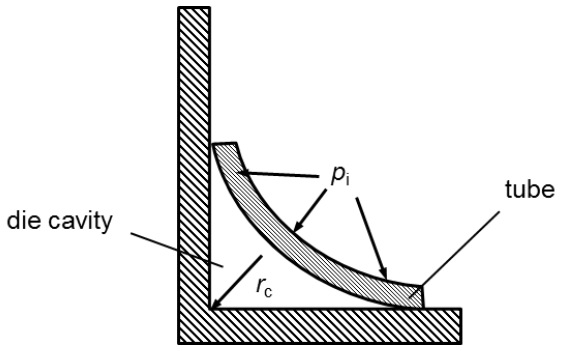

Fig. 5: Corner radius region in THF processes determined according to [34]

Another equation [51] empirically deduced to determine the maximum necessary internal pressure is:

$$p_{i\max} = 1{,}2\,\sigma_{UTS}\,\frac{t_0}{r_c} \tag{6}$$

with the initial tube wall thickness t_0. Using *Eqn.* (6), the course of internal pressure versus the ratio of the die cavity radius r_c to the tube wall thickness t_0 for a stainless steel micro-tube had been developed, *Fig. 6*. It is obvious form this figure that the

smaller the ratio r_c/t_0 the higher is the necessary amount of internal pressure to form the radius r_c.

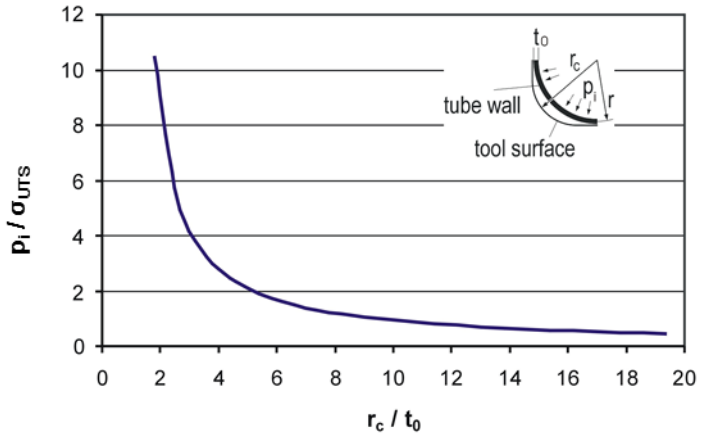

Fig. 6: p_i/σ_{UTS}-ratio versus r_c/t_0-ratio according to [52]

Bursting pressure

For the prediction of the internal pressure p_{ib} at the moment of the bursting of straight tubes within the state of free expansion, the statement investigated in [28] under the use of the membrane theory

$$p_{ib} = \sigma_{UTS} \frac{2t_0}{D_0 - t_0} \tag{7}$$

has shown to be applicable. Here, σ_{UTS} is the tensile strength of the material. Hence, the amount of p_{ib} should not be exceeded as long as the tube is not in contact with the surrounding die cavity. Only when large areas of the expanded tube received alignment to the die cavity the internal pressure is to be increased higher than p_{ib}.

Fig. 7 shows the comparison of bursting pressure obtained from experiments and predictions by *Eqn.* (7) for axisymmetric bulge parts of different tube material, wall thickness and diameter. Experimental information is obtained from [28] and from formability tests at Engineering Research Center, Ohio State University published by

[34]. As can be seen, predictions agree with the experimental findings within a reasonable range.

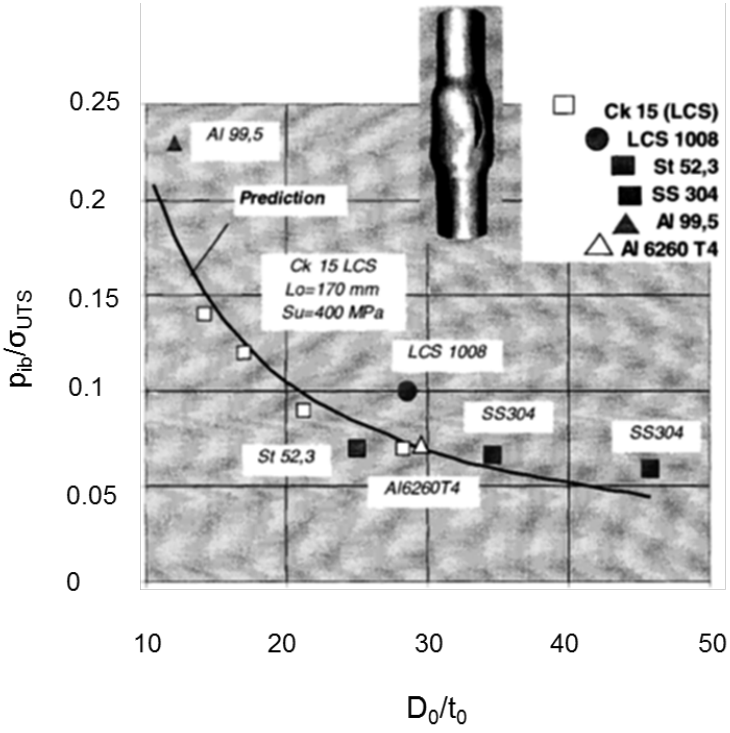

Fig. 7: Comparison of p_{ib}/σ_{UTS} ratios of macro-tubes obtained from experiments and predictions for different materials, tube diameter and wall thickness values after [34] (diagram also contains results developed by [28])

Calculation of axial force F_a

Simultaneous with internal pressurization, compressive axial forces are generated by the axial sealing punches in order to seal the tube ends as well as to compensate the thinning in the expansion zone by moving tube material into those regions. In today's tube hydroforming applications, hydraulic cylinders are used as axial drives to apply the axial forces into the tube walls. The forces provided by the axial cylinders should be:

- Sufficiently high in order to countervail the internal pressure at pressurization start. The sealing force F_p is the equivalent to the reaction force on the projected punch face due to internal pressure p_i.
- High enough to overbear the friction between outer tube surface and die walls. The axial force will be equivalent to the value of friction force F_f.
- Sufficiently high to cause the tube wall deforming. F_u is the component equivalent to the longitudinal stress acting on the tube cross section area. For practical purposes, flow stress, or the ultimate tensile strength σ_{UTS} respectively, of the tube material is used in calculations [34].

According to [53], a typical end position of a tube being bulged is represented in *Fig. 8*. Hence, the axial force F_a acting on the tube ends can be made up from the force equilibrium in *Fig. 8*:

$$F_a = F_p + F_f + F_u \tag{8}$$

The sealing force F_p results from the reaction force of the internal pressure acting on the punch front. The following applies:

$$F_p = p_i \frac{\pi}{4}(D_0 - 2t_0)^2 \tag{9}$$

with the outer diameter D_0 and the wall thickness t_0 of the tube end in the feeding zone.

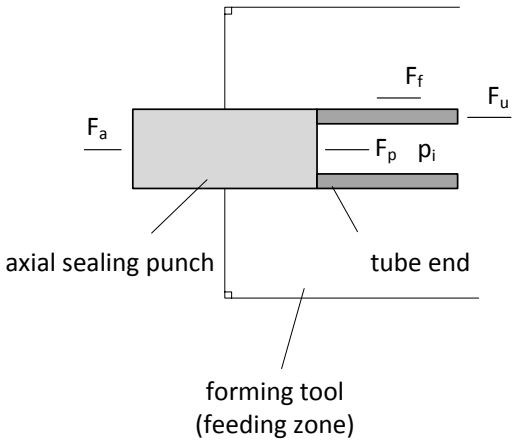

Fig. 8: Feeding zone with forming loads according to [53], schematically

As the tube wall comes into contact with the die shape with progressive expansion, with the axial force F_a also the friction force F_f must be overcome in this area. When Coulomb's frictional behaviour is taken as a basis, the following friction force is given:

$$F_f = \mu \, \sigma_N \, D_1 \, \pi \, l_f \tag{10}$$

with the coefficient of friction μ, the instantaneous tube diameter D_1 in the die and the length l_f where frictional movement occurs [53].

The force F_u is the axial force component that is initiated in the tube wall which together with the action of the internal pressure maintains the plastic flow of the tube material. By means of derivations using the upper bound theory it can be shown [49], that for thin walled tubes (if wall thickness to tube diameter ratio t_0/D_0 is below 0.3):

$$F_u = 1.12 \, \pi \, D \, t_0 \, \sigma_{yp} + \pi \, (D_0 - t_0) \, t_0 \, p_i \tag{11}$$

with the yield stress σ_{yp}, the tube outer diameter D_0 in the feeding zone and the tube wall thickness t_0 at this area.

For practical use according to [54], a rough estimation of F_u can also be made by:

$$F_u \approx \alpha \, \sigma_{UTS} \, \pi t_0 \, (D_0 - t_0) \tag{12}$$

with α = 1.2…2.0, the initial tube dimensions D_0 and t_0, and the ultimate tensile strength σ_{UTS}.

Finally, two important issues should be added:

- Generally, the internal pressure p_i and the position (stroke) of the axial punch x are controlled and varied versus the time t to obtain the desired part geometry within the process limits. Hence, the axial force F_a of the axial punches results from the selected process control with $p_i(t)$ and $x(t)$.
- For a suitable design of the axial punches the maximum amount of axial force F_a is of interest to ensure that these can be built with an adequate durability. This maximum force F_a generally arises at the end of the hydroforming process during the calibration of the component with $p_{i,\,max}$.

Process Limits and Process Failures

A successful executed THF process requires that all processing parameters are situated within a process window, *Fig. 9*, in order to avoid the typical failure modes [28].

The reason is that the workpiece shapes attainable with hydroforming processes are limited by the occurrence of failures like wrinkling, necking or bursting of the tube wall and buckling of components with long, unsupported workpiece areas [27,28,45,49,55,56].

To meet the process window, all process parameters must satisfy the following requirements:

- The axial force F_a must be large enough to ensure a safe sealing of the hollow profile.
- The maximum internal pressure p_i may not lead to a necking of the tube wall.

- The maximum applicable axial force $F_{a,\,max}$ must always lie underneath the buckling load.

Both, the mechanical loads and the internal pressure can only be increased up to boundary values, until following failure modes may occur [53]:

- Depending on the initial tube parameters (dimensions and specifics), a critical axial compression stress σ_z leads to buckles or wrinkling.
- A critical internal pressure p_i leads to necking of the tube's wall, if the pressure is further increased, cracks arise.
- If the chosen bending angle is too large, crinkles and defects along the tube's (oval) cross section appear.

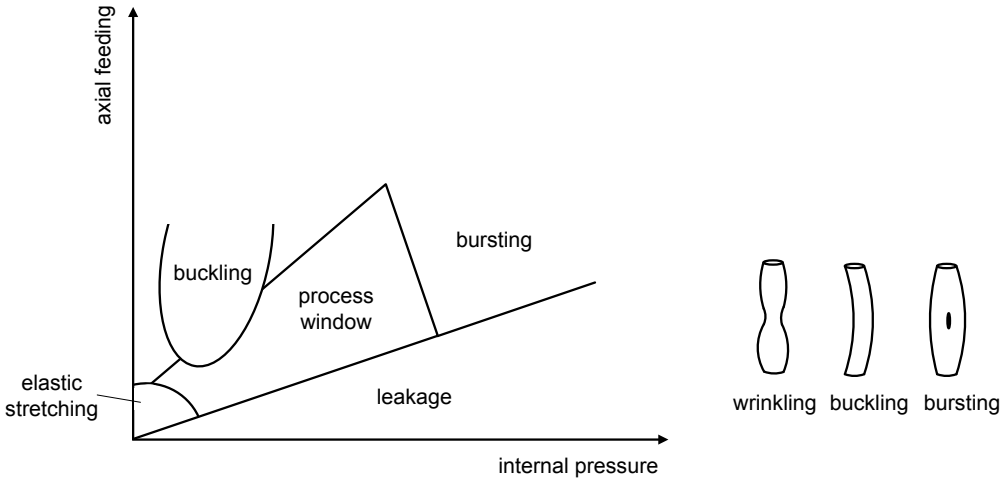

Fig. 9: Process window (left) with load conditions according to [28] and common failure modes [53] which limit the THF process: wrinkling, buckling and bursting

Regarding a forming process with tension-compression stress, the following can be stated. The larger the failure free area, the larger is the ratio *axial compressive stress to tangential tensile stress,* σ_z/σ_t. This ratio also influences the decrease in wall-thickness t_0. The process control must maintain a sufficiently high axial compression stress σ_z, in order to minimize the tangential stress σ_t and to force tube material towards the die cavity. Also the initial tube parameters influence the process limits.

The reliability on buckling and local wrinkling depends on the tube parameters length l_0, diameter D_0, wall thickness t_0 and tube material [28].

An exact prediction of the occurrence of such failures is comparatively time-consuming due to the usually complex forming operations. Based on the assumption of simplifying basic conditions, certain predictions can be made concerning necking of the tube wall and buckling of the workpiece, e.g. [27,45]:

- For the start of necking in the case of rotationally symmetric expansion of straight tubes, a criterion was investigated in [27] that was established under the assumption of a constant ratio of the axial to tangential stress $\sigma_z / \sigma_t = \text{const.}$ Accordingly, this form of necking occurs when the logarithmic strain in wall thickness direction

$$\varepsilon_t = \ln \frac{t}{t_0} \tag{13}$$

  corresponds to the negative strain hardening coefficient -n of the tube material with the wall thickness t_0 of the initial tube, and the local wall thickness t of the expanded tube. The requirement $\sigma_z / \sigma_t = \text{const.}$ does not apply generally to conventional hydroforming processes. However, fundamental investigations have shown that it can be used for a first estimation [49].

- In conjunction with FEA-process simulations, today forming limit diagrams (FLDs) are used for the prediction of the start of necking. Also here the simplifying assumption is made that the ratio of expansion growth is constant during the forming process.

- From practical experience it is known, that possible rotationally symmetrical expansions of straight tubes obtained by hydroforming are feasible from about 12% (aluminium alloys) up to 40% and more (stainless steel). Depending on the component geometry and length increased values may be achieved [55].

2.2.3 Laser-assisted process

In general, high deformation rates can lead to cracks and rupture very easily during forming processes. Thus, heating has been widely used for assisting in forming processes, largely due to improved material flow and reduced strength at the elevated temperature. Due to the dependence of the yield strength on temperature, forming at elevated temperatures eases processing of the materials.

Fig. 10 shows an example of the flow curve for an austenite stainless steel (AISI 304) steel at different forming temperatures. With an increase in heat the true stress decreases.

Thus, introducing heating leads to reduced forming loading and helps to process materials with extend forming ability including component/part-forms and dimensions or aspect ratios.

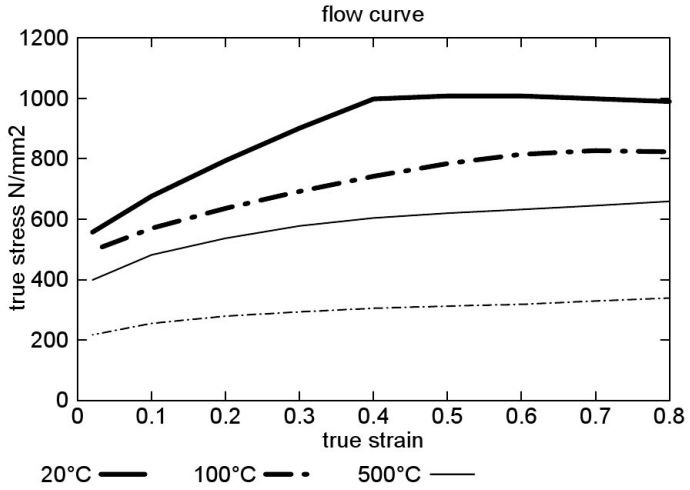

Fig. 10: Reduction of the yield stress during warm forming: Yield stress depending on the deformation degree during cold and warm forming [56]

Heating with laser is especially effective for forming sheet metals or thin sections from bulk materials. Since forming mostly takes place at localized areas of the work piece only, selective heating is sufficient and is advantageous in most cases. It offers a possibility to heat only the areas of the work piece where strongest deformations

are required. In today's production technologies the laser can be used in the processes such as bending, deep drawing, stamping, can-extrusion, etc. [58-61]. Transparent tools made of sapphire permit the guidance of the laser radiation directly onto the workpiece within the closed tool set during the processes [15].

Due to the high lateral resolution by minimized focusability down to a few microns, laser processes have in particular become established within the manufacture of miniature and micro-parts [5,56,59-61].

Thus, especially for the hydroforming of micro-tubes the impact of selective laser heat could help increasing the forming ability in the forming zone (provided that an increase in formability of micro-tubes takes place under heat influence which to find out is subject of the study).

Size effects in microforming

As already mentioned in *Chap. 1*, the forming behaviour, the tribological conditions and operation accuracy are influenced by the size-effects. They appear to be the most important (process limiting) factors in microforming. Therefore, the influence of the microstructure on the forming result is one of the main aspects to consider. With decreasing size, the influence of single grains and their orientation has to be taken into account, in particular if only a few grains are present in one dimension [8]. Also anisotropy and / or the texture of the material must be taken into account. From literature it is known that those parameters often lead to reduced process stability and reliability. As suggested in [62] a possibility to reduce the impact of size-effects is to influence the microstructure during the forming by heating the workpiece. According to [63,64], the above-mentioned flow stress at higher temperatures is been reduced by a higher number of activated slip systems inside the grain structure. Due to that, anisotropic material behaviour is reduced which results in a less inhomogeneous forming with improved repeatability.

Looking at the above mentioned facts, laser heat seems the most suitable choice for the heating of the micro-tube during the forming process compared to other methods, as it offers

- Local heating of the tube, allowing to limit the heat impact to the forming zone (heating of the entire micro-tube e.g. by magnetic induction probably could have enlarged the risk of instabilities such as wrinkling due to reduced material stiffness during axial feeding)
- Energy input and thus the forming temperature can easily be controlled via the current of the used laser source
- Laser radiation allowing minimal process time as well as handling time of the tube during experimental investigations which could not be achieved with heat transfer from e.g. pre-heated tools

Description of the forming ability during hot forming as an example of steel

Normally, in forming processes with increased temperature mostly high-alloyed steel and steel with higher strength (higher C-content) are formed. The temperature range of usually 600°C … 800°C is named as the area of warm forming. Besides that, some manufacturers apply lower temperatures, especially for impact extrusion processes. In some cases, forming between 160°C to 350°C shows a significant improvement of the formability without noticeable change of the basic material. For austenitic steel, in particular stainless steel, 200°C - 450°C is a common temperature range [65].

Since austenitic stainless steel, and in particular AISI 304 stainless steel is object in this study, it is essential to point out some of the general and specific characteristics.

If the chrome concentration arises over 12.5%, steel becomes rustless and with that non-corroding. Alloying elements such as molybdenum and nickel support this effect. Depending upon the content of alloying elements and carbon the stainless steel differs in its metallurgical structure. Three main groups are differentiated in /1/ ferritic, /2/ martensitic and /3/ austenitic steel. In general, the cold-formability of austenitic steel is better than the one of ferritic steel. However, due to the strain-hardening of

austenitic steel during cold forming its power requirement is larger compared to the cold forming of ferritic steel. Parallel to the strain-hardening of austenitic steel, another hardening effect occurs: the austenitic (face-centred cubic, fcc) structure changes to martensitic (body-centred cubic, bcc) structure [65].

The hardness of the martensite leads to an increase in strength. This hardening depends on the content of nickel. The higher the nickel content, the smaller is the cold hardening [65].

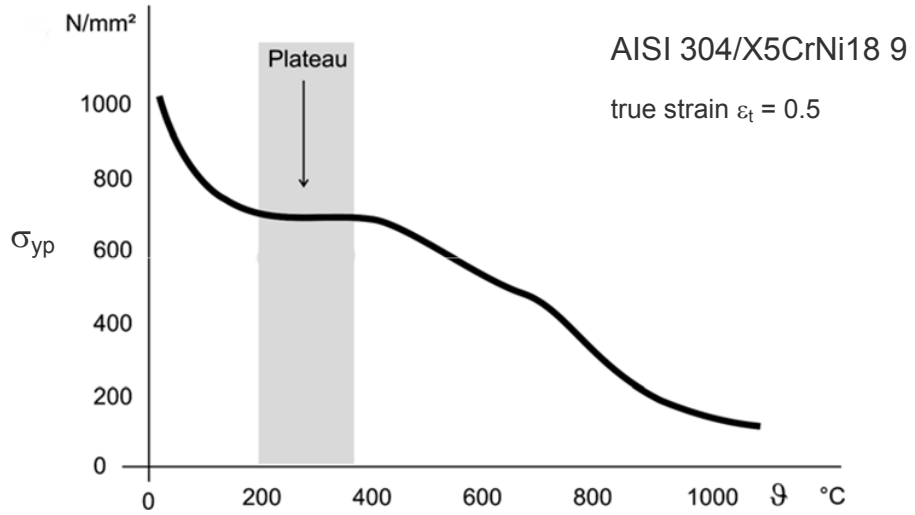

Fig. 11: Function of temperature-yield stress of stainless steel AISI 304 [66]

An increase in temperature to approx. 350°C can affect the forming of stainless steel favourably [65]. The flow curve [66] of AISI 304 at a degree of true strain $\varepsilon_t = 0.5$ is characterized by a plateau of reduced yield strength σ_{yp} between ca. 200°C and 400°C, *Fig. 11*. Thus, with regard to experimental investigations, the area of steady material ability is a tremendous advantage if the forming temperature probably cannot be hold absolutely constant.

CHAPTER 3

SELECTED MATERIALS AND MATERIAL ANALYSIS

This chapter addresses three major topics regarding the materials used during the study.

- The first part of the chapter addresses the methodology concerning: How adequate tube materials and dimensions have been selected for a later miniaturized THF process. Finding appropriate material is important because there is no material database existing and there are no reports which characterize the mechanical properties such as the forming ability of micro-tubes, which would simplify the choice of those tubes suitable for micro-hydroforming application. And as can be seen later, mechanical properties of the same material changes depending on the delivery.
- The second part of the chapter gives an overview of the used tube materials and dimensions and focuses on the approach to systematically applying several testing methods to collect significant information about the formability of the chosen micro-tubes.
- And finally, part three deals with the material analysis to verify and/or extend the manufacturer's information regarding the mechanical properties of the investigated micro-tubes, e.g. the ultimate tensile strength obtained in tensile tests, elongation, hardness etc. Additionally, microstructural analyses had been performed to get information about grain sizes and possible anisotropies with the objective to be able to understand obtained forming results.

3.1 Considerations on tube selection

In principle, all materials and alloys used for deep drawing or stamping can be used for hydroforming applications as well [67]. Hence, micro-tubes made of material typically used for micro-forming applications were analysed in a first step.

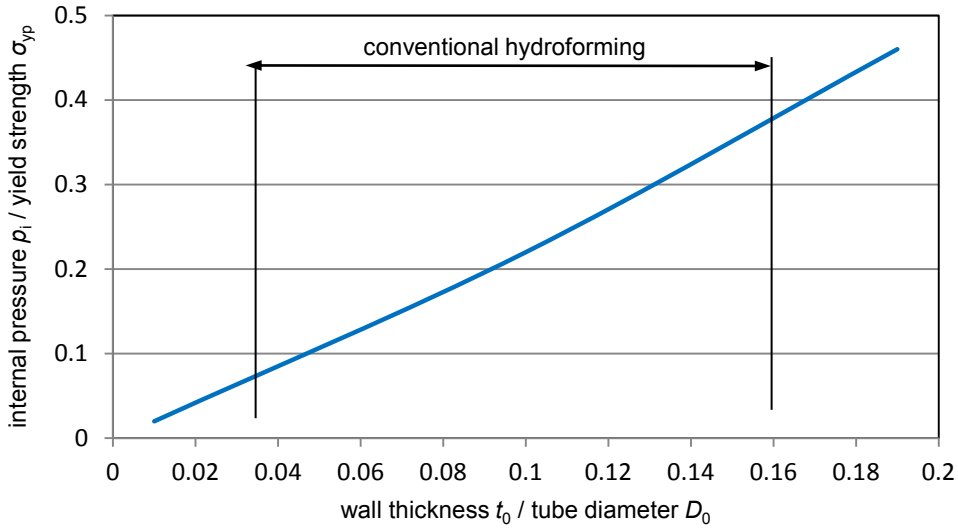

Fig. 12: Ratio t_0 / D_0 versus p_i / σ_{yp}

It can be shown with *Eqn.* (1), *Chap. 2*, that for a tube expansion without the support of an axial stress, the ratio between the needed pressure for the tube expansion and the yield strength of the material, p_i/σ_{yp} is proportional to the ratio of tube wall thickness to tube outer diameter t_0/D_0. This relationship is shown in *Fig. 12* [67], supplemented with the range of t_0/D_0 ratios used in current applications for the conventional hydroforming of tubes [69]. Thus, micro-tubes had been investigated with the same t_0/D_0 ratio compared to those being used in conventional THF processes, *Fig. 12*.

It was found that micro-tubes available on the market have dimensions in the range of $t_0/D_0 = 0.05$ up to 0.16, which is identical to the ratios of hydroforming tubes for conventional applications. Smallest offered tube diameters are about 0.2 mm and smallest wall thicknesses about 0.015 mm. Available micro-tubes of two different manufacturers/suppliers are exemplarily shown in *Fig. 13* and *Table 2*.

Regarding the typical maximum values of internal pressures presently used in conventional THF applications (200 up to 400 MPa), it seemed that this pressure can also be applied to micro-parts.

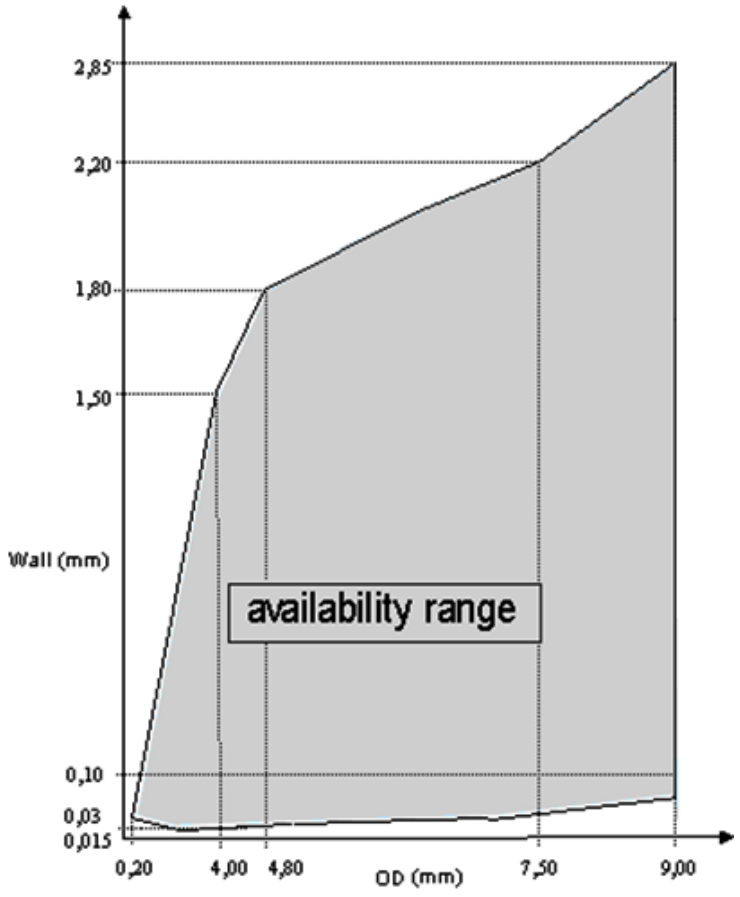

Fig. 13: Manufacturer's ('Minitubes', France) availability range of mini- and micro-tubes [70]

h = zughart / hard drawn w = geglüht / annealed hh = halbhart / half - hard R = Ring / coil

AD OD	WD WT	ID ID	1.4301 AISI 304				1.4306 AISI 304L				1.4541 AISI 321				1.4401 AISI 316				1.4404 AISI 316L				1.4435 AISI 316L				1.4571 AISI 316Ti			
			h	w	h	R	h	w	h	R	h	w	h	R	h	w	h	R	h	w	h	R	h	w	h	R	h	w	h	R
0,25	0,100	0,05													•												•			
0,30	0,060	0,18					•												•	•										
	0,100	0,10	•																											
0,40	0,100	0,20	•																											
0,45	0,125	0,20	•																											
0,45	0,150	0,15	•																											
0,50	0,075	0,35	•																											
	0,100	0,30	•																								•			
	0,150	0,20	•																								•			
	0,190	0,12	•																											
0,55	0,100	0,35	•																											
0,60	0,100	0,40	•																											
	0,125	0,35																									•			
	0,150	0,30	•																								•			
0,65	0,080	0,49	•																											
	0,100	0,45					•																							
	0,120	0,41	•																											
	0,125	0,40	•																											
	0,150	0,35	•																											
0,70	0,050	0,60	•																											
	0,100	0,50	•																											
	0,150	0,40	•																											
	0,175	0,35	•																											
	0,200	0,30	•																											
	0,250	0,20	•																											
0,75	0,150	0,45	•																											
0,80	0,100	0,60	•																								•			
	0,150	0,50	•																											
	0,200	0,40	•												•															
	0,250	0,30	•		•																						•			
	0,300	0,20																									•			
	0,350	0,10																									•			
0,81	0,280	0,25									•																			
0,85	0,100	0,65	•																											
	0,150	0,55	•																											
0,90	0,100	0,70	•																•											
	0,150	0,60	•																								•			
	0,200	0,50	•																								•			
	0,250	0,40	•																											
0,92	0,150	0,62																									•			
0,95	0,150	0,65	•																											
	0,175	0,60	•																											
1,00	0,050	0,90	•																											
	0,100	0,80	•	•							•																•			
	0,150	0,70	•			•					•	•															•			
	0,200	0,60	•	•		•													•								•	•		
	0,250	0,50	•																•								•	•		
	0,300	0,40	•																								•			
	0,350	0,30	•								•																			

Table 2: Stainless steel micro-tube dimensions and materials available from 'Rieck' [71]

3.2 Used materials and sequence of experimental investigations

Fig. 14 gives an overview of the investigated tube materials as well as the sequence of the studied experiments:

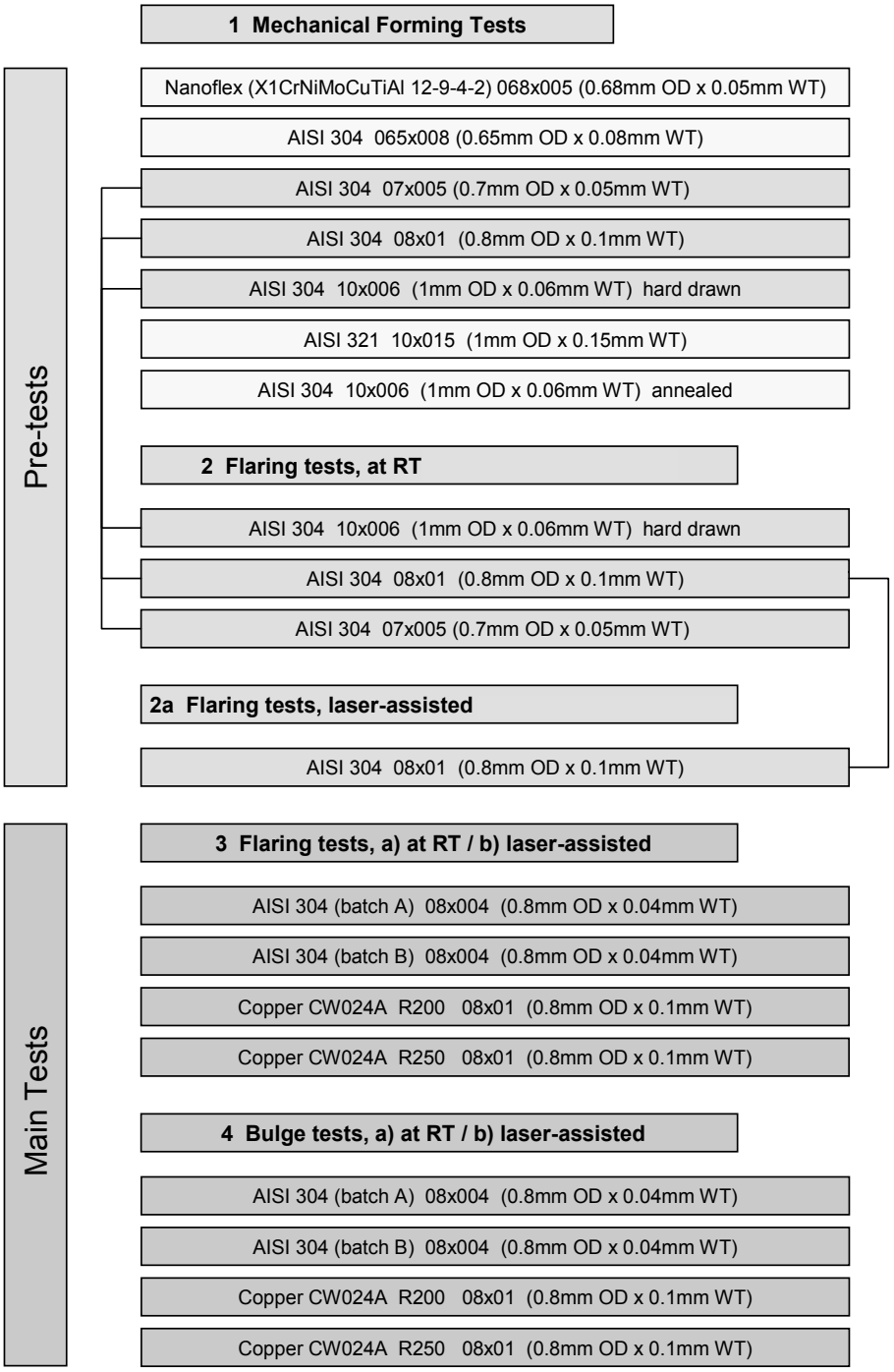

Fig. 14: Investigated tube material and sequence of experiments

Initial trials were performed on micro-tubes that had been offered by a supplier for free. The delivered samples in lengths of a few centimeters were used for experiments such as bending tests, simple tensile tests, and mechanical expansion tests. The overall objective was to obtain primary and general information about the tubes' forming ability. The tubes used for these tests are summarized under point '1', *Mechanical Forming Tests* (it should be noted here that due to minimal order quantities, approx. 500 to 1500 m, it was not possible to obtain amounts of tubes in lengths of approx. 1 m from the suppliers and/or manufacturers with which more extensive initial experiments compared to the samples in lengths of a few centimeters could have been performed).

After the initial trials, a selection was made and the micro-tubes presented in section '2' were investigated applying the *flaring test*, described in detail in *Chap. 4.3*. For simplicity reasons, a mechanical load gage was used initially and all forming data was recorded manually. The aim of the first tests was to collect information about suitable tube diameters and wall thicknesses (for the flaring test, bulge test and the following hydroforming trials) as well as wall thickness / diameter aspect ratios t_0/d_0, forming loads, expansion diameters and scattering of the investigated micro-tubes.

Furthermore, the assumed most suitable micro-tube (AISI 304 0.8x0.1) was investigated under warm forming conditions, *Fig. 14*, experiments '2a'. A laser beam was used to increase the temperature to up to 300°C. First information about enhanced process limits as well as (probably reduced) influence of size effects should be gathered. The temperature of 300°C was chosen since it was firstly approximately in the centre of the area suggested by [65], cf. *Chap. 2.2.3 Laser-assisted process* and secondly in the centre of equal yield strength (the 'plateau' of the AISI 304 flow curve) which could be - as already mentioned above - a tremendous advantage if the forming temperature probably cannot be hold absolutely constant and scatters slightly during the experiments.

Based on the experience gained with the test series ‘2/2a’, a few hundred metres of a stainless steel micro-tube with an outer diameter D_0 of 800 µm were ordered for further experiments. The wall thickness t_0 of the stainless steel tube (AISI 304) was 40 µm. After the first lot was used up during the study, new material had to be ordered expecting the same chemical composition and the same mechanical properties. In the course of the investigation the two lots are denoted as “-a” for the first lot (AISI 304-a), and “-b” for the second lot (AISI 304-b) respectively. Additionally, two sets of copper micro-tubes had been purchased to extend the investigations to non-ferrous material.

Fig. 15: Universal testing machine 'Zwick BX100/SN5A ' with flaring test setup

According to *Fig. 14*, both stainless steel batches (AISI 304-a and AISI 304-b) as well as the copper tubes (CW024A) differed in their mechanical properties. In test series '3', the material properties were investigated by applying the flaring test at a universal testing machine ‘Zwick BX100/SN5A’, *Fig. 15*. Trials were performed at room temperature and laser-assisted heating at 300°C.

In test series '4' hydraulic free bulging tests were performed with AISI 304 and CW024A micro-tubes at room temperature and laser-assisted heating at 300°C.

Major aspects of the bulge test were:

1. It should be examined if the forming results (e.g. maximum expansion diameters, elongations etc.) obtained by the flaring test can be reproduced by the free hydraulic bulging. If so, then the flaring test could be used as an alternative (easy-to-handle) testing method in the future in contrast to the hydraulic bulge tests.
2. Obtained forming results (forming diameters, maximum achievable internal pressures, elongations etc.) should be the basis to define the dimensions of a "demonstrator part" to be hydroformed in a micro-hydroforming prototype machine (closer described in *Chap. 6*).

3.3 Material analyses

As mentioned, AISI 304 and CW024A tubes were selected as test specimen materials. The austenitic stainless steel AISI 304 (ref. to EN 10088-3: 1.4301 and/or X5CrNi 18-10) features a high ductility and excellent drawing and forming properties. The material is commonly used in applications like the automotive and construction industry, the chemical industry, cooking and food processing equipment, kitchen sinks, hospital surgical equipment, hypodermic needles, feed water and other tubing and sanitary fittings to name a few. Typical mechanical properties of material used for forming applications are 500 – 700 MPa ultimate tensile strength σ_{UTS}, 360 MPa yield strength, 50% elongation at break and a Vickers hardness (HV10) of ~200 [72].

The CW024A copper also corresponds to the following designations: C106, UNS C12200, ISO Cu-DHP. CW024A is phosphorous de-oxidised non-arsenical copper that is 99.9% pure. It is typically used in applications like refrigeration, gutters and roofing, gas plants, hydraulic air and oil lines, air conditioning, heater units, plumbing pipe and fittings. It is typically supplied as round tube, half hard sheet and soft sheet. C106 / CW024A material has an excellent response to cold working. Hot working is good, but as an example with forging of brass rated as 100, the hot forge-

ability of C106 / CW024A is rated at 65. Annealing can be done by rapid cooling after heating to approx. 370 – 650°C. Mechanical properties vary widely according to condition (soft/half hard etc.), however typical values are 50…340 MPa proof stress, 200…400 MPa ultimate tensile strength σ_{UTS}, 5…50% elongation and 40 to 120 HV Vickers hardness [73].

To verify the material properties of the delivered micro-tubes, tensile tests, hardness measurements and microstructural investigations were performed on them. However, the material tests were only conducted on the tubes which were investigated in the 'main' test series 3 and 4 of the study and on the stainless steel tubes AISI 304 0.8x0.1.

The mechanical properties of the test materials were determined by tensile tests to verify the manufacturer's information. The experiments were conducted on a universal testing machine Zwick BZ100/SN5A. For each material tube samples of 40 mm in length were taken for the tensile tests. The free clamping length L_0 of the samples was 12 mm. Before each test, a small piece of wire was introduced into each tube end (outer diameters of the wires corresponded to the inner tube diameter) so that the tubes could not be crushed in the clamping area. Every measurement was repeated three times and each average value was taken as the result, *Table 3*. For comparison, the table also includes the values taken from the manufacturer's test reports.

It is conspicuous that the ultimate tensile strength (593 MPa) of the second delivery batch (batch B) of AISI 304 08x004 is far below the value (700 MPa) determined by the manufacturer and thus much lower than the ultimate tensile strength σ_{UTS} of delivery batch A, which was 730 MPa (manufacturer's information), and 690 MPa (measured) respectively. Furthermore, in both cases (batch A and B) higher yield strengths and thus lower elongations were measured.

Material	Outer diameter [µm]	Tube roundness [µm]	Wall thickness and thickness tolerance [µm]	Ult. tensile strength [MPa] (manufacturer information / measured)	Yield strength [MPa] (manufacturer information / measured)	Elongation at fracture [%] (manufacturer information / measured)	Hardness HV 1 (manufacturer information / measured)
AISI 304	800	-20/0	100±1	not listed / 1157	not listed /	not listed / 7.8	work-hardened / 372
AISI 304 (batch A)	800	±20	40±0.5	730 / 690	344 / 477	53.7 / 36.7	not listed / 205
AISI 304 (batch B)	800	-7.5/+6.4	40±3	700 / 593	329 / 408	53 / 31.2	not listed / 165
CW024A (R200)	800	-10/0	100±5	not listed / 236		not listed / 37.3	not listed / 45
CW024A (R250)	800	-10/0	100±5	247-250 / 296		30 / 13.7	not listed / 49

Table 3: Tube dimensions, tolerances and mechanical properties

Regarding the copper tubes, the values of the minimum required ultimate tensile strengths σ_{UTS} could be achieved. The σ_{UTS} of the R200 (R200 means at least a σ_{UTS} of 200 MPa) was 236 MPa and the one of the R250 (≥250 MPa) was determined to 296 MPa. Also, the indicated elongations of the copper materials did not match the manufacturers' data.

A reason for the differences compared to the manufacturers' information could not be found. All tensile tests were undertaken with identical test conditions during the study. However, it must be stated that sample lengths have been investigated which differed from the tube lengths used in the manufacturer's tensile tests.

For the hardness determinations a testing machine GNEHM, type Brickers 220 was used. As the program HV1 was chosen. The load duration was 12.5 seconds at a test load of 9.805 N. Again, every measurement was repeated three times and the mean values were taken as a result. Measured values are listed in *Table 3*. Due to recrystal-

lization annealing, the hardness values of the 08x004 stainless steel tubes were –as expected- well below the value of steel tubes with a wall thickness of 100 µm which were delivered in work-hardened condition. The measured hardness of the C106 / CW024A copper tubes are also represented in *Table 3*.

To analyse the grain structure and measure the grain size, samples were embedded in plastic moulding on the one hand in thickness direction (longitudinal tube direction) and on the other perpendicular to the longitudinal tube direction and afterwards polished. Finally the materials were micro-etched using a mixture of aqua regia (nitro-hydrochloric acid) and "Vogel's" pickling inhibitor for the stainless steel tubes, and Cu m5 (mixture of distilled water, hydrochloric acid and ferric-III-chloride) for the copper tubes respectively. The recipes had been taken from [74].

A digital microscope, type Keyence VHX-600 was used to visualize the grain structures, *Fig. 16*. In longitudinal direction of the AISI 304 0.8x0.1 tube, (1) left, a deformation texture caused by the drawing process of the material can clearly be seen, whereupon a significant anisotropic behaviour is expected during the formation tests. On the contrary, the AISI 08x004 micro-tubes, (2) and (3), show a consistent polycrystalline grain size distribution, grain shape distribution and structural arrangement in both the longitudinal and the section perpendicular to the longitudinal tube direction. Grain sizes of the AISI 304-a were determined to 8-9 ASTM (American Society for Testing Materials) which corresponds to grain diameters between 22 µm and 16 µm, and 7-8 ASTM (between 35 µm and 22 µm) of the AISI 304-b respectively, and which all indicates 'fine-grained' microstructures.

On the four micrographs in *Fig. 16* below, (4) - (5), the grain structures of the copper micro-tubes are visualized. The R250 copper tubes are characterized by a distinctive smaller grain size compared to the R200 grain structure. Grain sizes were determined to approx. 9 ASTM for the R250 copper tubes which indicates a fine-grained structure and corresponds to grain sizes of approx. 15 µm. R200 grain sizes refer to ASTM 6 - 7 which are mean grain size diameters in the range of 30…45 µm.

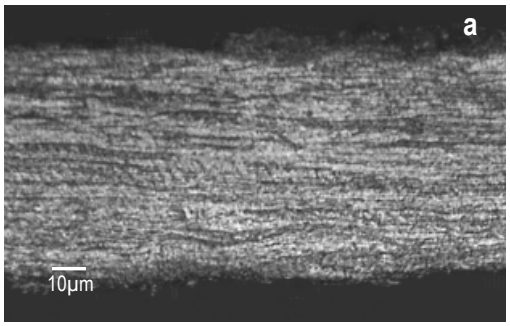

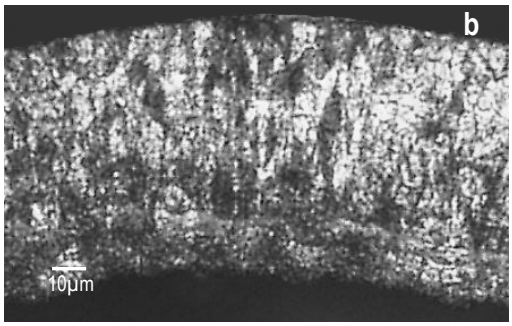

(1) Stainless steel AISI 304 0.8x0.1

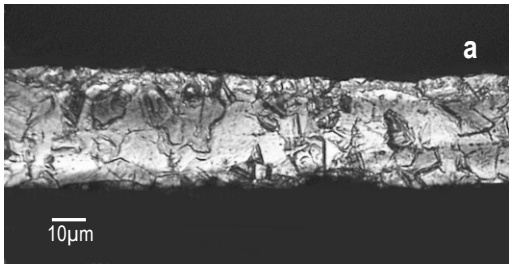

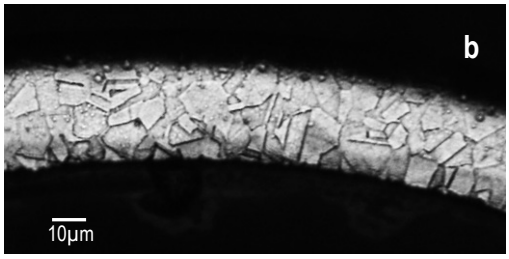

(2) Stainless steel AISI 304-a 08x004

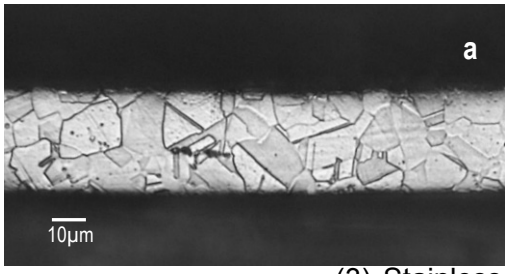

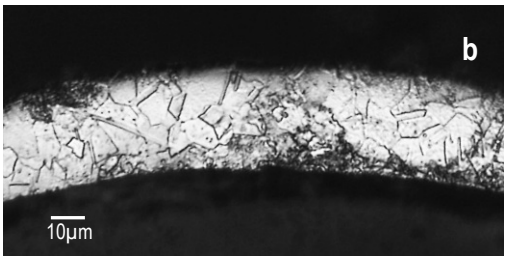

(3) Stainless steel AISI 304-b 08x004

(4) Copper CW024A R 200 0.8x0.1

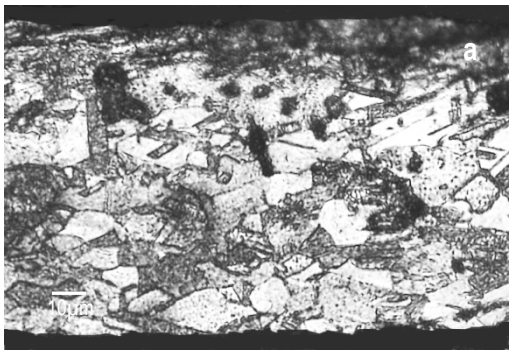

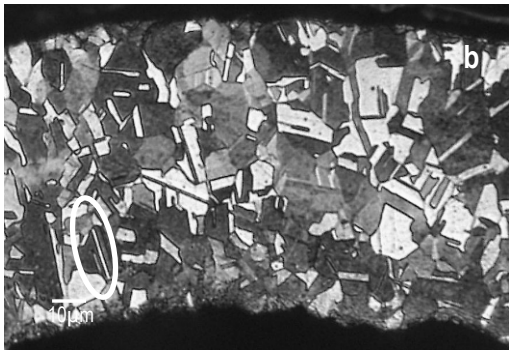

(5) Copper CW024A R 250 0.8x0.1

Fig. 16: Metallographic micrograph sections of the test materials, a) longitudinal tube direction, b) circular cross section of the tube

In the copper structures, the so-called crystal twins can be observed. Such crystals can be found in both the R200 and the R250 copper tube structures that are marked with white ovals in *Fig. 16* below. From literature is known, e.g. [75,76], that especially metals and alloys with fcc (face-centred cubic) lattice such as copper and stainless steel often contain those twins. In this case, two possible ways for their formation need to be considered: /1/ thermally formed twins so-called recrystallization twins, resulting from a recrystallization of the material and /2/ mechanically formed twins which arise due to an external load. In both cases those twins are generally a hint of a remarkable anisotropy which could lead to a likely inhomogeneous forming behaviour later on.

CHAPTER 4

DETERMINATION OF TUBES' FORMABILITY WITH FLARING TESTS

4.1 Introduction

As mentioned in *Chap. 3*, there has not been any research to characterize material properties on micro-tubes formability, particularly for circumferential ductility in biaxial stress state. However, this should be of substantial interest for the selection of applicable micro-tubes material for the tube hydroforming process. The current information available on micro-tubes formability is based only on uniaxial tensile tests though the hydroforming process applies multi-axial stresses.

In this study a testing method was used to investigate the tubes' formability under more realistic conditions which apply multi-axial stresses that are present in the hydroforming process.

4.2 Aim of the test

Since the ductility of a material is an important parameter that determines the forming limit of a hydroforming process, its evaluation is essential.

In order to evaluate the material behaviour, especially the circumferential ductility of micro-tubes, the flaring limit was investigated experimentally. The flaring limit is related to the circumferential ductility of a micro-tube and was determined as a property that defines the maximum flared expansion. In the study, the flaring limit was defined as the relative expansion ratio ε_f as:

$$\varepsilon_f = (d_f/d_0)-1 \quad (14)$$

Where d_0 and d_f are the initial micro-tube and final maximum expansion diameters, respectively.

4.3 Short description of the flaring test

Previous researchers have studied the material behaviour of tubes by means of the expanding test (now commonly referred to as a flaring test). Manabes and Nishimuras investigations [77,78] initially dealt with the effects of the mechanical properties and sizes of tubes, lubricants and cone-angles on the flaring process.

In the publication of Almeida et al. [79] and Alves et al. [80] the emphasis is focussed on deformation modes, forming limits and on establishing formability principles for the benefit of those who design thin-walled tubular parts in daily practise. Theoretical (numerical) investigation based on finite element method supported by experimental investigation validated the experiments.

The stress-strain distribution was meanwhile studied analytically combining the volume incompressible condition, Levy-Mises equation and the Theory of Plasticity by Lu [81] and Fischer et al. [82] to clarify the deformation behaviour during flaring.

Since all above mentioned studies dealt with tubes with outer diameters D_0 >20 mm, there has been a lack of information considering the material behaviour of micro-tubes. Thus far, no research results obtained from flaring tests regarding micro-tubes of the materials investigated in this study have been published. As the formability is one of the most important parameters that determine the forming limit during the hydroforming process, the flaring limit was investigated which provides information about achievable expansion ratios in the micro tube hydroforming process.

4.4 Experiment procedure

The mechanical expansion experiments conducted refer to DIN EN ISO 8493. According to this standard, seamless and/or welded tubes may be applied to the test which, however, is usually applied to tube diameters larger 1 mm. Additional information can be found in [83].

In this study, standard tubes featuring an outer diameter $D_0 \leq 1$ mm have been investigated. Furthermore, all selected tubes covered the t_0/D_0 *ratio r*ange according to *Fig. 12*. The sample to be expanded consists of a tubing section whose length L_0 is large enough that there is still sufficient length outside the tube holder after the procedure. The expanded area cannot extend into the area of the tube holder.

The samples are taken from the ends of the tubes. Their cut faces lie perpendicularly to the longitudinal axis of the tubes. The exact length of a tube was measured using a digital sliding calliper. In order to reduce the influence of a comparatively rough tube ends surface that could influence an early material failure (notch effects caused by grinding marks) the specimens were ground down with sandpaper (1200 grit) to set their nominal lengths. To guarantee an identical treatment of each specimen, the specimens of each test series were all together placed into a multi-holder and were then ground down to the same extend and to an equal length. The sample edges should not be rounded (deviating from the standard test for macro-tubes) in order to avoid a reduction of the wall thickness at the beginning of the procedure. However, all samples are slightly de-burred to the same extent.

The experiments were performed at room temperature using the universal testing machine Zwick BZ100/SN5A under an upper spindle displacement rate of v_a = 1.2 mm/min. The principle kinematics and geometry definitions can be seen in *Fig. 17*. The conical tool with the semi-angle of α is fixed in the chuck collet of the machine and aligned with the longitudinal axis of the micro-tube placed in the tube holder. Prior to inserting the sample into the holder, it was cleaned precisely using pressurized dry air. Before conducting each experiment, the conical tool and the end of the micro-tube were cleaned with isopropanol.

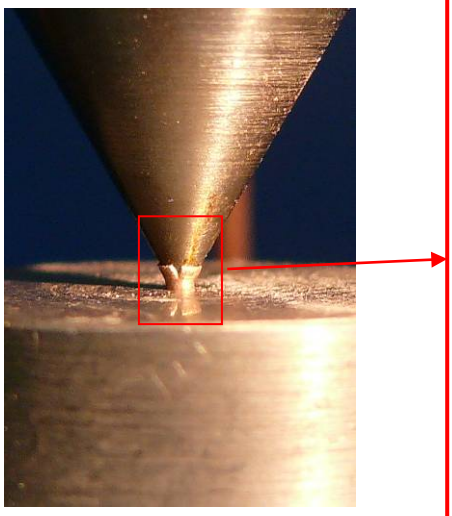

Experimental setup

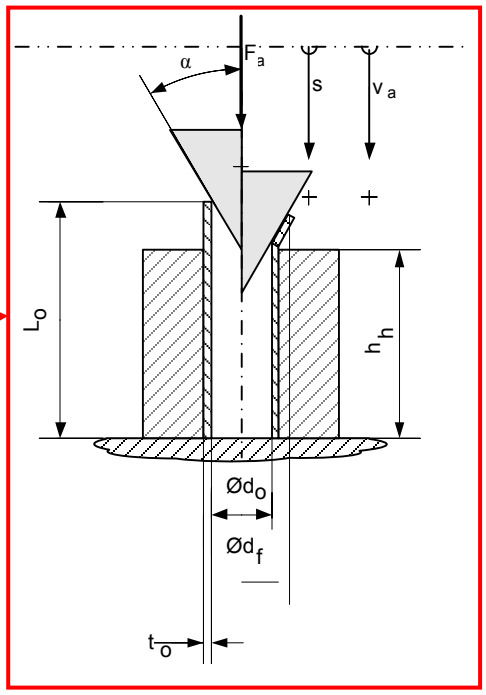

Flaring test, schematically

Tube dimensions:	Initial tube length L_0
	Initial inner tube diameter d_0
	Initial wall thickness of the tube t_0
	Inner tube diameter after forming d_f
Tool dimensions:	Semi-angle of the conical forming tool α
	Height of the tube holder h_h
Kinematics:	Axial forming load F_a
	Spindle displacement rate v_a
	Axial displacement of the forming tool s

Fig. 17: Conical tooling and the flaring test schematically

Before each test, the expand cone was oiled and moved until it just touched the inner edge of the micro-tube. After resetting the micrometre gauge and the load micrometre, the conical punch is pressed into the sample, until at least one tear appeared at the outer diameter of the expanded sample. During the test neither the sample nor the conical tool was allowed to turn. The sample surface was continuously observed

from a visual range of approx. 250 mm with normal visual acuity, particular in the main expansion area. In appropriate steps, the axial load affecting on the tube's end was read off from the indicating calliper and its value was recorded as one with the corresponding axial displacement. The press was stopped either at the point a fracture appeared or if buckling and/or wrinkling occurred, also if the flaring diameter could not be increased any further.

After backing out the conical tool from the tube and taking the tube out of the holder, the expansion diameter at the border of the flaring zone was measured using a Zeiss reflected-light microscope with charge-coupled device camera *AxioCam MRc*.

A remark on the measuring techniques of the expansion diameters

The two techniques to determine the forming diameter are shown in *Fig. 18*. Application of each type of technique depended on the appearance of the widened tube end. Two cases had been distinguished:

1. No crack or only a very small crack/beginning of crack appeared after forming. => Diameter could be determined via "diameter" or "radius" measurement mode of the microscope' measurement programme.

2. As a result of the high radial tensile stresses inside the tube wall a few tube ends practically 'exploded' so that the crack(s) wide opened. => A line along the inner edge of the tube wall could be manually designed and the measurement programme determined the surrounded area. The expanded diameter was then calculated via the according circumference of the determined area minus the distance of the crack width(s).

Since the measurement points had been manually set, the inaccuracy in measurement was assumed to be in the entire micrometre range. Thus, the measured values had been rounded up to the nearest 1/100 mm.

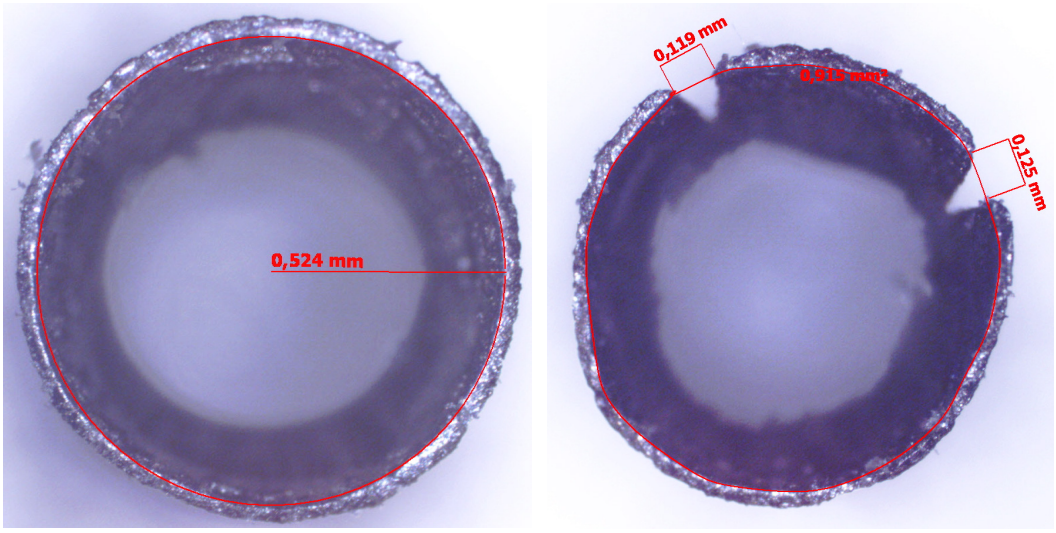

Fig. 18: Determination of the achieved expansion diameter with the integrated measurement programme of the Zeiss reflected-light microscope

4.5 Laser-assisted flaring test

After the cold-forming flaring tests have been conducted, the next aim of the investigating was on the influence of heat by means of laser-energy on the forming behaviour. Since applications of micro forming technologies are limited by problems arising from size-effects, several researchers have investigated micro-forming processes under the assistance of heat to approach to these problems. Experimental investigations with laser heat have shown that the variation in the material behaviour could be reduced, leading to more process stability and reliability. Laser energy increases the temperature of the material during forming and the formability in the required area of the work piece and reduces the flow stress as well as the anisotropy of the material [62].

With the objectives defined above, laser-assisted flaring tests were performed in order to obtain information about:

- improved formability
- reduced forming loads
- reduced scatter

The experimental setup was consistent with the flaring test performed at room temperature. The heat energy was introduced using the laser source described in *Chap. 4.5.1*. For measurement of the forming temperature ϑ_f a pyrometer was used, defined in section *4.5.2*.

4.5.1 Description of the laser source

A laser source with the following specifications had been used for the experiments:

Name:	„Hochleistungs-Diodenlaser System 25W“
Manufacturer:	Albers Laser, Konstanz, Germany
Type:	101
Semiconductor:	GaAs (Gallium Arsenide)
Maximum power:	25 W
Wave length:	810 nm (Infrared)
Operation mode:	CW and pulse …10 kHz
Numeric aperture :	0.2
Fiber coupling:	200 µm
Focussing lens:	50 mm
Image scale:	1:1

To transmit the laser beam to the tooling, a fibre optical cable was used. For holding the focusing lens a cylindrical device was mounted at the end of the fibre cable. The image scale of the focusing unit was 1:1, which means the distance “beam exit (fibre) – focussing lens” corresponded to the distance “focussing lens – focal point”. The cylindrical focussing unit was then attached to a clamping device which was mounted on the test table. To set or to change the focal diameter by varying the focal length, the entire focussing optics could be moved along its longitudinal axis by simply loosening the screw of a clamp. The adjustment of the spot was realized with the aid of an integrated pilot laser beam. This visible pilot laser point was adjusted so that it corresponded to the given tube diameter. The experimental setup is shown in *Fig. 19*.

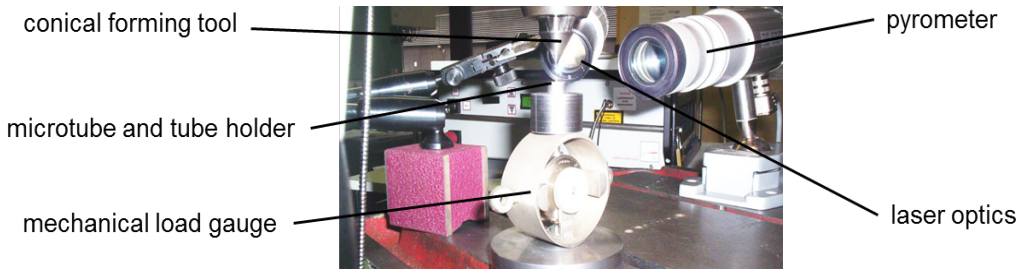

Fig. 19: Experimental setup (early laser-assisted trials)

4.5.2 Description of the pyrometer used for temperature measurement

For the temperature measurement of the laser-assisted tests a stationary digital pyrometer type Cella Temp PZ 27 had been used. By using a special filter, the high energy of the laser could be isolated against the much lower infrared radiation of the object, so the measurement was not tainted. According to the manufacturer's specifications the pyrometer was designed for measurements on metals starting from low temperatures of about 100°C. In preliminary test however, only a measurement range starting at 160°C until 1200°C could be measured accurately. Within the tests, sheet metal surfaces were heated by varying the laser radiation and the temperatures were recorded. Results had been verified by using two other laboratory-infrared thermometers. Specifications of the pyrometer used can be seen in the following table.

Specification sheet of the pyrometer type Cella Temp PZ 27 (Fa. Cellar)

Sensor:	photodiode
Spectral range:	1.8 ... 2.2 µm
Focus:	0.2 … 0.4 m
Uncertainty of measurement:	0.75% of measured value or 5 K (whichever is the greater value at an emission degree ε = 1.0 and ϑ_a = 23°C)
Repeatability:	1K

4.5.3 Laser-assisted procedure

To meet the specified performance criterion of a forming temperature ϑ_f = 300°C, which was defined in the test program, the laser settings were determined in preliminary tests. First problem was that a heated micro-tube having a wall-thickness in the range of a few micrometers cools down abruptly due to heat conductance when it comes into contact with the cool surface area of the forming cone. Therefore, before starting the expansion process the cone was moved down, to get in contact with the tube end and was charged with a preliminary axial load F_a = 0.2 N. The focal point of the laser beam was then focused predominantly onto the area of the conical forming tool, just touching the tube end a little. At a laser power of approximately $P_{out,\,l}$ = 15 W the flaring test was started after the temperature ϑ_f had stabilized to slightly above 300°C. By carefully selecting the focus diameter by defocusing it was possible to keep the forming temperature to an acceptable constant level. The uniform heating of the forming cone was verified by directing the pyrometer on the sides and back of the cone during laser impact.

4.6 Test program

Table 4 gives an overview of each test series which were conducted to determine the forming potential and the work piece characteristics of the examined tubes. A minimum of ten specimen tubes per test series were tested.

At first, in test series 2 stainless steel tubes AISI 304 with different outer diameters D_0 as well as different wall thickness / diameter ratios t_0/D_0 were investigated. All ratios corresponded to *Fig. 12* (mentioned in the previous chapter), and covered the range of t_0/D_0 = 0.05 … 0.16. Their tensile strengths were each in the range σ_{UTS} = 1100 ... 1200 N/mm^2 according to the information in the manufacturer's inspection certificate (0.7x0.05), and the information stated by the supplier (1.0x0.06). As the early access to these tubes was limited the tensile strength of these micro-tubes could not be verified in the materials testing laboratory.

As the supply of the 0.8x0.1 tubes was sufficient enough for a larger number of tests, tensile tests and additional to the flaring tests conducted at room temperature, warm-forming flaring tests could be conducted as well. According to the test program (series 2a), the forming behaviour under the influence of laser heat at 300°C was investigated. Mechanical properties of the examined tube materials can be found in *Table 3*, *Chap. 3.3 Material analyses.*

Since only a mechanical force gauge to determine the axial load of the forming cone was used in test series 2/2a and the procedure parameters axial load F_a and stroke s were manually recorded, only three curves were created. Although, the results of all ten investigated tube samples were taken into account of the evaluation of the statistics. Only the initial exploratory tests were conducted using manual recordings and the mechanical gauge, all subsequent later tests were performed using the automated universal testing machine.

Based on the initial experiments carried out within the test series 2/2a a tube with an outer diameter D_0 of 800 µm was favoured. The tubes were not too small so that they could be handled (cut, ground, be seen etc.) in an effective way. Secondly, they meet the requirements of real micro-parts, which two of its three room dimensions, according to the common definition in the area of micro-manufacturing, should be within the range of 1000 µm. Since the 1.0x0.06 tube showed a distinctive enhanced formability compared to the 0.8x0.1 tube, because of the smaller wall thickness/diameter ratio t_0/D_0, the tubes to be ordered should match an aspect ratio similar to the one of the 1.0x0.06 tube which was $t_0/D_0 = 0.06$ which should have the additional advantage of reduced forming loads due to a smaller wall thickness.

As a result, a stainless steel micro-tube having an outer diameter $D_0 = 800$ µm and a wall thickness $t_0 = 40$ µm made of AISI 304 had been ordered. Additionally two varieties of micro copper tubes had been purchased which together with the stainless steel tubes would be the subjects of test series 3.1 and 3.2.

Within test series 3.1 stainless steel tubes made from AISI 304, and with the same size but different mechanical properties were investigated. They came from two dif-

ferent delivery batches. In each case, the forming temperature was varied and the expansion diameter as well as the forming load was determined.

Test Program **Flaring Test**								
Test parameters					**Procedure parameters**			
Material	Tensile Strength [N/mm²]	Tube dimensions [mm]		Wall thickness / Diameter ratio	Temperature [°C] T_{form}		Flaring Diameter [mm]	Axial load [N]
	σ_{UTS}	D_0	t_0	t_0/D_0	RT	300	d_f	F_a
Test series 2: Variation of tube dimensions => Determination of Flaring Diameter d_1 and Axial Load F_a								
AISI 304	1171	0.7	0.05	0.071	O		d_f= ?	F_a = ?
	1157	0.8	0.1	0.125	O			
	n.k.	1	0.06	0.06	O			
Test series 2a: Variation of the forming temperature ϑ_f => D Determination of Flaring Diameter d_1 and Axial Load F_a								
AISI 304	1157	0.8	0.1	0.125	O	O	d_f = ?	F_a = ?
Test series 3.1: Variation of the forming temperature ϑ_f – AISI 304 => Determination of Flaring Diameter d_1 and Axial Load F_a								
AISI 304-a	690	0.8	0.04	0.05	O	O	d_f = ?	F_a = ?
AISI 304-b	593				O	O		
Test series 3.2: : Variation of the forming temperature ϑ_f – Copper CW024A => Determination of Flaring Diameter d_1 and Axial Load F_a								
CW024A (R200)	236	0.8	0.1	0.05	O	O	d_f = ?	F_a = ?
CW024A (R250)	296				O	O		

Table 4: Test program of the flaring test

Analogous to the investigations of the stainless steel tubes in test series 3.1, the ordered micro-tubes made of copper were subjects of the flaring test in test series 3.2. Again the material, CW024A, and the dimensions were the same; however the strengths of the tubes varied. Forming tests at room temperature and at 300° C were carried out.

4.7 Test results and process parameters

The process parameters and test results of each micro-tube investigated are shown in *Fig. 21* - *Fig. 27*. At each figure the respective test series, the studied tube material, the tube dimensions and the tool parameters are represented at the top left. For a better understanding the schematic illustration of the kinematics already pictured in *Fig. 17* is located in the upper right angle. The middle screen shows the records of the process parameters obtained from each conical expansion test series. The forming results including microscope pictures of individual tube specimens can be taken from the lower third of each figure.

4.7.1 Visualization and description of the results - test series 2 / 2a

Expansion diameters

Stainless steel tubes with the dimension 1.0x0.06 showed the largest mean expansion. The relative expansion of its middle flare diameter of 1.43 mm was 63%, which is equivalent to an absolute expansion of 550 µm. The mean expansion of the tubes with the dimensions 0.8x0.1 and 0.7x0.05 amounted to 300 µm (50%), and 250 µm (42%) respectively. Scatter around the achieved mean flare diameter $d_{f,\,mean}$ was 10% (1.0x0.06), 11% (0.8x0.1) und 14% (0.7x0.05).

The effect of laser heat

In line with test series 2a, scatter could significantly be reduced during the warm forming process, *Fig. 20*. The use of laser heat and the simultaneous forming at

300°C caused a decrease down to 3% (11% at room temperature) around the achievable mean value of the expansion diameter. Also, the mean expansion diameter $d_{f,mean}$ could be increased from 50% at room temperature to 55% at a temperature ϑ_f of 300°C, although the maximum expansion diameter of 960 µm achieved at room temperature could not be reached during warm forming. The largest measured expansion was 940 µm.

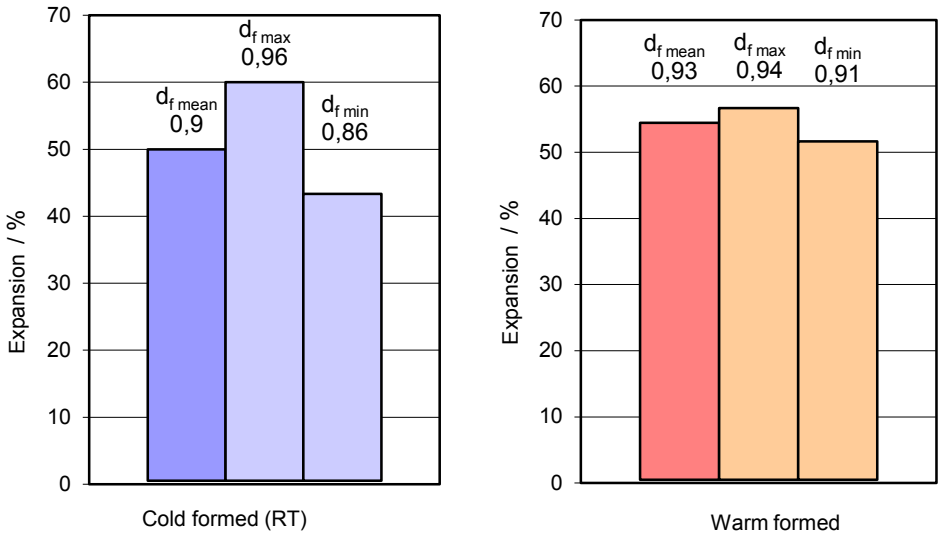

Fig. 20: Increase of the mean measured expansion diameter and reduction of scatter of the 0.8x0.1 AISI 304 micro-tube under the influence of thermal laser energy, test series 2 (cold formed, left) and test series 2a (warm formed, right)

With regard to the forming loads, cf. *Table 5*, an expected significant reduction of the maximum axial loads F_a during laser-assisted flaring compared to the values achieved at room temperature was not observed. The forming loads measured of $F_{a(RT)}$ = 160 N for laser assisted and $F_{a(300°C)}$ = 167 N for room temperature were comparatively equal.

Scatter around mean axial load

However, scatter around $F_{a,\ arithm}$ could significantly be reduced from 19% at room temperature - which was even a rather low value compared to the scatter around $F_{a,\ arithm}$ of both the 0.7x0.05 (40%) and 1.0x0.06 (41%) micro-tube - to 6% during warm forming.

Material AISI 304	0.7 x 0.05 [mm]	0.8 x 0.1 [mm]	1.0 x 0.06 [mm]	0.8 x 0.1 [mm]
Test series	2	2	2	2a
Forming temperature ϑ_f	RT	RT	RT	300°C
Arithmetic mean axial load $\overline{F_{ax\ arithm}} = \frac{1}{n}\sum_{i=1}^{n} F_{ax_i}$ [mm]	95	160	216	167
Maximum axial load $F_{a,max}$ [N]	117	175	266	172
Minimum axial load $F_{a,min}$ [N]	78	143	177	162
Scatter around $\overline{F}_{a_{arithm}}$ absolute [mm] / relative [%]	38 / 40	31 / 19	89 / 41	10 / 6

Table 5: Forming loads of flaring test series 2 and 2a

Test parameters:

Stainless steel AISI 304
Tube 0.7x0.05

Tube dimensions:	L_0 = 6.2 mm
	d_0 = 0.6 mm
	t_0 = 50 µm
Tool dimensions:	α = 30°
	h_h = 5.5 mm

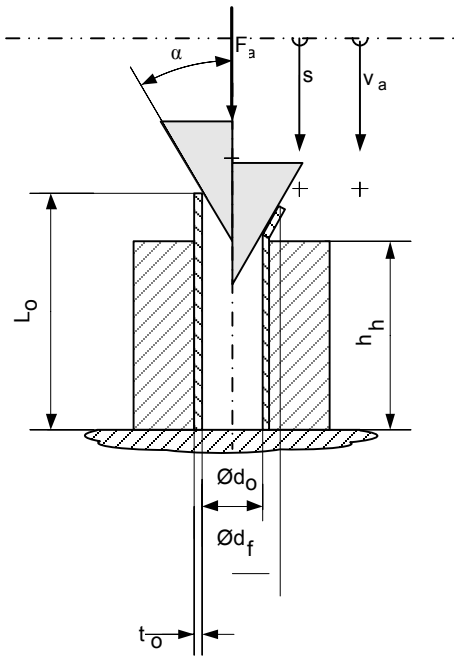

Procedure parameters:

Spindle displacement rate: v_a = 1.2 mm/min.

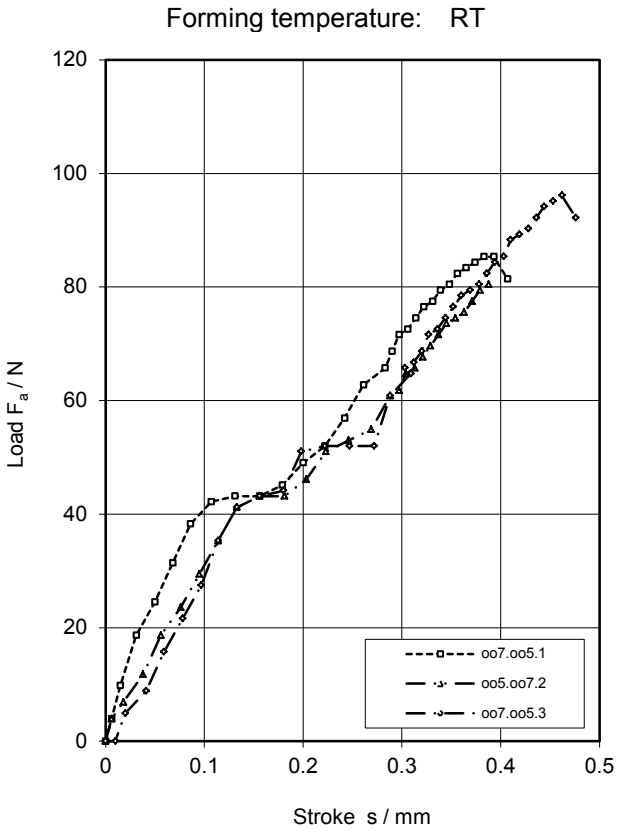

Forming results:

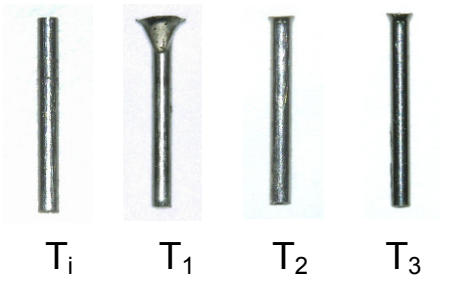

T_i: Initial tube
T_1: Specimen No.1 (007.005.1)
T_2: Specimen No.2 (007.005.2)
T_3: Specimen No.3 (007.005.3)

Fig. 21: Micro-tube AISI 304 0.7x0.05 - Forming results and procedure parameters with point of fracture at constant spindle displacement rate v_a, test series 2

Test parameters:

Stainless steel AISI 304
Tube 1.0x0.06

Tube dimensions: L_0 = 7 mm
d_0 = 0.88 mm
t_0 = 60 µm
Tool dimensions: α = 30°
h_h = 5.5 mm

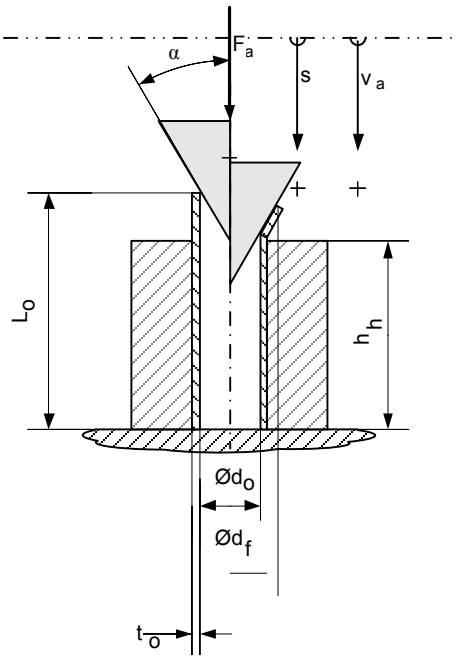

Procedure parameters:

Spindle displacement rate: v_a = 1.2 mm/min.

Forming temperature: RT

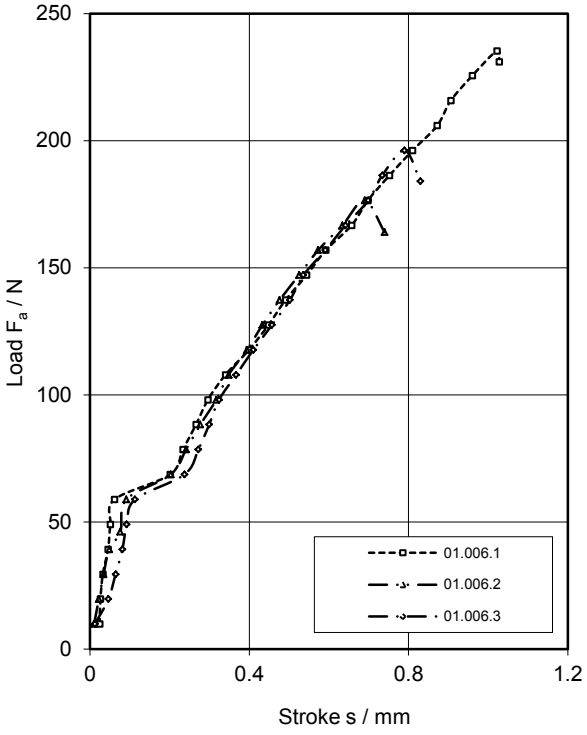

Forming results:

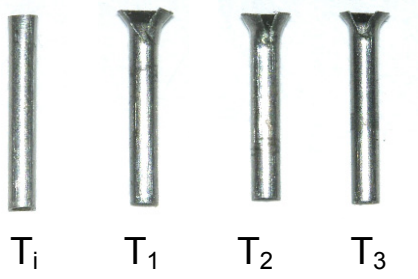

T_i: Initial tube
T_1: Specimen No.1 (01.006.1)
T_2: Specimen No.2 (01.006.2)
T_3: Specimen No.3 (01.006.3)

Fig. 22: Micro-tube AISI 304 1.0x0.06 - Forming results and procedure parameters with point of fracture at constant spindle displacement rate v_a, test series 2

Test parameters:

Stainless steel AISI 304;
Tube 0.8x0.1

Tube dimensions: L_0 = 6.2 mm
d_0 = 0.6 mm
t_0 = 50 µm
Tool dimensions: α = 30°
h_h = 5.5 mm

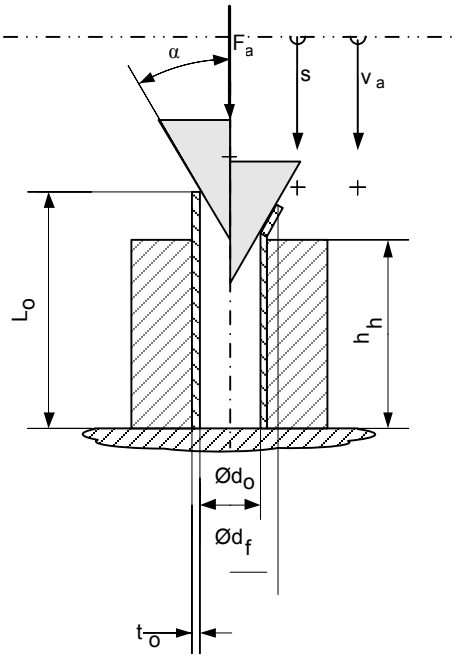

Procedure parameters:

Spindle displacement rate: v_a = 1.2 mm/min.

Forming temperature: RT

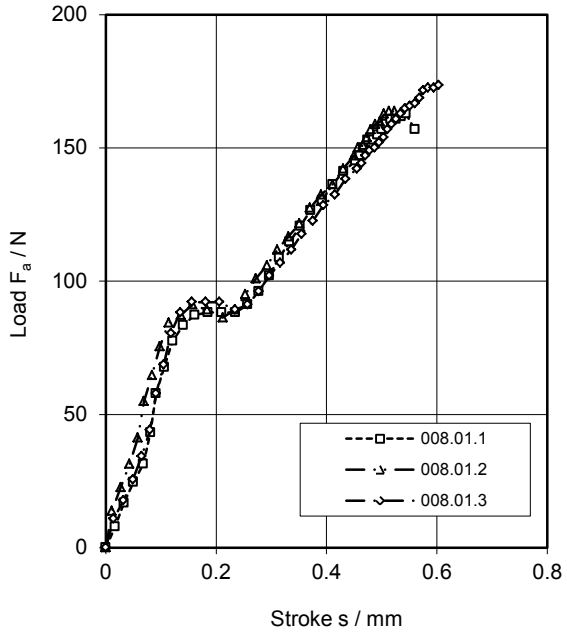

Forming results:

T_i T_1 T_2 T_3

T_i: Initial tube
T_1: Specimen No.1 (008.01.1)
T_2: Specimen No.2 (008.01.2)
T_3: Specimen No.3 (008.01.3)
(Formed at room temperature)

Fig. 23: Micro-tube AISI 304 0.8x0.1 - Forming results and procedure parameters with point of fracture at constant spindle displacement rate v_a, test series 2

4.7.2 Visualization and description of results - test series 3.1 and 3.2

In test series 3.1 the experiments were performed on tubes of the same material and same dimensions. Micro-tubes made from AISI 304 stainless steel were investigated, with an outer diameter D_0 of 800 µm and a wall thickness t_0 of 40 µm. The entire test parameters can be seen in *Fig. 24* and *Fig. 25* (upper section).

4.7.2.1 Stainless steel tubes AISI 304 – delivery batch A

The load/stroke curve of the 08x004 micro-tube from delivery batch A determined at room temperature, *Fig. 24* (centre), shows a conspicuous progression compared to the courses determined within test series 1, and 1b respectively. Due to the global loss of stability, bulging (deformation) occurred in the area of the excess length of the tube. Since this phenomenon could already be observed in tests in line with series 2/2a, if the excess lengths were not chosen appropriately, the test tube length L_0 was shortened as a result. However, at an average axial load F_a = 56.5 N with a standard deviation s = 1.2 N (scatter 3.2 N) a load maximum was reached, but bulging throughout still occurred. The penetration of the tube end proceeded until the cone had forced the expanded and bulged tube towards the upper surface of the tube holder respectively. In none of the penetrated tube samples cracks appeared, consequently maximum possible expansion diameters d_f could not be achieved. Additional information about failure modes and the explanation of stability and/or instability cases can be found later in *Chap. 4.8.1, Explanation of the forming behaviour.*

Expansion diameters – delivery batch A

The mean measured value of the achieved forming diameter d_f was determined to 1.005 mm with a standard deviation s = 0.0093 mm, which relates to a relative expansion of 40%. The second series AISI 304 08x004 tubes according to the test program, *Table 4*, was carried out at a forming temperature ϑ_f = 300°C. Again laser heat was used to obtain the temperature. Astonishingly, the mean value of the maximum achievable flaring diameters could not be increased, in contrast to the above investigated AISI 304 0.8x0.1 tubes in line with test series 2/2a. However, it must be noted that again loss of global stability (bulging or buckling) inside the tube walls occurred

and throughout all tests had to be stopped before cracks occurred so maximum expansion diameters could not be obtained. The relative expansion ratio ε_f was 0.36 which led to a mean value of the forming diameter d_f = 0.980 µm with a standard deviation s = 0.0085 mm.

The average value of the maximum achieved axial load F_a amounted to 43.6 N until bulging occurred with a standard deviation s = 0.3 N. In other words, any bulging took place within a range of only 1.1 N around the arithmetic mean of F_a. As can be seen in the expansion diameter / axial load diagram in *Fig. 24*, with one exception a slight reduction of scatter of measured maximum expansion diameters during warm forming could also be attained.

4.7.2.2 Stainless steel tubes AISI 304 – delivery batch B

Compared to delivery batch A, a much lower axial load F_a was required to induce the workpiece failure of the AISI 304 micro-tubes of delivery batch B, cf. diagram *Fig. 25* (centre). Failure appeared only twice at both room temperature and a forming temperature ϑ_f of 300°C in terms of loss of global stability. The cases of failure are exemplarily figured as pictures of formed micro-tubes, *Fig. 25* (below left). At room temperature a mean value of F_a was determined to 45.7 N with a comparatively high standard deviation s of 5.2 N and a scatter of 37% which, nevertheless, corresponds approximately to the values of both the 0.7x0.05 and the 1.0x0.06 AISI 304 stainless steel tubes identified in test series 2/2a. Note, that all three types of AISI 304 tubes offer a similar wall thickness/diameter ratio t_0/d_0 in the range of 0.05 to 0.07.

Due to laser-assistance, scatter of the forming load F_a could again be decreased, *Fig. 25* expansion diagram below right. The arithmetic mean F_a was 29 N with a standard deviation of 2.9 N. Furthermore, the effective forming loads during warm forming at 300°C could be reduced to an amount of approximately 2/3 compared to the mean value obtained at room temperature.

Expansion diameters – delivery batch B

The mean flare diameter d_f achieved at room temperature was 1.030 mm (standard deviation s = 0.020 mm) which relates to an expansion of 43%. Corresponding to the investigated tubes of delivery batch A, again the expansion could not be increased during warm forming at 300°C. Attained diameters measured on average 0.990 mm (standard deviation s = 0.024 mm) which is an increase of 37.5%, similar to the determined value of AISI 304 batch A tubes.

Though it must be noted, that comparatively high maximum expansion diameters and low minimum expansion diameters were measured at both cold formed and warm formed AISI 304 batch B micro-tubes, which can clearly been seen in the diagram below right in *Fig. 25*. As a result, scatter around arithmetic mean expansion diameter of batch B tubes was twice as large as of delivery batch A, at room temperature as well as at 300°C.

4.7.2.3 Copper CW024A R250

With one exception, all tube samples of R250 could be expanded until at least one crack occurred. On average, this case of failure started at an axial load F_a of 60.8 N with a standard deviation s = 8.9 N.

The arithmetical mean measured value of the forming diameter was d_1 = 1.18 mm with a standard deviation s of 0.084 mm which is a relative expansion of 97% (!), or an absolute increase of Δd = 580 µm related to the initial inner tube diameter respectively. The maximum reached flare diameter d_1 was 1.30 mm. The flare diameter of the micro-tube, whose penetration had been stopped due to the instability case, measured only a d_f = 1.07 mm.

Warm forming

As it could already be observed within test series 3.1, the expansion tests of stainless steel AISI 304 micro-tubes, Laser-assisted heating of the tube's end to 300°C did not increase the obtained flare diameter. On average this was 1.14 mm (standard deviation s = 93 µm), which implies a reduction of approx. 3.5% compared to the mean measured value at room temperature. The initial diameter d_0 tube end could be

Test parameters:

Tube: Stainless steel AISI 304; 08x004 (batch A)

Tube dimensions: L_0 = 5.6 mm
d_0 = 0.72 mm
t_0 = 40 µm

Tool dimensions: α = 30°
h_h = 5.5 mm

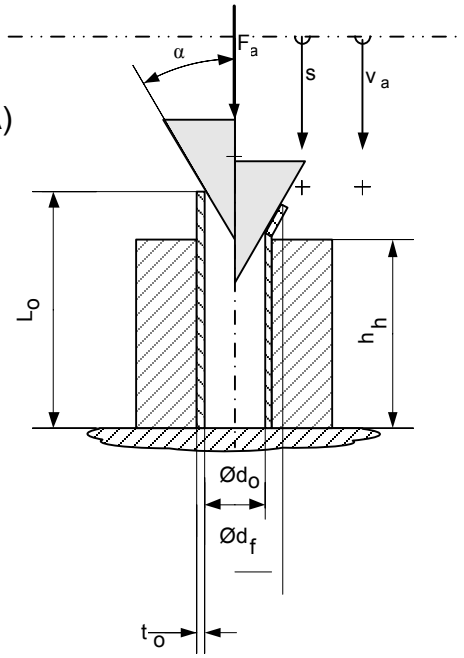

Procedure parameters:

Spindle displacement rate: v_a = 1.2 mm/min.

Forming temperature: RT

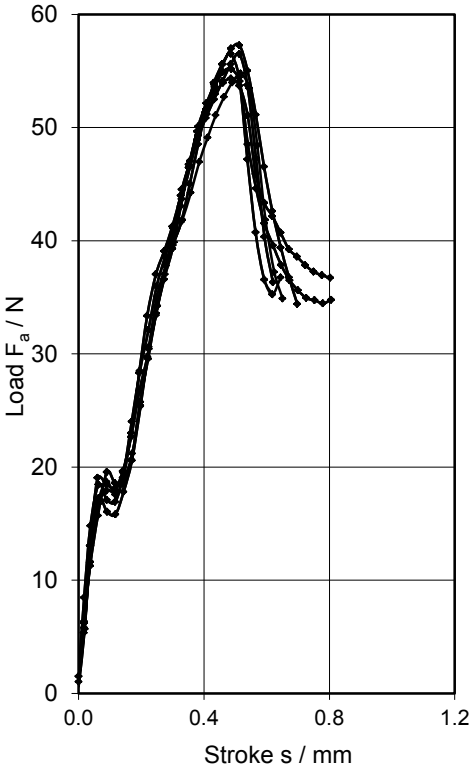

Forming temperature: 300°C

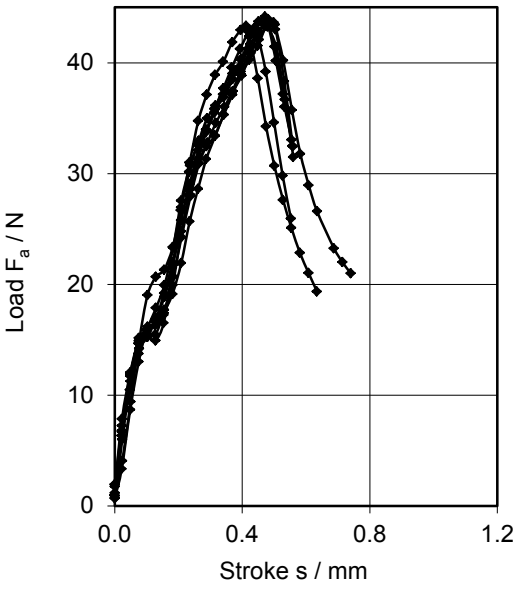

Forming results:

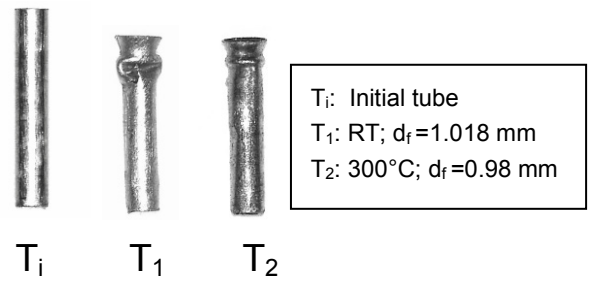

T$_i$: Initial tube
T$_1$: RT; d_f =1.018 mm
T$_2$: 300°C; d_f =0.98 mm

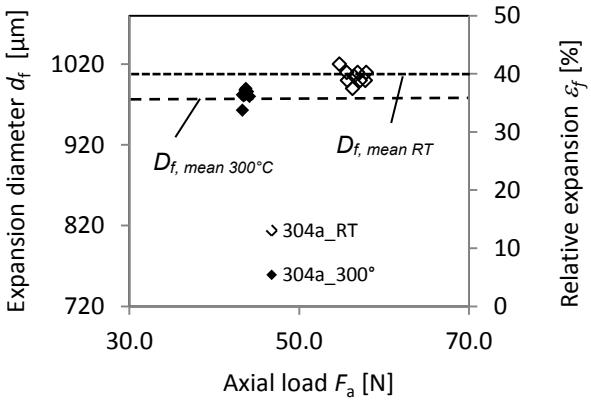

Fig. 24: Micro-tube AISI 304 0.8x0.04 (batch A) - Forming results and procedure parameters with point of fracture at constant spindle displacement rate v_a, test series 3.1

Test parameters:

Tube: Stainless steel AISI 304; 08x004 (batch B)

Tube dimensions: L_0 = 5.6 mm
d_0 = 0.72 mm
t_0 = 40 µm

Tool dimensions: α = 30°
h_h = 5.5 mm

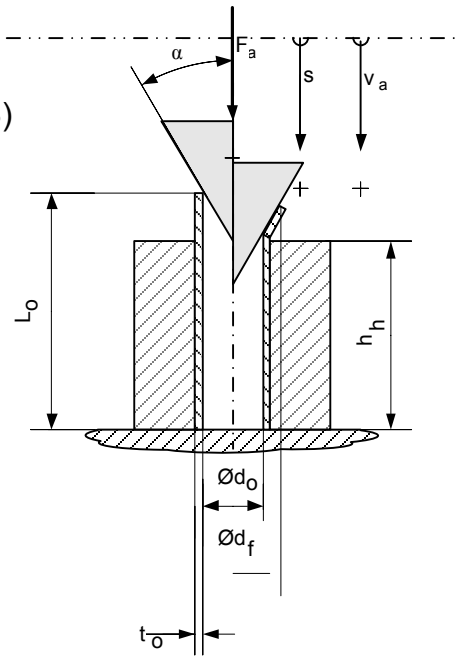

Procedure parameters:

Spindle displacement rate: v_a = 1.2 mm/min.

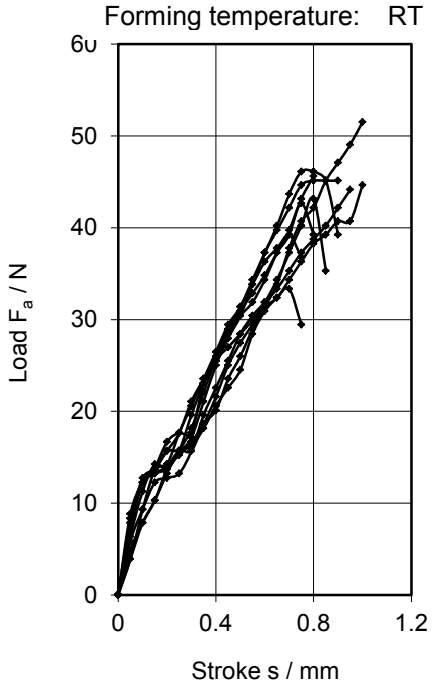

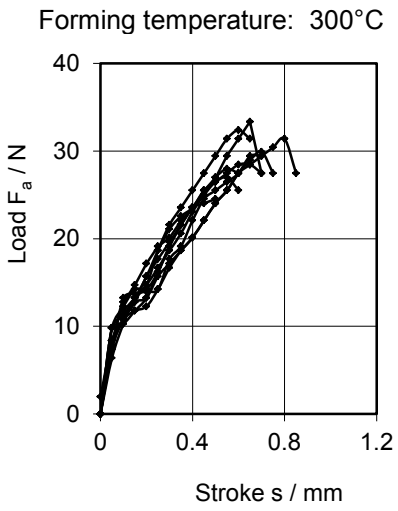

Forming results:

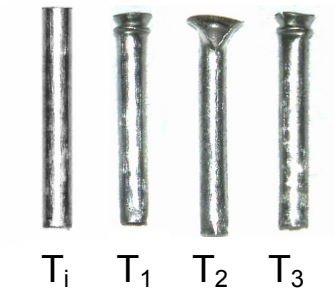

T$_i$: Initial tube
T$_1$: RT; d_f =1.04 mm
T$_2$: 300°C; d_f =0.99 mm
T$_3$: 300°C; d_f =0.99 mm

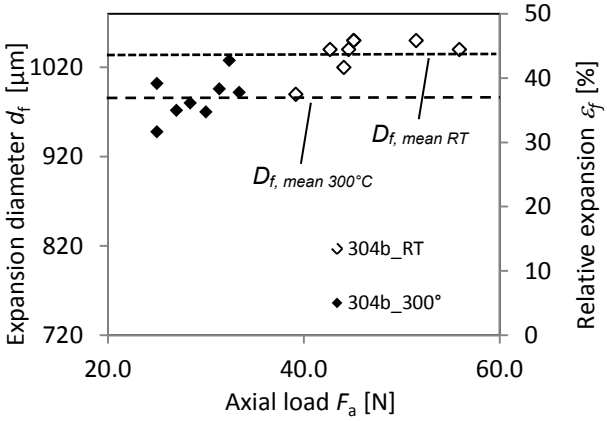

Fig. 25: Micro-tube AISI 304 0.8x0.04 (batch B) - Forming results and procedure parameters with point of fracture at constant spindle displacement rate v_a, test series 3.1

Test parameters:

Tube: Copper CW024A R250; 0.8x0.1

Tube dimensions: L_0 = 7.0 mm
d_0 = 0.6 mm
t_0 = 100 µm

Tool dimensions: α = 30°
h_h = 5.5 mm

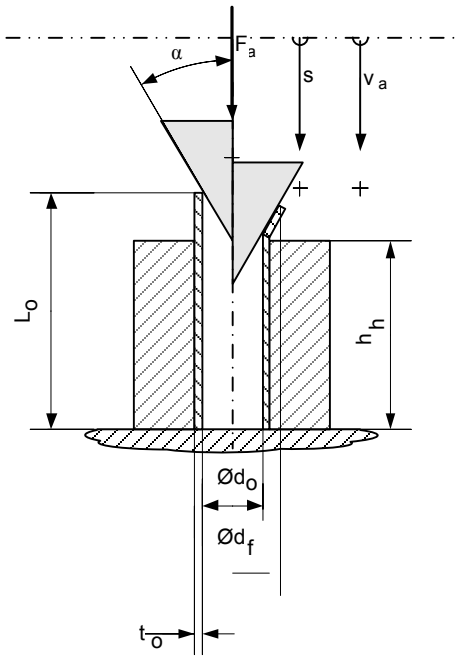

Procedure parameters:

Spindle displacement rate: v_a = 1.2 mm/min.

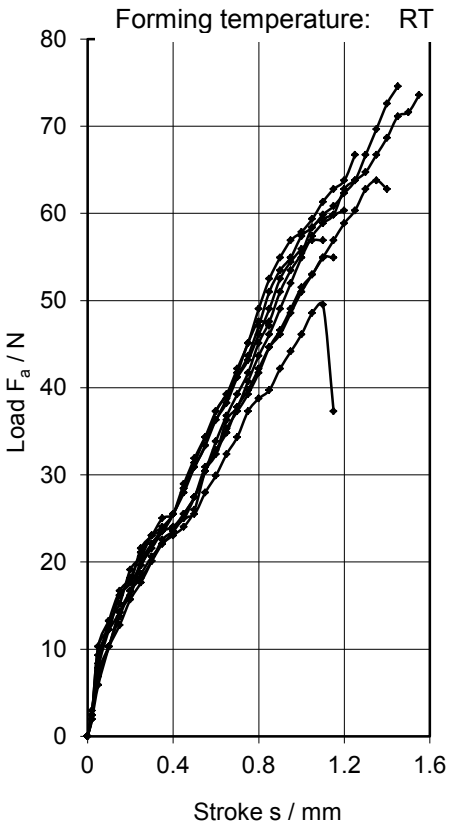

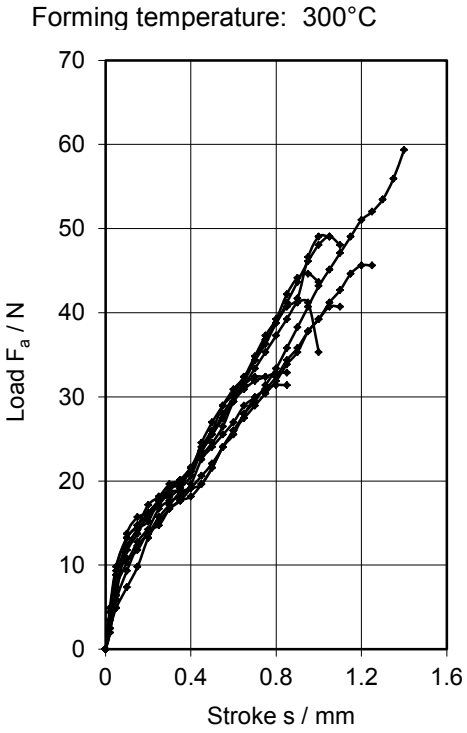

Forming results:

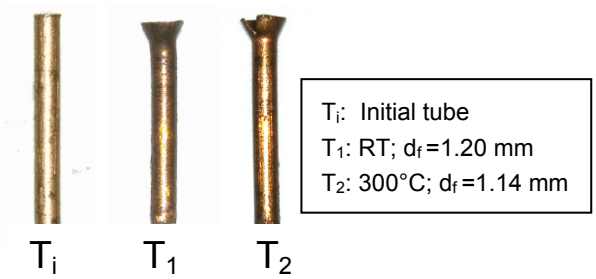

T$_i$: Initial tube
T$_1$: RT; d_f =1.20 mm
T$_2$: 300°C; d_f =1.14 mm

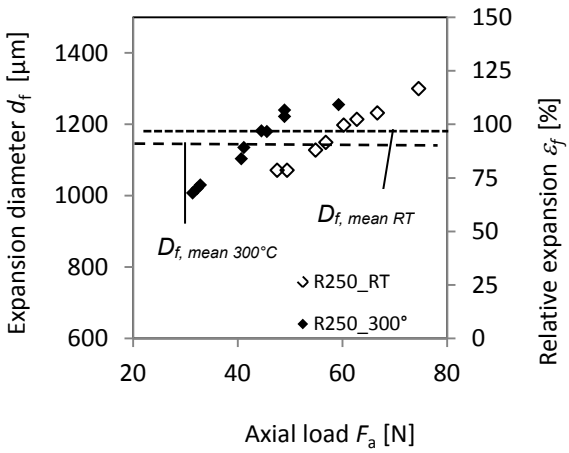

Fig. 26: Micro-tube Copper CW024A R250 - Forming results and procedure parameters with point of fracture at constant spindle displacement rate v_a, test series 3.2

Test parameters:

Tube: Copper CW024A R200; 0.8x0.1

Tube dimensions: L_0 = 7.0 mm

d_0 = 0.6 mm

t_0 = 100 µm

Tool dimensions: α = 30°

h_h = 5.5 mm

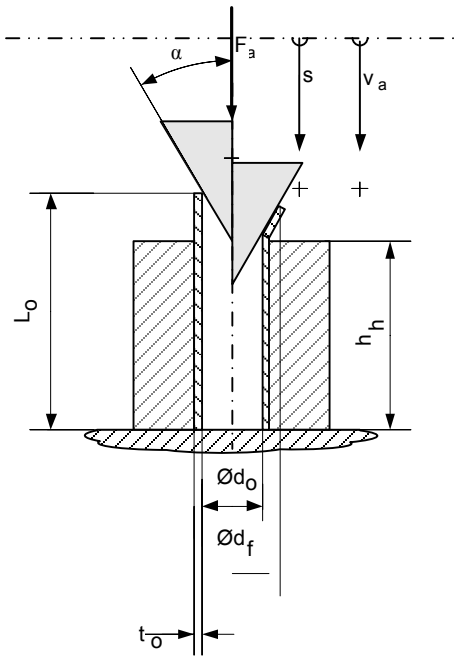

Procedure parameters:

Spindle displacement rate: v_a = 1.2 mm/min.

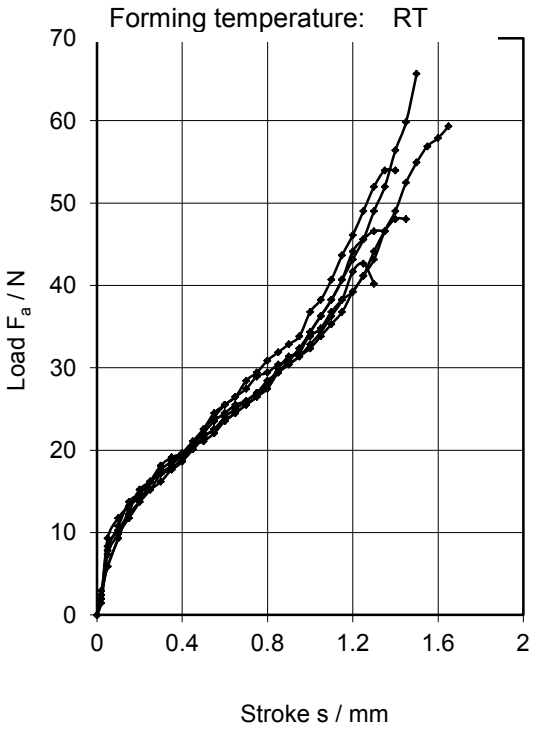

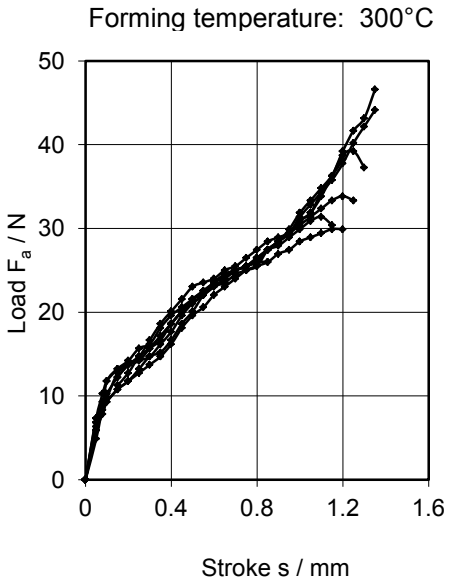

Forming results:

T$_i$: Initial tube
T$_1$: RT; d$_f$ =1.17 mm
T$_2$: 300°C; d$_f$ =1.11 mm

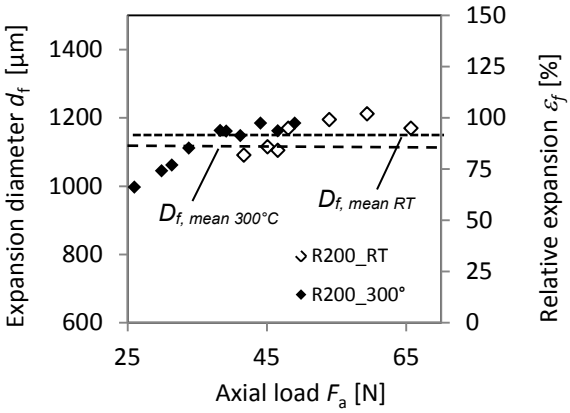

Fig. 27: Micro-tube Copper CW024A R200 - Forming results and procedure parameters with point of fracture at constant spindle displacement rate v_a, test series 3.2

expanded by 540 µm, complying with a relative expansion of still 90%. As represented in *Fig. 26* in the expansion diagram below right, scatter could not be reduced compared to the R250 micro-tubes formed at room temperature.

Additionally, a decrease of the range of variation of the achieved maximum axial load F_a during warm forming could not be observed.

4.7.2.4 Copper CW024A R200

Expansions

The mean value of the flare diameter achieved at room temperature was determined to d_1 = 1.15 mm with a standard deviation s = 47 µm. This corresponded to an expansion of 550 µm, or a relative expansion ratio ε_f = 0.92 respectively.

In warm forming, the tube end was widened by an average of 520 µm corresponding to ε_f = 0.87, which resulted in a mean flare diameter d_1 of 1.12 mm. Just as the scatter around the mean forming diameter of R250 micro-tubes, the range of dispersion also could not be reduced, this can be seen in the expansion diagram below right in *Fig. 27*.

Forming loads

The mean axial load F_a of investigated R200 micro-tubes was determined to 51.5 N with a standard deviation s of 8.6 N. Through warm forming at 300°C this value reduced to F_a = 36 N with a standard deviation s = 7.6 N. However, the range of dispersion could not be decreased during laser-heating compared to the forming tests obtained at room temperature.

4.8 Discussion

4.8.1 Explanation of the forming behaviour

All investigated micro-tubes show similar characteristics for their load-stroke curves. However apart from these similarities, the results of the investigation can be divided into two cases, stability and instability, and described according to [84].

If the test could be performed just before a crack occurred, it could be described as the stability case. In this case three phases were defined; (1) the elastic deformation, (2) bending deformation and (3) steady-state deformation. The instability case is characterized by two forming phases; (4) fracture and (5) local buckling.

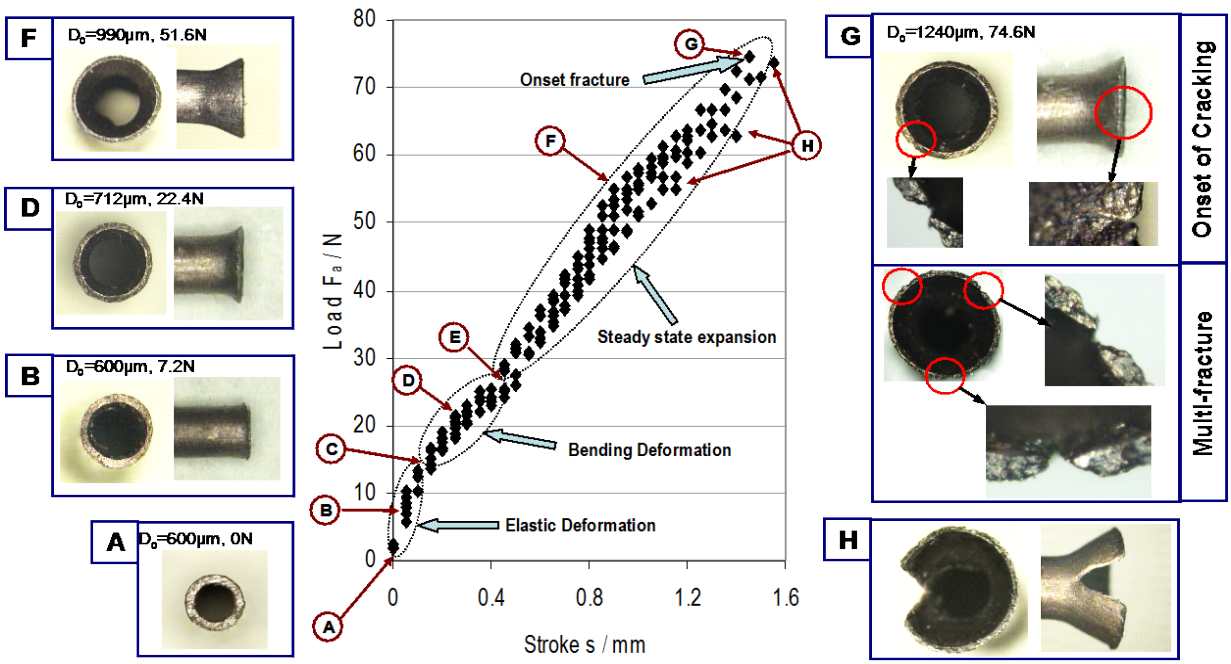

Fig. 28: Load / Stroke curve of a flaring test exemplarily presented by a micro-tube made from copper CW024A (initial outer diameter D_0 = 800 µm and wall thickness t_0 = 100 µm) according to [84]

As it can be seen on the load-stroke curve as an example of CW024A R250 in *Fig. 28*, at the first stage, points A to C, the load F_a grows steeply as the conical punch was axially pushed into the tube. Some flaring tests were stopped in different deformation modes in order to measure the expanded diameter during the procedure. Hence, it could be found out that the deformation mode of this first stage was elastic. Thereafter, the axial load F_a gently inclines from points C to E. In this second stage the leading edge of the micro-tube began to slide along the conical surface of the tool. The tube walls were now bent outwards, still without its inner surface completely contacting the conical punch. The third stage is the region from points E to G. The curve progression is again almost linear. The inner micro-tube surface was now in plane contact with the cone and with further increasing the load F_a it slid along the conical tool surface.

Steady-state expansion deformation occurred until signs of necking (thinning of the wall) along the circumferential edge of the tube, followed then by at least one crack at the edge of the micro-tube, point G, caused by the loss of local material stability. The first of the instability cases occurred if the tool further penetrated into the tube. The amount of load F_a suddenly dropped and the fracture got larger along the meridian direction of the expanded flange, point H. The axial tool movement was stopped and the expansion diameter as well as the wall thickness was then measured under the microscope. Multi-fractures could be observed at the tubes' edge, especially during the tests with copper tubes at RT. A high number of 50% of the R200 samples formed at room temperature showed more than one crack at their cutting edges, *Fig. 29*.

Second of the two instability phenomena observed which limited the expansion of the tube during the experiment was the loss of global or local stability. If for example the excess length of the micro-tube was not selected appropriately, bulging caused by the loss of global stability stopped the steady-state expansion. These cases were mainly observed with the AISI 304 08x004 micro-tube, delivery batch A. It was not possible to cut the tubes in appropriate lengths, so that no global buckling occurred. Without exception, every sample was bulged under the axial load F_a before a load maximum could cause the beginning of cracks; refer to *Fig. 24* below left.

In other cases, lateral buckling caused by the minimal tilting tolerance of the micro-tube inside the specimen holder, especially in combination with high axial loads determined the end of the flaring. In many cases, this phenomenon happened to the AISI 304 1.0x0.06 micro-tubes in line with test series 2, where maximum axial loads of more than 200 N could be attained.

4.8.2 Formability of examined copper tubes at RT

It can be seen from and *Fig. 27* that the R250 can be expanded further than the R200 copper micro-tube, *Fig. 26*. This can be explained by its considerable smaller grain size, cf. *Fig. 16*, which enables the micro-tube a more uniform expansion along its radial direction. As can be seen in *Fig. 29*, right, the R250 copper tube features an almost similar wall thickness along its expanded circular cross-section. On the contrary, the cross-section of the R200 copper tube is characterized by areas with comparatively large wall thickness as well as regions with thin wall thickness.

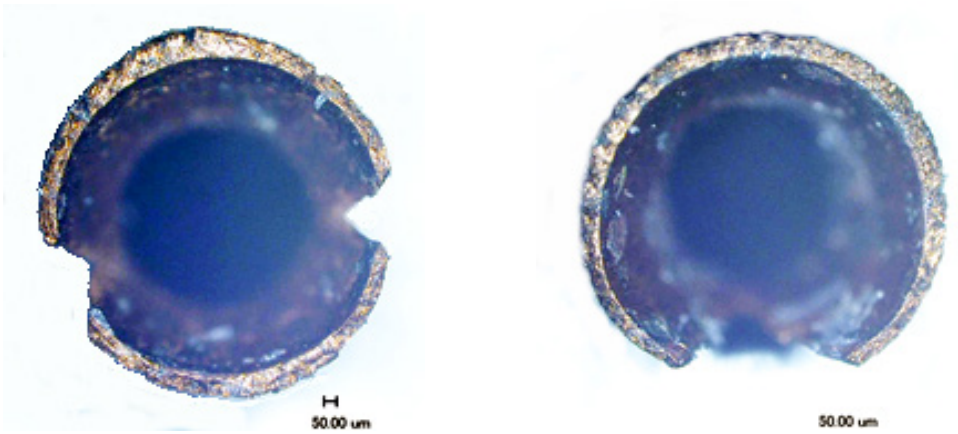

Fig. 29: Effects of grain size and grain structure on the forming behaviour of expanded copper micro-tubes, R200 w/coarse grain size (left), R250 w/fine grain size right

The bigger the grain size compared to the micro dimension of a micro-tube, especially to the wall thickness, less grains are placed in the cross-section, which is illustrated in *Fig. 30*.

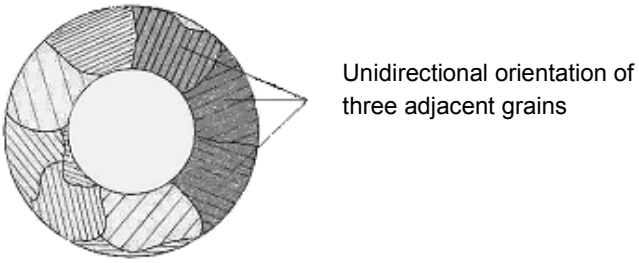

Fig. 30: Unidirectional orientation of the gliding planes (perpendicular to the hoop stress direction), schematically [85]

This results in a reduced probability with regard to a uniform distribution regarding the orientation of the grains across the circular cross-section [85]. Thus, zones exist in which forming is more and sometimes less possible, depending on the orientation of the gliding planes inside the grains.

The more grains in the circumferential cross sections the larger the probability of a uniform different orientation of the crystal slip systems (orientation of the gliding planes) which in turn effects a more uniform yielding of the material. This effect explains the more uniform wall thickness of the R250 copper tube compared to the R200. More gliding planes had been present to ensure an enlarged radial expansion (with that a larger expansion diameter) of the R250 compared to the R200. This finding corresponds to the research results recently obtained by [13] in line with similar investigations on formed stainless steel micro-tubes. In some particular areas of the tubes' cross sections with larger grain sizes localized necking was evident. However, in areas with more uniform smaller grain sizes, no obvious localized necking but a more uniform reduction of the wall thickness had been observed. In addition, in most areas close to the failure only one large grain across the thickness of the material could be detected.

Differences in formability of AISI 304 08x004 micro-tubes (batch A and B) at RT

In contrast to the copper tubes, the more solid 08x004-a compared to the 08x004-b tubes showed a lower expandability. Despite the higher elongation measured in the tensile tests, 36.7% and 31% for the AISI 304 batch A, and batch B respectively, the

08x004-a achieved a smaller flaring diameter. As already mentioned above and shown in the photograph in *Fig. 24*, below left, an early loss of global stability which led to buckling of the micro-tube, was assumed as the reason. The maximum flaring until cracks occurred was not possible with this specimen.

4.8.3 The influence of laser heat on the forming behaviour

It is remarkable that the influence of laser heat has not led to the assumed effects, to be specific to an increase in expansion diameter compared to forming at room temperature. As found out in test series 2a, the mean measured flare diameter of micro-tube AISI 0.8x0.1 could be increased and the scattering of all measured expansions could be reduced under the influence of laser energy, cf. diagram in *Fig. 23* below. However, these effects could not be repeated with both the stainless steel and copper micro-tubes investigated within test series 3.1, and 3.2 respectively.

Stainless steel tubes

The AISI 304 08x004 stainless steel micro-tubes with the influence had a lack of increased expandability and scatter; a few theories were hypothesised and investigated further. It was thought that the local impact of the laser energy could contribute to premature material failure. If this concept was correct one should have been able to observe cracks predominantly in the area receiving the lasers energy but this was not observed, batch B tubes, *Fig. 31* (right). Additionally regarding the batch A tubes which failed before cracking, verified under a microscope no signs of unequal heat distribution effects could be observed.

As a reason for the decrease in expansion diameter under the influence of laser heat, it is assumed that due to the considerably smaller wall thickness (AISI 304 0.8x0.1: 100 µm; AISI 304 08x004: 40 µm) the axial punch force caused an easier shift of material in radial direction. Conversely, the thicker the tubes' wall the more axial load can be transmitted into a material yield in longitudinal tube direction. Thus, the material was "compressed" and similar to the conventional tube hydroforming pro-

cess fed towards the main forming zone which enabled a higher expansion. It is further assumed that this effect was additionally supported by the longitudinally oriented texture of the single grains; cf. *Fig. 16* in *Chap. 3.3*, top left. The elongated grains (emerged due the manufacturing process) limit the amount of elongation possible in the longitudinal direction. Elongation measured during tensile test was only 7.8%, cf. *Table 3, Chap. 3.3.* However, as the elongated grains decrease elongation possibilities they conversely greatly increase the compressibility of the material without bulking or bulging. Thus, the tube material of AISI 304 0.8x0.1 could be easier (com)pressed together by axial load then widened under the influence of the rate of radial load of the 60° cone as the thinner tube material AISI 304 08x004 delivery batch A and B which resulted in an increase of expansion diameter of the 0.8x0.1 tubes.

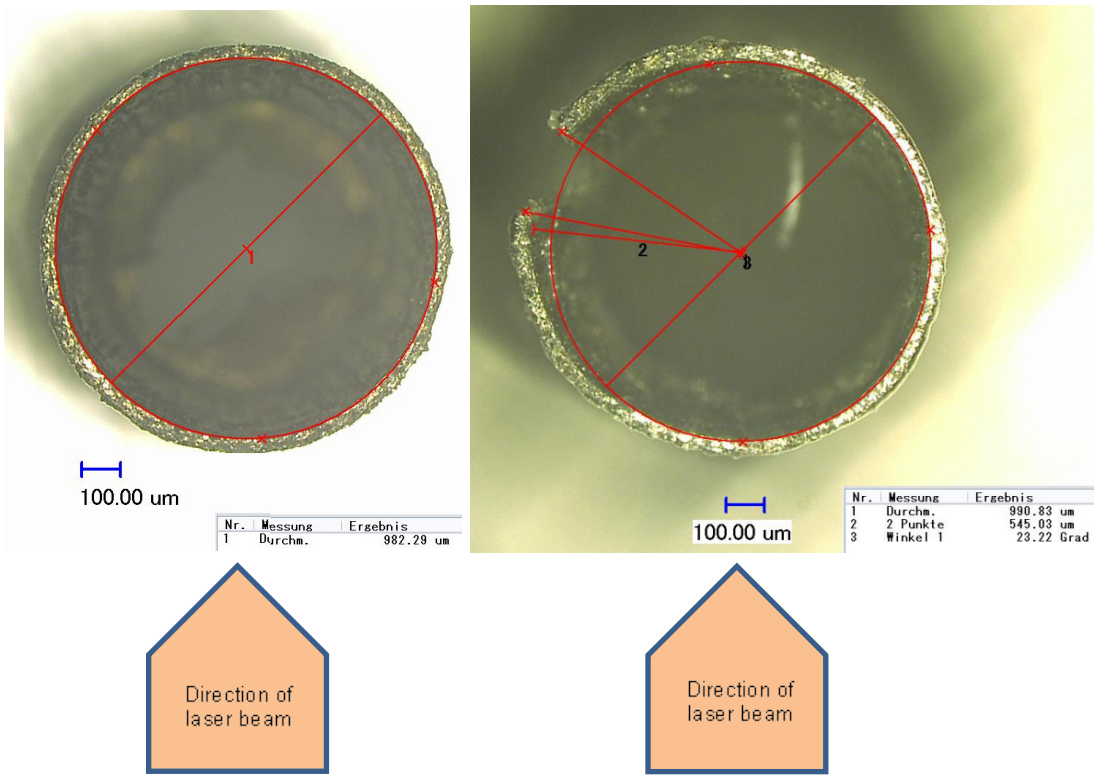

Fig. 31: Achieved expansion diameters at 300°C forming temperature, AISI 304 delivery batch A left and batch B right and incident angle of laser beam

Copper tubes

In the research with the copper tubes and laser heat; the results observed were different to the behaviour of the stainless steel tubes. There was no increase in flare diameter and no reduction of scatter. The ductility of copper reduces with the increase in temperature.

4.9 Conclusion

As mentioned, the information derived by uniaxial tests, e.g. tensile tests information from suppliers, was insufficient to define hydroforming limits on micro-tubes. Therefore, a testing method to identify the forming behaviour of the tubular micro-material based on multi-axial stretching was necessary. The first investigation about expansion ratios was completed by applying the flaring test.

It could found that mechanical material specifications like the yield and tensile strength and also criteria like grain sizes, grain structures as well as tube dimensions play an important role with regard to the maximum achievable diameters of micro-tubes. However, further research could be done (ideally by metallurgists) to investigate and in turn to be able to interpret these "micro-specific" issues in depth. With regard to an engineer who has to design a forming process, for him it is more important to get information about effective expansion limits.

For an engineer who has to design the tools with all its dimensions for his forming machine is interesting mostly after having accomplished the flaring test, how large in diameter may the die cavity be, how large is the formability of the micro-tube used for THF? One gathered information about achievable expansion diameters, one has found maximum values and one has mean values now. But if an engineer designs a tool based on either one of those values, he also needs to take a look at the scatter, especially at the minimum obtained expansions of the tube investigated to give him a good idea of yield or failure rate. In other words, if a designer builds a tool only based on the achieved mean values, and do not consider for example three or more very low outliers, he will produce a high failure rate during manufacture. That

means designers have to orientate themselves basically on the lowest expansion diameter or accept a high failure rate. It's obvious that especially the copper microtubes show a large scatter range, for example R250 with a lowest expansion diameter which was 0.11 mm and even 0.13 mm below its according arithmetic mean values at RT and 300°C respectively.

However, the flaring test is of limited use to make a conclusive statement regarding possible expansion during "real" micro-hydroforming process. Dissimilar to the flaring test, the tube hydroforming process has no compression loads in the main area forming zone which could help to increase the expansion of the tube. Furthermore, the mechanical flaring test involves some tribological issues that do not exist in THF. Thus, to be able to get more "realistic" expansion ratios, the tube material has to be examined with a closer to reality hydroforming simulation, which will be a hydraulic free-bulging experiment. This will also verify if during mechanical flaring test the scatter was influenced by the tribology.

CHAPTER 5

DETERMINATION OF TUBES' MECHANICAL PROPERTIES WITH HYDRAULIC FREE-BULGING

5.1 Introduction

The earlier investigations could contribute to a better understanding to what may be expected to be found in real micro tube hydroforming applications. These earlier experiments including initial material, tensile, flaring tests and laser heat assisted flaring tests can differ from real world tube hydroforming. Missing from these tests are the identical multi-axis stresses present in the hydroforming process. In THF the load application and tribology as included in the flaring test are not present so further investigation was necessary to get a clearer understanding.

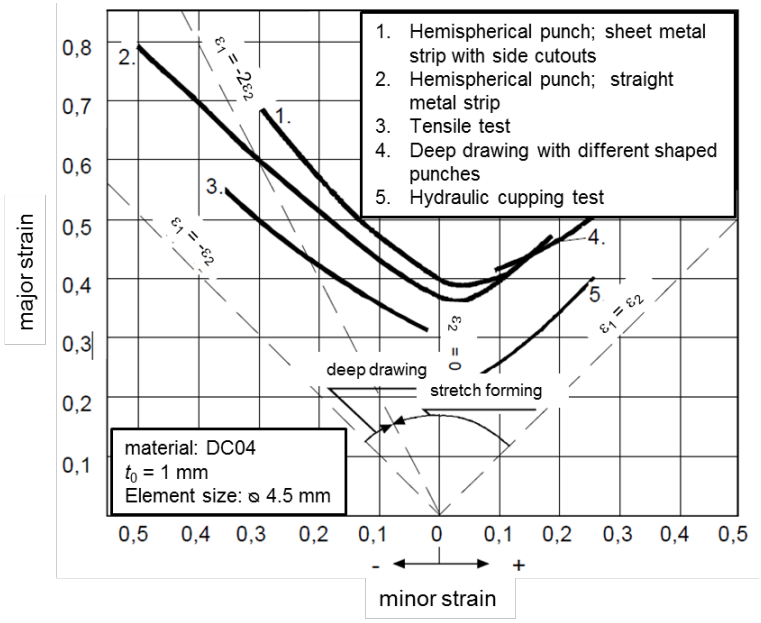

Fig. 32: Forming limit curves of identical materials established by different test methods [86]

As can be seen in *Fig. 32*, different test methods on the same specimen can result in significantly different forming limit curves which warrant the need for further study.

5.2 Aim of the test

Therefore, a method is needed to approximate the real conditions in THF. The best way to determine characteristic parameters for tube hydroforming (for example the maximum possible expansion diameter of a micro-tube) is the use of a technological process that comes as close as possible to the real forming process. In this case, contrary to the flaring test, a forming liquid should be used to obtain the same tribological conditions as exist in the real forming process. In current hydroforming processes, many tubular components are made by a simple calibration process. In those cases, the tube ends are not forced towards the die cavity, and as a result there is an almost pure plane stress condition. The bursting test with fixed tube ends is able to produce such a stress state. The test enables accurate characterization of tubes using the real loads of a real hydroforming process. The free expansion is even part of the hydroforming process, until the expanded tube touches the cavity just before applying the calibration pressure.

In this study the bulge test was used to attain two objectives: determining the forming limit and prediction of forming loads.

- Forming limit: As mentioned in *Chap. 2*, the ductility of a material is one of the most important parameters determining the forming limit in the hydroforming process, thus its evaluation is of high relevance. The expansion limit was investigated as it is related to the circumferential ductility of a micro-tube; as it is a property that determines the maximum achievable expansion. Similar to the flaring limit obtained during the flaring tests the expansion limit was defined as the relative expansion ratio ε_b in the hydraulic bulge forming experiments as:

$$\varepsilon_b = (D_1/D_0)-1 \tag{15}$$

where D_0 and D_1 are the initial tube and final maximum expansion diameters which could be achieved, respectively.

- Forming loads: As previously mentioned in *Chap. 2.2.2, Hydroforming fundamentals*, the design and optimization of hydroforming processes requires a mathematically empirical formula for the prediction of a suitable process control to determine the amount of forming loads during the hydroforming operation. As mentioned previously, the prediction of the internal pressure p_{ib} at the moment of fracture within the state of free expansion of a tube, *Eqn.* (7)

$$p_{ib} = \sigma_{UTS} \frac{2t_0}{D_0 - t_0}$$

has shown to be valid in conventional 'macro' tube hydroforming processes. The bulge test was also conducted to prove if the validity of the formula can be transferred 1:1 into a down-scaled micro process.

5.3 Short description of the burst test

The burst test involves a Free Hydraulic Bulging (FHB), which means the tube is expanded freely by internal pressure only, without getting into contact with a die. Besides the determination of a maximum pressure at which the specimen fails, other parameters such as the change in wall thickness and the maximum radial expansion can be observed. All values are important because they reflect on both strain-hardening properties and the size possible for a bulged tube. However, it must be taken into account that the test method is sensitive to the loading path. The deformation properties are dependent on the tube end conditions, free or fixed tube ends, which in turn are defined by the forming application. If the ends are free to move, the tube will self-feed, drawing material in as the pressure builds or if the ends are fixed, two-dimensional tensile strains will develop. If the ends are fed in, tensile and compressive strain fields will develop [34]. This study only investigated fixed tube ends as the first micro-hydroforming machine would not support axial feeding but only fixed tubes.

5.4 Experimental tooling and procedure

For the bulging of tubular specimens a standalone tool - closer described in *Chap.* 5.4.2 - was designed. The tool had been developed for the sole purpose to investigate tubular specimen of different material, wall thickness and diameters. No tooling changes are necessary for different material or wall thickness changes, only one simple modification -the exchange of upper and lower die half- is needed for use of different tube diameters.

5.4.1 Tooling requirements

Since the intention was that the tooling should be practice-orientated and in the future be used by industrial and research institutions, simplicity, low cost and easy operation were the main criteria in the design process. Further, the tool should be easily adaptable to different hydraulic pressures without requiring expensive and complicated pressure circuits usually comprising pressure control valves, flow control valves, relief valves, check valves and related plumbing, etc. Only a connection to a pressure transducer was required to be able to monitor the values of the forming pressure levels during the procedure.

Requirements for the tool set included tube sizes D_0 from 0.65 mm to 1 mm (available size ranges from all manufactures) internal pressures p_i up to 4,000 bar, provisions to lock the tube ends in place and a window to observe the tube expansion during the bulging.

With regard to a reliable sealing of the tube ends extra care had to be taken to tool deflections, to avoid pressure losses.

5.4.2 Design and function of the tooling

Based on the above requirements an experimental apparatus was manufactured for the bulging of tubular specimens, *Fig. 33*. The stand-alone test rig designed consists of a solid frame (pos. 1) including a square window. The tube to be investigated is contained by a set (an upper and lower) of dies (pos. 2 and 3) which are placed in the

square window. In this way, expansion tests for different tube diameters can be conducted by an easy exchange of the die inserts with different clamping radii.

Pos. no.	Name
1	frame
2	upper die
3	lower die
4	stop plate
5	sealing punch
6	sealing punch with bore hole
7	pressure ring
8	connection nuts
9	pressure ring

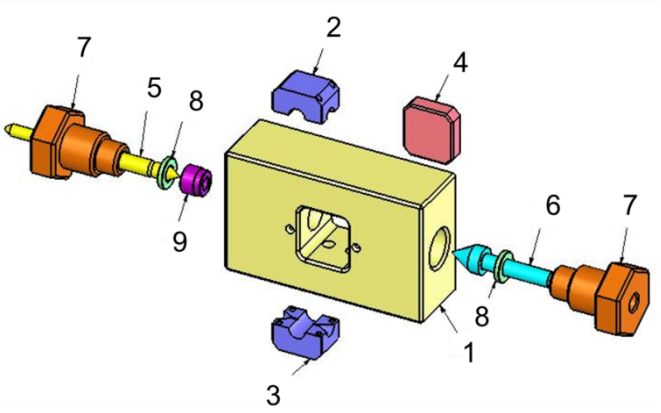

Fig. 33: Part's list and CAD of the test rig designed

Both die halves are positioned by using alignment pins to assure a centrically positioning along the longitudinal axis of the tubular specimen. Further on, the die halves are clamped by two screws carrying the closing force F_c, which would usually be applied by the hydraulic press. To ensure that the longitudinal axis of the tube falls in line with the axes of the female threads which carry the sealing punches, a stop plate (pos. 4) allows the exact alignment of the die-package to the tube's centre line. After the tube has been placed into the die cavities, the ends of the tube are lightly pressed against the 60° countersinks of the die inserts by conical sealing punches (pos. 5 and 6) having an outer angle of 58°, *Fig. 34*. After this pre-sealing the cavity of the tube is flooded with forming liquid until all the air has been eliminated. Filling is done through the bore hole of one of the two punches. As the connection nuts (pos. 7) of the punches are then tightened to a defined axial force F_a, a circular line contact (*Fig. 34*, shown as cross-section, coloured in red) creates stresses which, in turn, produce localized yielding and thus the sealing of the tubes. By this, no further sealing components such as rubber elements are necessary (ref. to *Chap. 6.4.4 Concept studies for axial sealing punches*).

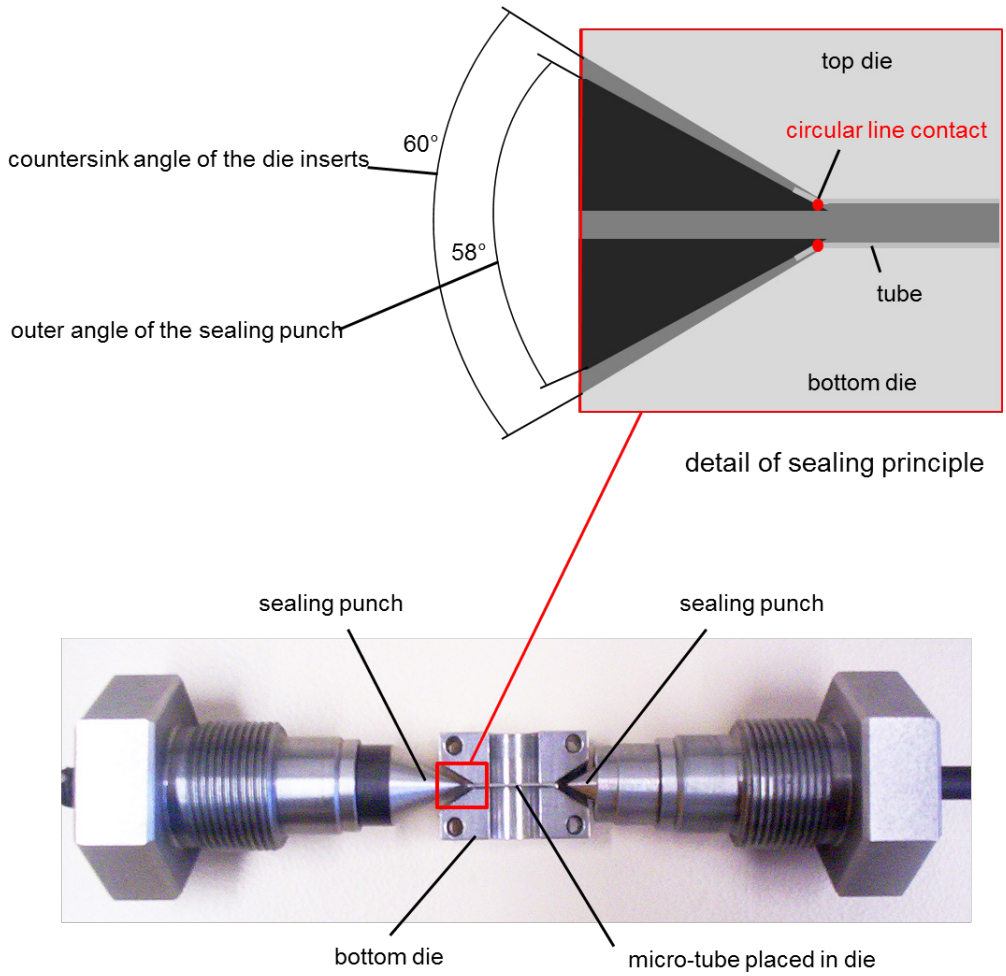

Fig. 34: Sealing principle of the 58° sealing punch angle and 60° angle of the die inserts

To meet the requirements for a sufficient sized free expansion zone the die inserts cover a circular hollow area of 10 mm diameter to the inserted micro-tube. This covers the range of the required minimum bulge width suggested by [40], and the area of the 'window' schematically shown in Fig. 35 is large enough to monitor the expansion during the process using a camera or other instruments. To avoid plastic deformation of the tubes at the edges of the clamping in the area of the transition region to the free expansion area the edges were fitted with small 0.2 mm radii. The clamping width is determined to 3 mm on each side (according to Hielscher [40] who suggests a clamping zone: 1/6 * D_0), which is wide enough to assure that no

axial stresses caused by the conical sealing punches occur which, in turn, may force tube material into the free expansion area.

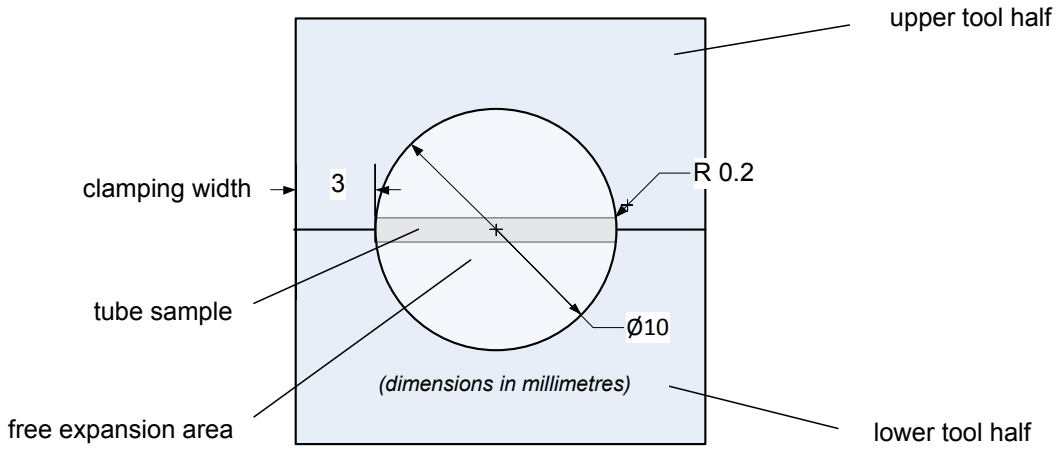

Fig. 35: Geometry and dimensions of the tooling, schematically

FE analysis of the tool components

The design of the tool was accompanied utilizing FE analyses. The simulations intend to minimize the risk of leakage due to vertical shifting of the tool halves caused by lateral forces induced by the sealing punches. As a boundary condition, a maximum internal pressure p_i of 4000 bar was defined. The resulting deflections of the frame of the test device are shown in *Fig. 36*.

A 'Mises' stress simulation of the test device frame showing the maximum in the area of the internal threads of the screws which are responsible for the clamping of the tool halves, represents *Fig. 37* (frame cut by symmetry conditions).

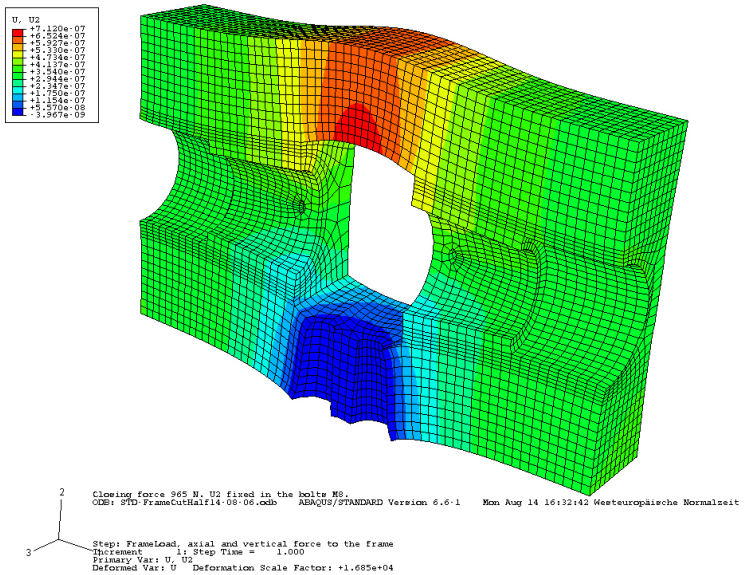

Fig. 36: Tool frame deflections under a load of 4000 bar internal pressure

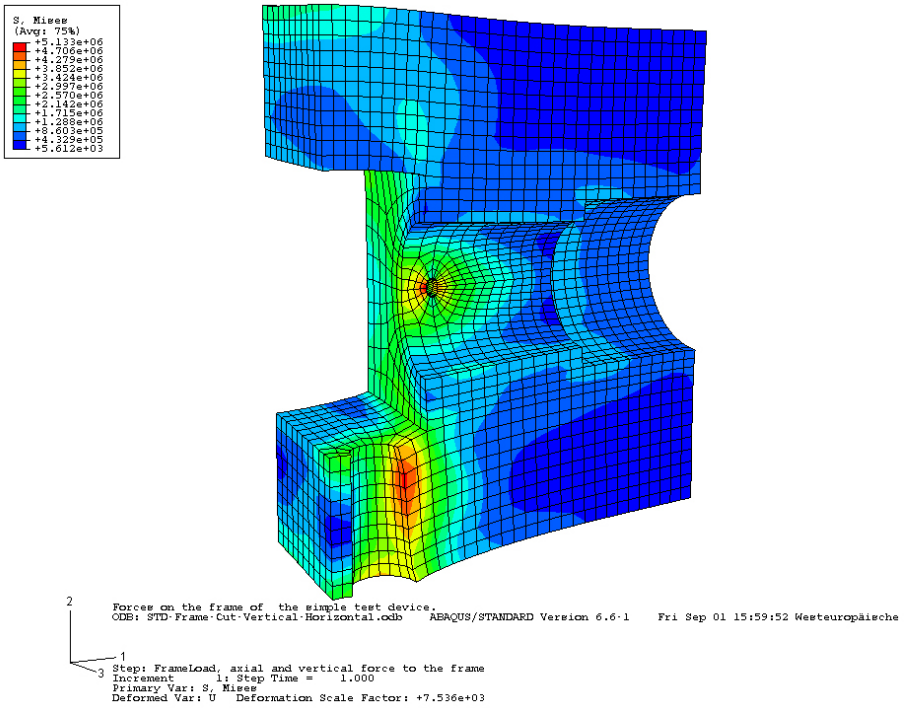

Fig. 37: 'Mises' stress FE simulation of the test rig designed

From the results obtained by the FE analyses of the test device frame it could be concluded that the distortion of the frame would not cause any appreciable shifting of the die inserts inside the frame window in which the inserts are placed. So leakage due to vertical shifting of the tool halves caused by lateral forces induced by the sealing punches was not to be expected. Further on, suitable tool materials and frame dimensions could be defined after the study.

Besides the frame components of the test device, another important part to be analysed by means of FEA is the conical sealing punch and its hole, which is shown in *Fig. 38*.

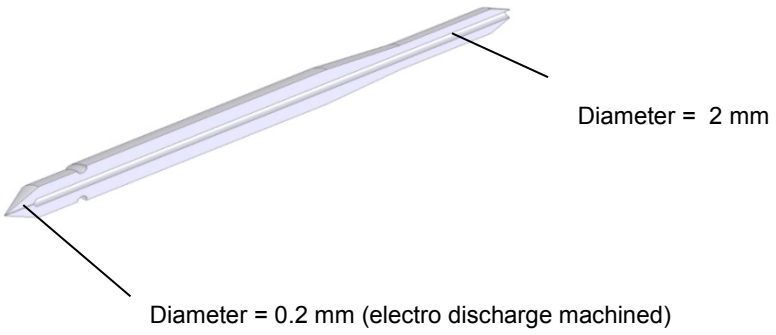

Fig. 38: *Conical sealing punch with the injection drilling*

Fig. 39 shows the simulation results of the punch tip under internal pressure p_i of 1,000 bar and under the influence of a maximum clamping torque of 30 Nm. Clearly recognisable is the main stress area in which the punch presses the tube towards the inner 60°cone of the tool. Here, the localised yielding and plastic flow of the tubular material occurs and broadens to the above mentioned annular area seal.

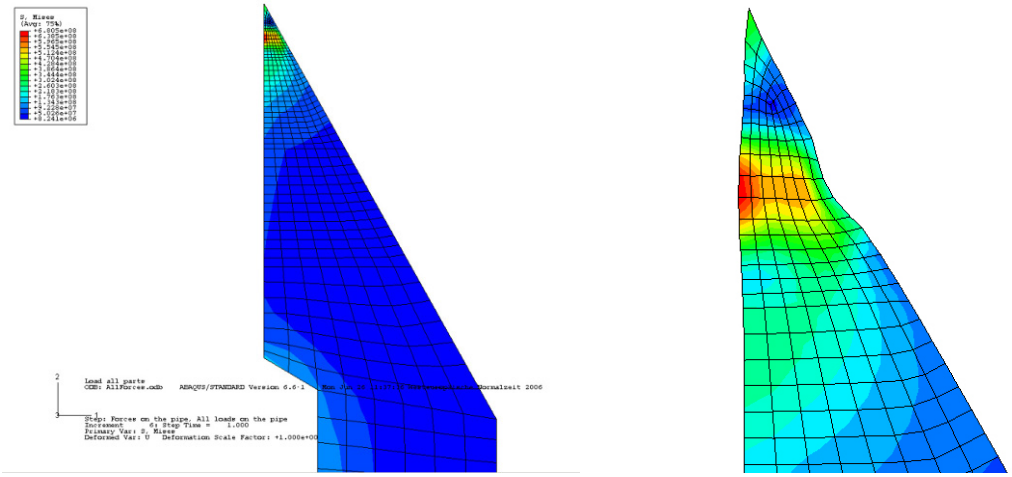

Fig. 39: Equivalent stress Distribution (N/mm²), Conical punch with boring diameter 0.2 mm

In principle there are materials which are able to withstand the stresses from these studies. Both sealing punches had been manufactured using the tool steel 1.2379 which was also hardened to 60 HRC.

The design of the free expansion zone

From literature, e.g. [28,40] it is known that attention should be drawn to the design of the length of free expansion zone and the clamping zone of tubular material. FEA analysis and burst tests showed that the expansion length is one of the most important issues. Because of changed stress conditions, the strains in axial direction increase when the length of the free expansion zone decreases. Even at high radial expansion diameters and expansion lengths (four times the initial tube outer diameter) very good results could be obtained. If the expansion length included three times the outside diameter, still acceptable results had been achieved. The experimental evaluation by [40] is illustrated in Fig. 40. With expansion lengths twice the outer tube diameter, significantly different results arose in comparison to the experiments with larger expansion length / outer diameter ratios. From about 10% radial expansions the necessary internal pressure as well as the maximum achieved expansion increased. The results for the triple and quadruple outer diameter were almost equal.

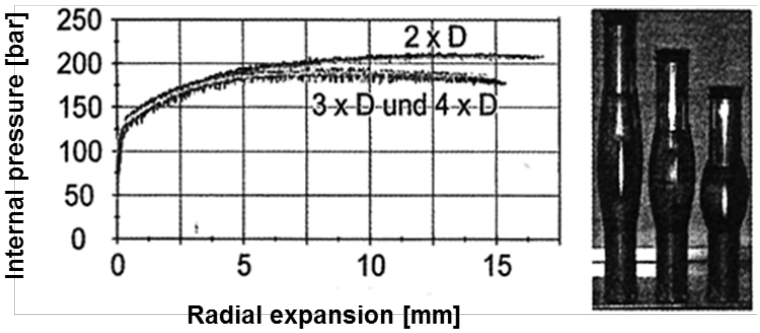

Fig. 40: Variation of the expansion zone length [40]

Additionally to the experiments at room temperature experiments with laser-heated tubes should be conducted. The introduction of the laser beam and pyrometer for measuring the temperature of the heated, a sufficient area or 'window' had to be considered to allow for these devices. The window should also provide enough space to be able to use a sensor and/or a camera for online measurement of the expanded tube diameter.

When designing the tool, the dimensioning of the clamping length turns out as a compromise. On the one hand, the clamping length to decrease the reaction forces on the projected clamping area of the tube caused by the internal pressure should be minimized. Thus, the risk of an opening of the die halves and with that a leakage may be reduced. On the other hand, a sufficiently long clamping zone generates higher sticktion. Thereby, axial movement of the tube which in turn could cause leakage would be prevented. Additionally, if the clamping length is not long enough and not enough sticktion is present, axial displacement (tube feeding) could influence the forming area and result in wrinkling and/or buckling due to compression forces.

5.4.3 Peripheral machine components

The hydraulic pressure system used for this tool set is composed of an electronically driven spindle press, a 3/2-port hydraulic control valve, a check valve and a safety

head with rupture disc and associated plumbing. The maximum forming pressure for the system is 4,000 bar (400 MPa), which should be sufficient for burst tests of micro tubes with a maximum diameter of 1 mm according to *Fig. 6* in *Chap. 2.2.2.4 Prediction of forming loads*. The flow rate of the spindle press was proportional to the DC input signal of the controller, and was 0.07…9 ml/min. According to a flow rate pre-set in the low range, a forming time of about 5…10 seconds was to be expected, depending on the dimensions of the tubes examined. It must be noted that during the experiments the exact flow rate had not been determined, since a flow meter was not adapted to the tubing system.

In order to control the pressurization, control and data acquisition LabVIEW software was used, described in *Chap. 6.8 Control system*. To enable the measurement of the internal pressure of the liquid that effects the expansion of the tube, a pressure transducer (measuring system: DMS) had been integrated into the high-pressure circuit.

5.4.4 Tube dimensions and material

For the selection of tube dimensions four criteria were relevant. Firstly, the size range of the tubes should correspond to the installation space of the tool, in particular to the given tube diameter of the die halves. Secondly, the tubes should be formed with pressure level according to *Eqn.* (7) that could be achieved by the pressure intensifier. Thirdly, the application of this formula requires, therefore, that *thin-walled* tubular workpieces are formed to meet the requirements of the shell theory. The shell theory assumes that there is a biaxial stress state. The stresses in wall thickness direction can be neglected according to [28], since these are small compared to other stresses. Therefore, the tube samples should have the inner diameter/wall thickness ratio $d_0/t_0 \geq 20$ proposed by [88].

Test program

Burst test

Test parameters						**Procedure parameters**									
						Temperature [°C]									
						(*) Temperatures aimed at could not be achieved with the laser source used									
Material	Tensile strength [N/mm²]	Tube dimensions [mm]			Volume flow [ml/min]										Pressure [bar]
	σ_{UTS}	L_0	D_0	t_0		RT	150	200	250	300	350	400	450	500	p_i
Test series 1: Variation of the material => Determination of bursting pressure p_b															
AISI 304-a	690	10	0.8	0.04	not measured	O									p_{ib} = x
AISI 304-b	593			0.04		O									
CW024A (R200)	236			0.1	0.07 (set to minimum)	O									
CW024A (R250)	296			0.1		O									
Test series 2: Variation of the temperature - Stainless steel => Determination of bursting pressure p_b															
AISI 304-b	593	10	0.8	0.04	not measured		O	O	O	O	O	O	O	O	p_{ib} = x
Test series 3: Variation of the temperature - Copper => Determination of bursting pressure p_b															
CW024A (R200)	236	10	0.8	0.1	0.07 (set to minimum)		O	O	O	O	O	O	(*)	(*)	p_{ib} = x
CW024A (R250)	296						O	O	O	O	O	(*)	(*)	(*)	

Table 6: Test program of the hydraulic free bulging

5.4.5 Test program

Table 6 provides an overview of the experimental parameter combinations. Per variation, at least ten samples were formed. The test program was divided into three test series. The tests to determine the strain capacity and the workpiece characteristics at

room temperature were summarized in test series 1. The overall goal of this first investigation was to determine the maximum possible expansion diameter D_1 and the bursting pressure p_{ib} at room temperature. In one series the sample material was varied, in another the tube sections of stainless steel AISI 304 were examined from two different deliveries. The tubes made of copper material differed in the previous annealing treatment. All material parameters can be found in *Chap. 3.2 Used materials and sequence of experimental investigations*. The variation of the materials was carried out on micro-tubes with outer diameter D_0 = 0.8 mm. The wall thickness of the stainless steel tubes was t_0 = 0.04 mm, t_0 = 0.1 mm of the copper tubes respectively.

The goal of test series 2 and 3 was to identify the maximum achievable flare diameters D_1 and burst pressures p_{ib} of the tubes when heated by laser energy. Eight different temperatures from ϑ_f = 150°C to ϑ_f = 500°C in steps of $\Delta\vartheta$ = 50°C were examined. A total number of 24 micro-tubes had been formed, three at each temperature step. To measure the forming temperature a pyrometer had been used. Since the pyrometer had only a range from about 150°C, no experiments could be carried out in the temperature range RT < 150°C accurately. In contrast to the studies of the test series 1, investigations with stainless steel tubes of the delivery batch A (304-a) could not been accomplished due to numerous previous initial trials during the study, such as flaring tests and tests for the handling and cutting of tubes, the material supply had been depleted.

5.4.6 Procedure of the bulge test

Preparation of the specimens

Every tubular test piece was directly cut from the wrought material delivered in lengths of one meter. To ensure a flawless seal when pressurized, the specimens had exactly to be cut in specific lengths. The appropriate length has been determined in preliminary tests. If the tube was too long tube samples bore the risk of premature tearing at the collar of the conically expanded end by crossing the strain capacity of

the tubular material. If the sample length was chosen too small, no circular line contact causing an insufficient sealing surface between the 58° / 60° cones of the punches and the tool respectively. Hence, the tubes were cut to 16.50 to 16.75 mm in length L_0 depending on the tube material and dimension used and the two ends of the tubes were deburred and finely ground (down to 1200 grit) to obtain a low roughness depth and that minimized the risk of notch effects.

Execution of the test

The experiments were carried out by placing the specimen into the bottom die half. It must be noted that some of the tubes drifted along their longitudinal axis due to asynchronous tightening of the lock nuts of the sealing punches. In order to increase the static friction, the tube ends were additionally fixed with superglue in the contact area. During pre-tests, in some cases the clamping force for the tube to be pressurized was not sufficient enough. As a result, under the axial force F_a the tube was pushed towards the free-forming zone and thus the tube ends could not be sealed. After closing the die halves, placing the die in the frame and tighten the screws which generate the closing force, the tube was first pre-filled to avoid blisters in the forming liquid. Having fixed the clamping screws the fluid was pressurized. With moving the spindle press at the pre-set volume flow V_{fl} the internal pressure rose to expand the free expansion zone of the tube between the two supporting dies until bursting. The internal pressure was recorded ten times a second for precise pressure changes and exact bursting point. Reaching that point, the bulge test was stopped. The experimental setup is represented in *Fig. 41*.

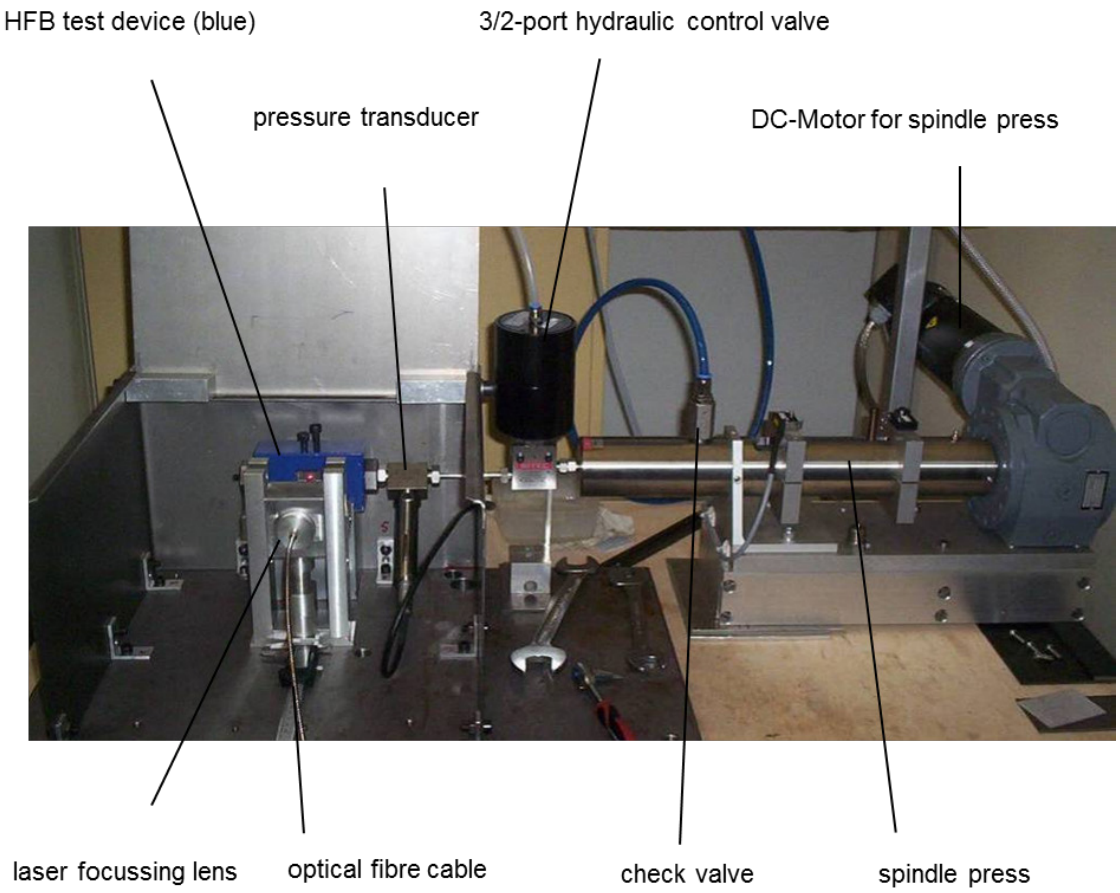

Fig. 41: Experimental setup for the hydraulic free bulging experiments

The measurement of the expanded micro-tubes

After taking the tubes out of the forming tool halves, the circumferential expansion diameters were measured by means of a Zeiss reflected-light microscope with charge-coupled device camera *AxioCam MRc* which had also been used for the flaring tests.

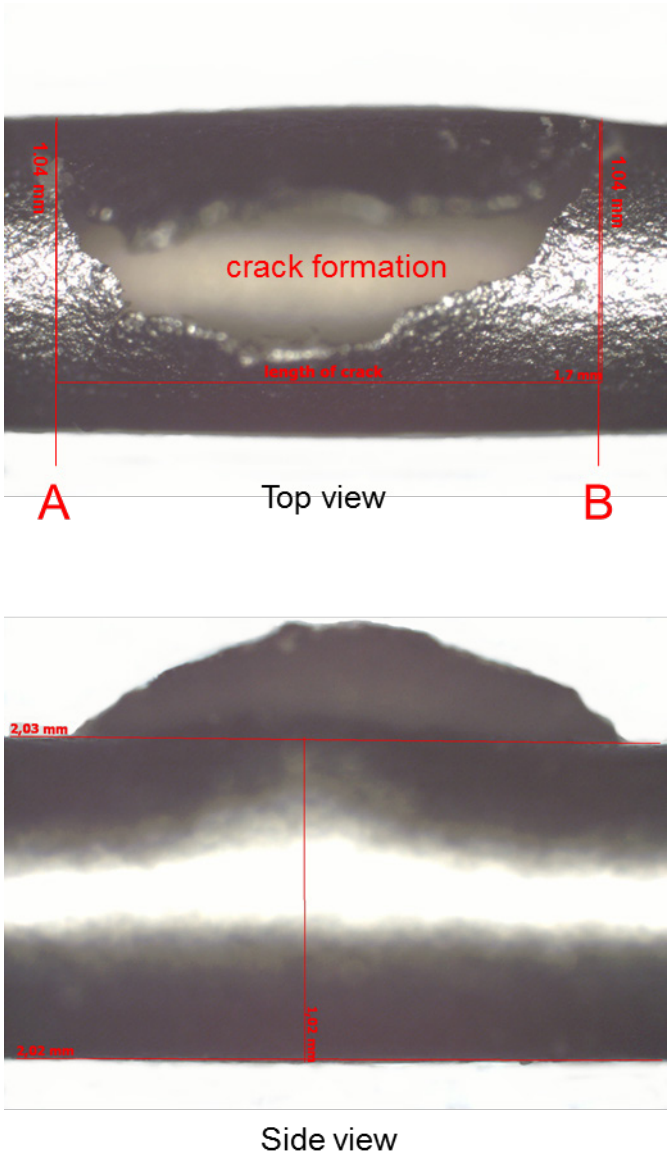

Fig. 42: Measurement of the expanded micro-tubes

The procedure for determining the expansion diameter D_1 is illustrated in *Fig. 42*. Since the tube is under the influence of several hundred bar of internal pressure p_i, the tube is literally exploded. In most cases the bursting led to a relatively large gaping fracture. The tubes' initial circular cross section changed to a slightly elliptical shape in the area of the fracture. Thus, the expansion diameter had to be determined in several steps. Firstly the forming diameter was measured in the top view (*Fig. 42* above) from both sides just in the area without fracture but as possible nearby the beginning and end of the crack. It was assumed that the expansion diameter within

the length of the longitudinal fracture (between points A & B in the top view) was almost similar. The second measurement was performed in side view. As can be seen in the lower photograph in *Fig. 42*, two parallel lines in longitudinal tube direction have been put into the picture. The start and end of each line was the position of the two constructed lines perpendicular to the longitudinal direction of the tube which had been constructed into the first photograph. A second expansion diameter was now measured in between those parallel lines. Finally, the maximum achieved expansion diameter was determined by the arithmetic mean value of both the established diameters in top and side view, respectively.

Similar to the flaring test measurements, the measurement points had to be set manually. As with the flaring tests, since the uncertainty of measurement was to be assumed in the range of 1 to 10 µm the measured values have been rounded up to the nearest 1/100 mm.

5.4.7 Laser assisted investigations

Again the laser source according to the specifications represented in *Chap. 4.5.1* had been used for the investigations.

To transmit the laser beam to the tooling, an optical fibre cable was used. For holding the focusing lens a cylindrical device was mounted at the end of the fibre. The image scale of the focusing unit was 1:1, which means the distance "beam exit (fibre) – focussing lens" corresponded to the distance "focussing lens – focal point". The cylindrical focussing unit by itself was then attached to a clamping device which was mounted on the test table. To set or to change the focal length, the entire focussing optics could be moved along its longitudinal axis by simply loosening the screw of a clamp.

For the temperature measurement of the laser-assisted experiments again the stationary digital pyrometer type Cella Temp PZ 27 (Cellar) had been used. A closer description as well as the specifications can be found in *Chap. 4.5.2*.

During the tests, the aim was to achieve a most uniform heating of the deformation zone as possible. Using the 50 mm focussing lens, mentioned in the above laser specifications, with a magnification ratio of 1:1, the focal radius was $w_f = 0.2$ mm, in due consideration of the specifications of the laser source. With regard to the demonstrator part "camera shaft" (*Fig. 55* & *Fig. 80*), the length of the main forming zone of the shaft comprises about 2 mm. It was therefore considered to try to evenly heat up the micro-tube in a useful range of about 2 mm. Therefore, to enlarge the laser-affected zone of the heated micro-tube the laser beam had to be defocused by enlarging the distance between focusing lens and micro-tube.

The required shift of the focusing unit relative to the focal point was determined by calculation using the technical data of the laser. The numerical aperture A_N, which describes the ability of an optical element to focus light is generally the product of the sine of the half object-side opening angle γ and the refractive index n of the immersion medium.

$$A_N = n \cdot \sin \gamma \tag{16}$$

In this case, of the optical fibre, the numerical aperture is described by the sine of the acceptance angle of the fibre and corresponds to the beam opening diameter of the fibre end face.

With $n = 1$ for air and $A_N = 0.2$, we obtain a half-acceptance angle $\gamma = 11.54°$ according to *Eqn.* (16).

The desired defocusing Δx_{def} results from the trigonometric relation

$$\Delta x_{def} = \frac{w_{def}}{\tan \gamma} \tag{17}$$

with the desired radius of the defocused focal point $w_{def} = 1$ mm and can thus be determined to

$\Delta x_{def} = 4.89$ mm.

Laser Procedure

After inserting the tube specimen into the tooling, the focal position was identified by measuring the maximum achievable temperature at the spot. Then for defocusing, the laser optics in the holder had been moved by the above calculated amount Δx_{def} = 4.89 mm relative to the determined focus position. After having turned on the pilot laser, the appearing focal spot became visible approximately in the size of the theoretically determined value (2* w_{def} = 2 mm).

Material: AISI 304	**Focal point centre**		**1 mm off-centre**		**2 mm off-centre**	
	ϑ_{max} [°C]	Δt [s]	ϑ_{max} [°C]	Δt [s]	ϑ_{max} [°C]	Δt [s]
Tube front side						
1st measurement	250	8.4	235	9.8	200	16.3
2nd measurement	250	8.3	235	10.0	200	16.1
3rd measurement	250	8.4	235	9.6	200	16.5
Tube back side						
1st measurement	236	8.7	223	11.5	191	18.1
2nd measurement	236	8.5	223	11.9	191	17.9
3rd measurement	237	8.6	223	11.8	191	18.1

ϑ_{max} Maximum achieved temperature

Δt Time of temperature rise until reaching ϑ_{max},

Table 7: Verification of heat conductance

To verify an appropriate choice of the allegedly enlarged focal spot and due to that a uniform heat input into the main forming zone, preliminary tests were undertaken before having started the laser-assisted bulge tests. Hence, a tube specimen made from stainless steel AISI 304 (batch B) was marked with very fine strokes at a distance of exactly 1 mm over its long side using a fine marker. After placing the specimen into the tooling, it was filled with the forming fluid and pressurized to 115 bar

(11.5 MPa). The laser power was set to $P_{out,l}$ = 3 W cw (continuous wave) and the laser beam was positioned into the centre of the micro-tube's longitudinal side. To measure local temperatures of the heat-affected zone, the measuring spot of the pyrometer was shifted from the centre along the millimetre scale attached to each side of the tube axis. The procedure was repeated measuring the local temperatures at back side of the tube, i.e. 180° faced away from the laser spot. Measured values are shown in *Table 7*.

It can be concluded that in the range of 1 mm to each side around focal point the largest difference in temperature was 27°C (centre point, front side - 1 mm aside, backside). However the difference between the temperature in the focus at the front and the area 2 mm off-centre at the back of the tube was already 59°C. With regard to the demonstrator part *camera shaft* with its length of a main forming zone of approx. 2 mm, the difference of 27°C was considered as 'not marginal' but acceptable for the range of about 2 mm.

Starting time of laser impact

Laser energy could not be introduced simultaneously with pressurization. The reason was that at hydrostatic pressure equal or near zero, the forming fluid began to boil when the temperature arose over 100°C due to laser impact. A remedy could be found by a time-delayed onset of laser impingement. However, the laser starting point was not chosen time-dependent but pressure dependent. Corresponding values of pre-pressurization can be found under point 'procedure parameters' in *Fig. 50* - *Fig. 52*.

Effects of laser light absorption in copper

The absorption curve (*Fig. 43*) of copper shows a hyperbolic inclination in the band of wave length λ = 0.5 … 1 µm. It is obvious, that the laser light of the used laser source with a wave length λ of 810 nm will mostly be reflected, vs. above specifica-

tion sheet of the laser source. As a result, even at nominal laser power of $P_{out,l}$ = 25W only a maximum forming temperature of approx. 300°C could be achieved.

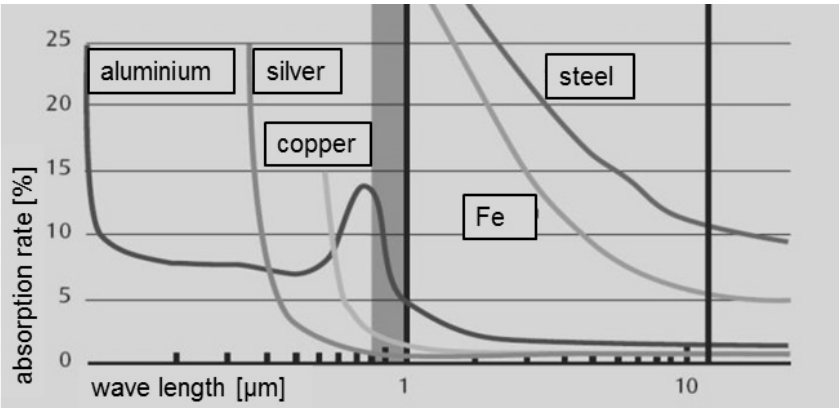

Fig. 43: Absorption curves of different metals (German Copper Institute)

To achieve higher temperatures the focal lens had to be moved from its defined defocal length Δx_{def} = 4.89 mm closer (reduced to Δx_{def} = 2.6 mm) towards the copper tube sample. The focal spot reduced and with that the fluence increased, which in turn afforded higher heat impact. Even though, the danger of laser burn-through magnified whereupon the pre-pressurizing of copper tube bulge tests was increased in comparison to the pre-pressurized stainless steel tubes.

To verify the heat conductance, the above-mentioned temperature tests accomplished with stainless steel tubes were repeated now with copper tubes. The laser power was set to 24 W. Subject of the experiment was the R250 copper tube. The measurements were undertaken three times. Mean measured maximum values are represented in *Table 8*.

During the experiments the laser power was set to 25 W whereby a maximum tube temperature ϑ_{max} of approx. 400°C on average could be achieved. It must be concluded that compared to the stainless steel tubes the heat conductance was more inhomogeneous.

Material: Copper R250	Focal point centre		1 mm off-centre		2 mm off-centre	
	ϑ_{max} [°C]	Δt [s]	ϑ_{max} [°C]	Δt [s]	ϑ_{max} [°C]	Δt [s]
Tube front side	277	2.0	251	3.1	200	5.4
Tube back side	228	6.2	206	22.5	153	53.3

ϑ_{max} Maximum achieved temperature

Δt Time of temperature rise until reaching T_{max},

Table 8: Verification of heat conductance, copper tubes

Acquisition of temperature data

For data acquisition, the temperature of the tube specimens which was measured by the pyrometer was recorded ten times a second with the windows based software Cella Mevis.

5.5 Forming results

5.5.1 Experimental results established from investigations performed at room temperature

In *Fig. 44 - Fig. 47* the forming results and process parameters are compared. The test parameters, including the investigated material and the tube dimensions as well as the procedure parameters can be taken from the top half of the figure. The diagram shows the recorded data of the forming pressure p_i versus the forming time t_f until it came to workpiece failure due to bursting. Examples of investigated micro-tubes before and after expansion are represented in the lower half of the image. Below, the diagram visualizes the achieved forming diameters D_1 of the tube specimens versus the applied maximum internal pressure p_{iB} at bursting.

Forming Pressures

As it can be seen from the diagrams on top of *Fig. 44- Fig. 47*, the curve progressions of the recorded forming pressure vs. forming time of both the AISI 304 (both batches) and the copper micro-tube material show similar characteristics. The forming pressure p_i grows steeply with linear inclination until maximum pressure p_{iB} was obtained. There were four exceptions in the AISI 304 stainless steel tubes, two each in batch A and batch B, the issue was due to leakage. Another leakage at process start, cf. ΔT in p_i/t-Diagram Cu R 200, *Fig. 46* no issue of liquid sealing was observed at any time. Nevertheless, the achieved forming time when bursting occurred shows a comparatively large range of variation. It can be seen from all four diagrams conducted at room temperature that the end forming time scattered in a range of 50% relative to its determined mean values.

Test parameters:

Material: Stainless steel AISI 304 (batch A)

Tube dimensions: L_0 = 16.5 mm, D_0 = 0.8 mm, t_0 = 40 µm

Procedure parameters:

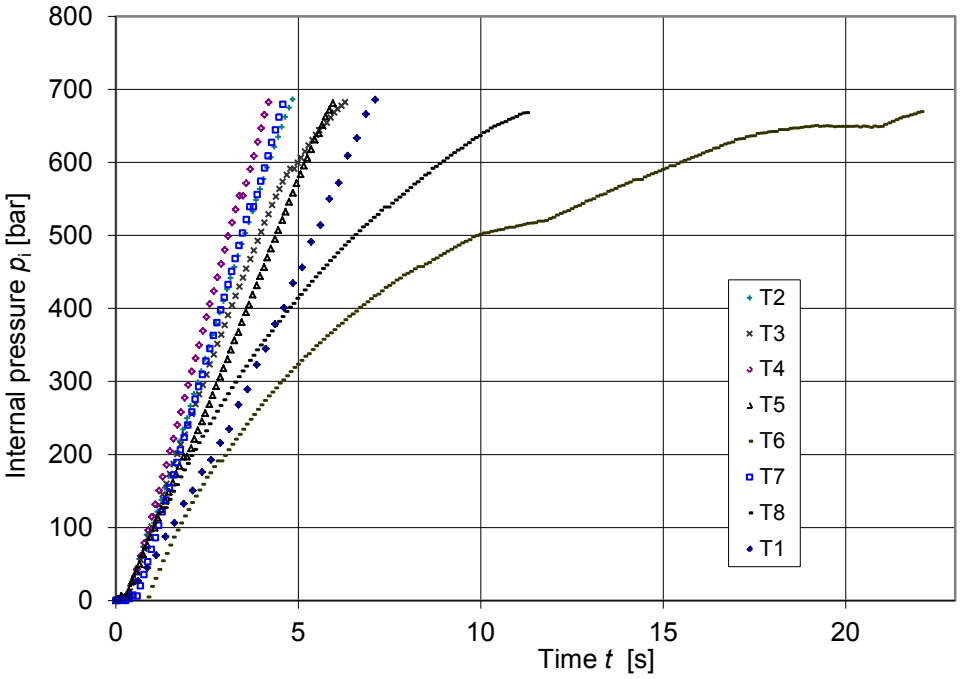

Forming results:

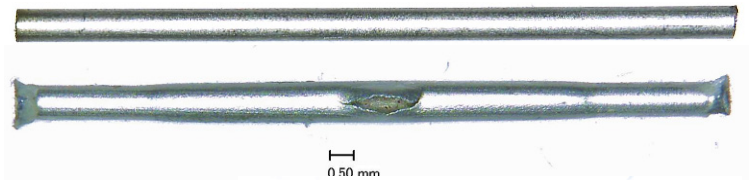

T_i: Initial tube

T_1: AISI 304 tube (batch A) formed at RT

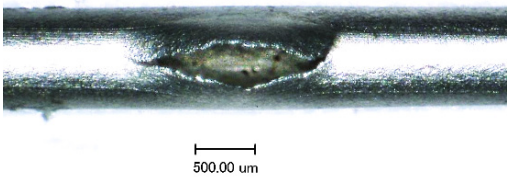

T_1: Section of fracture

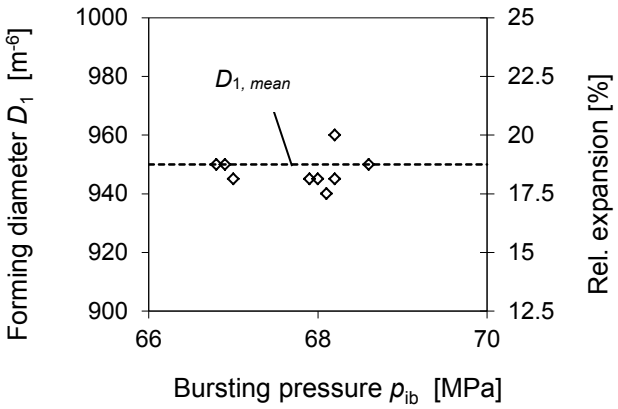

Fig. 44: Forming results and procedure parameters with point of fracture and mean expansion diameters - stainless steel AISI 304 (batch A)

Test parameters:

Material: Stainless steel AISI 304 (batch B)

Tube dimensions: L_0 = 16.7 mm, D_0 = 0.8 mm, t_0 = 40 µm

Procedure parameters:

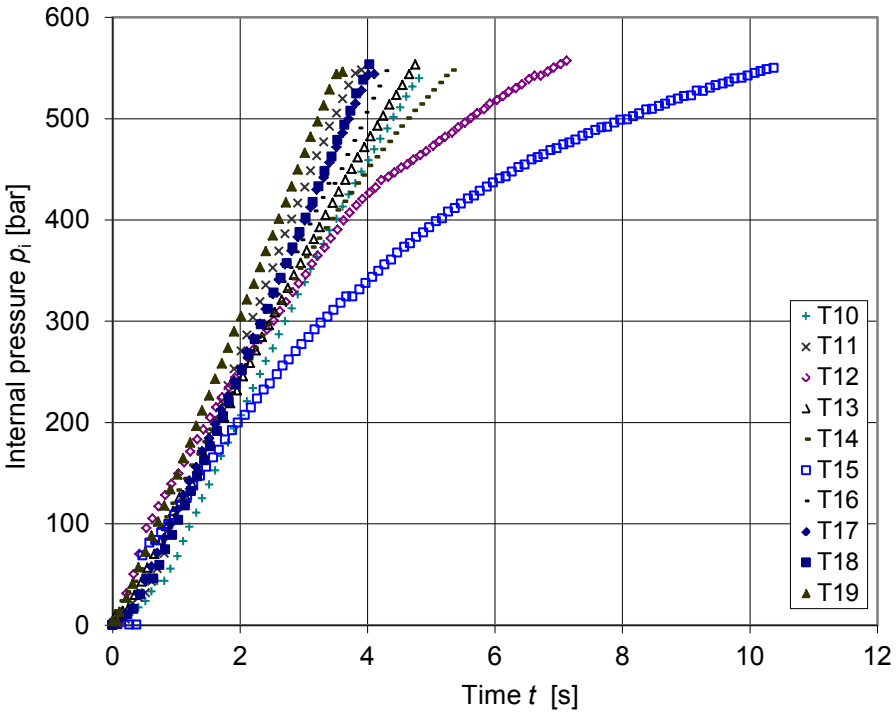

Forming results:

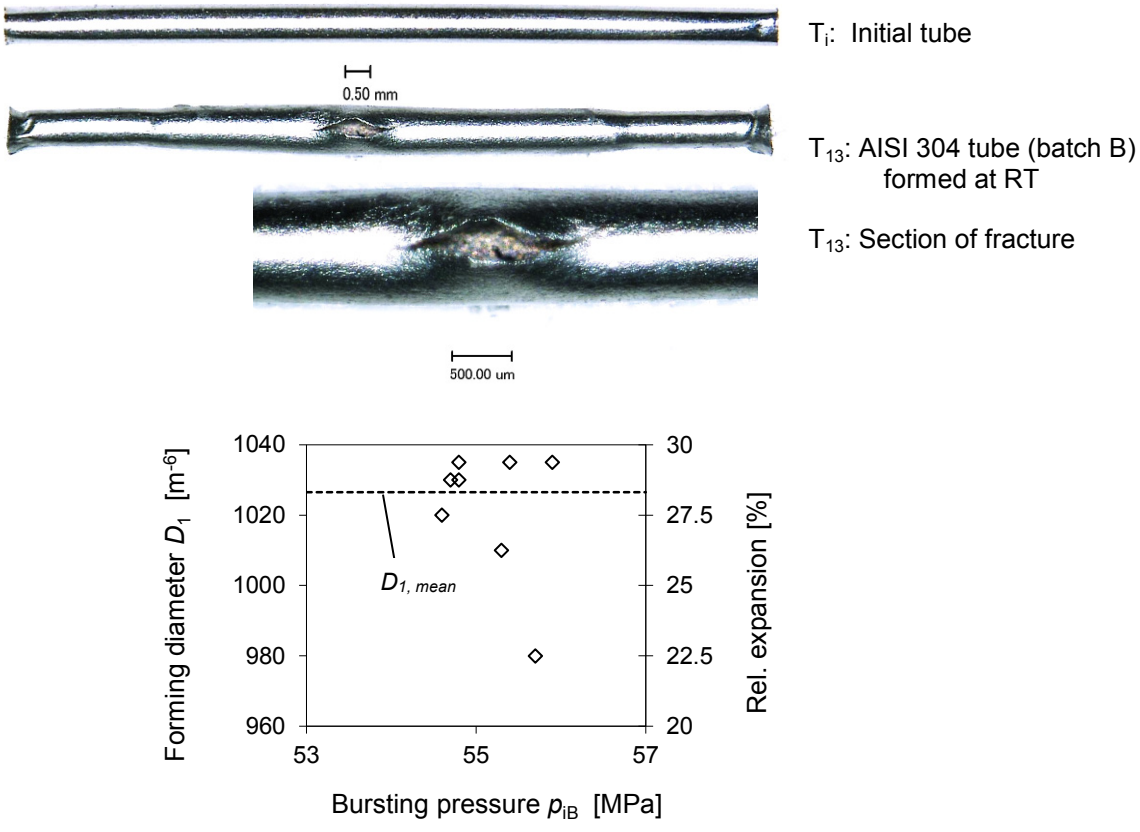

T_i: Initial tube

T_{13}: AISI 304 tube (batch B) formed at RT

T_{13}: Section of fracture

Fig. 45: Forming results and procedure parameters with point of fracture and maximum achievable expansion diameters - stainless steel AISI 304 (batch B)

Test parameters: **Material: Copper CW024A (R 200)**

Tube dimensions: L_0 = 16.75 mm, D_0 = 0.8 mm, t_0 = 100 µm

Procedure parameters: Volume Flow: V_{fl} = 0.07 ml/min. (minimum set)

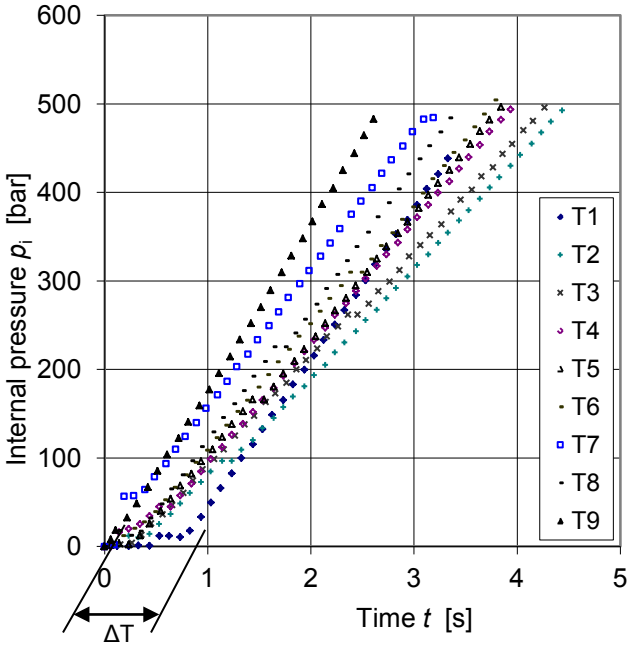

Forming results:

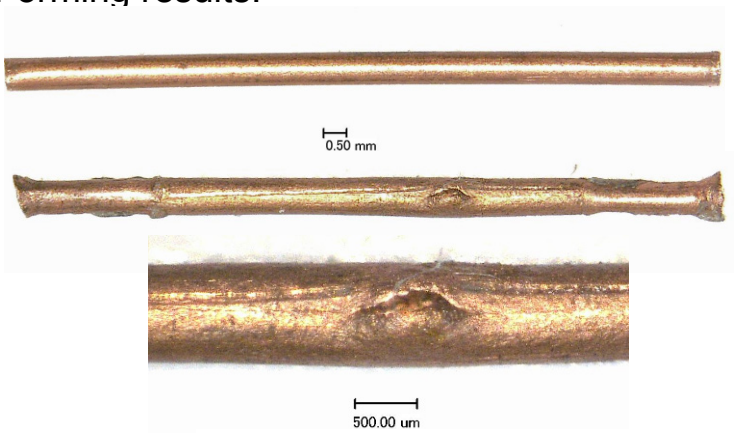

T_i: Initial tube

T_2: Cu tube (R 200) formed at RT

T_2: Section of fracture

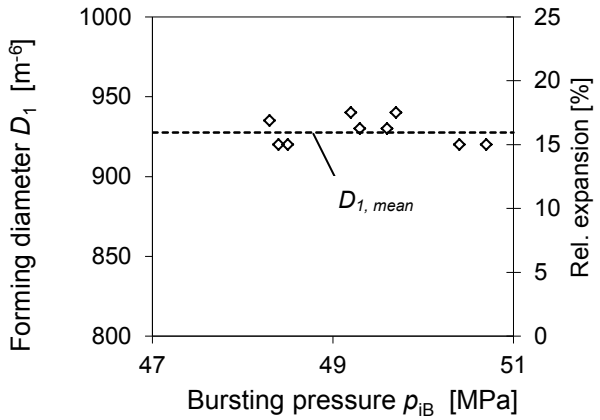

Fig. 46: Forming results and procedure parameters with point of fracture and achievable expansion diameters - Copper CW024A (R 200)

Test parameters:

Material: Copper CW024A (R 250)

Tube dimensions: L_0 = 16.75 mm, D_0 = 0.8 mm, t_0 = 100 µm

Procedure parameters:

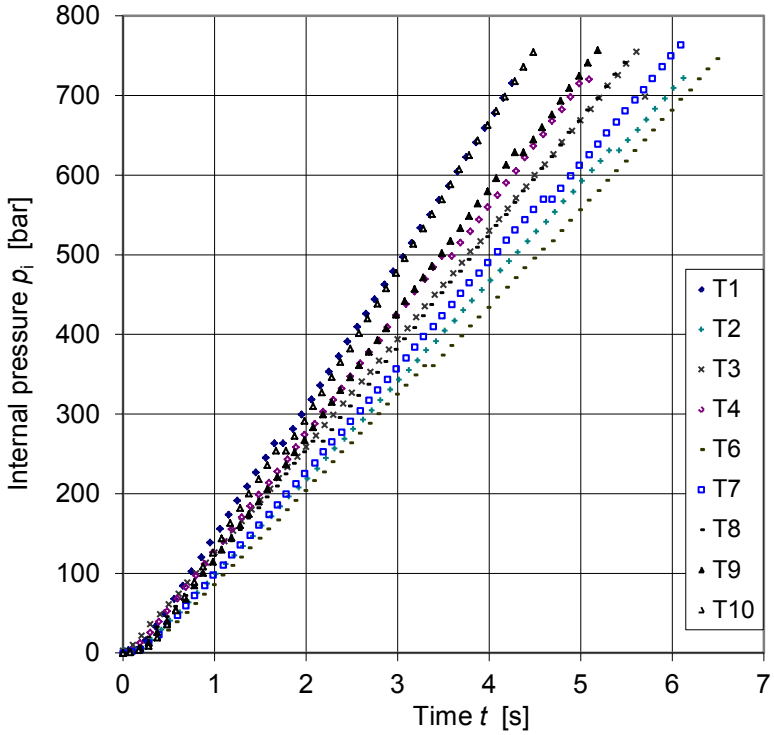

Forming results:

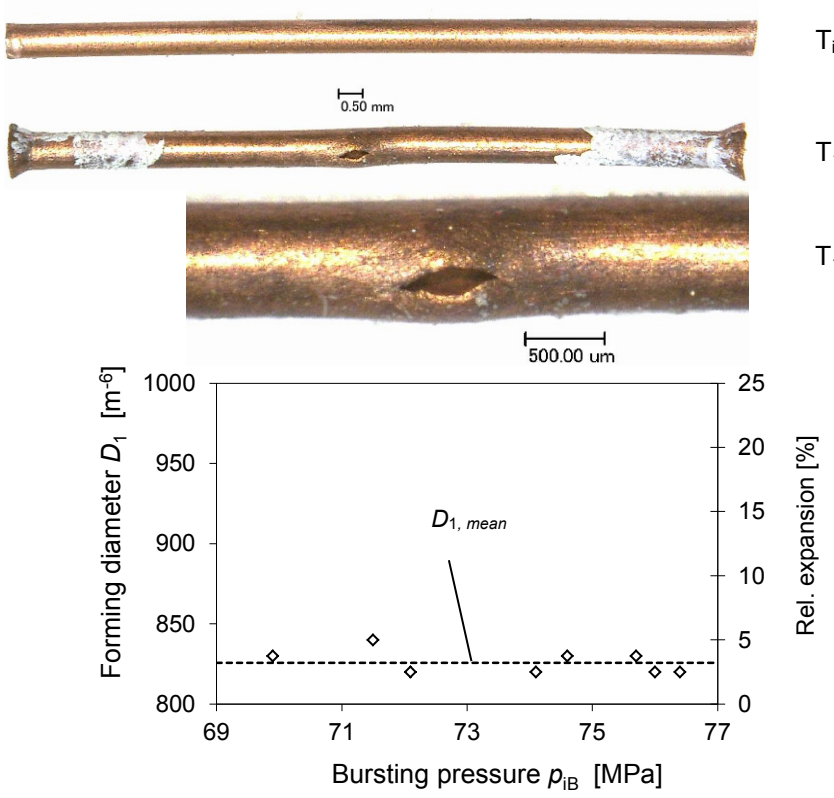

T_i: Initial tube

T_1: Cu tube (R250) formed at RT

T_1: Section of fracture

Fig. 47: Forming results and procedure parameters with point of fracture and achievable expansion diameters - Copper CW024A (R 250)

Achieved bursting pressures

The average values of the bursting pressures p_{ib} conducted at room temperature can be established from the p_i/t-diagrams and are summarized in the following:

- Stainless steel AISI 304, batch A: mean bursting pressure p_{ib} = 67.8 MPa with a standard deviation s of 0.68 MPa (scatter 1.8 MPa)
- Stainless steel AISI 304, batch B: mean bursting pressure p_{ib} = 54.9 MPa with a standard deviation s of 0.57 MPa (scatter 1.9 MPa)
- Copper CW024A (R 200): mean bursting pressure p_{ib} = 49.4 MPa with a standard deviation s of 0.81 MPa (scatter 2.4 MPa)
- Copper CW024A (R 250): mean bursting pressure p_{ib} = 73.5 MPa with a standard deviation s of 2.22 MPa (scatter 6.5 MPa)

Deformation modes and distribution of the fracture localisation

In all room temperature experiments, the internal pressurization led to a uniform radial expansion at each point along the tube length. However, depending on the micro-tube, different bulge formations could be observed. Pressurization of AISI 304 tubes caused a clear uniform bulging from the opening radius of the tool to the middle of the free expansion length. In contrast, copper micro-tubes almost showed no bulging along their tube lengths. The corresponding deformation modes can be found in the microscope photographs in *Fig. 44* - *Fig. 47*.

However, what applied for both, the copper and the stainless steel tubes is that prior to the workpiece failure, a local disproportionate bulging appeared just in the bursting area. As can be seen in the schematic (*Fig. 48*), the bursting area of the investigated AISI 304 stainless steel tubes was not necessarily in the middle of the tube. While the cracking of batch B tubes took place predominantly in the center of the free expansion zone, i.e. in the middle of the tube, the cracks of the batch A tubes were spread relatively uniform over the tubes' longitudinal axis. Regarding the examined copper tubes, without exception, bursting occurred in the center of each tube.

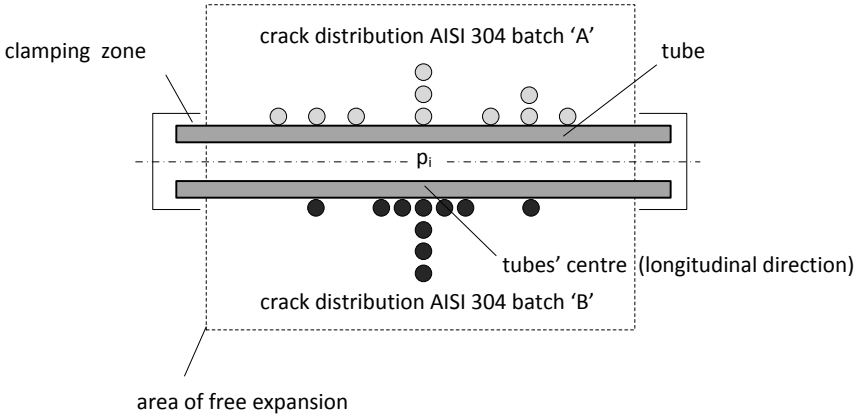

Fig. 48: Distribution of the crack formation of AISI 304 micro-tubes along their longitudinal axis (batch A above, batch B below)

Achieved forming diameters

The D_1/p_{ib} diagrams in *Fig. 44* - *Fig. 47* show the achieved forming diameters at room temperature of the micro-tube versus the applied maximum internal pressure at bursting. The established mean values are summarized in the following:

- Stainless steel AISI 304, batch A: mean outer forming diameter D_{1b} = 0.95 mm (corresponds to a relative expansion of 18.4%) with a standard deviation *s* of 5.6 µm (scatter 20 µm)
- Stainless steel AISI 304, batch B: mean outer forming diameter D_{1b} = 1.03 mm (corresponds to a relative expansion of 28.3%) with a standard deviation *s* of 20.7 µm (scatter 80 µm)
- Copper CW024A (R 200): mean outer forming diameter D_{1b} = 0.9275 mm (corresponds to a relative expansion of 15.9%) with a standard deviation *s* of 8.6 µm (scatter 20 µm)
- Copper CW024A (R 250): mean outer forming diameter D_{1b} = 0.826 mm (corresponds to a relative expansion of 3.2%) with a standard deviation *s* of 7.2 µm (scatter 20 µm)

5.5.2 Forming results achieved at variable forming temperature

As an example how the tests were accomplished, *Fig. 49* shows the curvatures of both the temperature and the forming pressure p_i of a micro-tube made of stainless steel AISI 304 batch B. In the represented case, the stainless steel specimen burst when a forming temperature ϑ_f of 350°C was reached. Similar to the curve progression of the investigated micro-tubes at room temperature, the internal pressure shows a linear increase until workpiece failure due to bursting.

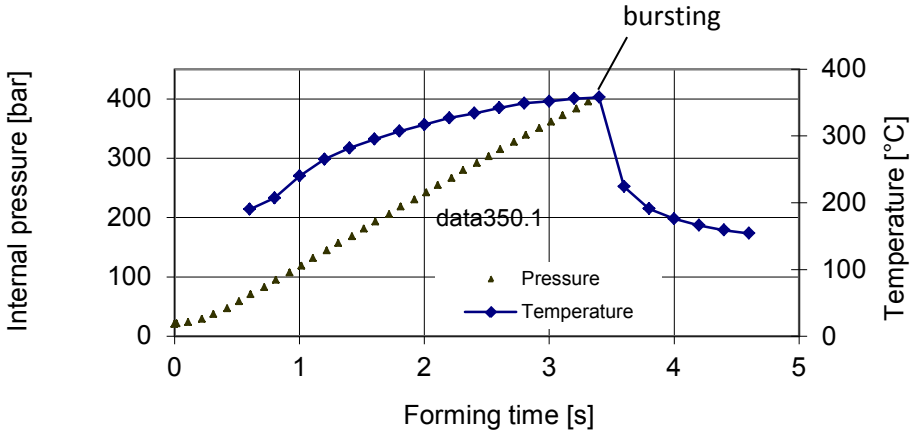

Fig. 49: Internal pressure and forming temperature versus the forming time, exemplarily shown as an example of an expanded stainless steel micro-tube made of AISI 304

The starting point of the pressure curve is the point of pre-pressurization, i.e. in the case of the stainless steel tubes at 20 bar (2 MPa). As mentioned previously, the pyrometer used for temperature measurement only offered a limited measurement range starting from approx. 150 °C. As a result, the beginning of data recording was delayed. In this example, first data could be recorded starting at above 200°C as can be seen on the starting point of the temperature graph.

Test parameters:

Stainless steel AISI 304, batch B

Tube dimensions:
L_0 = 16.7 mm
D_0 = 0.8 mm
t_0 = 40 µm

Volume flow: V_{Fl} = 0.07 ml/min.

Procedure parameters:

Laser power P_L:	2 - 6 W cw (continuous wave)
Focal length f':	50 mm
Defocussing $\Delta f'$:	4.89 mm
Laser impact:	simultaneous to pressurization
Pre-pressurization:	2 MPa

Forming results:

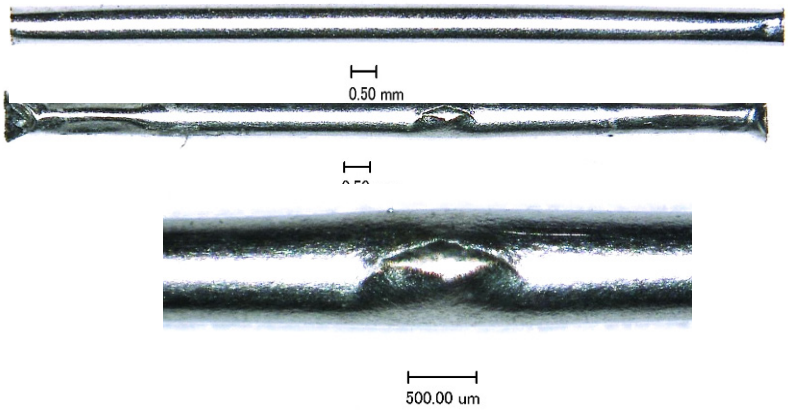

T_i: Initial tube

T_2: AISI 304 tube (batch B) formed at 350°C

T_2: Section of fracture

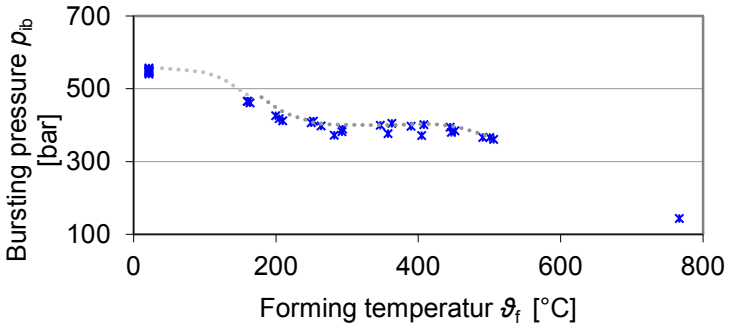

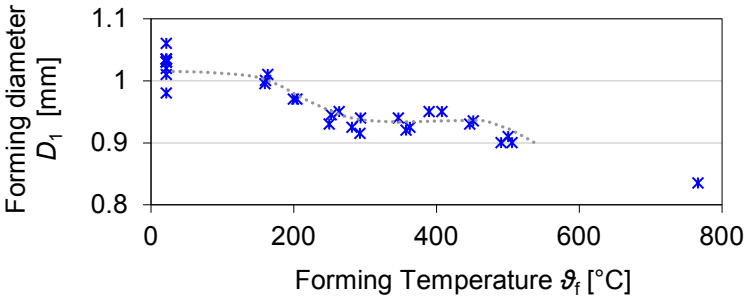

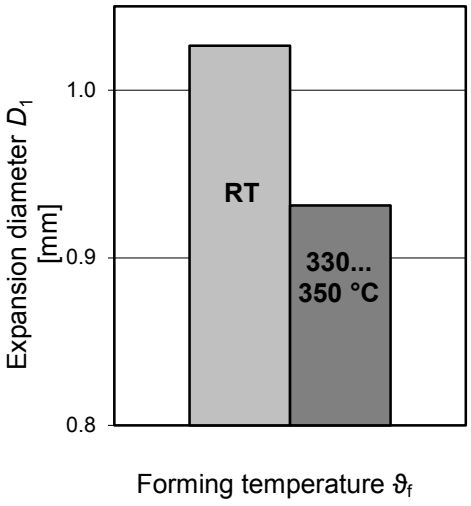

Fig. 50: Warm forming results and procedure parameters with point of fracture and achievable expansion diameters - Stainless steel AISI 304, batch B

Test parameters:

Copper CW024A, R 200

Tube dimensions:
L_0 = 16.60 mm
D_0 = 0.8 mm
t_0 = 100 µm

Volume Flow: V_{Fl} = 0.07 ml/min. (minimum set)

Procedure parameters:

Laser power P_L:	20 - 25 W cw (continuous wave)
Focal length f':	50 mm
Defocussing $\Delta f'$:	2.6 mm
Laser impact:	simultaneous to pressurization
Pre-pressurization:	9 MPa

Forming results:

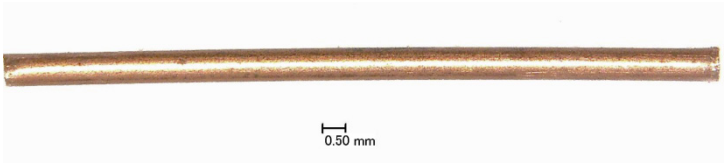

T_i: Initial tube

T_2: Copper CW024A (R 200) formed at 300°C

T_2: Section of fracture

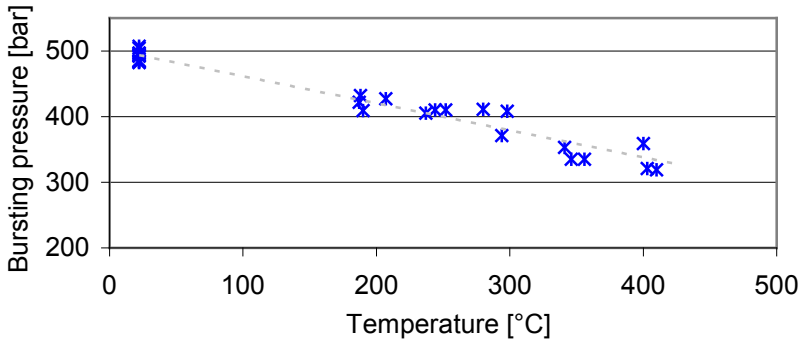

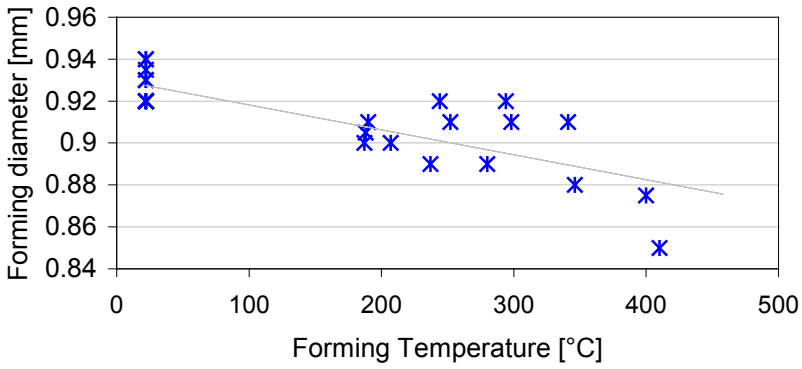

Fig. 51: Warm forming results and procedure parameters with point of fracture and achievable expansion diameters - Copper CW024A, R200

Test parameters:

Copper CW024A, R 250

Tube dimensions:
L_0 = 16.60 mm
D_0 = 0.8 mm
t_0 = 100 µm

Volume Flow: V_{Fl} = 0.07 ml/min. (minimum set)

Procedure parameters:

Laser power P_L:	20 - 25 W cw (continuous wave)
Focal length f':	10 mm
Defocussing $\Delta f'$:	2.6 mm
Laser impact:	simultaneous to pressurization
Pre-pressurization:	9 MPa

Forming results:

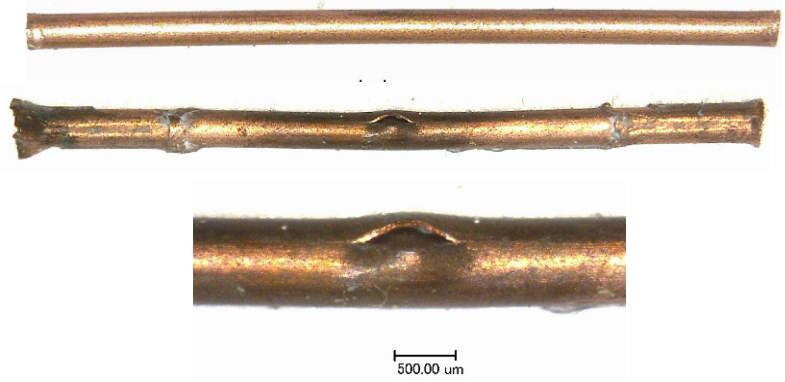

T_i: Initial tube

T_2: Copper CW024A (R 250) formed at 300°C

T_2: Section of fracture

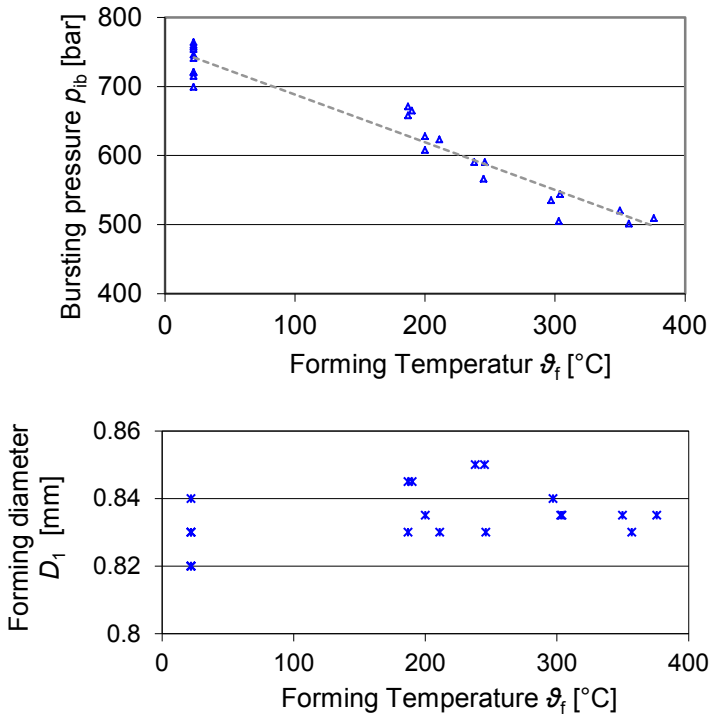

Fig. 52: Warm forming results and procedure parameters with point of fracture and achievable expansion diameters - Copper CW024A, R250

Fig. 50 - Fig. 52 show the test parameters and forming results in comparison to the variable process parameter forming temperature ϑ_f. The test parameters include the investigated material and the tube dimensions of each test series shown in the upper third of each figure. According to the test program, *Table 6*, the forming temperature was increased in each test series by steps of 50°C. The obtained values of at least three specimens per temperature step had been recorded. The correlative diagrams visualize the maximum bursting pressures p_{ib} of the corresponding forming temperatures as well as the determined forming diameters D_{1b} at the point fracture occurred.

Bursting pressure at variable forming temperature – AISI 304, batch B (test series 2)

In *Fig. 50*, the p_{ib}/ϑ_f - diagram shows the obtained bursting pressures versus the respective forming temperature of the investigated AISI 304 stainless steel tubes (batch B). The values measured at room temperature are taken from the studies of test series 1 and then placed into the diagram. Adding the values achieved at forming temperature range 150…500°C it can be seen that with an increase in temperature the curvature of the bursting pressure p_{ib} declines steadily from approximately 550 bar (55 MPa) to approximately 400 bar (40 MPa) where it roughly stays constant in a temperature range between 250…400°C. Scatter of obtained bursting pressure p_{ib} values was ~200 bar (20 MPa). Horizontal shift of each temperature measuring point (of each 50°C point/step) was approx. 20°C. After a temperature of approximately 400°C, declination of the pressure curve continued in the same rate as before the constant area between 250…400°C. The last measuring point at a temperature ϑ_f of approximately 760°C was accidentally recorded, as a result of a too high laser output power setting.

In summary, it can be determined that the mean value of internal pressure at room temperature of 549 bar (54.9 MPa) reduced to approx. 400 bar (40 MPa) at a forming temperature ϑ_f between 250…400°C which corresponds to a relative decrease of 27%.

Achieved tube expansions at variable forming temperature– AISI 304, batch B

The determined forming diameters D_{1B} are visualized versus the forming temperature ϑ_f in the second diagram, at the bottom of *Fig. 50*. It is obvious that the curvature of the expansion diameters correlate to the maximum internal pressures measured at each 50°C step when fracture occurred. A drawn average line and/or trend line resembles the course of measuring points shown in the p_{ib} / ϑ_f graph figured above. Thus, the achieved maximum expansion diameters could not be increased during laser-assisted warm forming procedure.

To be able to gain a comparative value in terms of a reduced forming feasibility at room temperature, apart from the test program ten micro-tube samples were formed at a temperature approximately in the mean range of the "temperature plateau", i.e. in the range of 330 to 350°C. The achieved forming diameters d_{1b} as well as the average value of 0.93 mm when bursting occurred are illustrated in the diagram on the right, *Fig. 50* , bottom. As one can see, this correlates to a relative expansion of 16.4%, in fact a reduction of approx. 44% compared to the achieved forming diameter obtained at room temperature.

Bursting pressure at variable forming temperature - Copper CW024A

In *Fig. 51* and *Fig. 52*, the first of the two diagrams shows the maximum obtained pressures when bursting occurred versus the forming temperature. The measurement points at each 50°C step show a slight horizontal shift as could already be observed during warm forming experiment of the stainless steel micro-tubes. The established trend lines of both the investigated R200 and R250 copper tubes show a steadily decrease. Within the investigated temperature range, the decrease seems to be linear. The vertical shift of the measuring points associated with each temperature step indicates no reduction in scatter compared to the tests accomplished at room temperature. As a result, the maximum achieved internal pressures of both investigated R200 and R250 tube materials reduced from 494 bar (49.4 MPa) and 735 bar (73.5 MPa) - both at RT - to approx. 350 bar (35 MPa) at 400°C, and 530 bar (53 MPa) at 350°C respectively.

Achieved tube expansions at variable forming temperature

The measured forming diameters D_1 of the investigated copper tube samples are represented in the appropriate graphs in *Fig. 51* and *Fig. 52*. As the R200 copper tubes still could be enlarged at room temperature to a mean expansion diameter of approx. 0.93 mm, which was a relative increase of almost 16% though its formability decreased during warm forming. A tendency towards reduced achievable forming diameters D_{1b} is recognizable. With regard to the appropriate R250 diagram, in some cases during warm forming some tubes slightly increased forming diameters. Both investigated copper tubes still show a relatively large scatter that obviously could not be reduced during the laser-assisted forming compared to cold forming investigations.

5.6 Discussion

Interpretation of the curve progression of bursting pressure p_{ib} vs. forming time t_f

Compared to results from existing research from investigations applied to macro-tubes, the inclinations of all established p_{ib}/t_f curves show a distinctive difference. From literature, i.e. [87,89] it is known that an instantaneous pressure corresponding to the beginning of tube yielding, the volume of the tubes starts to increase rapidly. As a consequence, internal pressure drops which can be identified typically as a decrease in the curve progression. Thus, it is possible to identify the yielding point of the investigated macro-tube material with the help of the bulge test. However, the results have shown that for down-scaled FHB processes it is not possible to identify the yielding point of the investigated micro-tube material due to the fact that the bulging of the tube wall is too low in relation to the small tube volume. Perhaps a lower flow rate of the pump would have solved the problem.

Large range of dispersion in forming time

The forming time when bursting occurred shows a comparatively large range of dispersion. It can be seen from the four diagrams established at room temperature that

the end of forming time approximately scattered in a range of 50% relative to its determined mean values. It was assumed that unequal amounts of remaining air inside the tubes could be significant reasons for the difference in forming time. Due to the compressibility of air probably different time to build up internal pressure was needed. In any case the time shift is not a critical aspect of the burst test but its influence needs to be noted.

As mentioned previously, in two cases of each investigated stainless steel batch the curve progressions showed a curved progression due to leakage. It was assumed that leakage was probably caused by an unevenly tightening of the lock nuts of the sealing punches so that the clamped tube was moved in longitudinal direction. So a circular contact line could not be properly achieved to produce localized yielding and thus the sealing of the tubes. Another case of leakage could be observed in line with the R200 tests. Just at the beginning of pressurization leakage occurred, cf. *Fig. 46* p_i/t diagram. However, after a time delay ΔT of approximately one second the according curvature continued with a linear progression until workpiece failure from bursting occurred.

Starting time of laser impact

Because the forming fluid began to boil when the temperature was raised over 100°C due to laser impact, the laser energy was introduced with a specific time delay after the tubes were pre-pressurized to $p_{i,\,start} = 20$ bar during the laser-assisted warm forming tests. The laser starting point was not time-dependent but pressure dependent. However, in most cases, the maximum bursting pressures were obtained at different forming time. It was assumed that once again a remaining quantity of air inside the pre-filled tube was the probable reason.

Interpretations of temperature scatter (around each 50°C step)

Fig. 49 illustrates the correlation of the internal pressure p_i and the forming temperature, and the correlation of the bursting pressure and forming temperature at work-

piece failure (bursting). As the example of the AISI 304-b shown in this figure, bursting pressure p_{ib} of ca. 400 bar (40 MPa) was achieved after approx. 3.5 seconds, which correlated to an increase in temperature to approximately 350°C. Due to different temporal bursting times observed during bulging tests at room temperature, cf. *Fig. 44* - *Fig. 47*, all p_i/t curves differ in their angle of inclination. Thus, both the pressures as well as the temperature curvatures of each repeated test differ in their intersection points. It is assumed that this is the reason for the scatter around the aspired temperature values, cf. p_i/ϑ_f and D_1/ϑ_f diagrams in *Fig. 50* - *Fig. 52*. It was not possible to repeat the maximum achievable forming temperature from test to test in spite of unchanged laser settings.

Plateau at 304b warm forming similar to plateau of 304 yield curve

As mentioned previously, during warm forming experiments regarding the AISI 304-B batch a temperature measurement ϑ_f of approx. 760°C was accidentally recorded. If establishing an average line (trend line) in the p_i/t diagram represented in *Fig. 50* which involves this measuring point the curve progression is similar to the AISI 304 flow curve with its plateau of constant yield stress between ϑ_f of approx. 250°C and 400°C, cf. *Chap. 2.2.3, Fig. 11*. Similar to the flow curve an area of constant maximum internal pressure p_{ib} matches the same temperature range.

Further on, *Fig. 50* lower diagram shows the forming diameter/temperature ratios D_1/ϑ_f. The curvature of the trend line that can be established is also similar to the AISI 304 flow curve.

General remarks on warm forming of copper tubes

Due to the reduced strength of the copper micro-tubes compared to the stiffer stainless steel tubes, special attention must be paid to fix clamping. In a few cases, due to tightening of the sealing locknuts the tube was setup under minimal compressive stress in its free forming area, so the influence of laser heat caused early process failure due to buckling of the tube. Two reasons can be found for this; first, volume dilatation caused by the impact of laser heat in combination with the compressive

stresses caused a bending moment; secondly, stiffness of the material due to heat impact was reduced so that the compressive stresses caused buckling of the softer material. Unexceptional this phenomenon happened to copper tubes, which compared to the stainless steel tubes, featured a low initial strength. Consequently, the initial length L_0 of the copper tube specimens had to be shortened compared to L_0 of the tubes investigated at room temperature to avoid buckling. The changed tube length L_0 can be found as one of the test parameters on *Fig. 51* and *Fig. 52*, top left. As one can see in the microscope pictures in *Fig. 51* and *Fig. 52*, the warm formed tubes still show a slight deflection in comparison to the copper tubes formed at room temperature and to the AISI 304 tube expanded at 350°C, *Fig. 46*, *Fig. 47* and *Fig. 50* respectively.

Achieved relative expansion ratios of micro-tubes compared to ratios of macro-tubes

In comparison with expansions of macro-tubes made of the here investigated material, micro-tube expansions attained a considerably smaller relative expansion ratio ε_b. Expansion tests of such macro-tubes, for example conducted by [67] with tubes with D_0 = 57.2 mm, t_0 = 0.6 mm and L_0 = 203.2 mm or by [90] with tubes with D_0 = 60 mm, t_0 = 1 mm and L_0 = 240 mm, showed an achievable ε_b in the magnitude up to 0.54. The reduction in formability is most likely to be attributed to the down-scaling of the hydroforming process. In general the tendency of the here developed results correspond also to findings summarized by [91], concerning sheet forming under tension, that the lower the ratio t_0/d_k of the wall thickness t_0 to grain size d_k the worse is the formability of the material. Nevertheless it must be noted that regarding both copper micro-tubes the R200 tube with a significantly lower t_0/d_k ratio show a slightly higher relative expansion ratio compared to the R250. It is assumed that probably due to differences in anisotropic behaviour R200 tubes could more easily expand in radial tube direction compared to R250.

Comparison of the relative expansions: Flaring test - free bulging test

One of the most important issues that was discovered during the study was the comparison of the relative expansions of the micro-tubes achieved in the free bulging tests vs. the conical flaring test. All the results can also be found in the according chapters 4 and 5. For clarity the results are compared against each other in *Fig. 53*. The average values of the achieved ε_b of both the stainless steel micro-tubes delivery batch A and B differ in a range of 35% to 50% from the average expansion ratios obtained by the mechanical flaring tests at room temperature, and at a forming temperature of 300°C respectively.

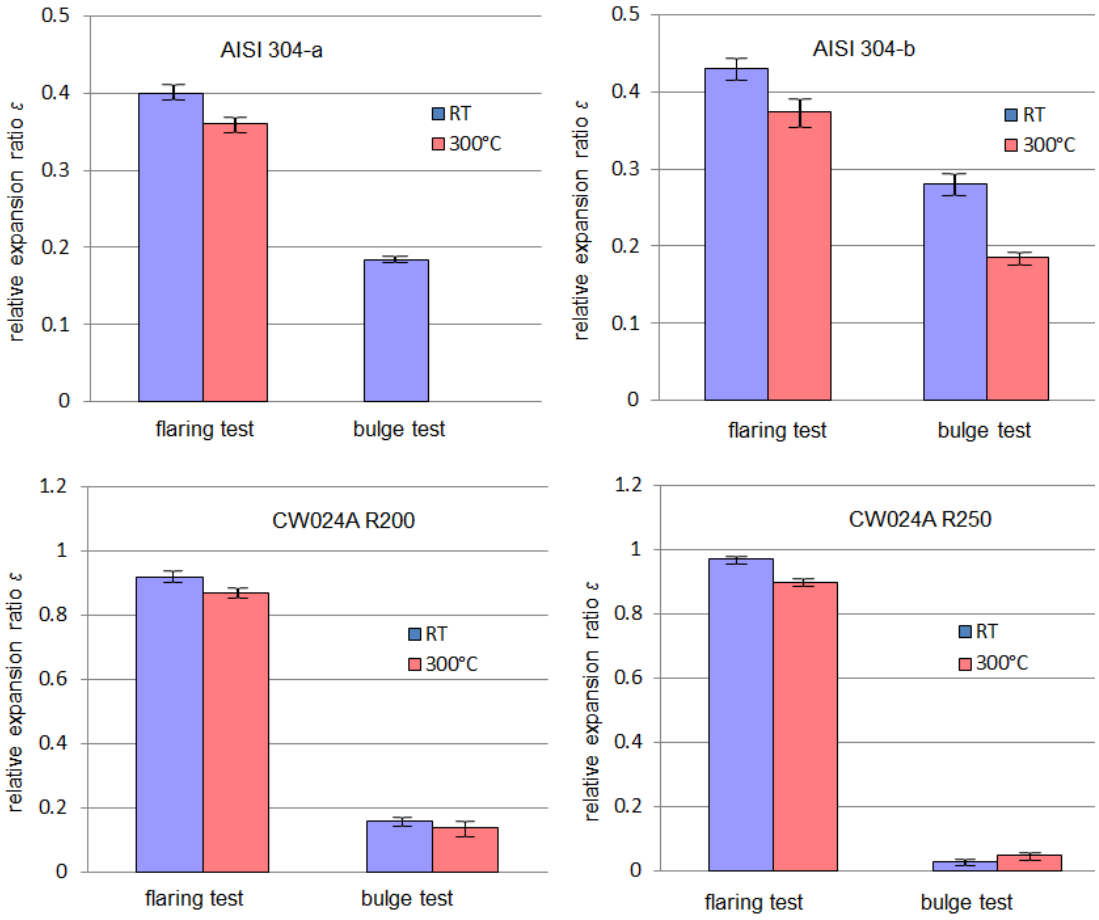

Fig. 53: Relative expansion ratios for hydraulically bulged stainless steel and copper micro-tubes in comparison with results obtained from conical flaring tests

However, regarding the investigated copper micro-tubes the difference between obtained forming diameters was even more significant. By applying the mechanical flaring test, the diameters of both the R200 and the R250 almost doubled compared to their initial tube diameters at room temperature as well as at a forming temperature of 300°C. On the contrary, the examined micro-tubes only expanded in the range of 3% to15% during hydraulic free bulging.

It is assumed that for down-scaled testing methods factors like tribology play a more important role than in macro testing methods and the reduced ratio of tube wall thickness and diameter to the grain size of the tube material have a significant influence on the forming results.

In summary, it can be stated that at least within the investigated tube materials and dimensions respectively, compared to macro-tube testing methods for tube hydroforming processes the flaring test cannot be used for a safe prediction of possible expansion diameters of the micro-tubes. Though, the bulge test is able to deliver adequate material properties for the THF process and thus would be the more accurate method to test different tubes and materials.

5.7 Conclusion

As already mentioned, todays' hydroforming processes generally use a mathematically empirical formula for the prediction of suitable process loads to determine the hydroforming operations.

Thus, one objective of the bulge test was to see if the existing theoretical correlation, *Eqn.* (7)

$$p_{ib} = \sigma_{UTS} \frac{2t_0}{D_0 - t_0}$$

which was proved in Klaas' dissertation [28] to be applicable for conventional macro-tubes can also be reliably applied to micro-tubes in a down-scaled process. As

already mentioned in *Chap. 2.2.2.4 Prediction of forming loads*, the formula enables the prediction of the bursting pressure p_{ib} for a known tensile strength σ_{UTS} of an analysed tube material.

For comparison, p_{ib}/σ_{UTS} ratios of the achieved results were added into the diagram, *Fig. 54*, which also contains the ratios of macro-tubes with outer diameters larger 40 mm analysed by [28] and [34]. It is obvious that all investigated micro-tubes do not significantly differ more from the theoretically calculated ratio (curvature) than the macro-tubes. Thus, with the obtained results it could be verified that *Eqn.* (7) can also be applied in the micro-scale as a first approximation, at least with regard to the examined stainless steel and copper micro-tubes.

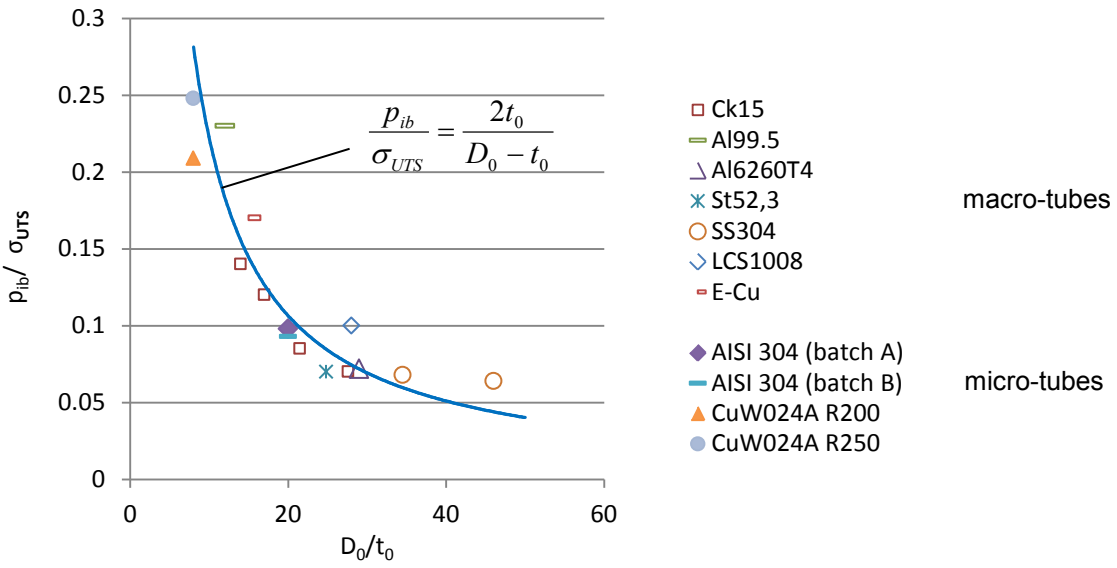

Fig. 54: Ratio p_{ib}/σ_{UTS} of micro- and macro-tube expansions (incl. results of macro-tubes developed by [28] and [34])

With regard to the development of a micro-hydroforming machine, especially to the determination of forming tool dimensions it is necessary to know about the forming abilities of the micro-tubes to be expanded. In comparison to the simpler flaring test, the bulge test could clearly identify achievable expansion diameters of the investigat-

ed micro-tubes. Thus, with regard to the tool design the required information about maximum cavity widths of the die could be provided.

It can be concluded that from engineering or manufacturing prospective one now has a much better understanding of the principles and behaviours present in micro-tube hydroforming. With what was studied it is now possible with confidence to begin the development of a successful micro hydroforming machine.

As for the laser assisted hydroforming process one has learned that though in many other methods of micro forming heat or laser assistance can be beneficial, at this time one has not seen satisfactory results that would warrant the added complexity to the first micro-tube hydroforming machine.

CHAPTER 6

FORMING MACHINE DEVELOPMENT

6.1 Introduction

In this chapter, the results regarding the development of several micro-hydroforming machine concepts are presented. To specify parameters for the layout and design of the machine concepts, a demonstrator part "camera shaft", was taken as the exemplary component that shall be producible with the final prototype machine, *Fig. 55*.

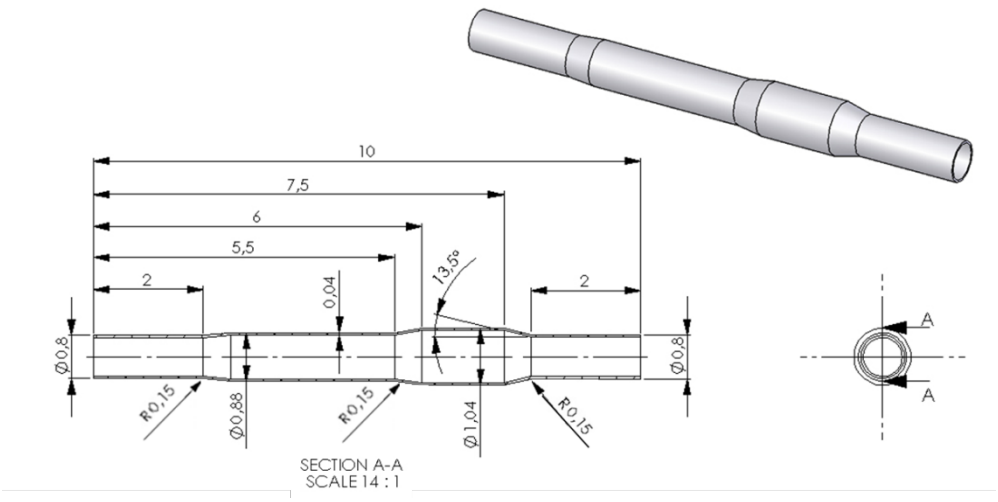

Fig. 55: Demonstrator part "camera shaft"

Requirements for the conceptual design of the micro-hydroforming machine components based on the micro-dimensions of the demonstrator and/or derived from the previous studies are documented in a specification sheet (see *Chap. 6.2*). The specification sheet contains functional requirements, like internal pressure, forces, strokes, speeds, etc. as well as structural design considerations, like precision, portability, stiffness, working space, accessibility, etc.

The development of the conceptual machine models was subdivided into the development and evaluation of essential subassemblies and functions of a hydroforming machine, shown schematically in *Fig. 56*. Emphasis was on (a) principle of press frame concepts, (b) the development of a tool unit including die geometry, principle of sealing mechanism and studies on sealing punch geometries (c) concept study of closing mechanism, (d) layout of high pressure system and (e) design and functions of control system and sensors.

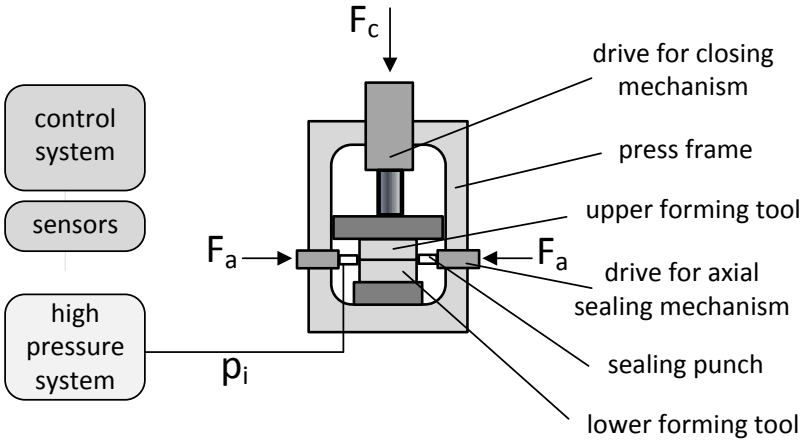

Fig. 56: Elements and functions of hydroforming machines

Due to the comparatively high forming loads (up to 4,000 bar internal pressure p_i), investigations on elastic deflection of forming tool elements and machine frame components resulting from these loads are particularly of interest when high accuracy of the formation is required. Thus, investigations concerning these issues were accomplished by use of FEA.

State of the art

At present, hydroforming presses exist solely for the manufacturing of conventional components, predominantly for the production of automotive parts [36]. Tubular components produced by these machines are characterized by cross section widths

above ca. 20 mm up to ca. 200 mm and larger, and lengths up to 3 m and more. Several new press concepts have been developed in the past for tube as well as for sheet hydroforming aiming at improvements regarding cycle time reduction by optimised movement of dies for loading and unloading the workpieces and regarding cost reduction by simplified press components, e.g. [92-95]. They basically differ in either the structure of press frame or principle of slide movement and the locking mechanism used. The following two basic principles of hydroforming presses are predominantly in industrial use today [36]:

(a) Traditional hydraulic presses have one or more large cylinders which both move the slide, carrying the top die, and apply the closing force during the hydroforming process, *Fig. 57*a. There also exist industrial used systems with two press slides in one frame which enable a more flexible use of the hydroforming technology [93];

(b) Presses with a drive for a fast movement of the top die and with a mechanical locking or stop of the slide during the forming process, *Fig. 57b*. One or more short stroke cylinders are used to apply the closing force. These short stroke cylinders can be located in the press bed or in the press slide. The direction of fast die movement may be similarly directed or perpendicular to the direction of the closing force applied by the short stroke cylinders.

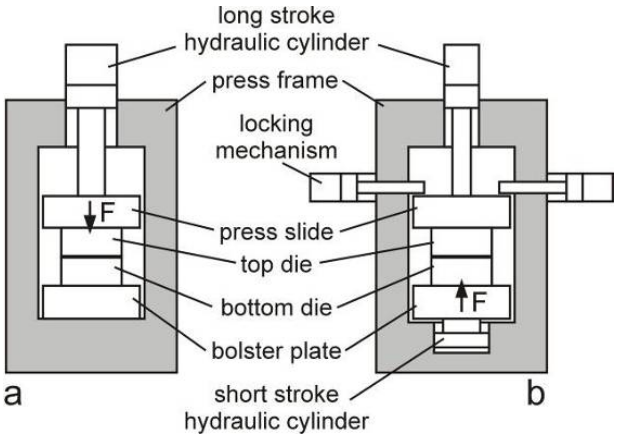

Fig. 57: Principles of common hydroforming press concepts for industrial production [36]

Due to the high amount of required vertical closing forces (up to 80,000 kN or more) and axial feeding forces (up to 4,000 kN), the drives to apply these loads are predominantly based on hydraulic cylinders. Also, the pressure intensifiers to pressurize the formed tubular component are hydraulic cylinders, increasing the pressure up to about 2,000 bar and in certain cases up to 4,000 bar [36]. A decisive reduction of cycle time was achieved during the past few years due to the reduction of filling time of the tubular component with the pressurizing media by using quick-filling-systems [94]. Depending on the machine size and the required machine stiffness, the press structure consists of three different frame types. Firstly, of a column frame with a top plate, a press bed and two or four cylindrical columns which also are used as guiding for the press slide, *Fig. 58* (left). Secondly, *Fig. 58* (middle) shows a split frame which can consist of a top plate, a press bed and either two side walls or four side columns (no guiding function of the press slide). The last frame type is a one-piece frame design, *Fig. 58* (right).

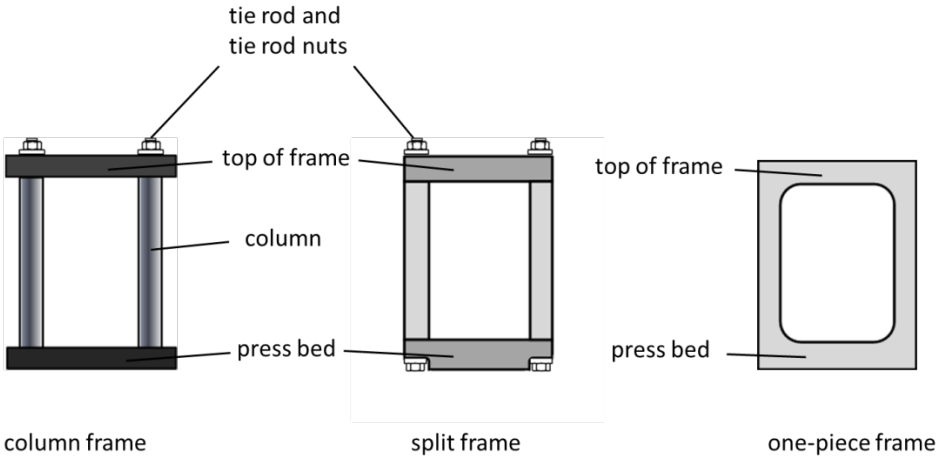

Fig. 58: Examples of press frames for hydroforming machines

Control systems for industrial hydroforming machines are based on conventional programmable logic controller systems, customized for the press control. Common sensors are used for measuring strokes, speeds and forces of all moved axes and for measuring pressures of the hydraulic system and the forming pressure.

6.2 Specification on the machine design

The following summarizes the main requirements for a hydroforming press and THF tooling [34]:

- Appropriate die closing force
- Appropriate bed size to hold the dies
- Adjustable/movable axial punches with computer controlled positioning
- Adjustable/movable rams for counter forces with free and position control
- Optional: automatic workpiece handling
- Appropriate internal pressure (2000 to 4000 bar or more) and fluid pumping capability with tight control
- High strength of the tooling against stresses due to large internal pressure and axial loading
- Good surface finish of the dies to minimize friction and increase formability
- Flexibility by interchangeable die inserts
- Good guiding systems (close tolerances, minimized clearance)

Based on these general requirements and on the findings of the previous studies as well as on the micro-dimensions of the demonstrator part (*Fig. 55*) the specifications of the micro THF prototype machine are defined in the following table:

	characteristic	**amount**	**remark**
1	***press frame***		in general: high stiffness required to minimize deflections/distortions
1.1	die space	min. 100 mm x 100 mm x 100 mm	width x depth x height
1.2	admissible deflection		to be defined
2	***drive for press slide***		closing of tooling during hydroforming (vertical)
2.1	principle		to be defined
2.2	control		most likely cascade control: transition and

			pressure (subordinate control loop)
2.3	max. force	~16500 N	acc. to *Eqn. (4) and Eqn. (6)* and the dimensions acc. to *Fig. 55*
2.4	max. stroke	120 mm	derived from the die space
2.5	max. speed	≥ 10 mm/s	depending on the aspired cycle time of ca. 6 parts per minute
3	***drives for axial sealing punches (2 pieces)***		sealing of tube ends, material feeding, fixing of hydroformed part during opening of tooling; mounted to bottom die
3.1	principle		to be defined
3.2	control		transition controlled, amount of displacement as a function of time independent control for each punch
3.3	positioning accuracy	+/- 0,015 mm	depending on the precision of axial drives and on clearance of guiding
3.4	max. force	800 N	derived from the demonstrator part dimensions acc. to *Fig. 55* an applied sealing system, cf. *Table 11*
3.5	max. stroke	3 mm	
3.6	max. speed		to be defined
4	***ejectors***		not used (lifting of part most likely initially manually)
2.5	***pressure intensifier***		filling and pressurizing the workpiece, mounted to one of the sealing punches to simplify high-pressure-piping the pressurizing medium is filled into the initial tube through a hole of one of the sealing punches; the air within the part will discharge through the gap between the opposite punch and the tube end
5.1	principle		to be defined
5.2	control (accuracy)	+/- 5 %	pressure controller, amount of pressure as a function of time
5.3	max. pressure	4000 bar	acc. to *Eqn. (6)*, *Table 3 and* the dimensions acc. to *Fig. 55*
5.4	volume flow	ca. 0.05 to 10	to be defined

		ml/min	
6	***pressurizing media***		(forming fluid)
6.1	type		oil-water-emulsion or solution
6.2	amount	ca. 2 ltr.	storage tank (without recirculation)
6.3	temperature equalization	20°C +/- 1°C	necessary to obtain a constant medium viscosity
6.4	filtration	50 µm	filter cartridge
8	***control system***		programmable solution: position-controlled, pressure-controlled or vs. time
	general specifications		
	assembly and disassembly		needs to be easy (as the machine is a prototype; improvements (parts exchanges) of the machine should be done easily)
	weight		lightweight as machine should be "portable"

Remark: "to be defined" means, the feature has been defined during or after the design studies described in this chapter

Table 9: Specification sheet of the THF prototype machine to be designed

6.3 Press frame concepts

In order to design a suitable press frame, different concepts had been created, analysed and evaluated. The developed conceptual models result from studies which had been conducted and from the design work which had been optimized with the assistance of numerical analysis.

Based on the functional requirements and structural design considerations expressed in *Chap. 6.3.1.,* four frame concepts described in *Chap. 6.3.2 Design studies*, were assessed.

6.3.1 Requirements

The die space of the frame should be large enough to contain relevant components of the forming tool. Furthermore exchange facilities of a tool must be given. To achieve this, an adequate stroke of the press drive must be taken into account. Regarding both axial drives and part handling (insertion of the initial micro-tube and removal of the final part) the frame has to include sufficient accessibility.

Deflections, caused by any stress during hydroforming process, must be controlled within a few microns range to obtain a high accuracy and a reproducibility of the components formed. That means, the stiffness of the frame parts must be high enough to endure the forces generated during the process.

The following design and performance-evaluation criteria were considered in the design of a micro-hydroforming prototype machine: stiffness, size, economic design and costs. Typically, the evaluation step involves detailed calculation of the performance of the design by using an analytical model. ABAQUS-software was used to carry out FE-simulations of loaded frame components. The dimensions of the critical elements of the frame were determined on the basis of the forming loads that are expected to be present. These dimensions had been based on keeping the nominal closing force of a maximum of 16.5 kN. The maximum closing force was determined using *Eqn.* (4).

Stiffness/Rigidity

Stiffness is defined as the ability of a designed structure to withstand loads against deformation and displacement in structure. The forming machine frame must meet these requirements to guarantee high quality of the hydroformed part. The frame should be able to withstand an approximate load of 16.5 kN in the vertical (z-axis) direction. Stiffness of the forming machine frame is generally of utmost importance for the high precision/accuracy requirement in micro technology.

Size

The size of the forming machine depends mainly on the required die space, the stroke and the size of the actuator for tool closing, space required for handling and maintenance of the machine parts and the formed component. The determined stroke for tool closing and opening is 120 mm. Another important consideration in the design is the “feeding” system. Main aim was to design a robust and compact structure. Above all, it has to be as small as possible to make it "portable" and to reduce weight.

Costs

Costs remain important criteria in all engineering designs. The following costs were considered: material, manufacturing, human cost and software.

Economic design

Flexibility and production time are important criteria in manufacturing. In this study, through the economic design of the forming machine frame, the intention was to achieve a flexible, time and cost saving system while still considering the functional and the total life cycle factors.

Functional requirements were that the frame has to be satisfactory and its design has to meet the required performance specifications. The performance specifications are a major task in problem definition.

The following specifications were considered:

- the frame should be easy to manufacture at acceptable cost
- assembly and disassembly of the frame should be easy and fast to save production time and for transport purposes
- the frame structure should be simple and easy to be assembled and disassembled without errors

- the frame structure should allow for the changing of machine components and forming equipment
- the frame structure should be designed for easy inspection and maintenance of forming machine components

6.3.2 Design studies

Based on the listed requirements, following four different frame concepts were developed as illustrated in *Fig. 59* and *Fig. 60:*

- Concept 1: Two column frame
- Concept 2: Four column frame
- Concept 3: C-frame
- Concept 4: Split frame

Concept 1: Two column frame

As shown in *Fig. 59* (left) the frame for this first concept consists of a top plate which will carry the drive to move the slide plate, two cylindrical columns (linear shafts), a slide plate guided by these columns for the movement of the top die, and a bottom plate to carry the bottom die. The vertical drive for the slide plate, and the top and bottom die are not shown in this figure.

As discussed, the most important decision-making criteria are: stiffness, size, economic design and costs. The advantage of this concept is its simplicity. However, a forming machine based on this concept provides a poor stiffness against torsion.

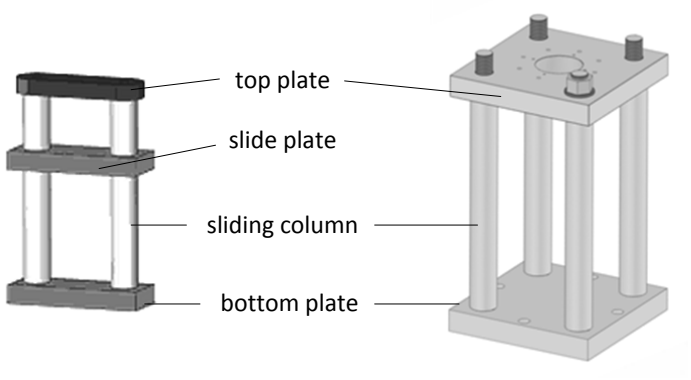

Fig. 59: Column frames: Concept 1, two column (l.) and Concept 2, four column frame (r.)

Concept 2: Four column frame

Similar to concept 1, this concept is also based on a column design, though now four instead of two cylindrical columns are used to connect bottom plate and top plate, *Fig. 59* (right). The four column frame is stiffer than concept 1, in particular regarding the inclination of top and bottom plate of concept 1 under non-concentric loads (loads outside the plane between the two columns). However, the stiffness against torsion is worse compared to the split frame, below, concept 4. Furthermore, column-design requires larger top plates and bottom plates in comparison to closed-frame constructions. Hence, a design with comparable deflections requires more material and with that will incur higher costs to implement this concept. Also the weight of this system will be higher which is contrary to the economic design evaluation goals.

Concept 3: C-frame

Fig. 60 shows a concept with a double-C-frame which carries a top plate and a bottom plate. This concept offers the advantage of a good accessibility to the die space. However, a major problem with this concept might be the inclination of the top plate and the bottom plate under load. The small stiffness against side forces could be in-

creased by mounting shear walls on the backside (in the top and bottom area) of both C-shaped side walls. That way, the accessibility would not be affected.

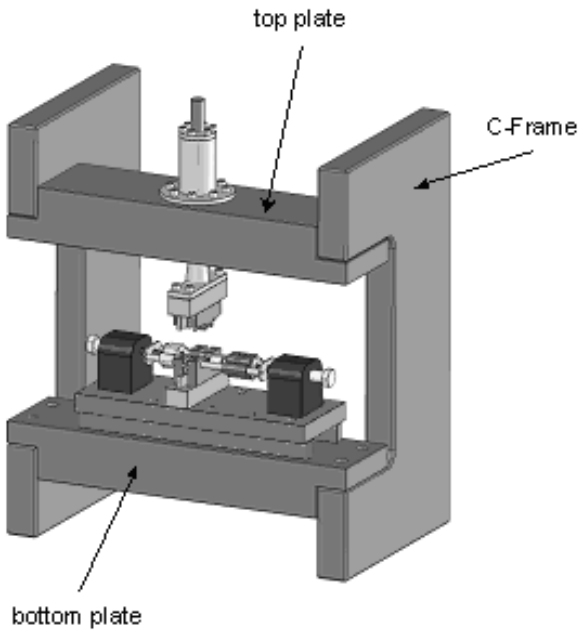

Fig. 60: 'C-frame' with two C-shaped side walls

Concept 4: Split frame

This split frame concept consists of a top and a bottom plate with two side walls, Fig. 61. It offers the advantage of an almost unrestricted accessibility to the die space from all sides due to its window-like O-shaped side walls.

The frame structure seems to be more robust than the one of the other concepts and it is assumed that this concept has the highest stiffness.

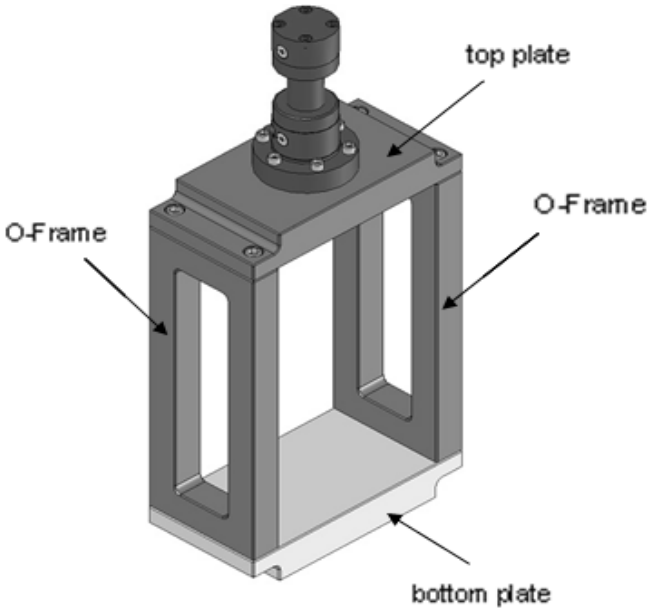

Fig. 61: 'Split frame' with two O-shaped side walls

6.3.3 Finite Element Analysis of the press frame components

To attain more information about frame stiffness, deflection, declination etc. concept 3 and concept 4 were further analysed by means of finite element method. The figures *Fig. 62* and *Fig. 63* present results of both frame components for concept 3 and 4 to determine the maximum strains, stresses and distortions under the influence of the maximum press load during the hydroforming process. The commercial FEA tool ABAQUS was used to perform the simulations.

Fig. 62 and *Fig. 63* also illustrate prepared symmetrical and half-symmetrical models of the frame components analysed. As a result, both frames investigated show an identical deflection of the centre of top plate to bottom plate which is about 2.5E-5 mm. However, the deflection of the C-frame consists also in an inclination of top plate and bottom plate of about 0,003°.

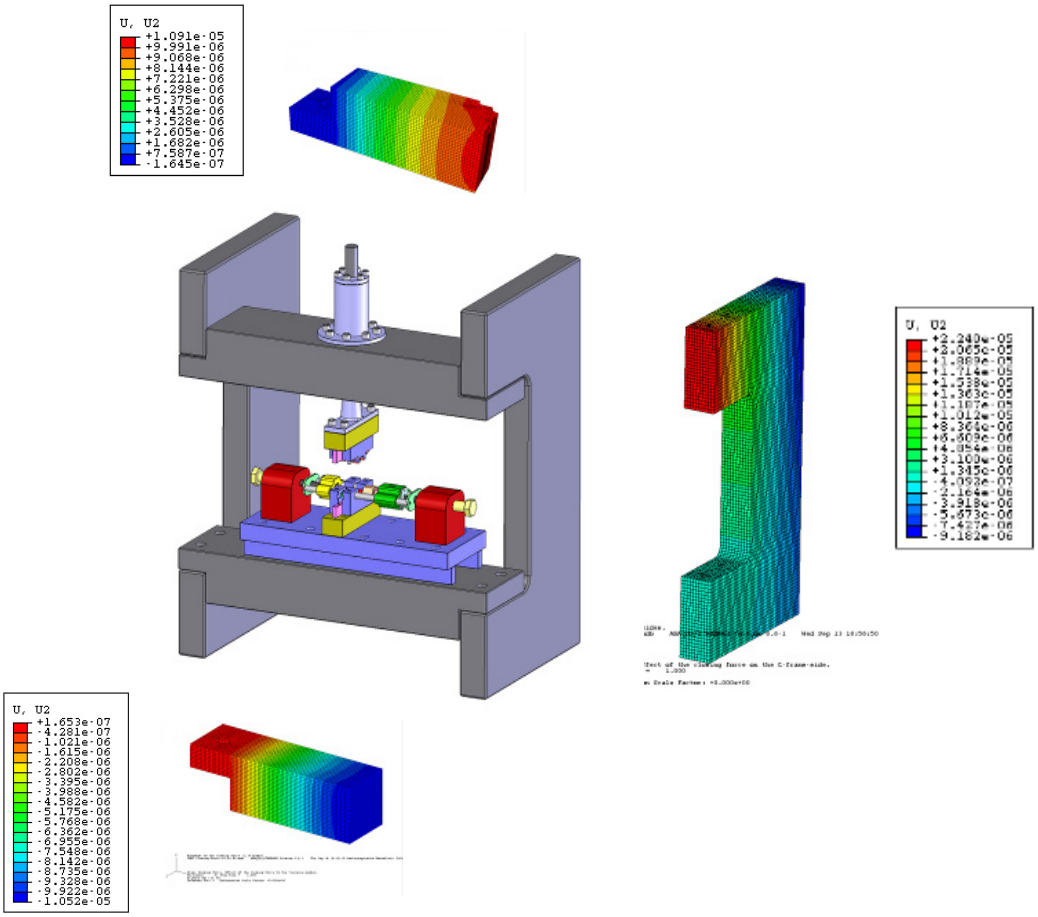

Fig. 62: FE simulation of the C-frame concept

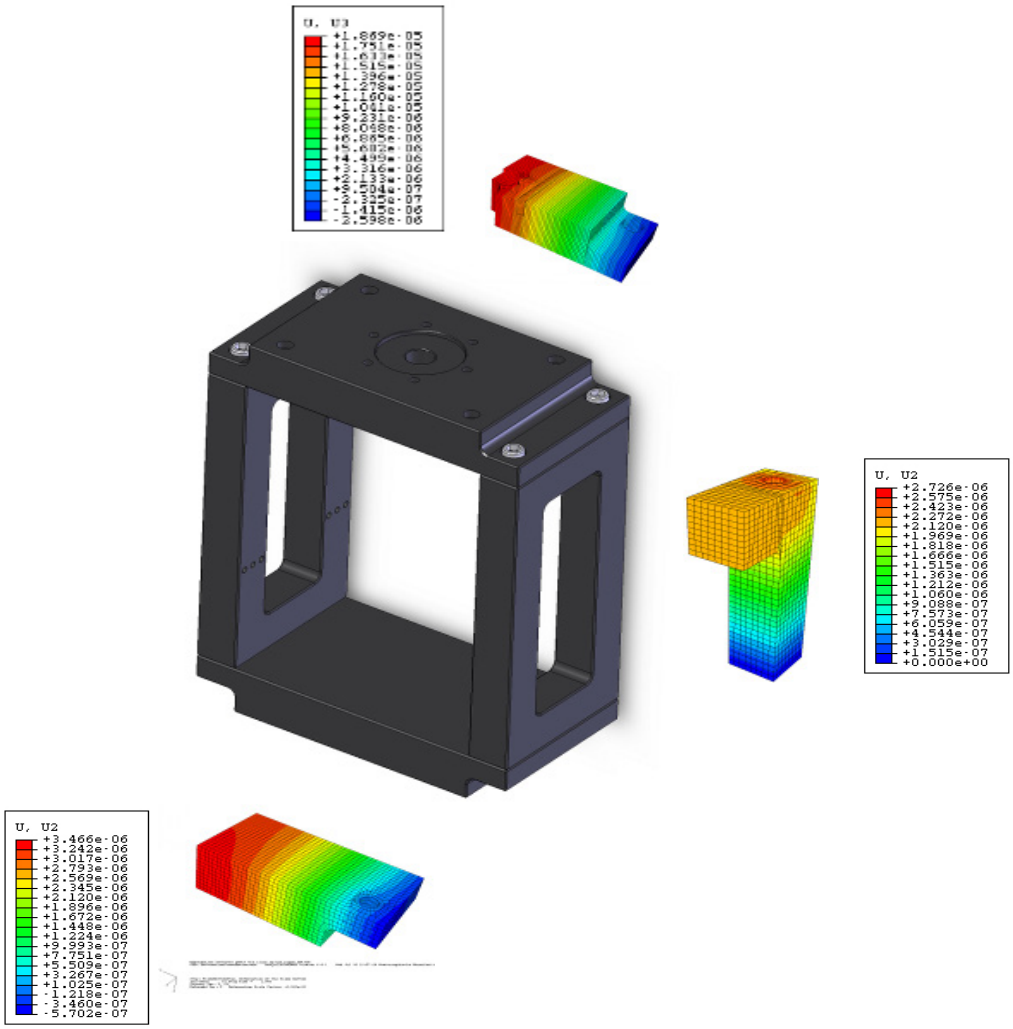

Fig. 63: FE simulation of the split frame concept

6.3.4 Conclusion - choice of the frame concept

The overall satisfactory points in a decision matrix were used as a basis for deciding which of the concepts is most suitable for the design of the frame structure. The split frame of concept 4 has the highest overall satisfactory points. This explains the deci-

sion to adopt this concept as the model structure for the frame design of a first prototype machine in this study.

	Two column frame	Four column frame	C-frame	Split frame
Stiffness/Rigidity	3	4	3	5
Size	4	4	3	4
Economic Design	4	4	5	5
Costs	4	3	2	3
Accessibility	1	3	4	3
Overall	**16**	**18**	**17**	**20**

Rating	Description
5	Complete satisfaction: objective satisfied in every respect
4	Considerable satisfaction: objective satisfied in the majority of aspects
3	Moderate satisfaction: balance between complete satisfaction and no satisfaction
2	Minor satisfaction: objective satisfied to a small extent
1	Minimal satisfaction: objective satisfied to a very small extent

Table 10: Decision matrix for the forming machine design

6.4 Forming tool module

For fundamental investigations of the micro-hydroforming process, a forming machine had been designed as a module could be used for investigations into free expansion of micro-tubes and also used on initial tests regarding the hydroforming of tubes in a die cavity. The idea was that the module to be manufactured can later be integrated into the close-to-production prototype machine.

In the following sub-chapters, considerations on functionality, tool design and tool deflections are presented. Concepts of major components of the module including the sealing punches with the axial drives and the die geometry are described and evaluated further on.

6.4.1 Design considerations and requirements to a flexible tool

It was particularly aimed at designing a die (tool) which can quickly be exchanged enabling the manufacture of various shaped micro parts. A large variety of hydroformed component shapes manufactured in conventional industrial production [36] has been taken into consideration. Thus, to design a flexible tool, from these 'macro' applications and from miscellaneous published classifications of hydroformed component shapes, e.g. [91,96], the following four shape-specific situations and its requirements to the tool design have been derived:

Situation 1 (schematically represented in *Fig. 64*): The tool must allow the forming of components having

- varying component shapes / cross sections
- equal component lengths *L*
- straight geometries (direction of both sealing punches in the same longitudinal axis)

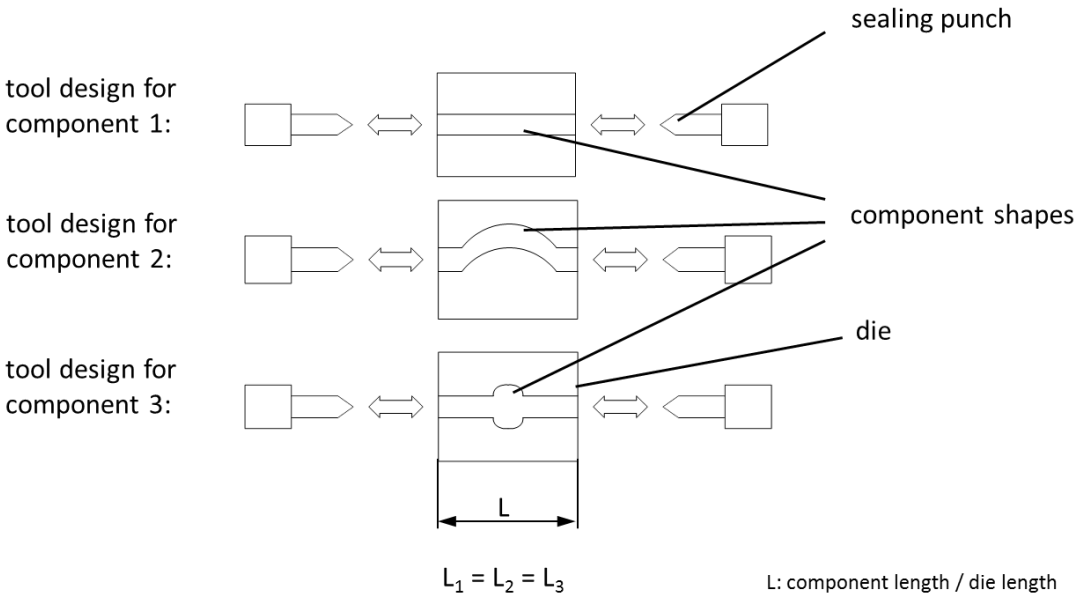

Fig. 64: Schematic of the flexible tool design according to 'situation 1'

The requirements to enable the flexibility of the hydroforming tool for situation 1, *Fig. 64,* consist of:

- The changeability of shape-specific die components (e.g. single die inserts or the complete forming tool with its basic die and shape specific inserts)
- The changeability of axial sealing punches for various tube diameters (depending on the used principle for tube ends sealing)

Situation 2 (schematically represented in *Fig. 65*): The tool must allow the forming of components having

- varying component shapes / cross sections
- varying component lengths *L*
- straight geometries

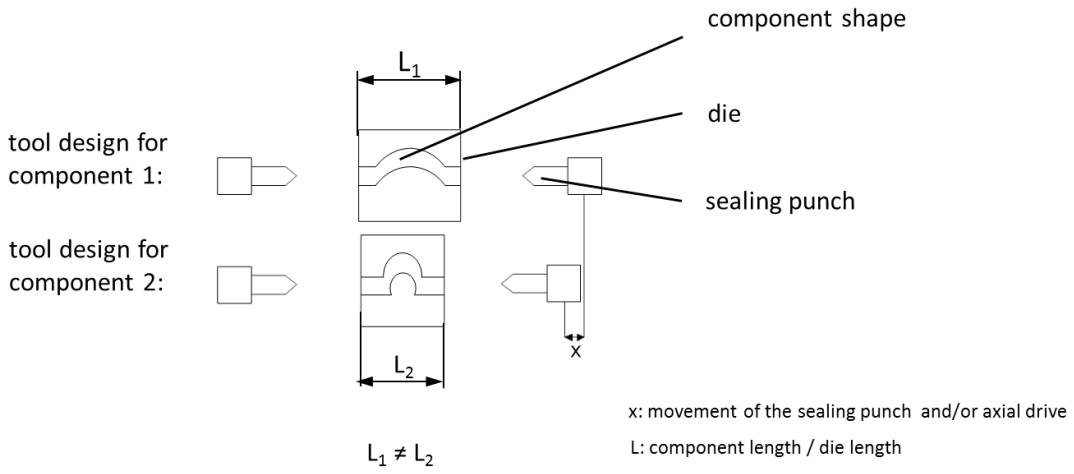

Fig. 65: Schematic of the flexible tool design according to 'situation 2'

The requirements to enable flexibility of the hydroforming tool for situation 2, *Fig. 65,* consist of:

- The changeability of shape-specific die components (e.g. single die inserts or the complete forming tool with its basic die and shape specific inserts)
- The changeability of axial sealing punches for various tube diameters (depending on the used principle for tube ends sealing)

- The adaptation of axial punch position (movement by the amount *x*) to the component length, and positioning of drive units respectively

Situation 3 (schematically represented in *Fig. 66*): The tool must allow the forming of components having

- varying component shapes / cross sections
- varying component lengths *L*
- bent part geometries (bent *only* in 'x-y-plane' => different direction of the sealing punches)

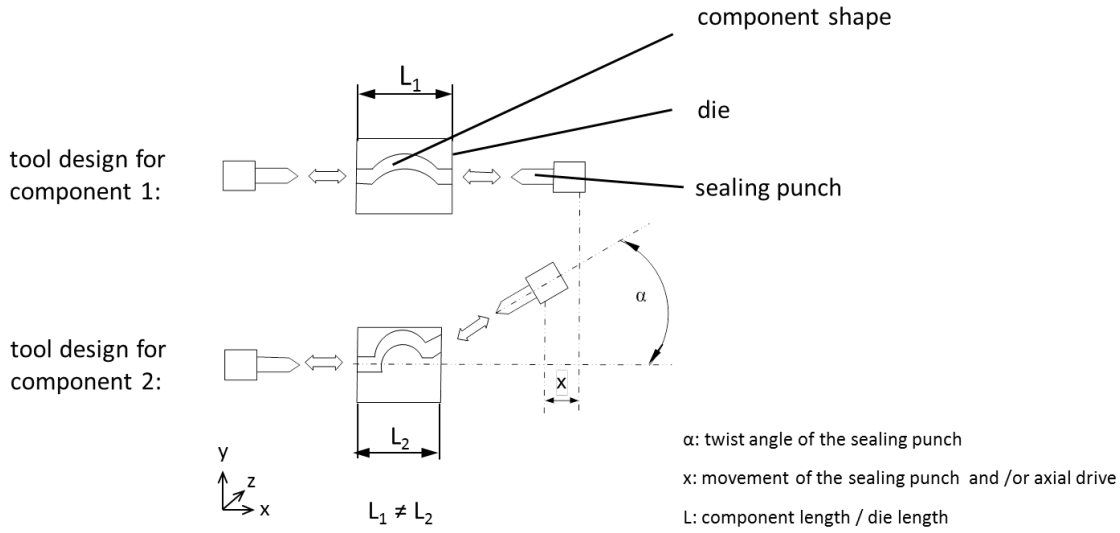

Fig. 66: Schematic of the flexible tool design according to 'situation 3'

For situation 3, *Fig. 66,* the requirements to enable the aimed flexibility of the hydro-forming tool consist of:

- The changeability of shape-specific die components (e.g. single die inserts or the complete forming tool with its basic die and shape specific inserts)
- The changeability of axial sealing punches for various tube diameters (depending on the used principle for tube ends sealing)
- The positioning of the drive units for axial sealing punches by adapting displacement *x* and/or *one* angle α

Situation 4 (similar to *Fig. 65*, but with a second twist angle 'x-z-plane'): The tool must allow the forming of components having

- varying cross sections
- varying lengths
- bent part geometries (bent in 'x-y-plane' *and* 'x-z-plane')

For situation 4 the requirements to enable the aimed flexibility of the hydroforming tool in this most complex situation consist of:

- The changeability of shape-specific die shape-specific die components (e.g. single die inserts or the complete forming tool with its basic die and shape specific inserts)
- The changeability of axial sealing punches for various tube diameters (depending on the used principle for tube ends sealing)
- The positioning of the drive units for axial sealing punches by adapting displacement and/or *two* angles α and β (β not shown in *Fig. 66*)

6.4.2 Flexible die cavity

Changeability of complete die

One possibility to provide a basis for flexible die cavities is to be able to replace the top die and the bottom die, respectively (*Fig. 67 left).*

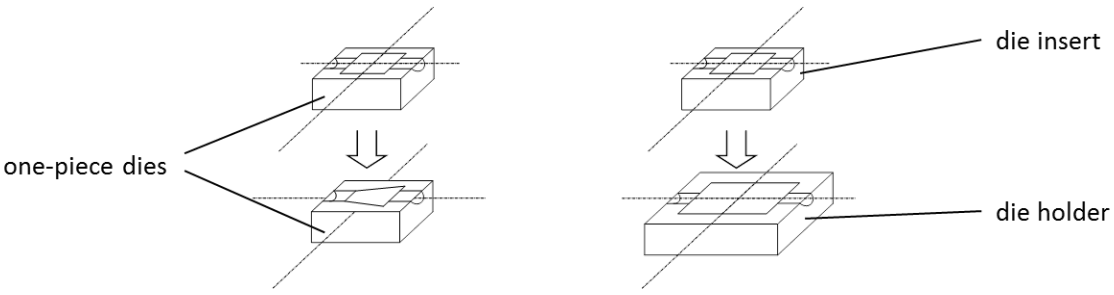

Fig. 67: Replacement of the complete one-piece die (left) and 'die insert' fitted into a basic die holder (right), only bottom dies are shown (left and right)

Depending on the principle layout of the tool which is generally used in today's industrial production (concept 1 or 2 according to *Fig. 68*), the effort for mounting and dismounting differs due to the difference in the mounting of the drives for the sealing punches.

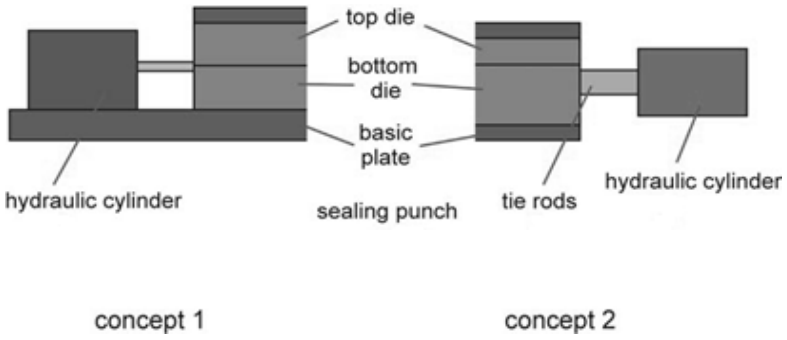

Fig. 68: Concepts of industrial hydroforming production tools [97]

Concept 1 shown in *Fig. 68* offers the advantage of an easier design of the die elements due to the mounting of the drive (the hydraulic cylinder) onto the base plate of the tooling. Concept 2 offers the advantage of a reduced influence of elastic die deflection on the position of the sealing punches relative to the die cavity.

For concept 1 in *Fig. 68*, to change to a new part geometry by changing the die cavities is comparatively simple, if there is no modification in part length to be considered. Regarding concept 2 in *Fig. 68*, changing to a new part geometry requires the disassembly and reassembly of the axial drives. However, this concept enables a higher flexibility when parts with different lengths and /or bent shapes have to be produced.

'Die insert' tools

A 'die insert' tool consists of a basic die holder and a die insert which contains the die cavity corresponding to the desired shape to be formed and which is fitted into the holder, *Fig. 67 (right)*. The axial drives for the sealing punches (hydraulic cylinders)

can be mounted to the basic plate of the tool (concept 1 in *Fig. 68*) or to the basic die holder (concept 2 in *Fig. 68*).

Independently from these concepts for the mounting of the punch drives, one important advantage is that die insert and basic die holder can be made from different tool materials. This enables the selective use of materials regarding machining properties, hardness etc. Also, dismounting and remounting of axial drives is not required. A disadvantage is the necessity to make adjustments for the accuracy of die insert and basic die holder and the reduced system stiffness due to additional gaps between tool elements.

Divided inserts

Fig. 69: Rapid interchange ability of separate inserts (Schuler)

Divided inserts offers more flexibility, *Fig. 69.* In the modern mass production individual inserts are built up to one cavity, thus the most complex shapes can be formed. In case of defects or wear only the appropriate elements have to be changed, whereby the spare part costs remain usually small. This illustrates the platform-design-strategy to save costs and to enhance flexibility. The main disadvantage of this system is the numerous interfaces between the individual inserts. Forming quality could be distorted at the interfaces between inserts. This can be disadvantageous in regarding the end product accuracy as reproducibility is one of the main requirements. Also the multiple interfaces of inserts require a large number of fastening spots.

6.4.3 Concept for a hydroforming tool unit

As a basis for a micro-hydroforming tool module, a design concept had been developed, which is illustrated in *Fig. 70*. The system consists of a bottom and a top die (top die not shown here) which can be mounted to a press table, and press slide (not shown here) respectively. The bottom die bears two guidance rods where the drive units with the slide carriage for the axial sealing punches are fastened. Hence, to switch to another part geometry both die halves have to be changed. Furthermore, due to the possibility to reposition the drive unit flexibly along the guiding pillar the system can be adjusted to different tool lengths.

An important advantage of this fastening concept is that the drive units as well as the sliding carriages with the sealing punches are not mounted on a base plate, but fastened at the end of the guidance rods which can clearly be seen in *Fig. 70*, in the upper and lower image. That means they are directly connected to the dies. Thus, a vertical shifting of the tube ends relative to the sealing punches due to an elastic deformation of the tool under the applied closing force F_c is minimized. A relative shifting, even in the range of a few micrometres, may cause leakage during the pressurization. In other words, the vertical displacement of the tool/tube would be equal to the vertical displacement of the sealing punches under the load F_c which results in stable sealing.

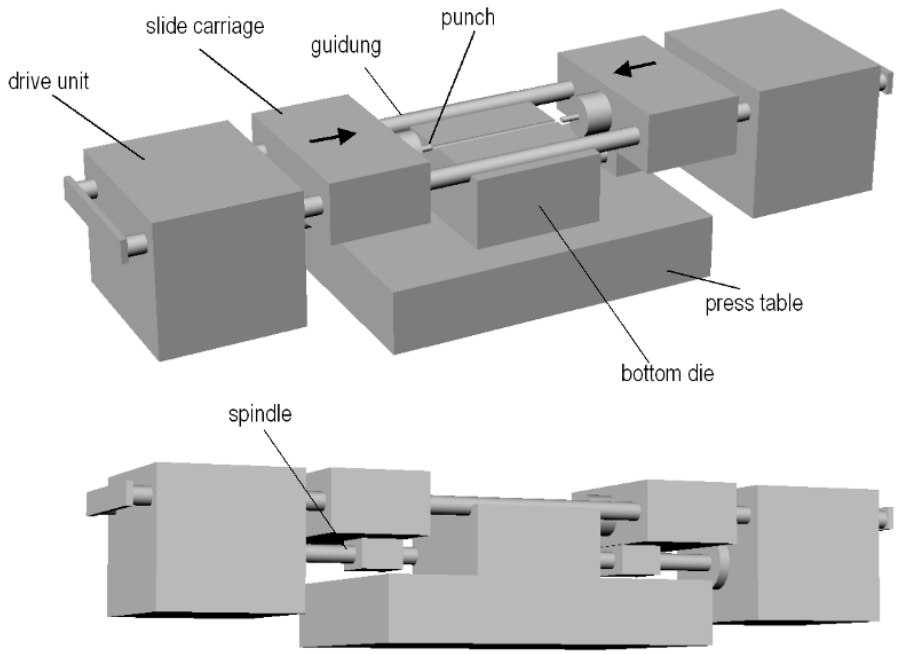

Fig. 70: Concept for the sealing of the tubes and movement of sealing punches [99]

6.4.4 Concept studies for axial sealing punches

The primary function of the axial sealing punches is to ensure the leakage-free sealing of the ends of the pressurised tube during the hydroforming process. The secondary function consists in supplying the pressurizing medium to the interior of the tube by a boring through the punch. The third function comprises axial feeding of tube material towards the main forming zone into the die cavity to enable an extended formability. For some industrial applications the sealing punches are designed to cover solely the primary and secondary functions.

Depending on the sealing requirements (e. g. internal pressure, contact area and with that the contact pressure per unit area), the length of stroke and on geometrical and material conditions, the punch material, its heat treatment and geometry must be tailored to the particular application. To increase the punch life span, low die loads should be used and notch effects and contact pressure should be minimized. If the

sealing punch is not strong enough it may break and the pieces may cause damage to the die [98].

In the following, different sealing punch concepts are presented, which are partly derived from existing designs and also represent new solutions.

Conical punch design

Fig. 71 shows the principle of the tube end sealing with a conical sealing punch. The conical punch forms the tube end into the conical end of the hydroforming tool and seals the pressurized tube during the forming process by applying a sufficient high axial load. According to the approved design of high pressure pipe connections it is suggested to use a cone angle of 60° for the hydroforming tool end and an angle of 58° for the conical punch. Movement of the punch towards the end of the tube results in an initial line contact, which has a theoretical area equal to zero, between the tube and the cones. An increase in axial force creates stresses that produce localized yielding and plastic flow at the seal contact. As the axial force is raised to a defined value, the line contact broadens to an annular area seal just wide enough to support the sealing thrust. Using this conical punch design no further sealing components such as rubber elements are necessary, though such elements are needed in conventional macro-hydroforming applications.

Another advantage of this concept is its flexibility. The conical punch is applicable for different tube diameters and tube wall thicknesses. However, an axial feeding of tube material, as described above, is not feasible with this punch geometry.

An important matter, and thus attention should be paid to, is that the conical punch may work similar to a wedge-acting tool which leads to lateral forces acting on the die halves. An elastic shifting of these tool halves due to these forces may cause a leakage of the pressurized tube.

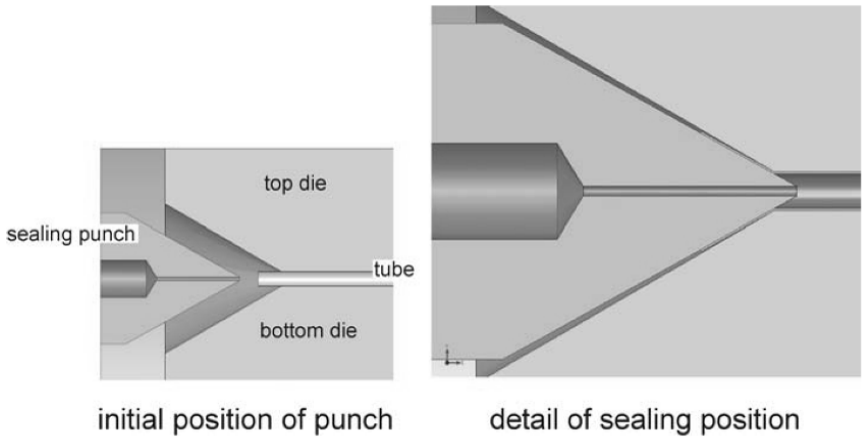

Fig. 71: Conical punch design [99]

Stepped punch design

A punch design proved in conventional 'macro' series production is presented in *Fig. 72*. Here the sealing occurs mainly due to a sharp corner surrounding the contact area between punch and tube end. When the punch gets in contact with the tube end, this corner is pressed into the tube front and creates the sealing.

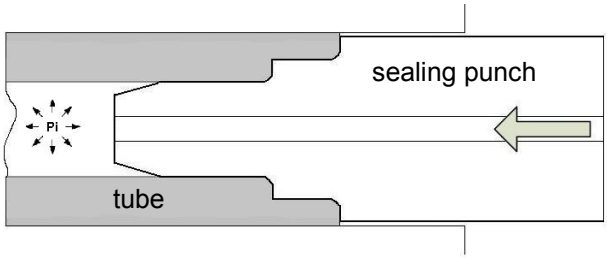

Fig. 72: Operating principle of a stepped punch [100]

The advantage of this design is that it enables an axial feeding of tube material. However, due to the adjustment of the punch geometry on a defined tube diameter and a defined tube wall thickness, its flexibility is constricted. As the sealing is achieved by the application of an axial force to the tube end, the use of this concept is restricted to hydroforming processes which require axial forces that are lower than the critical forces that cause wrinkling or buckling of the tube. For the design of the-

se stepped punches and the choice of punch materials the stress concentrations at the shouldered corners have to be taken into consideration.

Flange forming punch design

The principle behind this punch concept is derived from conventional forming processes to form flanges in tubes. *Fig. 73* shows the sealing process using this principle. Under the axial load F_a and the stroke x of the axial punch, a flange is being formed between the front faces of the sealing punch and the die halves which seals the tube. The major advantage of this concept in comparison to the conical sealing punch system is that there are no lateral forces created by the axial force of the sealing punch. Hence, higher axial forces can be applied through the punches thus improving the sealing reliability of the pressurized tube. Additionally this concept enables a certain flexibility as it can be used independently of the tube wall thickness. However, its application is reduced to a defined tube diameter and an axial feeding is not feasible. Depending on the critical force causing wrinkling or buckling of the tube, the flange forming process may be conducted within a separate tooling before the insertion of the tube into the hydroforming die.

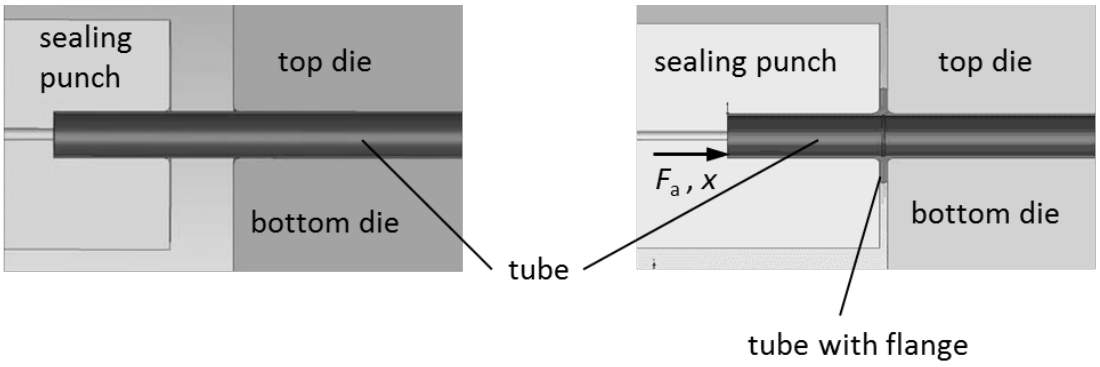

a) sealing punch starts pushing tube towards the die

b) formed flange seals the tube

Fig. 73: Flange forming punch design: a) start of flange forming (left) and b) end of flange forming and start of hydroforming (right)

6.4.5 FEA optimization of the sealing punch design

A general problem of the axial sealing punches is the reduced durability of these tool elements due to the high amount of stresses generated by the applied loads. From practical experiences it is known that this concerns particularly the punches with stepped design which are suitable for an axial feeding of tube material. To optimize the design of these tool elements stress analyses were carried out by means of FEA. *Fig. 74* shows the two-dimensional rotationally symmetric FE-model of the simulated punch geometry (outer diameter D_0 = 0.8 mm; wall thickness t_0 = 0.08 mm) with the applied loads as a half-section. These loads consist in the internal pressure p_i (black), acting to the inside of the boring which supplies the pressurizing medium into the tube as well as to the head of the punch and the contact pressure p_n (red) between tube wall and punch, estimated as the sum of the tube materials yield strength (AISI 304) and the hydrostatic pressure resulting from the internal pressure p_i. The FE analysis was simulated with a maximum internal pressure of 4,000 bar.

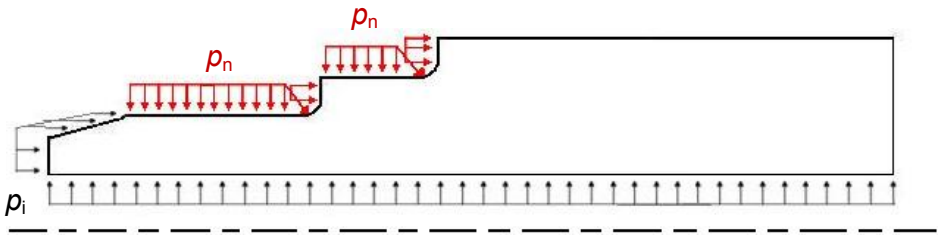

Fig. 74: Stepped punch model and applied loads (p_i black, p_n red) [99]

Fig. 75 on the next page shows the determined equivalent stress of punches with the boring diameters 0.2 mm (top) and 0.32 mm (middle) during the hydroforming process under an internal pressure p_i of 4,000 bar. It is evident from these figures that the smaller the boring diameter, the lower are the maximum equivalent stresses. For the investigated design, the maximum equivalent stress was reduced approximately 18 % when using of the smaller boring diameter. However, the smaller boring diameters lead to an increased flow resistance regarding the flow of the pressurizing medium which has to be supplied by these borings.

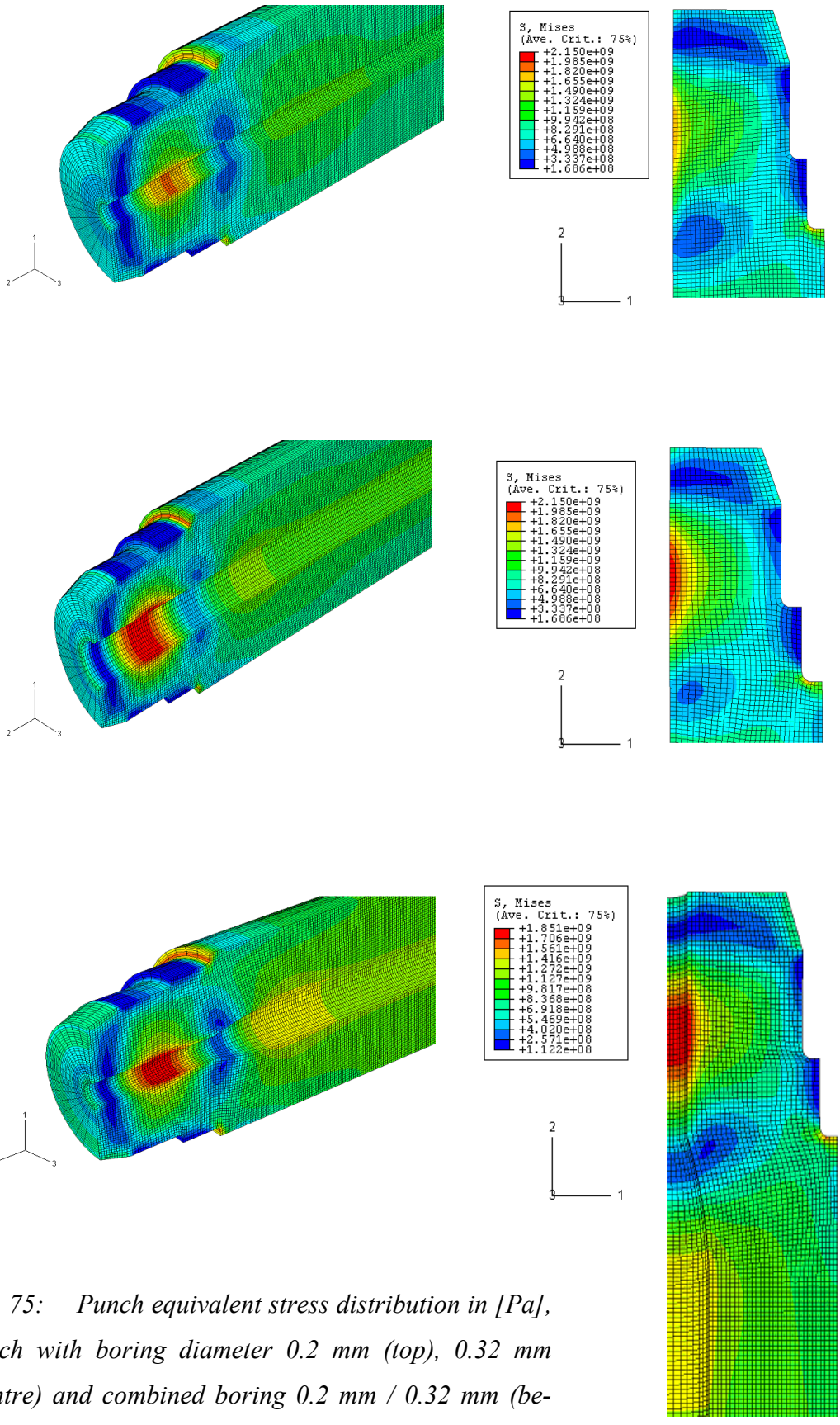

Fig. 75: Punch equivalent stress distribution in [Pa], punch with boring diameter 0.2 mm (top), 0.32 mm (centre) and combined boring 0.2 mm / 0.32 mm (below), please refer to Fig. 76 for additional dimensions

An improved design with a combined boring of 0.2 mm / 0.32 mm was investigated *Fig. 75* (bottom). The results show that there is no increase of stresses in comparison to the 0.2 mm diameter punch shown on top.

In principle there exist tool materials which are able to withstand the stresses resulting from these studies, e.g. the tool steel 1.2379 hardened to about 60 HRC. Consequently, for the use in the prototype machine two of the three here presented punch designs were manufactured using the above mentioned material. The chosen geometries of a stepped punch and a conical punch are pictured in *Fig. 76* and *Fig. 77*, respectively.

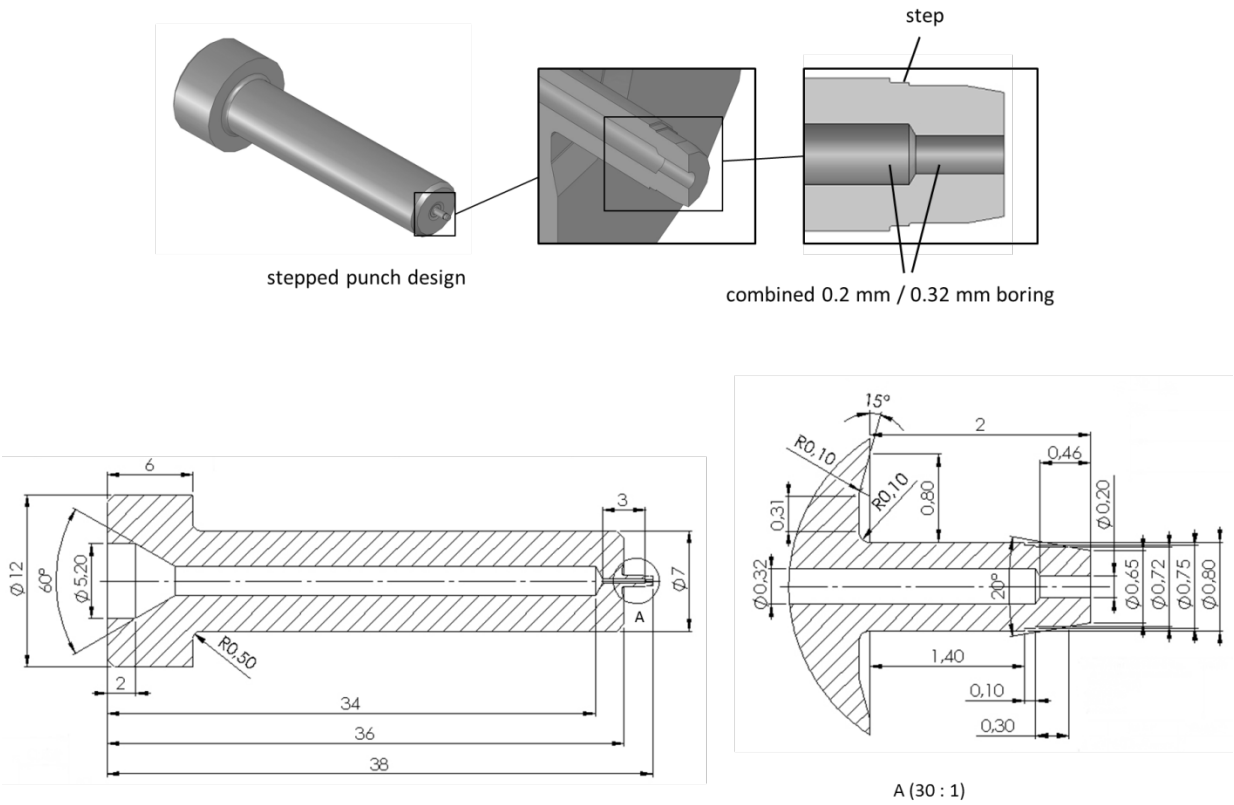

Fig. 76: Design and dimensions of a stepped (cylindrical) sealing punch with a combined 0.2 mm / 0.32 mm boring

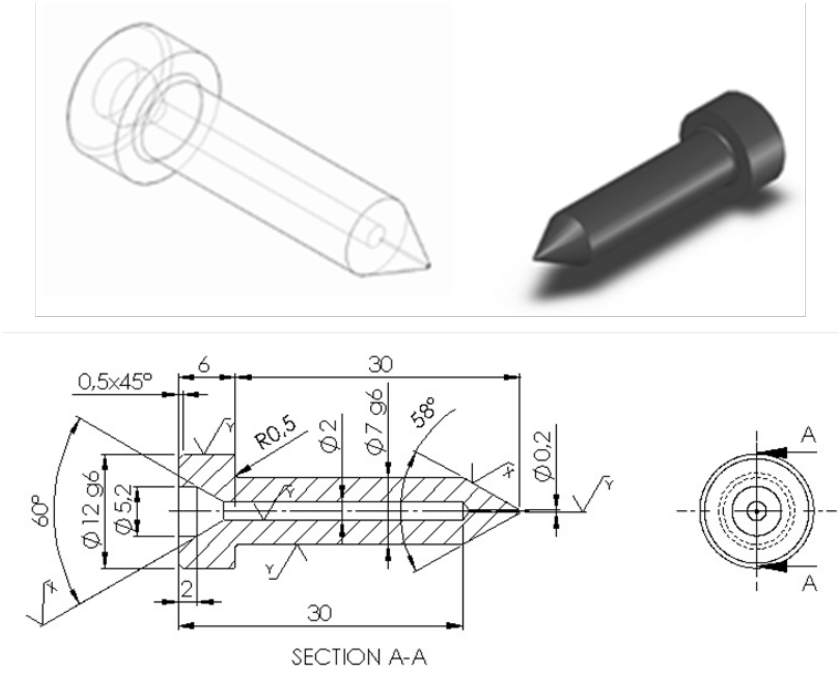

Fig. 77: Conical sealing punch for the prototype machine

6.4.6 Realization of the tool unit

The assembly of the complete tool unit with its essential components is pictured in *Fig. 78*. It contains both top and bottom parts of the micro-hydroforming tooling as schematically represented in *Fig. 79* (top). The tool inserts (*Fig. 79* below) which include the die cavity are located within the basic tool blocks. Adjusting plates, covering the contact areas between the basic tool blocks and the integrated tool inserts were used to adjust the correct position of the die-insert elements to each other and to the axis of the sealing punches. The assembly of the bottom tooling is fixed to the machine table. Only the two brackets which cover the axial drives were additionally fastened onto the machine table. The axial drives by themselves act on the sliding carriages with vertical clearance. As described above (*Chap. 6.4.3 Concept for a hydroforming tool unit*) the slide carriages which cover the sealing punches were mounted on the horizontal guiding pillars. Due to the clearance and the fact that the sealing punches are permanently aligned with the forming tool, vertical shifting of the tube ends against the sealing punches caused by elastic deformation of the tool under the applied closing force can thus be avoided.

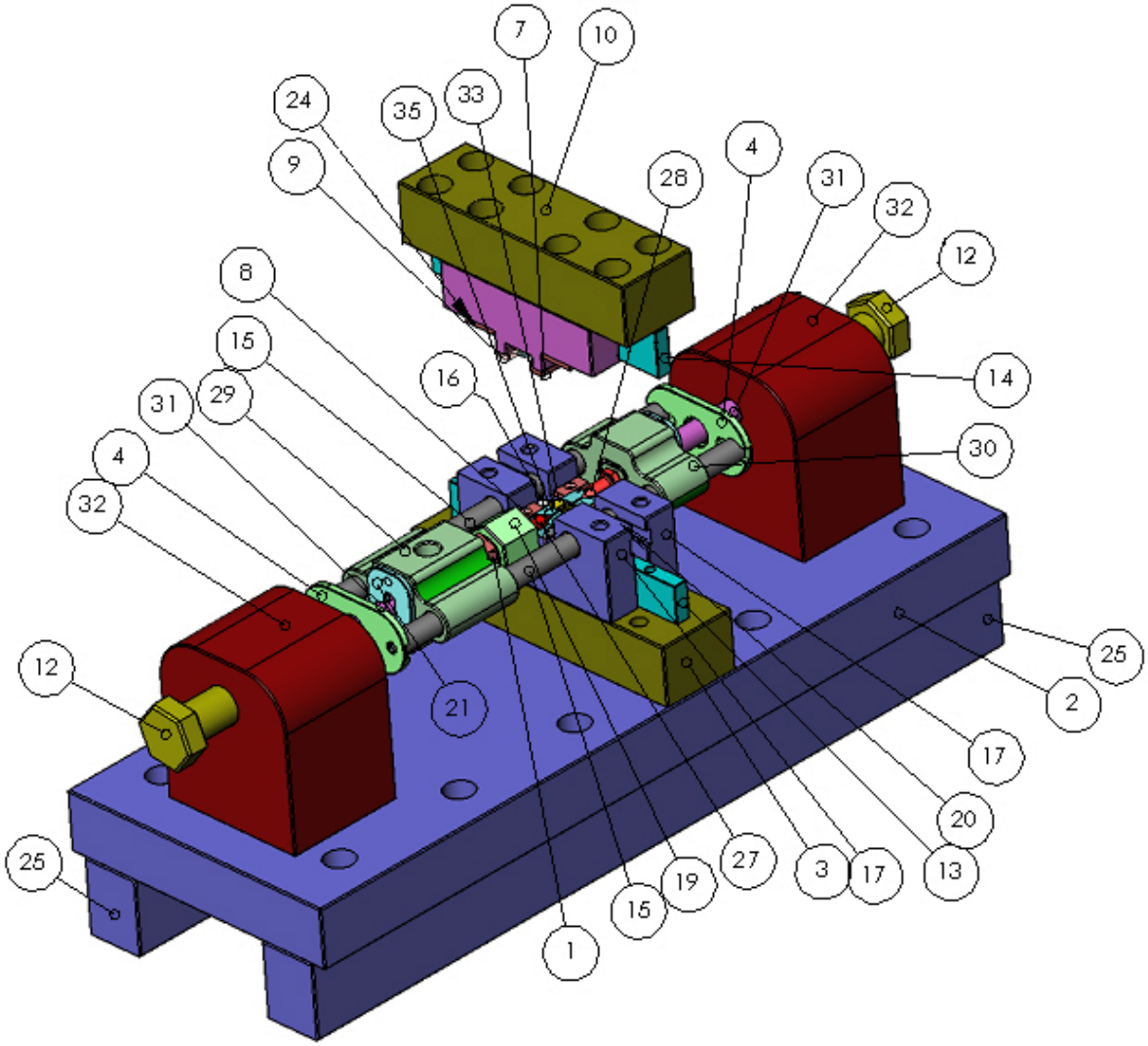

POS-NO.	TITLE	QUANTUM
35	blank holder	4
34	flexible tool cartrigde one form (top)	1
33	flexible tool cartrigde one form (bottom)	1
32	spindle retainer	2
31	spindle	2
30	slide carriage2	1
29	slide carriage1	1
28	sealing punch2	1
27	sealing punch1	1
26	sealing cone	2
25	rail	2
24	Pressure plate2	2
23	Pressure plate1	2
22	pressure plate spindle	2
21	plate	2
20	parallel key	2
19	nut metric 20mm	1
18	insert carrier (top)	2
17	insert carrier (bottom)	2
16	insert	4
15	guiding rod	2
14	flexible tool (top)	1
13	flexible tool (bottom)	1
12	fitting screw 24mm	2
10	cover plate	1
9	clamp2 (top)	2
8	clamp2 (bottom)	2
7	clamp1 (top)	2
6	clamp1 (bottom)	2
4	bridge	2
3	bottom plate	1
2	basic plate	1
1	adapter	1

Fig. 78: Assembly of tool unit with both top and bottom tool blocks and parts list

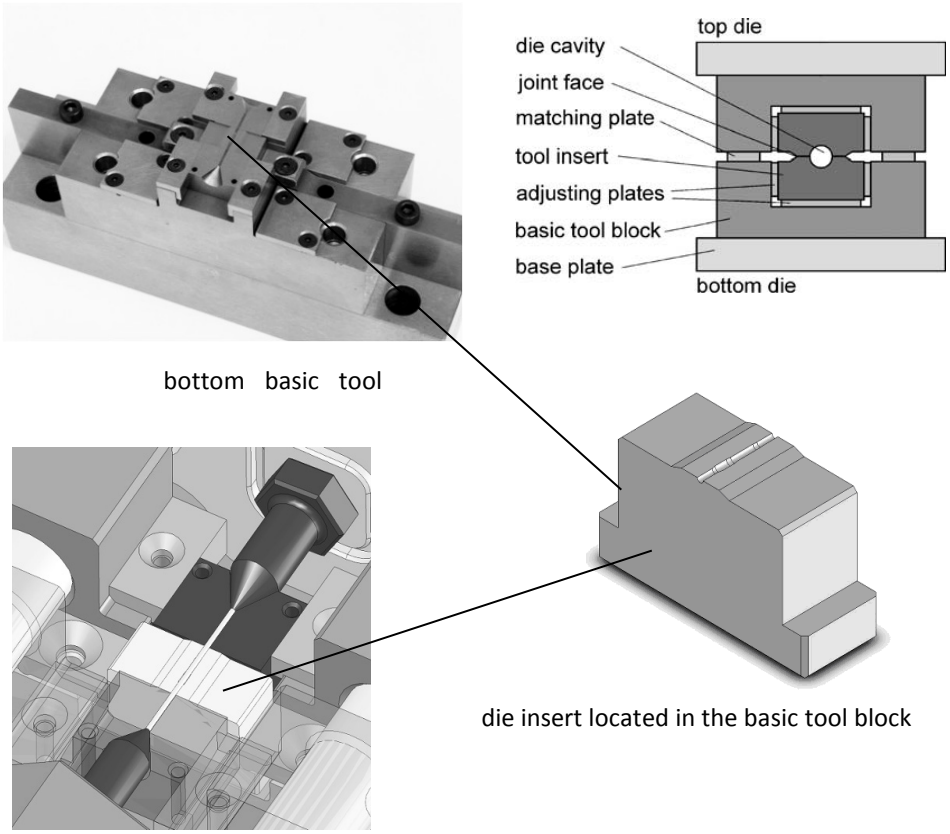

Fig. 79: Bottom basic tool block [101] of the micro-hydroforming tool (top left), cross-section (top right) [3] and die insert with cavity (right & left below)

Elastic tool deflection in macro-hydroforming

Referring to macro-hydroforming processes, a decisive factor for the magnitude of the elastic tool deflection is the level of applied internal pressure p_i. In general, at the end of the process, the internal pressure is increased to the target pressure $p_{i,\,max}$ to form the tube wall into the corner radii of the die cavity, this area may not have been formed during the main expansion of the workpiece. The necessary level of internal pressure is influenced significantly by: the local yield stress σ_{yp} of workpiece, the wall thickness t_0 of the formed component, the component shape, and the minimum corner radii r_c of the die cavity.

Miscellaneous conditional equations (cf. *Chap. 2.2.2.4 Prediction of forming loads)* are available for the determination of $p_{i,\,max}$, predominantly based on the correlation:

$$p_{i,max} = f(\sigma_{yp}, t_0, r_c) \tag{18}$$

The level of applied internal pressure affects, besides the sealing force F_a, particularly the required force F_c to close the top and bottom die during the forming process. Commonly, the opening and closing of the hydroforming tool is implemented by a press, predominantly hydraulically driven. The minimum closing force required, which has to be applied by this press to avoid the loss of contact between the two die halves during the forming process, can be estimated according to correlation (4) with:

$$F_{c,min} = A_p \, p_{i,max}$$

with the projected area of the formed component A_p being perpendicular to the closing direction. It is obvious from this correlation that the greater is the internal pressure $p_{i,\,max}$, the greater amount of force F_c is required. In addition to the deflection caused by $p_{i,\,max}$, the deflection due to F_c has to be taken into consideration also.

From practical experience it is known that the elastic tool deflection in macro-hydroforming processes caused by the acting loads can be about 0.5 mm [102]. Specific tool designs as well as adaptations in the design of the forming die cavities enable a reduction in faults within certain limits [3]. Scatter in the process loads as well as in the tube dimensions and material characteristics induce additional deviations in the dimensions of the hydroformed part. Typical accuracies for conventionally hydroformed macro-parts are within the range of 0.1 mm and up to about 0.6 mm as reported in [102] for the example of a hydroformed sub-frame made from a tube with an outer diameter of 52 mm.

Finite element analysis of die deflections

In order to investigate the accuracy of the hydroformed part geometry, analyses were carried out for an example cross-section of the hydroforming die inserts already shown in *Fig. 79*.

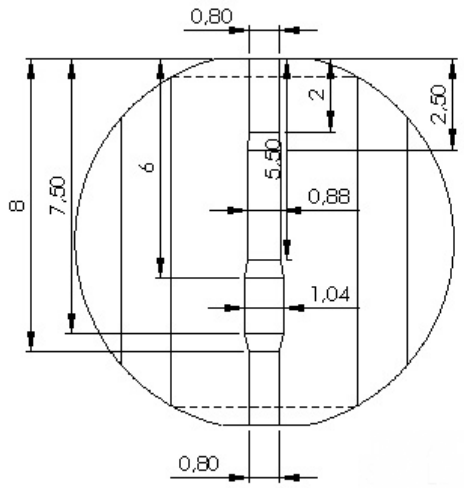

Fig. 80: Dimensions of the hydroformed part

The tool was developed for the forming of the cylindrical camera shaft. According to the dimensions illustrated in *Fig. 80*, the selected section represents a die-cavity diameter of D_1 = 1.04 mm, in which a tube with an initial diameter D_0 of 0.8 mm and variable wall thicknesses t_0 can be expanded.

Once again the commercial system ABAQUS was used to execute the simulations. Subject of the simulation was a tube specimen made of AISI 304 with a wall thickness t_0 of 80 µm. Linear-elastic behaviour of the die cavity was considered and elastic-plastic behaviour with strain hardening of the tube material. The required yield curve was taken from [103]. By means of a planar FE-model, cut by symmetry conditions (*Fig. 81* left), the influence of closing force and internal pressure on the tool deflection and on the hydroformed part accuracy was examined. Regarding the boundary conditions (BCs) of the model, the bottom die was fastened on the machine table (BC: fixed) whereas the top die was free to move (in vertical direction).

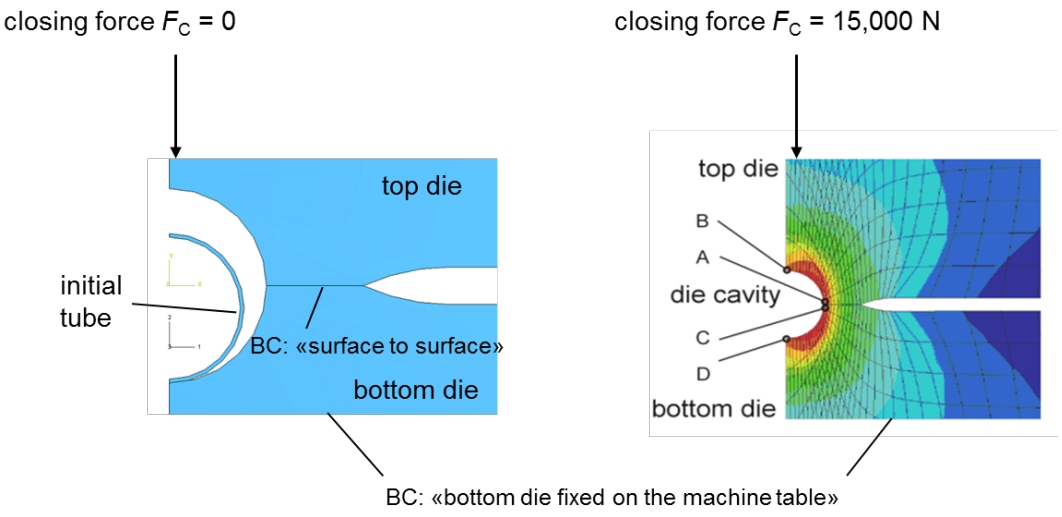

Fig. 81: Schematic of the initial FE-model (left) and areas of investigated deflections (right)

Two load cases and the resulting displacement of four positions of the die cavity (A-D) had been investigated with the above mentioned model: The positions A-D are illustrated in *Fig. 81* on the right. To simplify these simulations, in the first instance the internal pressure was applied directly onto the inner surface of the die cavity without consideration of the tube expansion.

As the result of the two load cases investigated, *Fig. 82* [99] shows that the curve progression of the acting press force vs. process time essentially influences the deflections of the hydroforming die cavity during the forming. The graphics on the left hand side illustrate the process control similar to a conventional hydroforming process: a constant closing force during the whole hydroforming process. On the other side an *adapted process control* with a closing force rising and lowering parallel to the internal pressure with an "offset force" has been simulated.

It is evident from *Fig. 82* that the conventional process control causes a more unfavourable alternation of the tool deflection on the investigated die cavity (positions A-

D) in comparison to the adapted process control. Further on, the amount of displacement was reduced by the use of an adapted process control, e.g. up to 50 % at position B in y-direction. Therefore, the adapted process control is recommended for the control system of a micro-hydroforming machine. The adapted process control can be utilized to reduce die deflection during the forming process and through this improve the formed part accuracy.

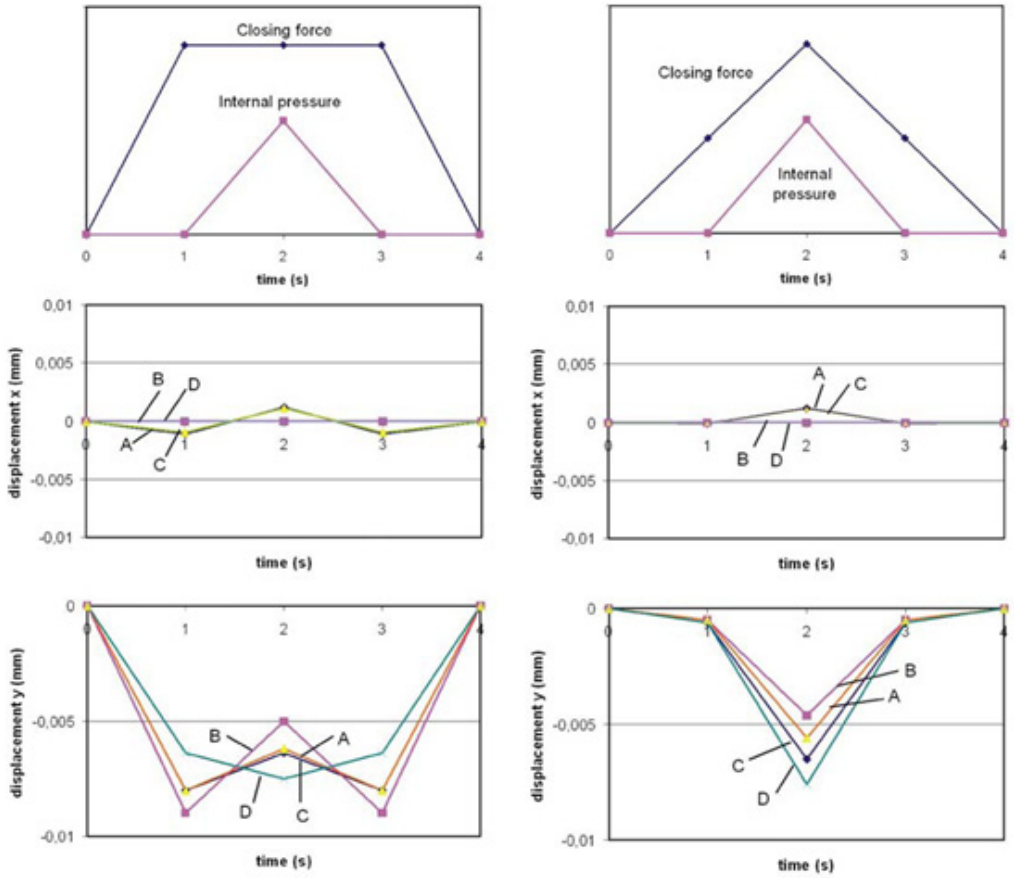

Fig. 82: Comparison: influence of conventional press force control, left and adapted force control on tool deflection, right

To subsequently determine the accuracy of the final hydroformed part geometry and to be able to draw comparisons the above mentioned part accuracy achieved during conventional hydroforming processes further simulations with the mentioned FE-model had been carried out. Again an expansion of 30 % was simulated but now applied to the stainless steel tube (AISI 304) placed in the model. The diameter of

the die cavity D_1 was 1.04 mm, according to the expansion of 30 %. Linear-elastic behaviour of the die cavity was considered and elastic-plastic behaviour with strain hardening of the tube material.

Fig. 83 shows the simulations of the tube model at the end of the forming process under 4,000 bar and the relieved situation with the opened tool. An adapted process control, as described above, was applied.

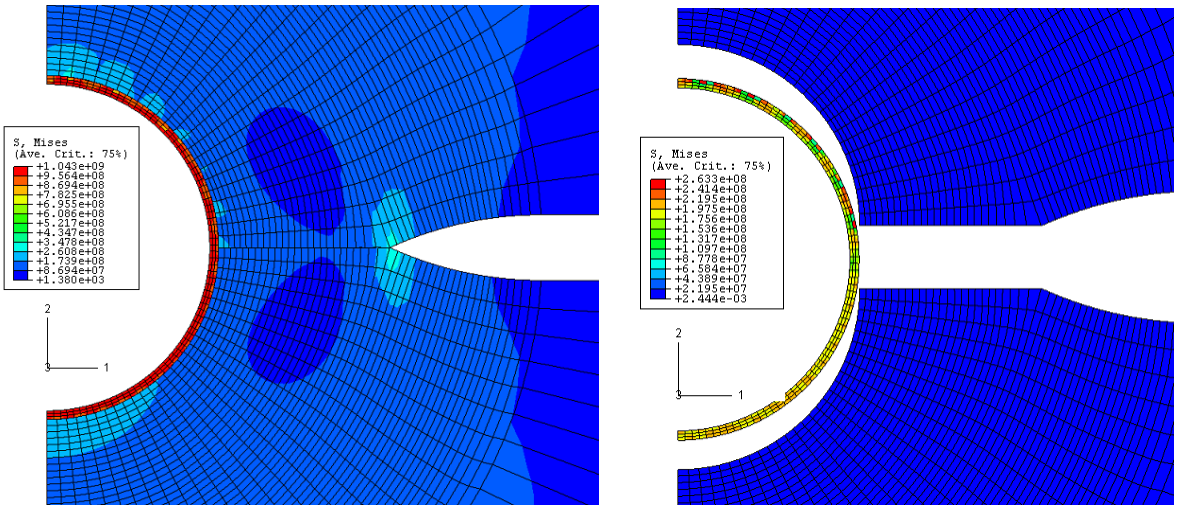

Fig. 83: Simulation results: Tube under internal pressure of 4,000 bar (left) and under relieved condition and open die halves (right)

The resulting dimensions after relieve and simulation of spring back of the expanded tube are:

Vertical diameter: 1.03692 mm (deflection: - 3.08 µm)

Horizontal diameter: 1.03723 mm (deflection: - 2.77 µm)

The conducted simulations show that accuracies in the range of about 3 µm are able to be achieved, disregarding any potential scattering due to variations in tube specifications, process control or friction conditions.

According to the example above for part accuracy of hydroforming processes today, (between 0.1 mm, 0.2% respectively, and 0.6 mm, 1.15% respectively, referred to an

expanded tube diameter of about 52 mm), the determined accuracy of about 3 µm (0.3% of the expansion diameter) is in the equivalent range, which can be commonly achieved by conventional tube hydroforming, even in a comparatively low magnitude.

6.5 Construction of the axial drives

The primary function of an axial driving system is the axial movement of the sealing punches towards the tube ends to ensure a leak-free sealing of the pressurised tube during the hydroforming process. The secondary function comprises of the axial feeding of the tube material into the die cavity during the forming process to enable an extended formability of the tube.

Three axial driving concepts are introduced and hereafter evaluated.

The driving system needed consider to accepting conical punches and also cylindrical punches as the initial tests may utilize an axial feeding system. Thus, the following requirements differ in detail relying on the sealing concept adopted.

6.5.1 Requirements on the axial driving system

Sealing forces

With regard to *Eqn.* (8) in *Chap. 2.2.2.4 Prediction of forming loads* the axial loads acting on the sealing punches consist of the axial force and the forces due to friction along with the sealing forces resulting from the internal pressure.

With reference to the tube dimensions outer diameter D_0 = 0.8 mm and wall thickness t_0 = 0.04 mm, the following axial forces required for the axial sealing and for the axial feeding respectively have been calculated:

Sealing principle	Required axial force / N	Axial feeding
Conical punch	670	no
Flange principle	163	no
Cylindrical punch	350	yes

Table 11: Required axial loads

Precision/Accuracy

For the axial feeding concept, the axial drive needs to have a very precise drive system. The mentioned axial forces as well as the displacement of the punches have to be determined and controlled versus the internal pressure. An infinitesimal variation of the internal pressure effects a force/displacement change which also affects the punch in the same way.

Using the conical punch sealing concept, the maximum required axial force of the punches can be directly generated to the tube ends.

Speed

When the process starts, the sealing punches are to be drawn near to the tube ends at an increased speed. During the forming process for the case 'without axial feeding' the speed essentially amounts to zero. In the case 'with axial feeding' the required speed corresponds to the speed of medium delivery realised by the pressure intensifier. For the here developed forming system, an increased speed of 360 mm/min and a speed of 16 mm/min during the forming time t_f were determined.

Stroke

Inserting of stepped (cylindrical) punches into the forming tool during axial feeding is to be considered as a critical phase relating to wear, friction, buckling etc. Hence, the stroke of the punches should be as short as possible. The punches should never

leave the tool halves during a cycle, in particular after the forming process when moving backwards. Otherwise punches may get jammed when re-entering the forming tool halves, even with the smallest backlash. However, the stroke needs to be long enough to ensure the proper handling of the part. A maximum required stroke of 3 mm was defined.

Stiffness/Rigidity

Due to the comparatively low axial loads admitted and the quasi-static behaviour of the drives, requirements regarding stiffness/rigidity were secondary.

6.5.2 Design studies on axial actuators

Pneumatic actuators

Pneumatic actuators are only suitable for the use of sealing punch drives in hydroforming applications when no axial feeding is required. Due to the compressibility of the pressurized air, no reliable control of the stroke is feasible. Hence, these systems are only applicable for the principles 'conical sealing' and 'flange sealing'.

Common magnet valves are sufficient to control these kinds of actuators in order to drive the conical sealing punches towards the tube ends. The major advantages are low costs, easy controllability (in terms of only advance and back the piston), less additional components are required, they are safe (pressurized air, max. 10 bar), clean and usually have a long work life. Due to the fewer required components which are less complicated to apply and integrate, costs are expected to be comparatively lower.

Relying to the controllability of pneumatic cylinders it must be stated, that adequate air regulators are available on the market. Nevertheless, an imprecise axial feeding by using cylindrical sealing punches is to be adopted therewith. The reason for this is the elastic behaviour of the pneumatic cylinder movement due to the compressibility of the compressed air.

Hydraulic cylinder

Hydraulic drives are commonly used when high powered solutions are required. In the present case, even the smallest hydraulic cylinders available on the market would be easily able to raise tenfold higher power than what is required. Hydraulics' are competitive and applicable for when comparatively higher forces are applicable and suitable for 'axial feeding' and 'non-axial feeding'. A disadvantage that must be taken into account is that an operation would take place practically under a low degree of efficiency. At the final control element, the valve necessary for regulating extremely high leakage currents would occur, which would cause a thermal warming of the hydraulics circuit as a consequence. Accurate controlling might become very difficult to achieve.

Linear actuators

Linear actuators represent a further feasible concept to drive the axial punches. Their principle enables an applications working with 'axial feeding' and 'without axial feeding'. They are suitable for stroke controlled application with sufficient precision in positioning, applicable for both 'axial feeding' and 'non-axial feeding' processing. A possible drawback is that some electric motors are only suitable to a limited extent for a force controlling application without movement.

6.5.3 Conclusion - selected actuators for the axial drive

	Pneumatic drive	Hydraulic drive	Linear actuator
Force generation	5	5	5
Speed	5	5	4
Controllability	2	3	5
Stroke	5	5	5
Precision/Accuracy	1	2	4
Cost	4	2	4
Overall	**23**	**24**	**32**

Rating	Description
5	Complete satisfaction: objective satisfied in every respect
4	Considerable satisfaction: objective satisfied in the majority of aspects
3	Moderate satisfaction: balance between complete satisfaction and no satisfaction
2	Minor satisfaction: objective satisfied to a small extent
1	Minimal satisfaction: objective satisfied to a very small extent

Table 12: Decision matrix for the axial actuators

Resulting from the above evaluation electric drives are supposed to be the most applicable drive components for the sealing of the pressurized workpiece and for the feeding of material towards the main forming zone of the tube. The selected linear actuators feature a recirculating ball-screw suitable for axial loads up to 800 N. The positioning accuracy of the actuator is 15 μm, enabling a precise axial movement of the axial punches when forcing tube material into the die during the forming process.

6.6 Development of the closing mechanism

In the following, the requirements on the closing mechanism including its drives/actuators as well as three different closing mechanisms are explored.

6.6.1 Functional requirements

The functional requirements of the closing mechanism include the requirements on force, stroke, speed, precision/accuracy, handling/assembling and maintenance.

According to previous considerations and calculations, the following functions may be required: (a) the drive should be able to supply a press force of approximately 15,000 N, relating to an internal hydro-static pressure of 4,000 bar, (b) the stroke should be able to afford enough space for a comfortable and fast tool displacement and part handling, (c) a speed of 50 mm/s is necessary to fulfil an aspired part production of approximately 6 to 10 parts per minute, (d) precision for force control of the concept to be applied is expected to be comparatively high, whereas precision of stroke control is secondary.

Considerations on the control issues

A basic issue involved is the synchronization of the required press closing force F_c with the internal pressure p_i. As already mentioned in *Chap. 6.3.3* a FE analysis showed an unfavourable alternation of the forming tool deflections due to a constant closing force during the hydroforming process (*Fig. 78*). However, the amount of displacement could be reduced by applying an adapted control with a closing force rising and lowering parallel to the internal pressure p_i. This strategy has been used to define the control precision by specifying the required amount of closing force versus p_i.

6.6.2 Concept studies

Based on the above mentioned requirements, several types of press drives had been investigated which are described in the following.

Double toggle joint mechanism

This concept, *Fig. 84*, comprises of an electric motor acting over a ball screw system. The nut fixed to the ball screw presses down an x-shaped element (nut pusher) which drives two toggle mechanisms. Each single toggle joint mechanism consists of a force element and an upper and a lower lever arm. The upper lever arms are fixed to a horizontal element which is mounted via a bearing at the lower end of the ball screw and which always remains on its position. By rotating the ball screw, the up and down moving force elements bend and stretch the lever arms whereupon the lower arm raises and lowers the press ram on which the upper tool block with the top die is fastened. Depending on the geometry (length of the lever arms) and the position of the moving components, the force of the spindle can be multiplied. The guiding system comprises four guiding columns, each carrying a roller type ball bearing bushing rolling up and down.

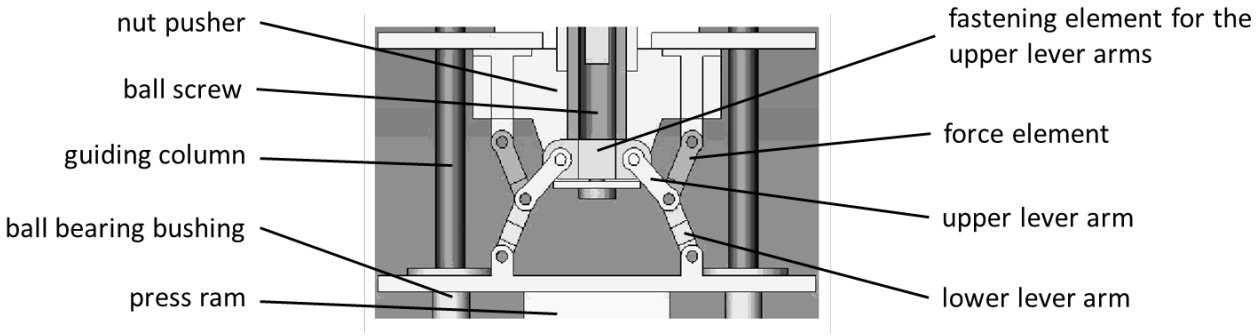

Fig. 84: Principle of the toggle joint mechanism as a press drive [104]

The principle of the toggle joint mechanism is shown in *Fig. 85* (left) below. When force is applied to the element *f*, forcing its movement, *e* moves as well and force applied is multiplied, because movement of the joint *g* produces a slight movement of *e*. This part *e* is in contact with the part and applies this amplified force. The multiplication only depends on the dimensions and geometric features of the joint, cf. equation on the right hand side in *Fig. 85*.

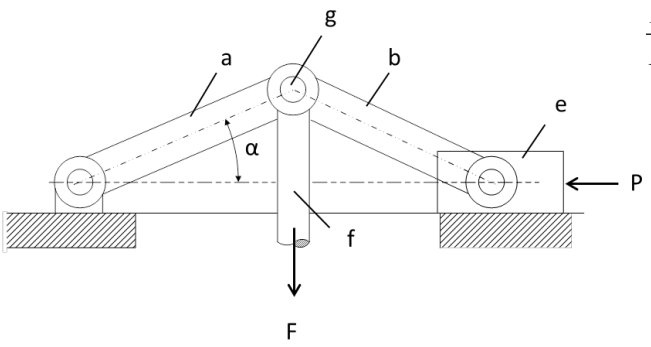

$$\frac{P}{F} = \frac{\cos\alpha}{2\sin\alpha} = multiplication\ coefficient$$

Fig. 85: Schematic of a toggle joint mechanism

Hydraulic drive

The hydraulic drive concept consists of three main parts: a tie rod cylinder mounted on the top plate of the closed machine frame, a servo solenoid valve with on-board electronics and a power unit. Most of the components are commercialised standard components, such as the pilot operated check valve, the mounting plate, hydraulic hoses and a number of connectors. The only type of a non-standard-part would be a connexion-plate of the upper die, which can be screwed onto the thread of the piston rod.

For the generation of the required press force, a pressure control is essential. In general, this may be achieved by the integration of either proportional pressure reduction valves or proportional pressure limitation valves. For both systems one needs electronics (integrated or external) to control the magnetic current. Another possibility is the application of steady valves as there are servo-operated valves and proportional solenoid valves (directional control valves).

Linear actuator with ball-screw spindle

Beside others, linear actuators based on ball-screw spindle systems are commonly used for axis drives of CNC-machines. Two types are available on the market: systems with an axially moved, non-rotating spindle in combination with a rotating, axially unmoved ball screw nut, and systems with a rotating spindle which is axially

unmoved combined with a non-rotating, axially moved ball screw nut. The principles are represented in *Fig. 86*. In general, the rotary motion of these systems is realised by electric servo motors. To reduce machine component dimensions, the second system would be to be preferred in present case.

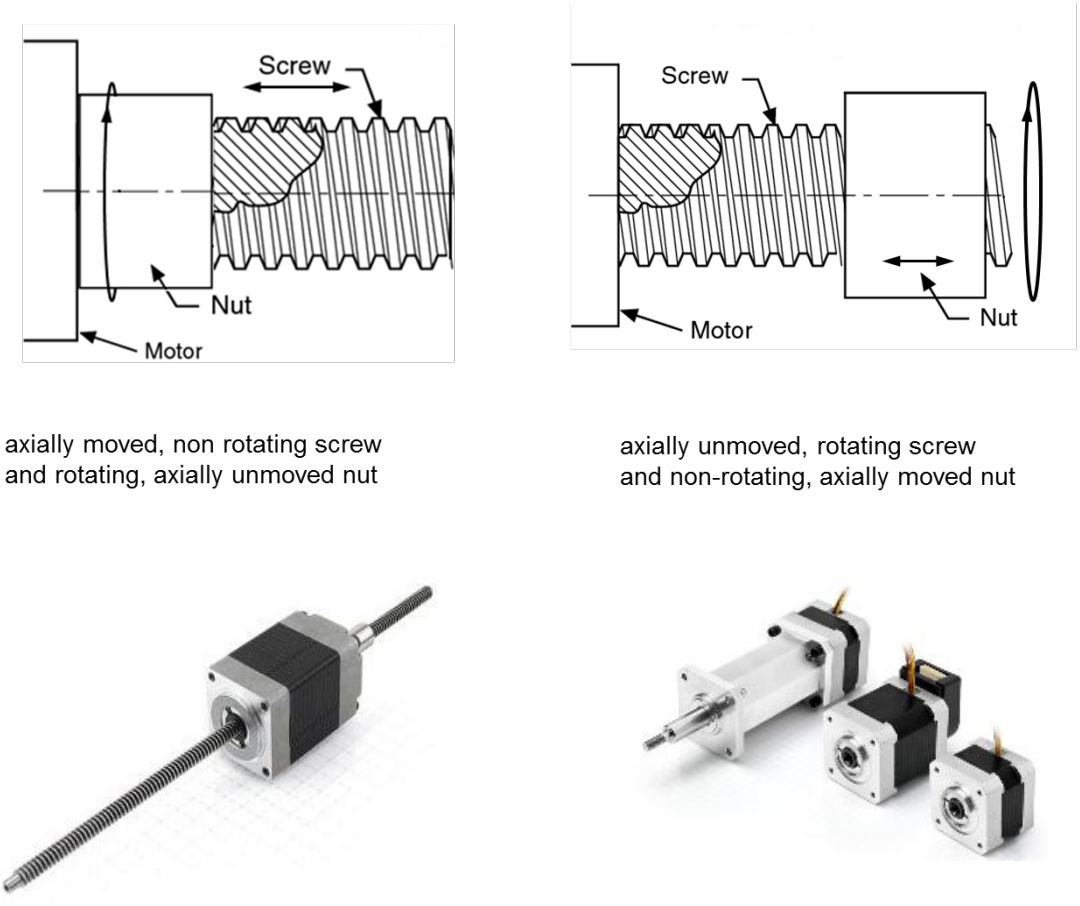

Fig. 86: Principles of spindle drives, above [Newport] and examples of linear actuators, below [Nanotec]

A suitable design of such ball screw spindle system for the developed machine concepts requires a diameter of the spindle of about 63 mm, considering permissible stresses, surface pressures and limits of buckling. These systems are suitable only to a limited extent for a force controlling application without movement, as it is necessary in the present case. An uneconomic oversized servo motor would be the conse-

quence using such systems here to enable the required force control. Additionally, non-uniform wear of the spindle will result from the fact that the maximum force is applied at one certain spindle position for any stroke.

Decision matrix

	Double toggle joint mechanism	Hydraulic system	Linear Actuator
Load (as high as possible)	5	5	4
Speed (high)	1	5	4
Stroke	3	5	5
Controllability	4	4	1
Damping of Speed	5	5	2
Economic Design	1	4	3
Costs	2	4	3
Accurate Positioning	4	4	4
Overall	**25**	**36**	**26**

Rating	Description
5	Complete satisfaction: objective satisfied in every respect
4	Considerable satisfaction: objective satisfied in the majority of aspects
3	Moderate satisfaction: balance between complete satisfaction and no satisfaction
2	Minor satisfaction: objective satisfied to a small extent
1	Minimal satisfaction: objective satisfied to a very small extent

Table 13: Decision matrix for the closing mechanisms

6.6.3 Conclusion - selected components of the closing mechanism

Features and functions of the selected hydraulic system

Based on the above mentioned requirements and on the evaluation results, a tie rod hydraulic cylinder equipped with a position measuring system was selected. To apply the hydraulic pressure to drive the hydraulic cylinder for tool closing, a custom-

ized 60-liter power unit had been chosen which was positioned under the machine table. The modular desktop-sized system enables a pressurization of 160 bar. Besides more than 50 standard parts; the major components of the hydraulic system are: a proportional pressure relief valve, a pressure control unit incl. a relief valve, a servo solenoid valve with on-board electronics, a pressure limiting valve as well as several check valves. Functions of the components mentioned are later explained in *Chap. 6.8.2.3 Control module of the press drive*. The complete system is shown in the hydraulic diagram at the end of this chapter, also *6.8.2.3*.

6.7 High Pressure System for forming fluid pressurization

In general a high-pressure system consists of several main components: a pressure intensifier to fill the workpiece with the forming medium and to generate the forming pressure, valves and safety devices to control medium flow, high-pressure piping, equipment for media supply and maintenance (e.g. filters, tanks), pressurizing medium and connection to the forming tool/workpiece. All of the components mentioned are commercially available expect for the connection to the forming tool/workpiece. The pressurizing media typically consists of oil-water emulsions.

The pressure intensifier is the primary component of the high-pressure system. To reach a decision regarding a suitable system three common principles have been investigated: (a) hydraulic driven pressure intensifier, (b) pneumatic driven pressure intensifier (air driven pump) and (c) mechanical driven pressure intensifier (spindle pump).

6.7.1 Requirements to a micro-hydroforming high-pressure system

Major requirements for a high-pressure system to enable the forming of the demonstrator part “camera shaft” and in the future similar micro-tubes consist of: (a) maximum pressure: minimum 4,000 bar, (b) “small” volume flow: 0.15 ml/s, (c) time for pressure generation: max. 3 sec, (d) pulsation-free high-pressure generation, (e) quality of controllability: +/- 5 bar.

6.7.2 High pressure intensifier - system studies

Hydraulic driven pressure intensifier

In conventional hydroforming processes the forming media is pressurised by an ordinary hydraulic power unit in combination with a single or double-acting pressure intensifier.

An intensifier consists of a stepped piston-cylinder arrangement with a fixed intensifier ratio. The low pressure fluid is pumped into the large cylinder (primary side) expelling the fluid from the small cylinder (secondary side) at an increased pressure. Common ratios vary from 1:5 to 1:30 depending on the secondary pressure required. The commercially available intensifiers are available which enable pressurisations up to 10,000 bar.

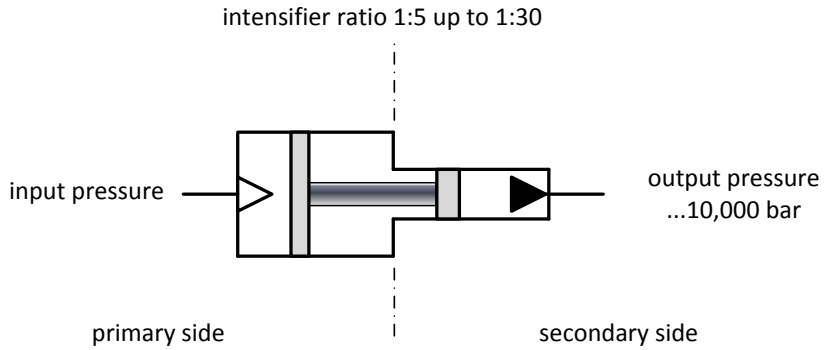

Fig. 87: Single-acting hydraulic pressure intensifier

With regard to a required process control, a pressure intensifier should be used which enables a sensitive internal pressure. Thus, only a single-acting pressure intensifier (*Fig. 87*) can be applicable. This is so that no additional valves in the high pressure range, which are necessary with double acting pressure intensifiers for switching between the chambers, affect the internal pressure unfavourably. The main advantages are: a) continuous, pulsation-free pressure build-ups up to 10,000 bar are

possible, b) pressure intensifiers are continuously adjustable. Though due to the very small flow volume required, an imprecise pressure adjustment/controlling is to be expected. That demands a complex and costly build-up/assembling of a control system with pressure regulators, valves etc. Furthermore, according to conventional hydroforming machines used today an additional filling unit to fill the workpiece with medium before pressurisation is required. High initial costs are expected which vary around €13,000 to €16,000 (only for intensifier) and may easily double or more for the additional control system and the filling system needed.

Air-driven pump

Air-driven intensifiers operate on the simple principle of an automatic reciprocating differential air piston. A large air-operated piston is connected to a smaller high-pressure piston to convert compressed air flow into fluid flow at high pressure. A range of single (*Fig. 88*, left) are offered by several suppliers. Maximum achievable outlet pressures add up to approximately 5,500 bar. Intensifier ratios may increase to 1:800.

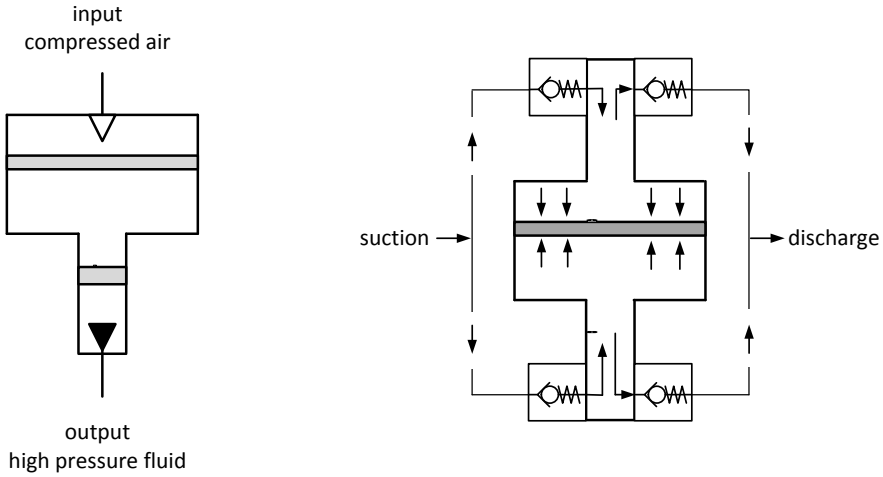

Fig. 88: Principles of air-driven pumps

Contrary to a single acting pump consisting of an air piston and high-pressure piston, double acting pumps (*Fig. 83*, right) have two high-pressure pistons which have a

more continuous flow and pressure. During operation the outlet pressure and flow can be controlled by regulating the air drive pressure with an air pressure regulator.

Major advantages are a) working pressure up to approx. 5,500 bar, b) no additional hydraulic drive is necessary c) low noise level d) easy maintenance e) low initial costs (typically less than €10,000) and finally air driven intensifiers are f) suitable for water, oil and several different chemicals.

As previously mentioned, when compressed air is applied to the pump, the pump will cycle at high speed to produce a high fluid flow. This specific advantage of an air-driven pump is one of the main drawbacks for the dimensioning of a micro-hydroforming machine. Regarding the minimised dimensions compared to the traditional hydroforming process, only a very small forming volume and with that a low volume flow is required. Supplementary, no pulsation-free pressure build-up or imprecise regulation is to be expected. The outlet pressure of the fluid is indirectly controlled by regulation of the air pressure. Relying on the high intensifier ratios compared to the hydraulic drive system, adequate control accuracy is not to be expected.

6.7.2.1 Spindle driven pressure intensifier

Fig. 89 shows a commercial spindle driven pressure intensifier. The high pressure is generated by a plunger which is driven by a mechanical drive consisting of an electric motor and a spindle gear. Maximum hydraulic pressures up to approximately 10,000 bar are achievable.

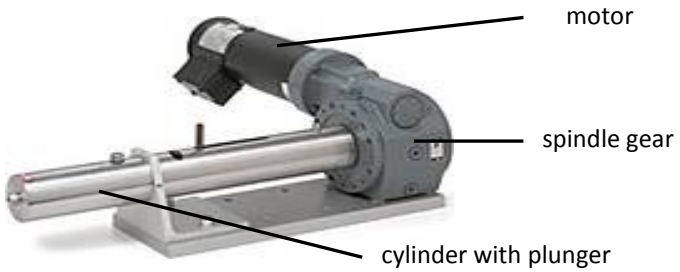

Fig. 89: Spindle driven pressure intensifier

The operation principle is shown in *Fig. 90*. The spindle press works as follows: In the first step the pump plunger has to advance to its end position. After closing the discharge valve v2, followed by an opening of the inlet valve v1, the fluid fills the cylinder since the plunger moves backwards. To pressurise the fluid, the pump plunger advances again until the required pressure is reached. The relief valve avoids the pressure generation back into the fluid reservoir.

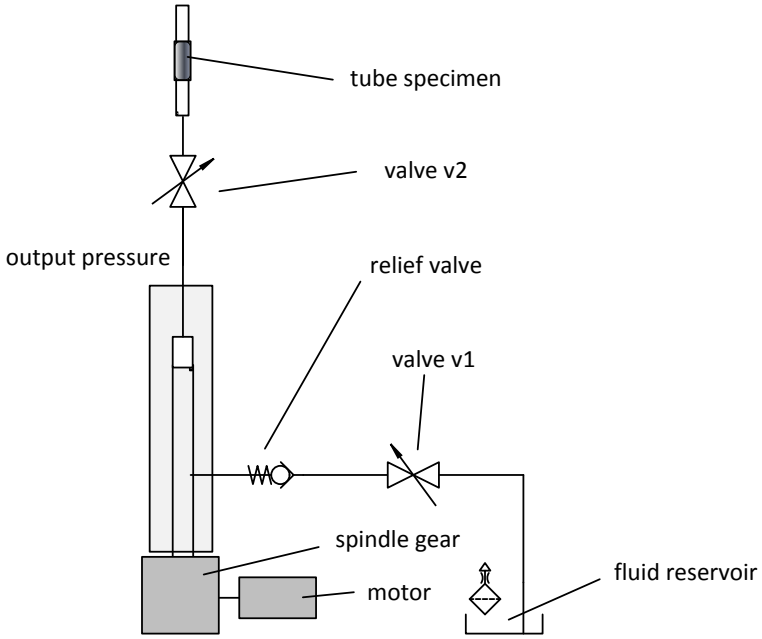

Fig. 90: Operating principle of a spindle pressure intensifier

Due to a comparatively easy controllability of the DC-servo motor, an accurate pressure control is to be expected. A further advantage is a low volume flow. One potential drawback is high costs particularly if the spindle press is supplied with integrated feedback control system; they can be up to € 30,000 and also may have a prolonged time for tube filling.

6.7.3 Conclusion - selection of the high-pressure generator

Theoretically all investigated systems are suitable to apply the required pressure of 4,000 bar. However, the systems differ in accuracy of pressure control when small

volume flows under high pressure are to be expected. Thus, and after evaluating all other criteria as mentioned in the decision matrix, the mechanical driven pressure intensifier (the spindle press) has been selected for the micro-hydroforming prototype machine.

	Hydraulic driven pressure intensifier	**Pneumatic driven pressure intensifier** (air driven pump)	**Mechanical driven pressure intensifier** (spindle pump)
Max Pressure (4,000 bar)	5	5	5
Small Volume Flow	1	2	5
Pressure Generation within the calculated cycle (conveyor speed) /filling time	4	2	4
Pulsation free HP-generation	4	1	5
Quality of Controllability	3	1	4
Capacity (small)	2	1	5
Overall	**19**	**12**	**28**

Rating	**Description**
5	Complete satisfaction: objective satisfied in every respect
4	Considerable satisfaction: objective satisfied in the majority of aspects
3	Moderate satisfaction: balance between complete satisfaction and no satisfaction
2	Minor satisfaction: objective satisfied to a small extent
1	Minimal satisfaction: objective satisfied to a very small extent

Table 14: Decision matrix for the high pressure generators

To be applicable with all oil-water emulsions or solutions and all kinds of oil which do not solidify under high pressurization, all wetted parts of the pressure generator are manufactured of stainless steel. Exclusively the packing of the piston is made of Teflon.

Further specifications of the spindle press are:

Working pressure:	4,000 bar
Swept volume:	7.5 ml
Capacity:	0.07…9 ml
Stroke:	100 mm
Type of actuation:	DC-servo motor, DC-tacho integrated
Speed:	3,200 1/min

Apart from the five main standard components (electromagnetic-operated 3/2-port pneumatic control valve, 10,000 bar high-pressure transducer, check valve, safety heads with rupture disc) the whole high-pressure cycle which was built up, comprises more than 30 further standard parts (tubing, fittings, collar screws, collars, etc.). Only the slide carriage was a component to be manufactured. As a result, a total number of more than 60 standard and non-standard parts including the pneumatic components to operate the 3/2-port hydraulic control valve are involved in the subassembly to apply the internal pressure. A detailed description and all functions of the components integrated can be found in *Chap. 6.7 Control System*.

6.8 Control system

6.8.1 Requirements

The micro-hydroforming process bears the risk of a process failure if the parameters have been chosen inappropriate. Therefore, the controlling system of the forming process is a critical component.

For the design of a hydroforming process a multitude of workpiece parameters, tool parameters and process parameters, which all have a decisive influence on the final product, must be considered. It was the aim to consider all the parameters and their effects to ensure the optimal process is achieved. The exact variation of the process parameters such as the internal pressure p_i, the axial loads F_a and/or axial feeding x in

combination with the press force F_c are essential to obtain a failure free forming result.

Another issue to be considered is the question of the command variable used. The process management may act on different variables. In the first instance, relying on conventional hydroforming processes, the internal pressure was selected as the command variable. According to this, the axial force and/or the axial displacement as well as the press force are to be assigned as p_i-dependent variables.

6.8.2 Realization of the machine control

Regarding the mentioned requirements and keeping in mind that especially for experimental use of a prototype machine, versatile data as well as data row combinations have to be integrated into the control software, LabVIEW was chosen as the 'overall' hydroforming machine system software. LabVIEW (short for Laboratory Virtual Instrumentation Engineering Workbench) is a platform and development environment for a visual programming language from National Instruments. The graphical language is named "G". In particular for prototype applications and laboratory use, its free programmability and the feasibility of easily embedding manually generated data rows into the program were decisive selection criteria.

LabVIEW for process control and SPS for an additional machine control system

In order to provide 'fixed' machine parameters, an independent SPS machine control was integrated into the process control. That means, the machine control is responsible only for the compliance of the set points given by the process control and has no influence on the process parameters.

This machine control had been divided into logical subsystems including an individual subroutine and each subsystem was discarded into the process control.

The tasks that could be performed via these basic modules include:

- initialisation of the machine (generation of the system pressure, query of the security arrangements)
- filling the spindle pump cylinder
- moving toward the ends of the tubes
- inducing the filling operation and/or
- sealing with defined axial forces (use of conical sealing punches without axial feeding)

If process modifications were necessary, single basic modules (which are alike) remain untouched and were implemented unchanged into the modified process.

The modules responsible for the compliance of the loads and the internal pressure were supposed to be carried out as external analogue control loops. Analogous regulator structures have the advantage that they are low-priced and can react quickly to monitoring variables. Moreover they require no computation time so that the main computer control is released of this task. The single sub-modules of the control system include periphery hardware components which are presented and described in the following.

6.8.2.1 Pressure intensifier control module

As described in *Chap. 6.7.2 High pressure intensifier - system studies* the pressure intensifier, which is responsible for the generation of the internal pressure is driven by a 110-V-DC-servo motor. To regulate the required volume flow and thus the necessary servo motor speed a DC-Servo-controller was chosen. Due to a 4-quadrant operation mode the controller is capable of driving the spindle motor in both directions. In consequence its high frequency capabilities, the selected controller gives rapid and smooth reaction to assure a fast and fine trim of the pressure needed. A further advantage is the feasibility of either a speed control or a torque control. It

was first implemented to use speed control; however torque control may be a good alternative.

As the pressure intensifier is only able to accomplish a few tube filling cycles per stroke, an individual control loop has been created to ensure a continuous tube filling. This control loop (independent from the process control) is operated by a logic module 'Siemens logo!'. The program implementation had been accomplished by combining stored functions with a small SPS program. Additionally the logic module comprised the option for making easy time-consuming changes through a simple user interface so as not requiring any re-programing of the software. However, all operations such as the program simulation or a creating/change of a program could be made on the controlling PC.

Additional components integrated in the high-pressure control loop are:

A high-pressure transducer (measuring system: DMS) for high-pressure up to 10,000 bar has been integrated into the high-pressure circuit to enable the measurement of the internal pressure of the liquid medium that effects the expansion of the tube. The acquisition is amplified by a strain gauge full bridge amplifier.

A double-piston air operated valve, normal closed type, 4,000 bar, is mounted close to the pressure outlet of the intensifier and has the function to disconnect the machine from the high pressure circuit when: the forming has been completed, the intensifier moves backwards to refill its pressure chamber or a sudden pressure drop (due to early tube bursting) occurs. In the last case, it acts as a «fail-safe» shut-off function. The two main common features of the high-pressure valves offered by a few suppliers are the two types of actuation: either hand-operated or air-operated. In order to meet the requirement of controllability, an air-operated valve was utilized; however it required a compressed-air circuit which had also to be integrated into the control system.

To control the air-operated 4,000 bar valve via the computer a standard 3/2-port-valve had been included in the compressed-air circuit. In order to avoid an expansion of the high-pressure back into the intake duct, a relief valve was mounted on the

intensifier inlet. To avoid potential destructive or dangerous unintentional overpressure in the high pressure system a safety head with rupture disc was integrated into the high-pressure circuit. The disc inserted would burst at system pressures above 4,000 bar.

6.8.2.2 Control module of the axial drives

The axial drive linear actuators (please see *Chap. 6.5*) had been selected to operate with two micro-step constant current drivers (bipolar-chopper drivers). Both drivers (for individual control of each actuator) are controlled via 5V output from the control computer attached to the machine.

As the internal pressure is to be the command variable of the control system, the impacts of the axial drives on the tube ends should respond to this. This could be accomplished by using two different control facilities. Either, one uses a force control (herewith the actual value is ascertained via load cell adapted to the sealing punches) or the actuators can be transition controlled. That way, displacement transducers mounted on each punch for individual transition control measured the actual values.

Which concept will turn out as the most adequate, could not found out during my studies and therefore must be determined in future experimental investigations.

6.8.2.3 Control module of the press drive

As discussed previously, a press with a hydraulic cylinder for tool opening and closing was selected.

Since the machine presumably required “forming error compensation” due to occurring deflections inside the frame and the forming tool, the control system was flexible enough to easily encompass these requirements.

The hydraulic cylinder displacement transducer could be cascade-controlled. That means that initially a transition control effects a steady positioning of the upper die

during the pressurisation of the tube. Hence, a control valve was included into the hydraulic circuit for the regulation of the piston position of the hydraulic cylinder.

In addition, a subordinate control loop operates the pressure controller, which enables the adjustment of the required press load as well as error compensation if needed. Thus, a second sensor (a pressure transducer to be implemented into the hydraulic press circuit) became necessary to measure the current system pressure. To regulate the set pressure a proportional excess pressure valve was further inserted into the circuit. Also a lock valve which avoids the piston and the upper tool from sinking down in an emergency case and a pressure limiting valve and a check valve were integrated in the hydraulic system. The complete system is shown in the hydraulic diagram, *Fig. 91*.

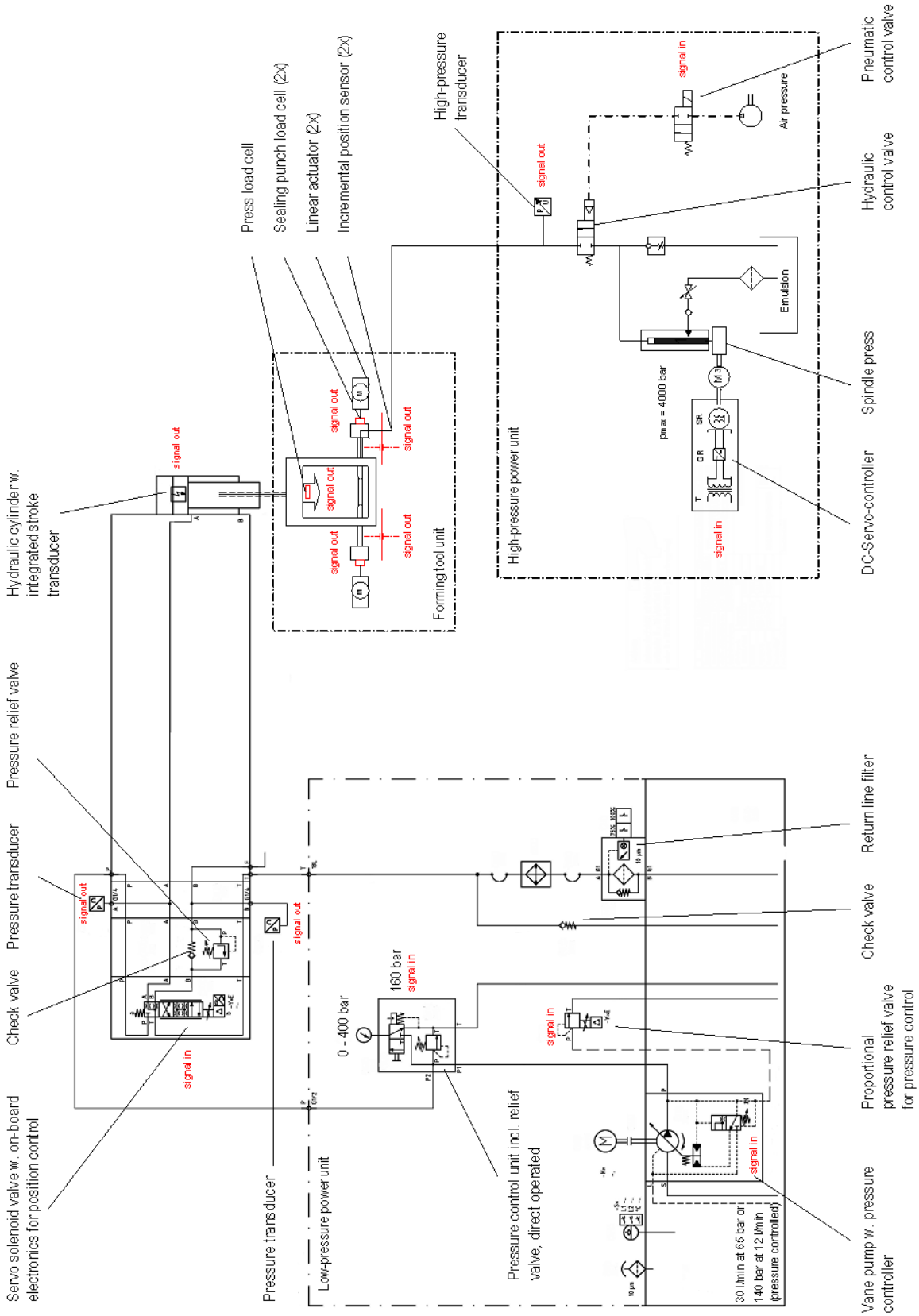

Fig. 91: Hydraulic plan

6.9 Inclusion of laser heat assisted hydroforming

One of the principal hypotheses investigated in this thesis was for the inclusion of laser heat with the expectations of increasing formability in the micro tube hydroforming process. In some micro forming technologies the inclusion of heat has contributed to increased formability though the research detailed in the previous chapters have conclude that the addition of laser heat does not increase formability enough to warrant the greater complexity and costs needed to include this in the prototype micro tube hydroforming machine. Nonetheless, investigations were still carried out to how a system could be included in the first THF prototype machine.

The main components needed to be investigated are:

- modified moulds that permit the transmission of laser heat
- appropriate laser selection
- laser mounting and direction of energy transmission
- integrating the laser into the control system

6.9.1 Hydroforming moulds permitting transmission of laser heat

It is easy to identify that traditional hydroforming moulds will not allow the transmission of laser energy to the forming part. As discussed earlier the moulds are made of structurally sturdy materials to prevent any deformation during the THF process so no portion of the forming part is visible during the forming process.

A feasible solution is to construct special moulds with ‘sapphire windows’ in the mould allowing the laser light to pass those windows. Sapphire combines the required transparency to laser radiation at all wavelengths $\lambda >$ ultra-violet (UV) with brilliant mechanical properties such as high compressive strength, hardness and Young's Modulus making it especially suitable for metal forming. Additionally a melting point of approx. 2050°C allows warm respectively even hot forming of e.g. steel without destroying the forming tool. The cutting and shaping a sapphire to be inserted into a typical hydroforming mould will create the ‘window’ that can pass the laser energy to the forming part. As the sapphire will now be the inner part of the

mould, where the tube will be expanded to form the part - the sapphire will need to be cut/machined, e.g. by laser ablation to become the forming section of the mould. *Fig. 92* represents a CAD drawing of a mould prototype including a 'sapphire window'.

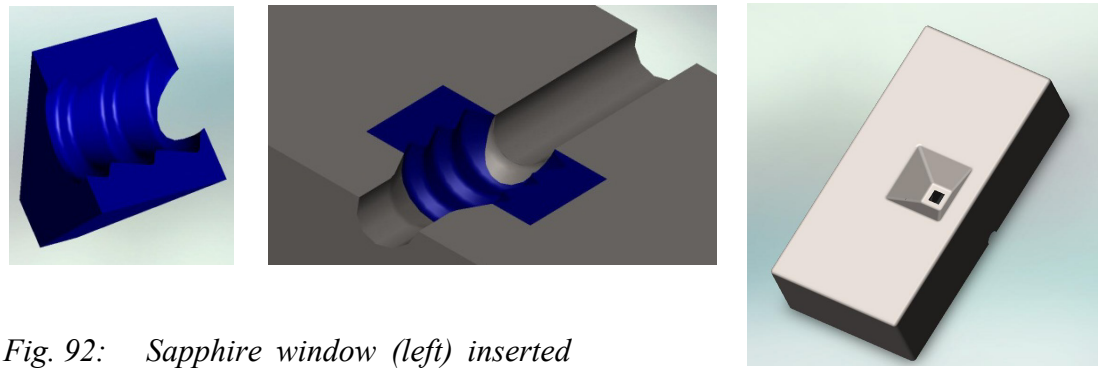

Fig. 92: Sapphire window (left) inserted into the tool (centre), and back side view of a possible forming tool (right)

However, including a sapphire and the special machining to form the material and include it into the mould will already greatly increase the cost and complexity fabricating moulds.

6.9.2 Lasers selection for hydroforming

For the purpose of laser heating a diode laser seems to be (from an applicant's point of view) the most suitable choice for the laser source as it offers several advantages in comparison to other laser systems:

- Comparatively low purchase cost
- Very high durability with often > 30,000 hours and low power degradation <<1% / 1,000 hours when operating at rated current which is an important requirement regarding process stability in mass production
- Robust, and compared to lamp-pumped lasers, long maintenance intervals

- Coupling and transport of radiation in fibre optical cables, this is of high importance regarding the direction of the laser light to the forming tool, cf. following sub-chapter
- Available with large output power (~up to 1,000 W) in combination w/low cost
- Easy pumping by electric current, that means the laser energy input and thus the resulting temperature into the workpiece can easily be controlled via the current of the diode laser
- Size, to meet the requirements of desktop size machine these lasers are available in 19" rack chassis which allows an easy positioning either in the electronic cabinet or underneath the machine table inside the housing
- Available in the required wavelengths (usually in the range of λ = ~800 - 1000 nm, however in case of an InGaAIP diode laser with λ = 635 nm also suitable for copper processing, cf. *Chap. 5.4.7 Effects of laser light absorption in copper*.

6.9.3 Applying laser heat during hydroforming

Adding the laser into the prototype machine is fairly straight forward. The laser only requires a reliable power source and a secure mounting system free from vibration and twisting/deformation forces from the THF process.

Directing the laser energy can be accomplished either by directly "guiding" the laser energy via an open beam through mirrors to the target location, or more feasibly direct the beam via glass fibre to the laser optics to point to the appropriate location on the mould.

The most likely area to position a ‘sapphire window’ would be in the bottom mould halve. The lower mould halve is always stationary with few parts and complexity present on the lower half of the mould. Therefore the laser energy would be directed from the bottom of the forming machine also making the installation of the laser less complex.

A possible mounting system could consist of an x-y- micro cross table and a third axis for the z-shift of the focal point. The focussing lens (focussing optics) can easily be fixed on the linear axes which in turn can easily be moved by micrometre screws if a re-positioning/adjustment of the lens is necessary after changing moulds for manufacturing different parts.

As the laser source as well as a fibre cable could entirely be placed underneath the machine table inside the housing, in the rare case of accidental discharge of the laser the machine and its casing should prevent the laser beam to come into contact with any person's eyes. Though on the final design a safety evaluation would need to be conducted to identify any safety risks and recommend if any additional light shielding or laser safety goggles would be necessary.

6.9.4 Integrating a laser into the control system

The last point to consider is the inclusion of the laser control into the control system for the THF machine. There are three points to consider: directing the laser energy, controlling the laser (turning it on and off during the appropriate sequence) and getting the forming part to the appropriate temperature.

Directing the laser energy should be fairly simple. As a diode laser should direct the energy through fibre optics to the machine, thus directing the energy is a matter of mechanically moving or mounting the cable to point to the appropriate area on the mould. The fibre optics will most likely have a unique position for every mould so need to be repositioned for any mould change.

The THF control system would view the laser as another step in the forming process. It would need to turn on the laser then either: if measure the temperature of the part wait until the critical temperature is reached, or if using a simple duration of laser energy time wait - then in either case start the pressure build-up for the start of the hydroforming process. The laser would be turned off through the THF controlling system before, during or at the completion of the hydroforming process. Using the

above proposed diode laser system this turn on/turn off signal could easily executed via analog 0-5 V outputs or a digital signal controlling the current of the laser source.

6.9.5 Conclusion of the laser inclusion

As it requires time to heat the tube - inclusion of the laser heat will not only increase complexity and costs but can add a significant amount of time for producing any part. Again for all these reasons with the minimal or negative increase in formability found in the earlier investigations it was concluded that a laser system was not necessary to include in the first prototype machine.

6.10 The prototype machine system realized

6.10.1 Description of the prototype machine

Based on the results obtained from the experimental work and theoretical considerations, cf. Chap. 4-6.8, a close-to-production machine system for performing the miniaturized hydroforming process has been created. The prototype machine with its main components is schematically represented in *Fig. 93*.

The press frame which includes the forming machine is mounted on a machine table. The encased table covers the high pressure system (spindle press and additional components) for the generation of the internal pressure, a hydraulic power unit for the press cylinder and an air compressor necessary for the air-driven valves. The control system, all electric and electronic devices and the computer are housed in an electric cabinet which is placed beside the machine, *Fig. 94*. For safety reasons, a housing made of 10 mm polycarbonate windows encases the hydroforming machine and covers all pressurized machine components. For maintenance as well as for manual workpiece exchange, the polycarbonate cover can be opened via a three-

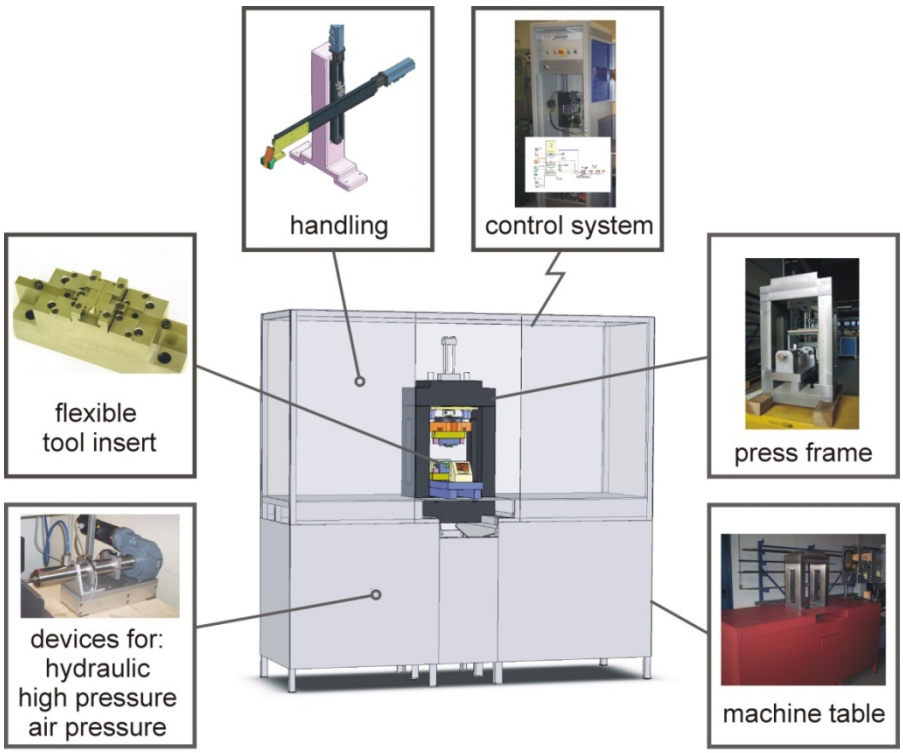

Fig. 93: Micro hydroforming machine assembly

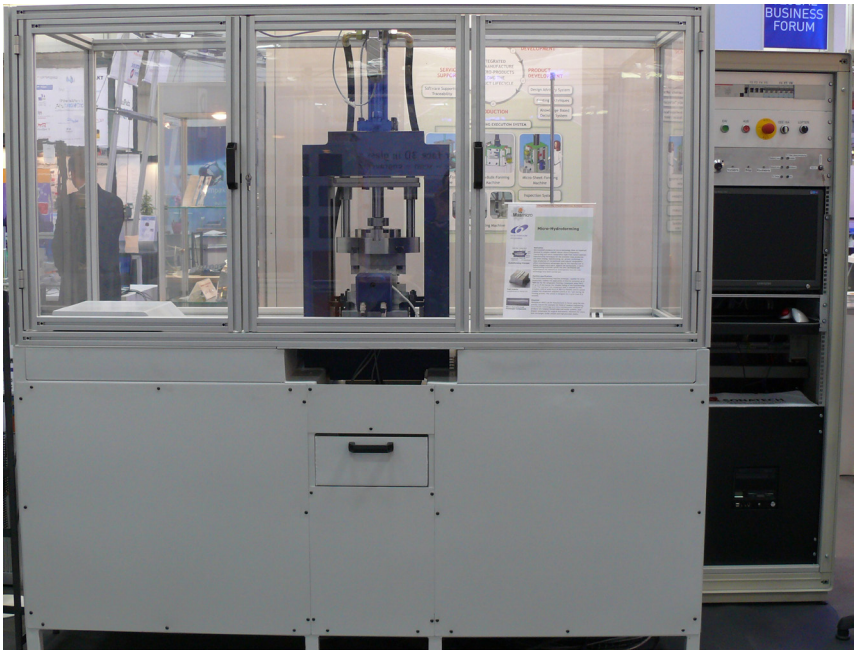

Fig. 94: Close-to-production micro-tube hydroforming machine

piece front door. Sufficient space on both the right and left side of the machine frame allows the future placing of a workpiece handling system.

The machine developed facilitates hydroforming of tubes made of different material with initial outer diameters of less than 1mm and internal pressures up to 4,000 bars.

To change to new product geometries flexible designed tool halves (with variable die geometries) can be exchanged quickly with a few easy steps. Two independently controllable linear actuators with ball screw allow axial tube sealing loads of up to 800 N of each sealing punch. The positioning accuracy of the movement is below one micron which corresponds to smallest micro part tolerances used in micro-manufacturing technologies today. The machine system can be driven with both cylindrical for THF-processes with axial feeding as well as conical sealing punches with fixed/clamped tube ends. However, the first machine experiments only utilized conical sealing punches, thus only forming trials without axial feeding are discussed in the following chapter. *Fig. 95* shows the lower tool assembly including the die insert with its shaping die geometry.

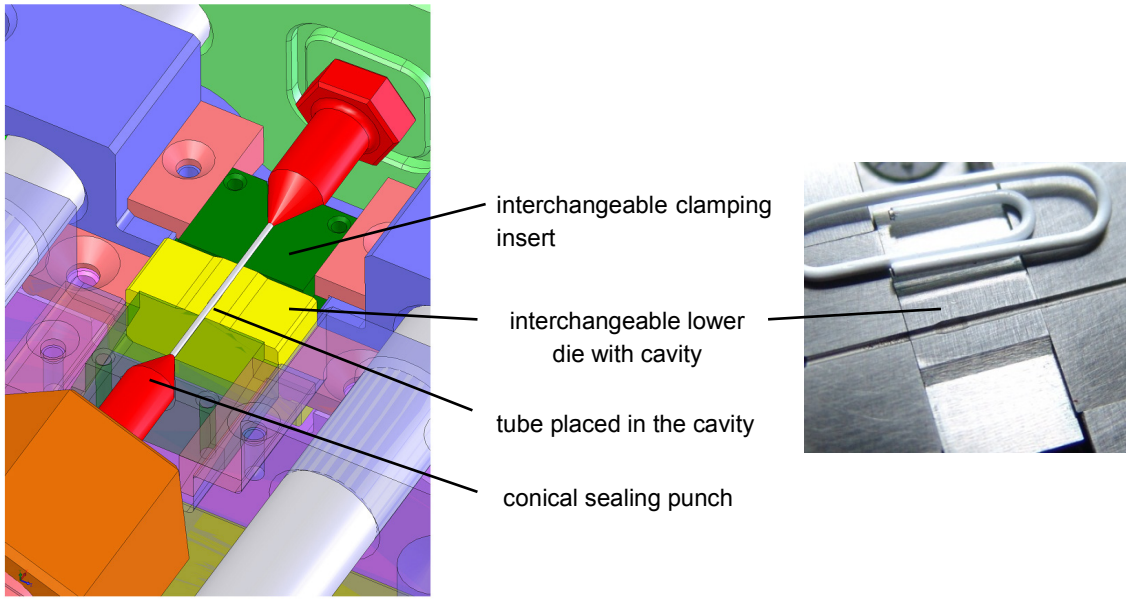

Fig. 95: Arrangement of the lower tool components (left) and lower die cavity with size comparison (right)

6.10.2 Achievable precision of the machine

Precision was one of the main requirements of the micro THF prototype machine system. With regards to the size-dependent effects it was tried to

- reduce the numbers of gaps/interfaces between machine components which may cause elasticity
- minimize clearance/bearing clearance

It was an aim to manufacturing machine components in narrowest tolerances. However, a compromise must be made for instance between "*small number of components* and *adjustment feasibilities*", especially regarding the tooling (adjustment plates for the tool inserts). Thus, it must be concluded that the precision of the machine will be limited to a certain extend by factors such as:

- clearance fit, e.g. of the alignment pins between upper/lower tool
- bearing clearance, e.g. guiding rods for the axial punches
- deflexions caused by forming/machine loads inside the tool/machine
- delivery condition (tolerances) of the micro-tubes, e.g. diameter tolerances

The precision of the machine shall be determined by the itemization represented in *Table 15* on the next page. By summarizing all of the individual machine and workpiece tolerances, the maximum overall tolerance arises to 142 µm. With regard to a part to be manufactured, its achievable precision/accuracy may thus be in the range of 9 to 142 µm. This means, if it is a part with a final circular cross-section, its ellipticity may - in a worst case - amount to the calculated value of 142 µm.

Characteristic	**Tolerance [µm]**
Outer tube diameter tolerance, e.g. AISI 304 stainless steel micro-tube 08x004, D_0 = 780-820 µm	0 to 40
Guiding pins between upper and lower tool half: boring was manufactured 8H7 (+15 µm / 0 µm); pin was 8h6 (0 µm / -9 µm)	0 to 24
Displacement of the forming tool (FEA cf. *Fig. 83* in *Chap. 6.4.6 Realization of the tool unit*)	3
accepted manufacturing tolerance acc. to the CADs: +/-5 µm	0 to 10
Guiding rods of the axial punches: Outer diameter of the rod was 14g6 (-6 µm / -17 µm), inner diameter of the slide carriage was 14H7 (+18 µm / 0 µm)	6 to 35
Unequal forming behaviour, difference in wall thickness after forming; e.g. copper R250, cf. *Fig. 29* in *Chap. 4.8.2 Formability of examined copper tubes at RT*	0 to 30
Resulting machine/part precision (sum of individual tolerances)	**9 to 142**

Table 15: Approximate determination of the machine precision

CHAPTER 7

FORMING EXPERIMENTS WITH THE PROTOTYPE MACHINE AND ANALYSIS

This chapter describes the first "real" tube hydroforming experiments using the designed prototype machine. The overall goal was to draw a conclusion at the end of the study on the miniaturized process, the designed tools and the other machine components. Measurements of the forming diameters in different tube areas of the micro-tubes should identify possible effects of elastic tool deflections on the final part geometry.

Following a short description of the experiments, the analysis of the experimental investigations of a first hydroformed micro part is given.

7.1 Investigated tube geometry and used materials

In line with the tube hydroforming experiments three different tube materials have been investigated which had been formed in the die geometry 'camera shaft'. The forming geometry is represented in *Fig. 96*.

Tube materials

The experiments were conducted with the following materials

- Stainless steel AISI 304 micro-tubes (batch B) - delivery status
- Stainless steel AISI 304 micro-tubes (original batch B) - recrystallized
- Copper CW024A (R200) micro-tubes - delivery status

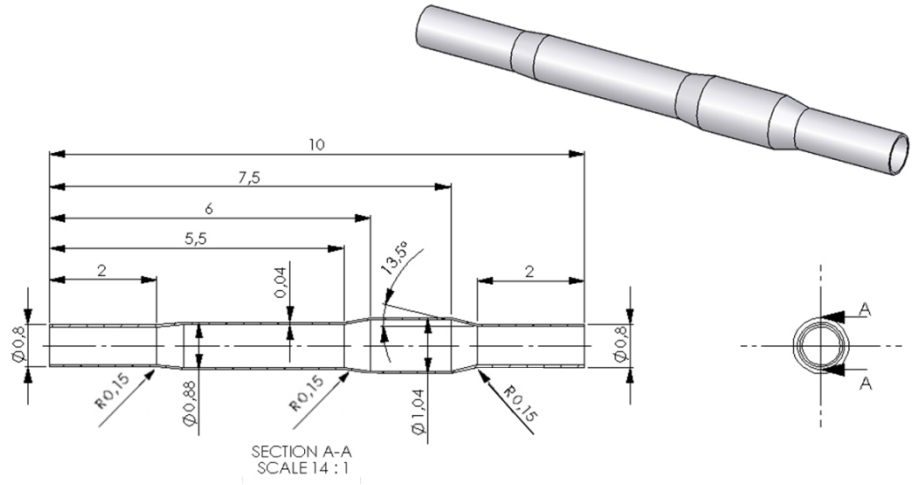

Fig. 96: Investigated tube geometry 'camera shaft', 2D and 3D drawing

Corresponding specifications of the materials as supplied can be found in *Chap. CHAPTER 3.* Tube properties of the recrystallization annealed AISI-304-b are listed in *Table 16*.

Micro-tube 08x004		**status: recrystallized annealed**	
Material:	AISI 304	Ult. tensile strength [MPa]:	513
Outer diameter [µm]:	800	Yield strength [MPa]:	275
Wall thickness [µm]:	40	Elongation at fracture [%]:	26.7
		Hardness HV 1:	150.1

Table 16: Mechanical properties of the recrystallized annealed AISI-304 micro-tube

7.1.1 Heat treatment of the AISI 304-b micro-tubes

During all forming experiments with the AISI 304-b tubes, early workpiece failure occurred due to bursting. Thus, the idea was to reduce potential dislocation density in the grain structure to a minimum by conducting an additional recrystallization annealing process causing a reduction of lattice defects in the crystallites which are

based on re-formation of the microstructure on the basis of nucleation and grain growth. However, the following issues were expected to be encountered:

- Formation of coarse grain size because of the low (initial) germination number due to only a low deformation degree of the tubes' delivery status
- In turn non-uniform forming
- Loss of strength of the final (hydroformed) part

Tube specimens pre-cut in length and ready for the experiment were annealed over a two hour duration at 620°C.

To analyse the influence of the heat treatment on the grain structure, tube sections were embedded in resin and their polished surface were micro-etched using a mixture of aqua regia (nitrohydrochloric acid) and “Vogel’s” pickling inhibitor. Compared to the grain structure of the original tubes, the grain size increased to 45-60 µm on average corresponding to 6-5 ASTM which refers to the ASTM definition in the transition region of a fine-grained to a coarse-grained structure. In the following, the recrystallized AISI 304 micro-tube is denoted as 'AISI 304-r' to clearly distinguish it from the other stainless steel micro-tubes used during the study.

Fig. 97: Microstructure of the recrystallized AISI 304-r micro-tube

7.2 Procedure of the tube hydroforming experiments

Every tubular specimen was cut from the wrought material. Depending on the dimensions of the die inserts and the conical clamping inserts the tubes had exactly to

be ground to lengths of 26.4 mm. Before each automated conducted test the tubular test pieces were manually placed into the lower die. Once pre-filled, the sealing punches were charged with the specific axial force F_a according to *Eqn.* (8) and *Eqn.* (9) - (12) (see *Chap. 2*), respectively. It should be mentioned that due to the fixed tube ends and application of the test without axial feeding one of the components of F_a - the friction force F_f - did not need to be determined. The tubes were pressurized with linear increase to the maximum internal pressure (calibration pressure) $p_{i,\,max}$ which had been established using *Eqn.* (6), cf. *Chap. 2*. For each of the tube materials, five samples were hydroformed.

Before conducting the trials, all required and determined process parameters had been programmed into the LabView control system of the prototype machine.

7.3 Forming results

The test results and the process parameters of the hydroforming experiments are shown in *Fig. 99* - *Fig. 101*. In each figure the tube dimensions and the applied process parameters are represented at the top, microscope pictures of the formed tube specimens are shown below. The lower pictures (of the stainless steel micro-tubes) show the resultant forming diameters D_1 of each tube section (A-D), *Fig. 98 (left)*. Corresponding values which express the circularity of the formed tubes can be found in *Chap. 7.3.1.*

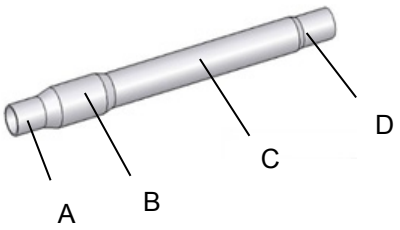

Fig. 98: Forming sections of the stepped tube diameters

For the measurement of the forming diameters of each tube section a digital microscope Keyence VHX-600 with charge coupled device camera was used. Tubular

specimens had been measured at least three times in each forming section including a horizontal (x-) and vertical (z-) diameter, i.e. rotated ninety degrees and measured.

7.3.1 Description of the test results

Stainless steel AISI 304-b (delivery status)

As can be seen from the microscopic pictures in *Fig. 99* the stainless steel AISI 304-B micro-tubes could not achieve the required relative expansion ratio ε_d which was given by the maximum diameter of the die in section (B). It was defined as:

$$\varepsilon_d = (D_{1(B)} / D_0) - 1 \tag{19}$$

where D_0 and $D_{1(B)}$ are the initial tube and maximum die diameters in tube section (B), respectively.

Before the tubes were able to expand to the aspired forming diameter $D_{1(B)}$ = 1.04 mm in the main forming zone, fracture due to bursting occurred which corresponds to the results obtained during the hydraulic free-bulging, cf. *Chap. 5.5.1 Experimental results established from investigations performed at room temperature*. (In these early forming tests the mean outer forming diameter D_{1b} was 1.03 mm with a scatter of 80 µm). The areas of each tube in which bursting occurred were evenly distributed around the tube circumference (at different points around the circumference), however always in the same section of the largest forming diameter. As an example of the measured forming diameters of the analysed tube sections, cf. *Fig. 98*, their values can be taken from both the tables (tube's horizontal diameters, and tubes vertical diameter, 90° twisted) on the right side of the microscope pictures in *Fig. 99*. On average, the expanded tube diameters of all investigated tubes measured in:

- Section A: $D_{1(A)}$ = 0.883 mm with a standard deviation of 0.024 mm and a mean concentricity tolerance $T_{(A)}$ = 22 µm
- Section B: could not be measured due to crack formation

- Section C: $D_{1(C)}$ = 0.984 mm with a standard deviation of 0.024 mm and a mean concentricity tolerance $T_{(C)}$ = 18 µm
- Section D: $D_{1(D)}$ = 0.882 mm with a standard deviation of 0.022 mm and a mean concentricity tolerance $T_{(D)}$ = 26 µm

Stainless steel AISI 304-b (recrystallized annealed)

Applying *Eqn.* (6) and according to the reduced ultimate tensile strength of the re-crystallized AISI 304-b stainless steel micro-tubes the process parameter calibration pressure $p_{i,\,max}$ was programmed to 154 MPa. In contrast to the hydroforming trials conducted on the original material, the recrystallized (annealed) tubes of the same material with the now reduced pressure could be formed successfully without failure due to bursting, *Fig. 100*. All investigated micro-tubes were formed until their entire outer surface contacted with the forming die. In these tests, the expanded tube diameters of all investigated tubes measured in average:

- Section A: $D_{1(A)}$ = 0.796 mm with a standard deviation of 0.042 mm and a mean concentricity tolerance $T_{(A)}$ = 77 µm
- Section B: $D_{1(B)}$ = 1.043 mm with a standard deviation of 0.041 mm and a mean concentricity tolerance $T_{(B)}$ = 74 µm
- Section C: $D_{1(C)}$ = 0.894 mm with a standard deviation of 0.038 mm and a mean concentricity tolerance $T_{(C)}$ = 71µm
- Section D: $D_{1(D)}$ = 0.787 mm with a standard deviation of 0.052 mm and a mean concentricity tolerance $T_{(D)}$ = 95 µm

Copper CW024A (R 200)

In analogy to the investigated AISI 304-b stainless steel micro-tubes in their delivery status, also the R200 copper tubes (which also could not be widened to D_1 = 1.04 mm during the early free-bulging tests which corresponds to the maximum die diameter) could not be hydroformed without occurrence of fracture, *Fig. 101*. Compared to the AISI-304-b stainless steel tubes, only very large forming radii between the

stepped forming diameters can be observed. The following tube diameters of the investigated copper micro-tubes in their individual sections according to *Fig. 98* had been achieved:

- Section A: $D_{1(A)}$ = 0.905 mm with a standard deviation s of 0.025 mm and a mean concentricity tolerance $T_{(A)}$ = 43 µm
- Section B: could not be measured due to crack formation
- Section C: $D_{1(C)}$ = 0.949 mm with a standard deviation s of 0.028 mm and a mean concentricity tolerance $T_{(C)}$ = 45µm
- Section D: $D_{1(D)}$ = 0.882 mm with a standard deviation s of 0.030 mm and a mean concentricity tolerance $T_{(D)}$ = 15 µm

Hydroforming experiment 'camera shaft'

Stainless steel AISI 304, batch B - delivery status

Test parameters:

Material: stainless steel AISI 304-B

Tensile strength σ_{UTS} : 593 MPa

Tube dimensions:
Tube length L_0 = 26.4 mm (*)
Outer diameter D_0 = 0.8 mm
Wall thickness t_0 = 40 µm

Procedure parameters:

Calibration pressure $p_{i,\,max}$ = 178 MPa
Axial sealing force F_a = 75 N
Volume flow: V_{Fl} = 0.07 ml/min.
Forming temperature: RT

Relative expansion ratio ε_d (**): 0.3

(*) overall length of die and clamping inserts
(**) According to *Eqn.* (19) and given die dimensions

Visualization of the forming results:

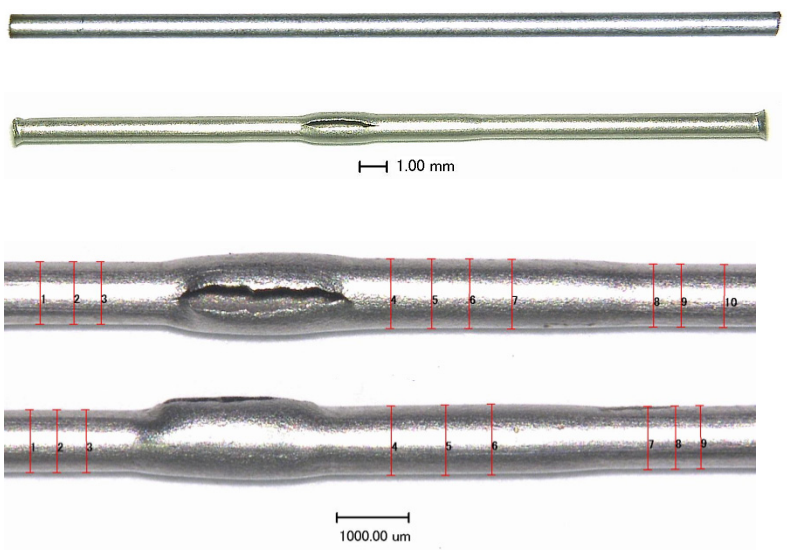

T_i: Initial tube

T_{01}: Hydroformed tube

T_{01}: Forming zone with section of fracture, top view

T_{01}: Forming zone, side view

Fig. 99: Forming results with test and procedure parameters of the hydroforming experiment 'geometry camera shaft' - stainless steel AISI 304 (batch B - delivery status)

Hydroforming experiment 'camera shaft'

Stainless steel AISI 304, batch B - recrystallization annealed

Test parameters:

Material: stainless steel AISI 304-B (recrystallization annealed)

Tensile strength σ_{UTS} : 513 MPa

Tube dimensions:
Tube length L_0 = 26.4 mm (*)
Outer diameter D_0 = 0.8 mm
Wall thickness t_0 = 40 µm

Procedure parameters:

Calibration pressure $p_{i,\,max}$ = 154 MPa
Axial sealing force F_a = 65 N
Volume flow: V_{Fl} = 0.07 ml/min.
Forming temperature: RT

Relative expansion ratio ε_d (**): 0.3

(*) overall length of die and clamping inserts
(**) According to Eqn. (19) and given die dimensions

Visualization of the forming results:

T_i: Initial tube after recrystallization

T_{13}: Formed micro-tube

T_{13}: Hydroformed prototype with cut ends

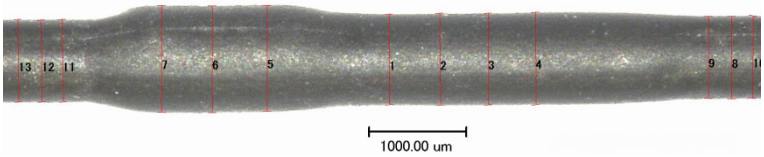

T_{13}: Forming zone and measurement of the stepped forming diameters, top view

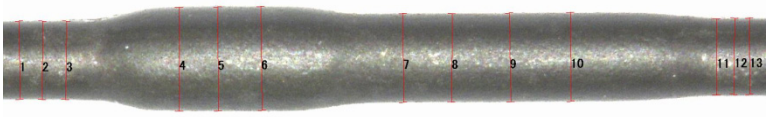

T_{13}: Forming zone and measurement of the stepped forming diameters, top view

Fig. 100: Forming results with test and procedure parameters of the hydroforming experiment 'geometry camera shaft' - stainless steel AISI 304 (batch B - recrystallized)

Hydroforming experiment 'camera shaft'

Copper CW024A (R 200)

Test parameters:

Material: Copper CW024A (R 200)

Tensile strength σ_{UTS}: 236 MPa

Tube dimensions:
Tube length L_0 = 26.4 mm (*)
Outer diameter D_0 = 0.8 mm
Wall thickness t_0 = 100 µm

Procedure parameters:

Calibration pressure $p_{i,\,max}$ = 70 MPa
Axial sealing force F_a = 20 N
Volume flow: V_{Fl} = 0.07 ml/min.
Forming temperature: RT

Relative expansion ratio ε_d (**): 0.3

(*) overall length of die and clamping inserts
(**) According to Eqn. (19) and given die dimensions

Visualization of the forming results:

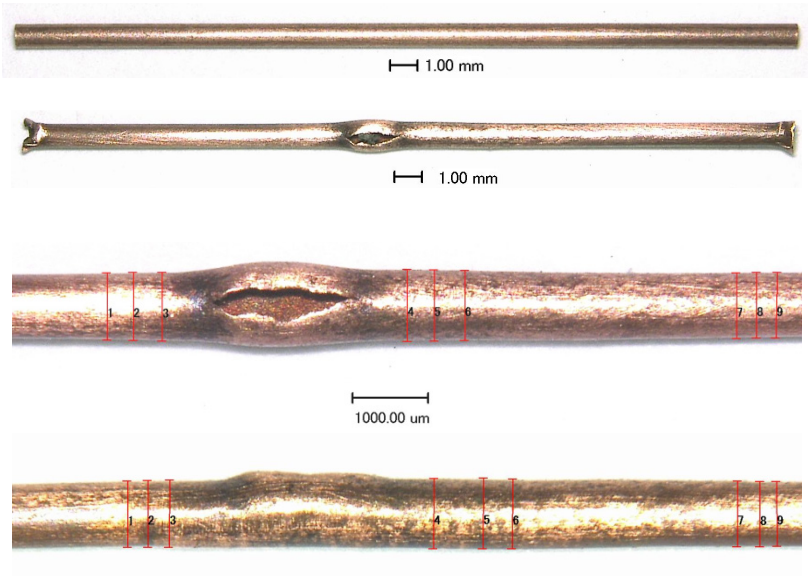

T_i: Initial tube

T_{22}: Formed micro-tube

T_{22}: Forming zone with section of fracture, top view

T_{22}: Forming zone, side view

Fig. 101: Forming results with test and procedure parameters of the hydroforming experiment 'geometry camera shaft' - Copper CW024A (R 200)

7.3.2 Discussion of the hydroforming results

In the failed forming results (due to bursting) using AISI 304-b and copper tubes, it can be seen that the achieved forming diameters are larger than the nominal diameters of the forming tool die cavity, cf. *Fig. 96*. A possible reason could be that the tensile stresses acting in circumferential tube direction changed to compression stresses after bursting of the tube samples which -after opening of the die halves- led to an opening (increase in diameter) of the tubes. At first there were the tensile stresses in circumferential direction σ_t according to *Eqn.* (1) in *Chap. 2.2.2.4* caused by the internal pressure p_i in the early stage of the free hydraulic bulging, then after bursting there were compression stresses inside the tube walls in circular direction, the still closed forming tool halves embarrassed the tube to open. After opening the die, the tube fracture widened through spring-back. It is assumed that the compression stresses in hoop direction caused also an increase in diameter of the neighbouring regions (diameters A, C & D*)* and the increase of the tube diameter was not only restricted to the area of the crack formation.

However, apart from this assumption also an opening of the die halves during the forming process could have happened. The recrystallized annealed AISI 304-r tubes that could be pressurized up to its calculated calibration pressure $p_{i,\,max}$ = 154 MPa showed two indentation lines along their longitudinal axis in the region of the largest forming diameter, cf. *Fig. 100 T_{13}*: *Forming zone top view,* which indicates a possible opening. A hint on this assumption might also be the increase in concentricity tolerance in all formed tube sections of the recrystallized tubes compared to the AISI 304-b and copper tubes. It is assumed that their forming pressure p_{ib} (fracture due to bursting occurred at less than 55 MPa, and less than 50 MPa respectively, according to the values achieved from the bulge test investigations, *Chap. 5.5.1*) of these tubes was not sufficient enough to attain an opening of the die. However, please note that in the hydroforming experiments described in this chapter no internal pressure had been measured. For the first hydroforming tests the software was only simple pro-

grammed, not programmed to acquire data, only a ramp was driven to attain the preset process variable $p_{i,\,max}$. Exact values are hence not known.

Another issue to consider is the coarse grain size of the recrystallized annealed stainless steel tubes. The danger of a non-uniform expansion has already been mentioned in *Chap. 7.1.1* which probably has occurred here and which is probably responsible for the increased eccentricity of the recrystallized micro-tubes.

Finally as a third reason for inaccuracy of the final part, spring-back behaviour must be named. Firstly elasticity of the micro-tube could have led to the eccentricity of the final part. As only or respectively less than one grain in the circumferential cross section of the AISI 304-r micro-tube was identified, it may be assumed that maybe also the elastic forming behaviour along the hoop was inhomogeneous/unequal.

It must be mentioned that elasticity due tool elements like the adjusting and matching plates (refer to *Fig. 79*) which were necessary to adjust the tool inserts could have caused a specific inaccuracy of the final part. For alignment of the tool inserts adjusting plates in sizes (thicknesses) of a few microns had been used which were stacked to ensure the correct position of the die inserts to each other and to the axis of the sealing punches. Also elastic deflections of the die insert by itself could have caused inaccuracy of the hydroformed part, please refer to below issue in the following conclusion.

Another issue that should be mentioned was the difficulty to place the tube at the beginning of the hydroforming process (cf. *Fig. 2*) exact into the longitudinally centre of the die cavity. This was not as trivial as it seemed, since a certain number of tubes could not be sealed by the conical sealing punches. Reason was that if the excess length on both sides of the tubes was unequal the length of the smaller overhang was not sufficient enough to create the infinite small circumferential line contact to ensure the sealing of the tube end.

Lastly, the low number of trials (5 per material) with regard to a descriptive statistic must be noted. This was due to the ending of the project and limitations to materials, no further experiments could be conducted.

7.3.3 Conclusion of the hydroforming experiments

The final hydroforming experiments at the end of the study have positively shown that in principle the first micro-hydroforming machine system is able to operate. To draw a definite conclusion, all accomplished considerations on machine components workpiece materials and dimensions must have been correct (in general). The most important points should be summarized in the following:

- With regard to the sealing system the tube ends could successfully be closed, apart from the problems mentioned in the above discussion, so that the tubes could be pressurized. It was critical (please mind the dimensions of only a few microns) if the sealing punches which were pushed via the sliding carriage along the guiding with a certain amount of guide clearance. A successful sealing implied that at any time the centre of the sealing punches' longitudinal axis was in the centre of the micro-tubes' axis. Just a slightly eccentricity towards each other could have led to an unequal circumferential contact pressure which could in turn have led to damage of the tube walls, especially in case of the just 40 µm thick AISI 304 micro-tubes.
- The control system worked. With the successfully formed AISI 304-r micro-tubes it could be shown that the pre-set process parameters matched the process window, cf. *Fig. 9* in *Chap. 2.2.2*.
- It also must be concluded that with all three investigated micro-tube (materials) a respectable accuracy as determined in *Chap 6.10.2 Achievable precision of the machine* could be obtained.
- In the future, one difficulty must be overcome. As mentioned above, it was difficult to place a micro-tube exact in the longitudinal centre of the die so that an equal excess length on both tube ends is sufficient enough to enable a sealing by the sealing punches. A solution may be to integrate a locator for exact positioning to the tool that could be deleted before starting the process cycle.

CHAPTER 8

CONCLUSION AND FUTURE WORK

8.1 Conclusion

This research project was intended to acquire basic knowledge about a miniaturized tube hydroforming (THF) process and tooling for the hydroforming of micro-components with the overall aim to carry out fundamentals of process design for industry to be able to start (mass-) producing micro THF-parts in the near future.

The following items were specific aims of this study:

- Establishment of material properties assessment methods
- Demonstration of a micro-THF prototype process
- Manufacture of 6 tubular micro-parts per minute

These items were specific objectives of the study:

- Investigation of the micro-tubes' relative expansion ratios, as compared to expansion ratios of macro-sized tubes
- Investigation of "conventional" testing methods to find out, if and/or how far they can also be used for the examination of micro-tubes
- Verification of technological laws and formulas used in the design of macro hydroforming process - if these can also be applied (and if, how far) for the development of a down-scaled process.
- Verification of an increase in formability and a decreased influence of size-effects during warm forming
- Examination and quantification of size-effects

Based on the intensively and extensively conducted theoretical and experimental research and development work, the following items are contributions as a result of this study:

- The world's first micro tube hydroforming prototype machine was successfully constructed and has produced the first tube hydroformed micro-components (see chapter *Forming experiments with the prototype machine and analysis*); cycle time per hydroformed micro-tube was ca. 10 seconds, handling of the workpiece not included

- A detailed description of a design study of machine / tool components (cf. chapter *Forming machine development*) serves as a methodology to enable design engineers further establishments and improvements of micro hydroforming machines of the 'next generation' in the near future.

- With an identified material testing method (hydraulic free-bulging) a tool is provided to process designers of future industrial micro tube hydroforming applications to successfully and efficiently pre-determine the forming behaviour of micro-tubes and to in turn successfully choose appropriate tube materials and suitable tube dimensions, chapter *Determination of tubes' mechanical properties with hydraulic free-bulging*.

- The feasibility to effectively determine real/existent expansion limits of micro-tubes will enable tool/machine designers of future industrial processes a safe dimensioning of forming tool geometries with a minimized danger of early process failure and thus to assure a most economic production.

- Existing theoretical correlations that serve in many cases as a basis for a determination of a 'macro' tube hydroforming process operation were verified as also applicable for the down-scaled process which also will allow engineers to pre-determine future micro hydroforming process controls.

- Size dependent effects could be observed and were identified as reasons, why currently used material testing methods in the 'macro' range - such as the mechanical tube flaring test (see chapter *Determination of tubes' formability with flaring tests*) - to determine tube material properties may not be applied to the miniaturized process

A remark on laser-assistance

In the laser assisted micro-hydroforming investigations one has learned that though in many other methods of micro forming heat especially laser assisted heat can be beneficial, however no satisfactory results regarding a significant increase in formability and/or a major reduction in scatter of the results that would warrant the added complexity and cost to a micro-tube hydroforming prototype machine could be seen.

8.2 Future work

Based on the experience gained throughout this study on micro-tube hydroforming, there are many ideas for future work. Among these, the four most important suggestions the author would like to express in the following:

(1) During the study, the bulge test turned out as a comparatively simple and effective instrument to prove the suitability of micro-tubes for micro-hydroforming applications. By applying the test, the maximum internal pressure the tube is able to withstand without fracture as well as maximum expansion ratios could be determined. However, from the author's point of view, the test method should be enhanced. As established in conventional THF applications, the bulge test provides the basis for accurate FE analyses of THF processes. To conduct the simulations the development of the true stress versus the true strain curve from the bulge test is necessary. By inducing a suitable device enabling the online measurement of the bulge height, the bulge height could be plotted as a function of internal pressure. Methods to hereafter determine the flow curve from the experiment are suggested and described in [105,106]. Obtained results of these investigations might serve as a basis for future

FEA simulations that from the author's point of view will need to be addressed in the future.

(2) Since only hydroforming experiments with fixed tube ends had been conducted, the formability of the investigated tube material should also be studied with axial feeding, i.e. by using the cylindrical sealing punches, which already had been manufactured but not been employed yet, and hence to draw a conclusion on the exact design of those machine components and if the already conducted design considerations were also correct.

(3) As mentioned, the hypothesized manufacturing time of 6 micro-tubes per minute could be achieved. However, the cycle time per unit was only obtained excluding the handling time of the micro-tube (inserting of initial tube and removing of the final part). The feasibility to increase the flow rate to further reduce the filling time must therefore be investigated. For economical mass-production an 'automatic handling system' needs to be designed and constructed in the near future.

(4) Even though all hydroformed micro-tube samples could be manufactured within the range of the predetermined precision (cf. *Chap. 6.10.2*) an improved final part precision needs to be achieved. A 'deflection compensation of the tooling' should be developed (e.g. based on a piezo-electric element that compensates tool deflections) which could be integrated into the tool block and be controlled via the machine control system.

In closing, the author would like to express his deepest desire and hope that his research efforts contribute to lay the foundation of the development of a new and modern manufacturing technology within the micro technology sector. He also wishes that he contributes to meet the requirements of a growing demand for miniaturized products of our daily life and that micro-THF as a new manufacturing method provides access to many other fields and applications, especially in the area of health care, medical devices and medical equipment.

APPENDIX:

SPECIFICATION SHEET – MICRO-HYDROFORMING PROTOTYPE MACHINE

A.1 Product specifications

	characteristic	**amount**	**remark**
1.1	***initial tube***		
1.1.1	outer diameter	0.8 mm	
1.1.2	wall thickness	variable	
1.1.3	length	10 mm	
1.1.4	material	variable	
1.1.4.1	yield strength		depending on material
1.1.4.2	tensile strength		depending on material
1.1.4.3	strain	53 %	
1.1.4.4	tolerances		depending on material
1.2	***hydroformed part***		
1.2.1	geometry	camera shaft	ref. to *Fig. 55*

A.2 Final machine specification

	characteristic	**amount**	**remark**
2.1	***press frame***		high stiffness required
2.1.1	die space	100 mm x 100 mm x 100 mm	width x depth x height
2.1.2	admissible deflection		to be defined
2.2	***drive for press slide***		closing of tooling during hydroforming (vertical)
2.2.1	principle		hydraulic cylinder
2.2.2	control		cascade control: transition and pressure (subordinate control loop)
2.2.3	max. force	~15000 N	
2.2.4	max. stroke	120 mm	
2.2.5	max. speed	10 mm/s	
2.3	***drives for axial sealing punches (2 p.)***		sealing of tube ends, material feeding, fixing of hydroformed part during opening of tooling; mounted to bottom die
2.3.1	principle		elec.: linear actuator
2.3.2	control		transition controlled, amount of displacement as a function of time independent control for each punch
2.3.3	positioining accuracy	+/- 0,015 mm	
2.3.4	max. force	800 N	
2.3.5	max. stroke	3 mm	
2.3.6	max. speed	25 mm/s	
2.4	***ejectors***		not used (lifting of part currently manually)
2.5	***pressure intensifier***		filling and pressurizing the workpiece, mounted to one of the sealing punches to simplify high-pressure-piping; the pressurizing medium is filled into the initial

			tube through a hole of one of the sealing punches; the air within the part will discharge through the gap between the opposite punch and the tube end (in the beginning of the arising axial load
2.5.1	principle		motor-driven spindle pump for the generation of a high pressure; the speed of the DC-motor is controlled by a DC-servo-controller (including a transformer and a rectifier)
2.5.2	control	+/- 2 %	pressure controlled, amount of pressure as a function of time
2.5.3	max. pressure	4000 bar	
2.5.4	volume flow	0.07 – 9 ml/min	
2.6	***pressurizing media***		
2.6.1	type		oil-water-emulsion or solution
2.6.2	amount	2 ltr.	storage tank (without recirculation)
2.6.3	temperature equali-zation	20°C +/- 1°C	necessary to obtain a constant medium viscosity
2.6.4	filtration	50 µm	filter cartridge
2.7	***deflection com-pensation of tool-ing***		an output of the control system is to be provid-ed; e.g. signals to a piezo-electric element which compensates tool deflection (principle to be defined, not realized during study)
2.8	***control system***		should be flexibly programmable: position-controlled, pressure-controlled or vs. time

A.3 Process sequence

	characteristic	amount	remark
3.1	***course of process***		see A.4
3.2	***values of manual input***		
3.2.1	min. closing force.	10000 (12000) N	w. axial feeding (without axial feeding, conical punches)
3.2.2	mean projected part area		necessary to calculate the increase of closing force in dependence of internal pressure
3.2.3	rest position of sealing punches (2 p.)	+0.267 (left) – 1.304 (right)	position during loading / unloading tube (depending on hydroformed part
3.2.4	initial forming position of sealing punches (2 p.)	ref.-point +/- 0 mm	first contact between tube ends and sealing punches
3.2.5	time interval	7 sec.	time for the forming process (including filling and calibration)
3.2.6	load curve		flexible input of internal pressure and stroke of sealing punches as a function of time (within time interval), e.g. curves with 10 interpolation points
3.2.7	curve for signal of “tool deflection compensation”		flexible input as a function of time (within time interval), e.g. curve with 10 interpolation points
3.2.8	stop criteria		necessary for automatic stop if failures occur, e.g.: - actual internal pressure is below a critical target (leakage), - sealing force exceeds a critical value (to avoid punch breakage), - pressure intensifier not filled before forming, - failures with part handling, - hydraulic oil temperature too high, - filtration system blocked, etc.
3.3	***sensors and data logging***		
3.3.1	press slide position		sensors for upper position / lower position

3.3.2	closing force		sensor and data logging of target/actual values
3.3.3	positions of sealing punches (2 p.)		e.g. incremental position sensor; data logging of target/actual values
3.3.4	load of sealing punches (2 p.)		sensors for force measurement; data logging of target/actual values
3.3.5	internal pressure		sensor for internal pressure measurement; data logging of target/actual values
3.3.6	part detection		sensors for the detection of correct inserted part
3.3.7	others		if required, e.g. sensors for oil temperature, medium management, etc. data logging for output as described at 2.7

A.4 Process sequence

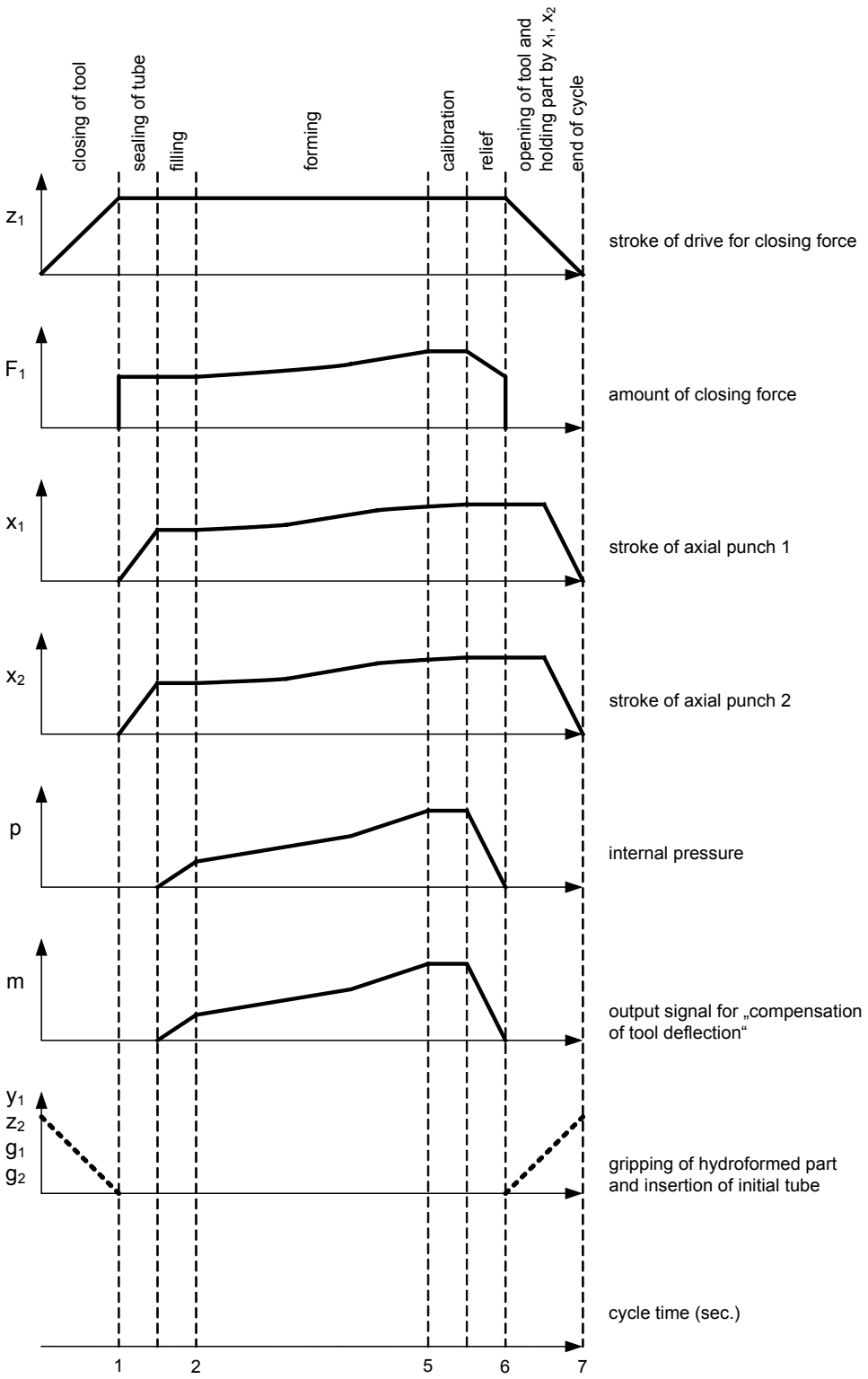

GLOSSARY

ABAQUS	Suite of software applications for finite element analysis
AISI	American Iron and Steel Institute
ASTM	American Society for Testing Materials
BFT	Bulge Forming of Tubes
CAD	Computer-Aided Design
CCD	Charge-Coupled Device
CW	Continuous Wave (continuous output beam)
DC	Direct Current
DMS	German acronym for Dehnungsmessstreifen (strain gauge)
EDM	Electro Discharge Machining
ETH	Eidgenössische Technische Hochschule (Swiss Federal Institute of Technologie), Zürich, Switzerland
EU	European Union
FE / FEA	Finite Element / Finite Element Analysis
FHB	Free Hydraulic Bulging
FLD	Forming Limit Diagram
HPF	Hydrostatic Pressure Forming
IC	Integrated Circuit (also reffered to as chip or microchip)
IHU	German acronym for Innenhochdruckumformen (Internal High Pressure Forming)
IHPF	Internal High Pressure Forming
LIGA	German acronym for LIthographie, Galvanik, Abformung (Lithography, Electroplating, Molding)
LBF	Liquid Bulge Forming

MASMICRO	Mass-Manufacture of Miniature/Micro Products (EU research project under the FP6 Framework Programme)
MEMS	Micro Electro-Mechanical Systems
MST	Micro Systems Technology
RT	Room Temperature
SPS	German acronym for Speicherprogrammierbare Steuerung (Programmable Logic Controller, PLC)
THF	Tube HydroForming

LIST OF REFERENCES

1. Vollertsen, F. et al.: State of the art in micro forming and investigations into micro deep drawing, Journal of Materials Processing Technology 151 (2004), pp. 70-79

2. Qin, Y.: Micro-manufacturing engineering and technology, 1st ed.; Elsevier, Amsterdam, Boston, 2010

3. Hartl, Ch., Anyasodor, G., Ptaschlik, T., Lungershausen, J., Lippert, S.: Investigation into reduction of die-cavity deflection in micro-hydroforming processes using FEA. International Journal of Advanced Manufacturing Technology 47, no. 9-12, special issue 'Mass-Manufacture of Micro-Products' (2009) pp. 835-858

4. Wilhelm, H., Lungershausen, J., Hartl, Ch.: A fiber laser system for 3D-processing of hydroformed micro components (orig.: Faserlasersystem für die 3D-Bearbeitung von Miniatur-Umformteilen), LASER no. 6 – Europäischer LASER Markt (2009), pp. 58-60

5. Hartl, Ch., Lungershausen, J., Eguia, J., Uriarte, L., Lopez Garcia, F.: Micro hydro-forming process and machine system for miniature/micro products. Proceedings from Euspen, 7th International Conference, Bremen; Germany (2007)

6. Neugebauer, R.: Hydroforming (orig.: Hydroumformung). Springer-Verlag Berlin Heidelberg (2007)

7. Engel, U., Eckstein, R.: Microforming - from basic research to its realization, Journal of Materials Processing Technology 125-126 (2002), pp. 35-44

8. Geiger, M., Kleiner, M., Eckstein, R., Tiesler, N., Engel, U.: Microforming. Annals of the CIRP Vol. 50/2 (2001), pp. 445-462

9. Vollertsen, F.: Size effects in manufacturing. 1st Colloquium Process Scaling, Bremen (2003), pp. 1-9

10. Geiger, M., Messner, A., Engel, U.: Production of microparts - size effects in bulk metal Forming, similarity theory. In: Production Engineering - Annals of the WGP (1997), pp. 55-58

11. Geiger, M. et al.: Metal forming of micro parts for electronics. Production Engineering 2, no.1 (1994), pp. 15-18

12. Geissdörfer, S., Engel, U., Geiger, M.: FE-simulation of microforming processes applying a mesoscopic model. International Journal of Machine Tools & Manufacture 46 (2006), pp. 1222-1226

13. Zhuang, W. et al.: Experimental and numerical investigation of localized thinning in hydroforming of micro-tubes. European Journal of Mechanics A/Solids 31 (2011), pp. 67-76

14. Kowalczyk-Gajewska, K.: Modelling of texture evolution in metals accounting for lattice reorientation due to twinning. European Journal of Mechanics A/Solids 29 (2010), pp. 28-41

15. Qin, Y.: Advance in Micro-Manufacturing Research and Technological Development, and Challenges/Opportunities for Micro-Mechanical-Machining, in Proceedings of Cutting Tool Congress, Milano, Italy, 2007

16. Vollertsen, F., Schulze Niehoff, H., Hu, Z.: State of the art in micro forming. International Journal of Machine Tools & Manufacture 46 (2006), pp. 1172-1179

17. Engel, U. et al.: Forming of metallic micro-parts (orig.: Umformtechnische Herstellung metallischer Kleinstteile). VDI-Z 136 (1994), Nr. 9, pp. 76-78

18. Xie, Y., Yu, H., Ruan, X.: Development and future of metal microforming technology. Chinese Journal of Mechanical Engineering 16, no.10 (2005), pp. 935-939

19. Qin, Y.: Micro-forming and miniature manufacturing systems - Development needs and perspectives. Keynote Paper (plenary address) of the 11th Int. Conference of Metal Forming, Sept. 2006, Journal of Materials Processing Technology 177, no. 1-3 (2006), pp. 8-18

20. Koc, M., Altan, T.: An overall review of the tube hydroforming (THF) technology. Journal of Materials Processing Technology 108 (2001), pp. 384-393

21. Grey, J.E., Devereaux, A.P., Parker, W.N.: Apparatus for making wrought metal T's. US Patent 2,203,868 (1939).

22. Mellor, P.B.: The ultimate tensile strength of thin-walled shells and circular diaphragms subjected to hydrostatic pressure. International Journal of Mechanical Sciences 1 (1960), pp. 216-228

23. Fuchs, F. J.: Hydrostatic Pressure - Its Role in Metal Forming. Mechanical Engineering, April 1966, pp. 34-40

24. Ogura, T., Ueda, T.: Liquid Bulge Forming. Metalworking Production 04 (1968), pp. 73-81

25. Al-Qureshi, H. A.: Comparison Between the Bulging of Thin-Walled Tubes Using Rubber Forming Technique and Hydraulic Forming Process. Sheet Metal Industries 7 (1970), pp. 607-612

26. Woo, D. M.: Tube-Bulging under Internal Pressure and Axial Force. Journal of Engineering Materials and Technology 95, no. 4 (1973), pp. 219-223

27. Sauer, W. J. et al.: Free bulge forming of tubes under internal pressure and axial compression. 6th Northamerican Metallworking Research Conference Proceedings, SME, Conf. University of Florida, Gainsville (1978), pp. 228-235

28. Klaas, F.: Upsetting & expansion of tubes by hydroforming (orig.: Aufweitstauchen von Rohren durch Innenhochdruckumformen). Doctoral Thesis, University Paderborn, Germany (1987)

29. Dohmann, F., Bieling, P.: Fundamentals and application of hydroforming (orig.: Grundlagen und Anwendung des Innenhochdruckumformens). Bleche, Rohre, Profile, Nr. 38/5 (1991), pp. 379-385

30. Dohmann, F., Dudziak, K. U.: Concept for the construction of tools and machines for hydroforming (orig.: Konzeption für den Bau von Werkzeugen und Maschinen zum Innenhochdruckumformen). Bänder, Bleche, Rohre 8, (1991) pp. 19-29

31. Schmoeckel, D., Hessler, C., Engel, B.: Pressure Control in Hydraulic Tube Forming. Annals of CIRP 41, no. 1 (1992), pp. 311-314

32. Böhm, A.: Numerical simulation of the hydroforming process with special consideration of expansion in closed dies (orig: Numerische Simulation von Verfahren der Innenhochdruckumformung unter besonderer Berücksichtigung des Aufweitens im geschlossenen Gesenk). Doctoral Thesis, University Paderborn, Germany (1993)

33. Dohmann, F.: Hydroforming, in Lange, K. (ed.) Metal Forming Volume 4, 2nd ed. (orig.: Innenhochdruckumformen, in Lange, K. (Hrsg.) Umformtechnik Band 4, 2. Aufl.) Springer Verlag, Berlin u.a. (1993), pp. 253-270

34. Koc, M.: Development of Design Guidelines for Tube Hydroforming. Doctoral Dissertation Engineering Research Center for Net Shape Manufacturing at Ohio State University, Columbus, OH, USA (1999)

35. Lang, L.H. et al.: Hydroforming highlights: sheet hydroforming and tube hydroforming. Journal of Materials Processing Technology 151 (2004), pp. 165-177

36. Hartl, Ch.: Research and advances in fundamentals and industrial applications of hydroforming. Journal of Materials Processing Technology 167 (2005), pp. 383-392

37. Hartl, Ch., Lücke, H.-U., Böhm, A.: Produktivitätssteigerung beim Hochdruckumformen - Massnahmen und Strategien. Proceedings of the 3rd Chemnitz Car Body Colloquium, Chemnitz, Germany (2002), pp. 169-182

38. Hartl, Ch., Lungershausen, J., Biedermann, H., Conzen, J.: Study of hydroforming processes for the production of micro-components. Proceedings from 1st Jubilee Scientific Conference Manufacturing Engineering in Time of information Society, Gdansk, PL (2006)

39. Hartl, Ch.: Materials and their characterisation for hydroforming. In: M. Koc (Ed.) Hydroforming for advanced manufacturing, Woodhead Publishing, Cambridge, UK (2008), pp. 77-92

40. Hielscher, C.: Semi-finished products inspection for the hydroforming of complex components (orig.: IHU-Halbzeugprüfung für die Herstellung komplexer Bauteile). Int. Conference „Hydroforming“, in Conference Procee-

dings: Hydroumformung von Rohren, Strangpreßprofilen und Blechen, Band 2 (2001), pp. 69-91

41. Jirathearanat, S.: Advanced methods for finite element simulation for part and process design in tube hydroforming. Doctoral Dissertation Engineering Research Center for Net Shape Manufacturing at Ohio State University, Columbus, OH, USA (2004)

42. Altan, T.; Jirathearanat, S.; Kaya, S.: Process Simulation for Hydroforming Components from Sheet and Tube - How can we improve the accuracy of the predictions? Proceedings of The 3rd Chemnitz Car Body Colloquium, Chemnitz, Germany (2002), pp. 131-132

43. Altan, T. et al: Formability and Design Issues in Tube Hydroforming, Proceedings of the International Conference on Hydroforming, Fellbach b. Stuttgart, Germany (1999), pp. 135-151

44. Bauer, H., Hartl, Ch., Haas, A.: Hydroforming-optimized process design with the aid of the FEA. Proceedings of the Advanced Technology Symposium on Tube Hydroformimg, Iron and Steel Society, Detroit, MI, USA (1999), pp. 98-105

45. Bieling, P.: Studies on upsetting & expansion of tubes to hollow shafts (orig.: Untersuchungen zum Aufweitstauchen von Rohren zu Hohlwellen). Doctoral Dissertation, Universität Paderborn, Germany (1992)

46. Dohmann, F.; Hartl, Ch.: Hydroforming-applications of coherent FE-simulations to the development of product and processes. Journal of Materials Processing Technology 150 (2004), pp. 18-24

47. Dohmann, F.; Hartl, Ch.: Tube hydroforming - research and practical application, Journal of Materials Processing Technology. 71 (1997), pp. 174-184

48. Dudziak, K.-U.: Process modeling for the hydroforming of stepped, hollow components (orig.: Prozessmodellierung für die Innenhochdruckumformung von abgesetzten, hohlen Bauteilen). Fortschrittberichte VDI Reihe 2 Nr. 368, Düsseldorf, VDI-Verlag (1996)

49. Hartl, Ch.: A contribution to the flexibility of hydroforming (orig.: Ein Beitrag zur Flexibilisierung der Innenhochdruckumformung). Doctoral Dissertation, University Paderborn, Verlag Shaker, Aachen (1995)

50. Jirathearanat, S.; Hartl, Ch.; Altan, T.: Hydroforming of Y-shapes - product and process design using FEA simulation and experiments. Journal of Materials Processing Technology 146 (2004), pp. 124-129

51. Bräutigam, M, Rutsch, H.: Hydroforming - the way out of the tight investment squeeze (orig.: Hydroformen - als Ausweg aus der Investitionsklemme). In: VDI Reports No. 946, VDI, Düsseldorf (1992)

52. Hartl, Ch.: Theoretical fundamentals of hydroforming (orig.: Theoretische Grundlagen der Innenhochdruckumformung). International Conference on Hydroforming, Fellbach b. Stuttgart, Germany, (1999), pp. 23-35

53. Koc, M., Altan, T.: Prediction of forming limits and parameters in the tube hydroforming process, Int. J. of Machine Tools & Manufacture 42 (2002), pp. 123-138

54. Hartl, Ch.: Deformation mechanism and fundamentals of hydroforming. In: M. Koc, (Ed.) Hydroforming for advanced manufacturing, Woodhead Publishing, Cambridge, UK (2008), pp. 52-76

55. Dohmann, F., Hartl, Ch.: Hydroforming - a method to manufacture lightweight-parts. Journal of Materials Processing Technology 60 (1996), pp. 669-676

56. Hartl, Ch.: Case Studies in Hydroforming. International Conference: Recent Development on Tube and Sheet Hydroforming, Columbus, OH (2003)

57. Kratky, A.: Laser-assisted forming (orig.: Laserunterstützte Umformverfahren). International Congress of the welding and joining technology, Vienna, Austria (2008)

58. Gillner, A., Holtkamp, J. et al.: Laser applications in microtechnology. Journal of Materials Processing Technology 167, no. 2-3 (2005), pp. 494-498.

59. Bayer, A., Gillner, A., Groche, P., Erhardt, R.: Laser-assisted forming of metallic micro-parts. Proceedings of SPIE - The International Society for Optical Engineering, Vol. 5063, Fourth International Symposium on Laser Precision Microfabrication (2003), pp. 157-162

60. Peng, X., Qin Y., Balendra, R.: Analysis of the laser-heating methods for micro-parts stamping applications, Journal of Materials Processing Technology 150, no. 1-2 (2004), pp. 84-91

61. Peng, X., Qin Y., Balendra, R.: A numerical investigation to the strategies of the localised heating for micro-part stamping. International Journal of Mechanical Sciences 49, no. 3 (2007), pp. 379-391

62. Wulfsberg, J.P., Hilpert, S.-E., Ostendorf, A., Samm, K.: Fundamentals of Laser-assisted Microforming. 1st Colloquium Process scaling, Bremen, Germany (2003)

63. Egerer, E., Neudecker, T., Engel, U.: Basic research on warm micro forming. In: Kopp (ed.), expansion of the forming limits in metal forming processes (orig.: Grundlagenuntersuchungen zum Halbwarmmikroumformen. In: Kopp (Hrsg.), Erweiterung der Formgebungsgrenzen bei Umformprozessen), Proceedings of: DFG-Kolloquium im Schwerpunktprogramm 1074 der Deutschen Forschungsgemeinschaft (DFG) (2001), pp. 82-88

64. Gillner, A., Bayer, A., Groche, P., Erhardt, R.: Laser-assisted micro forming of metallic components. In: expansion of the forming limits in metal forming processes (orig.: Laserunterstütztes Mikroumformen metallischer Bauteile. In: Erweiterung der Formgebungsgrenzen bei Umformprozessen), Proceedings of: DFG-Kolloquium im Schwerpunktprogramm 1074 der Deutschen Forschungsgemeinschaft (DFG) (2001), pp. 89-95

65. Schöck, J., Kammerer, M.: Material selection. In: Lange, K. (ed.) Extrusion - Economic manufacturing of metallic precision workpieces (orig.: Werkstoffauswahl. In: Lange, K. (Hrsg.) Fliesspressen - Wirtschaftliche Fertigung metallischer Präzisionswerkstücke), VDI-Buch, Springer, Berlin Heidelberg (2008)

66. Remppis, M.: Hot and cold-forming of steel - its possibilities and limitations (orig.: Kalt- und Warm-Umformung von Stahl - ihre Möglichkeiten und Grenzen). L. Schuler GmbH (1993)

67. Koc, M. Aue-u-lan, Y., Altan, T.: On the characteristics of tubular materials for hydroforming - experimentation and analysis. International Journal of Machine Tools & Manufacture 41 (2001), pp. 761-772

68. Research report, Deliverable: D14, The process configuration of laser-assisted hydro-miniature forming. Cologne University of Applied Sciences, Cologne, Germany (2005)

69. Bollinger, E., Jütten, W.: Tubes for hydroforming processes. In: Hydroforming of tubes, extrusions and sheets, Volume 1 (orig.: Rohre für das IHU-Verfahren. In: Hydroumformung von Rohren, Strangpressprofilen und Blechen, Band 1), DGM, Frankfurt 1999, pp. 127-133

70. http://www.minitubes.com (date of access: Mar. 10, 2009)

71. http://www.rieck-edelstahl.de (date of access: Mar. 10, 2009)

72. Klocke, F., Koenig, W.: Manufacturing 4 - Forming. 5th revised edition (orig.: Fertigungsverfahren 4 - Umformen. 5., neu bearbeitete Auflage), VDI-Buch, Springer-Verlag, Berlin Heidelberg (2006)

73. Copper - occurrence, extraction, properties, processing, use (orig.; Kupfer - Vorkommen, Gewinnung, Eigenschaften, Verarbeitung, Verwendung). DKI - Informationsdruck, Best.-Nr. i004, Deutsches Kupferinstitut, 02 (1997)

74. Petzow, G.: Metallographic Etching (orig.: Metallographisches, keramographisches, plastographisches Ätzen), 6th ed., Gebrüder Borntraeger Berlin Stuttgart (2006)

75. Han, W. et al.: Orientation Design for Enhancing Deformation Twinning in Cu Single Crystal Subjected to Equal Channel Angular Pressing. Advanced Engineering Materials 10, no. 12 (2008), pp. 1110–1113

76. Lobastov, A.I., Shudegov, V.E., Chudinov, V.G.: Study of the atomic structure of bcc and fcc crystals upon instantaneous plastic deformation. Technical Physics 42, no. 12 (1997), pp. 1460-1462

77. Manabe, K., Nishimura, H.: Forming loads in tube-flaring with conical punch - Study on nosing and flaring of tubes V. Journal of Japan Society for Technology of Plasticity 24, no. 264 (1983), pp. 47-51

78. Manabe, K., Nishimura, H.: Stress and strain distributions in tube-flaring with conical punch - Study on nosing and flaring of tubes VI. Journal of Japan Society for Technology of Plasticity 24, no. 266 (1983), pp. 276-282

79. Almeida, B.P.P. et al.: Expansion and reduction of thin-walled tubes using a die: Experimental and theoretical investigation. International Journal of Machine Tools & Manufacture 46 (2006), pp. 1643-1652

80. Alves, M. L. et al.: End forming of thin-walled tubes. Journal of Materials Processing Technology 177 (2006), pp. 183-187

81. Lu, Y.-H.: Study of tube flaring ratio and strain rate in the tube flaring process. Finite Elements in Analysis and Design 40 (2004), pp. 305-318

82. Fischer, F.D., Rammerstorfer, F.G., Daxner, T.: Flaring - An analytical approach. International Journal of Mechanical Sciences 48 (2006), pp. 1246-1255

83. Expansion test on tubes - Testing of Metallic Materials (orig.: Aufweitversuch an Rohren - Prüfung metallischer Werkstoffe), DIN 50135, Fachnormenausschuß Materialprüfung im Deutschen Normenausschuß (DNA), 08 (1965), pp. 94-95

84. Mirzai, Mohammad Ali. et al.: Deformation characteristics of microtubes in flaring test. Journal of Materials Processing Technology 201 (2008), pp. 214-219

85. Lungershausen, J.: Studies on hydroforming of micro parts (orig.: Untersuchungen zum Innenhochdruckumformen von Mikro-Bauteilen. Proceedings from 9th Int. Symposium of Students and Young Mechanical Engineers „Advances in Mechanical Engineering“, Gdansk University of Technology (2006), pp. 129-134

86. Hasek, V.: Deformation analysis using the power line method. (orig.: Formänderungsanalyse mittels des Liniennetzverfahrens). In: Metal Forming Vol. 3 (Umformtechnik Band 3), Springer Verlag, Berlin, Heidelberg, New York (1990), pp. 35-77

87. Jansson, M., Nilsson, L., Simonsson, K.: On constitutive modelling of aluminium alloys for tube hydroforming applications. International Journal of Plasticity 21 (2005), pp. 1041-1058

88. Lange; K.: Metal Forming Vol. 1: Fundamentals. (orig.: Umformtechnik Band 1: Grundlagen), Springer Verlag Berlin, Heidelberg, New York (1984)

89. Lianfa, Y., Cheng, G.: Determination of stress-strain relationship of tubular material with hydraulic bulge test. Thin-Walled Structures 46 (2008), pp. 147-154

90. Hielscher, C.: Tube testing for the production of complex hydroforming parts, in: Proceedings of the International Conference on Hydroforming, Stuttgart (2001), pp. 63-84

91. Vollertsen. F. et al.: Size effects in manufacturing of metallic components. Annals of CIRP 58 (2009), pp. 566-587

92. Kleiner, M. Homberg, W.: New 100,000 kN press for hydro sheet metal forming (orig.: Neue 100,000 kN-Presse für die Hydro-Blechumformung). In: Proceedings of the International Conference on Hydroforming, Fellbach b. Stuttgart, Germany (2001), pp. 351-362

93. Luecke, H.-U., Hartl, Ch., Abbey, T.: Hydroforming, in: Proceedings of the International Conference on Sheet Metal, Erlangen Nuremberg, Germany (1999), pp. 1183-1188

94. Schnupp, K., Kerschner, M.: Presses for hydromechanical drawing of panels for automobiles, in: Proceeding of the International Conference on Hydroforming, Fellbach b. Stuttgart, Germany (2003), pp. 409-421

95. K. Siegert, M. Haussermann, R. Rieger, A. Schwager: New press concept for hydroforming. In: K. Siegert (Ed.) Hydroforming of tubes, extrusions and sheet metals 1 (1999), pp. 123-138.

96. Dohmann, F., Hartl, Ch.: Possibilities of hydroforming with special attention to the molding of extruded profiles (orig.: Möglichkeiten der Innenhoch-

druckumformung unter besonderer Beachtung des Formens von Strangpressprofilen). Kolloquium: New developments in massive forming, Fellbach b. Stuttgart, Germany, (1993), pp. 255-279

97. Research report, Deliverable: D60, Forming machine system concepts - hydro-forming machine. Lead contractor: Cologne University of Applied Sciences, Cologne (2006)

98. Altan, T., Ngaile, G.: Tooling for tube hydroforming, Tube and sheet hydroforming, Fundamentals and Applications, ERC, Ohio State University (2003)

99. Research report, Deliverable: D40, Flexible tool-system structure designs for micro-hydroforming, Cologne University of Applied Sciences, Cologne, Germany (2006)

100. Conzen, J.: Finite Element Analysis of processes and tools for the laser-assisted hydro-forming of microcomponents (orig.: Finite Elemente Analysen von Prozessen und Werkzeugen für das laserunterstützte Hydroformen von Mikrobauteilen), Diploma Thesis, Fachhochschule Köln, Germany (2007)

101. Lungershausen, J.; Hartl, Ch.: Micro forming with high pressure (orig.: Mikroumformen mit Hochdruck), Maschinenmarkt - Das Industriemagazin 10 (2007), pp. 26-28

102. Vollertsen F: Accuracy in process chains using hydroforming. Journal of Materials Processing Technology 103, no. 3 (2000), pp. 424–433.

103. Doege, E., Meyer-Nolkemper, H., Saeed, I.; Flow curve atlas of metallic materials (orig.: Fließkurvenatlas metallischer Werkstoffe). Hanser Verlag (1986)

104. Research report Deliverable: D42, Forming Machinery Design Considerations. Lead contractor: Tekniker, Eibar, Spain (2006)

105. Strano, M., Altan, T.: An inverse energy approach to determine the flow stress of tubular materials for hydroforming applications. Journal of Materials Processing Technology 146 (2004), pp. 92-96

106. Hwang, Y.-M., Lin, Y.-K., Chuang, H.-C., Forming limit diagrams of tubular materials by bulge tests, Journal of Materials Processing Technology 209 (2009), pp. 5024-5034